



U.S. DEPARTMENT OF
ENERGY

PNNL-23060 Rev. 1
DSGREP-RPT-002, Rev. 1

Prepared for the U.S. Department of Energy
under Contract DE-AC05-76RL01830

Gas Release Due to Rayleigh-Taylor Instability within Sediment Layers in Hanford Double-Shell Tanks: Results of Scaled-Vessel Experiments, Modeling, and Extrapolation to Full Scale

SD Rassat
PA Gauglitz
LA Mahoney
RP Pires
DR Rector
JA Fort

GK Boeringa
DN Tran
MR Elmore
WC Buchmiller
ML Kimura

April 2014



Pacific Northwest
NATIONAL LABORATORY

*Proudly Operated by **Battelle** Since 1965*

DISCLAIMER

This report was prepared as an account of work sponsored by an agency of the United States Government. Neither the United States Government nor any agency thereof, nor Battelle Memorial Institute, nor any of their employees, makes **any warranty, express or implied, or assumes any legal liability or responsibility for the accuracy, completeness, or usefulness of any information, apparatus, product, or process disclosed, or represents that its use would not infringe privately owned rights.** Reference herein to any specific commercial product, process, or service by trade name, trademark, manufacturer, or otherwise does not necessarily constitute or imply its endorsement, recommendation, or favoring by the United States Government or any agency thereof, or Battelle Memorial Institute. The views and opinions of authors expressed herein do not necessarily state or reflect those of the United States Government or any agency thereof.

PACIFIC NORTHWEST NATIONAL LABORATORY
operated by
BATTELLE
for the
UNITED STATES DEPARTMENT OF ENERGY
under Contract DE-AC05-76RL01830

Printed in the United States of America

Available to DOE and DOE contractors from the
Office of Scientific and Technical Information,
P.O. Box 62, Oak Ridge, TN 37831-0062;
ph: (865) 576-8401
fax: (865) 576-5728
email: reports@adonis.osti.gov

Available to the public from the National Technical Information Service
5301 Shawnee Rd., Alexandria, VA 22312
ph: (800) 553-NTIS (6847)
email: orders@ntis.gov <<http://www.ntis.gov/about/form.aspx>>
Online ordering: <http://www.ntis.gov>



This document was printed on recycled paper.

(8/2010)

Gas Release Due to Rayleigh-Taylor Instability within Sediment Layers in Hanford Double-Shell Tanks: Results of Scaled-Vessel Experiments, Modeling, and Extrapolation to Full Scale

SD Rassat
PA Gauglitz
LA Mahoney
RP Pires
DR Rector
JA Fort

GK Boeringa
DN Tran
MR Elmore
WC Buchmiller
ML Kimura

April 2014

Prepared for
the U.S. Department of Energy
under Contract DE-AC05-76RL01830

Pacific Northwest National Laboratory
Richland, Washington 99352

Executive Summary

In Hanford Site underground waste storage tanks, a typical waste configuration is settled beds of solid particles beneath liquid layers. These sediment beds usually exist in layers due to incremental waste transfers into the vessel, and these layers can have different physical and chemical properties. One postulated configuration within the settled bed is a more-dense layer lying atop a less-dense layer. The different densities can be a result of differences in gas retention in the layers or different degrees of settling and compaction in the layers. If the density difference between the layers is sufficiently high, this configuration can experience a Rayleigh-Taylor (RT) instability, in which the less-dense lower layer rises into the upper layer. The motion from the RT instability has the potential to cause the release of some portion of the gas retained in these layers, and, because hydrogen is a component in the retained gas, this results in a potential flammable gas safety hazard.

Previous studies of gas retention and release in Hanford tank waste have not considered potential buoyant motion within a settled bed of solids. However, because future waste management operations may lead to sludge depths in double-shell tanks (DSTs) that are greater than in historical practice and this may create waste configurations where an RT instability could occur, consideration is being given to the RT instability. The postulated gas retention-release scenario is referred to as a deep-sludge gas-release event (DSGRE). The overall objectives of the present report are to provide quantitative information for a) predicting the conditions under which an RT instability might occur in waste stored in DSTs and b) estimating the size of the DSGRE should an RT instability occur. The overall effort includes conducting tests in different size vessels and developing a simple physical model (modified energy ratio) to support extrapolation of the results to estimate full-scale DST behavior. Also included in this report is a summary of numerical modeling studies of RT instabilities that were conducted to provide physical insights into the RT behavior and to support the extrapolation of the experimental results to full-scale DSTs. (The numerical studies were not conducted under the Quality Assurance plan for the project, so these results are For Information Only.)

RT instability gas-release tests were conducted in cylindrical, open-topped, clear-plastic test vessels placed on scales to record the mass of simulant added and the liquid lost due to evaporation. The three test vessels have nominal inner diameters of 10 in., 23 in., and 70 in. A silica-bentonite clay slurry simulant was added in two layers at the start of each RT test: the bottom sediment (slurry) layer contained hydrogen peroxide to generate oxygen gas over time; and slurry having no gas-generating components was layered on top. The latter was dyed to allow the two layers to be visually distinguished and to aid in observations of buoyant motion within the sediment bed. Finally, supernatant liquid (water) was added on top of the upper sediment layer. The testing included four different configurations for the thickness of the layers. In the first configuration, the initial total slurry and supernatant layer depths were geometrically scaled to match Hanford DST 241-AN-101 (1×, geometrically-scaled ratio of depth to vessel diameter) and the initial depths of the lower and upper slurry layers were equal (i.e., 1:1 lower-to-upper layer depth ratio). The second configuration also had equal initial depths of the lower and upper slurry layers, but the total slurry depth was other than 1× geometrically scaled. In the third configuration, the relative thicknesses of the initial lower and upper slurry layers were varied (e.g., 1:3 or 3:1 lower-to-upper depth ratio) using both 1× and 2× geometrically-scaled total slurry depth. In the fourth and final configuration, single slurry layers that matched the depth (and simulant composition) of the lower layers

in the first test configuration (1× geometrically scaled, 1:1 layer depth ratio) were used, but without an upper slurry layer.

RT instabilities were initiated by blending hydrogen peroxide in the lower slurry layer. The hydrogen peroxide decomposed to generate oxygen gas bubbles. Over time, oxygen bubbles that were retained in the lower simulant layer caused the overall liquid level to increase and reduced the bulk density of the lower layer in comparison to the upper layer. Eventually, the layers became unstable and all or a portion of the lower layer rose through the upper layer, causing gas to be released and causing the overall liquid level to fall. The liquid level was tracked throughout each RT instability test, which lasted from ~10 hr to several days, using time-lapse cameras focused on measuring tapes that were attached to each vessel. Analysis of the level data provided quantitative information on the retained gas volume fraction α as a function of time and the volume of gas releases. Other cameras mounted overhead (top) and along the side of the vessel provided panoramic views and qualitative information.

Multiple tests were conducted in each vessel, and results were obtained for quantifying the conditions for the onset of the RT instability, the release of gas during the RT instability, and the onset of spontaneous gas release in the single-slurry-layer tests. Based on previous studies, the retained gas fraction at the onset of the RT instability (α_{RT}) was initially expected to depend only on the dimensionless gravity yield parameter (Y_G) with Y_G being a constant value for the different configurations (total slurry depth and lower-to-upper depth ratio). The test results showed more complex behavior with thinner total slurry depths and smaller lower-to-upper slurry depth ratios both increasing stability of the layers and requiring a higher void fraction for the onset of the RT instability. Based on the test results, two correlations were developed for the stability criterion for onset of RT instabilities. One correlation used dimensionless parameters, specifically Y_G and ratios of slurry layer depths and tank diameter, and the second correlation was a dimensional, empirical fit to the data. The two correlations are similar, but have differences including tank-diameter dependence. Each correlation was used to extrapolate and estimate the void fraction and waste strength for the onset of RT instabilities in a full-scale DST. The waste strength for the onset of an RT instability, at a specified gas void fraction, differed by about a factor of two using the two correlations.

The observed motion and quantity of gas released depended on the test conditions. In addition to the initial RT instability in each test and the gas release caused by this motion, secondary gas releases also were observed. These secondary releases were often at a higher retained gas fraction and larger than the initial RT instabilities. Test results demonstrate that the quantity of gas released in RT instabilities generally increases with increasing α_{RT} , and considerably larger gas releases were often observed for α_{RT} values >0.2. An overall assessment of the test results shows that tests at higher α_{RT} are affected by being near or above the void fraction for neutral buoyancy in the supernatant water layer or being near the void fraction at which a spontaneous bubble-cascade gas release occurs. Excluding these high- α_{RT} tests and also excluding 23-in. vessel tests that were 2× geometrically-scaled total slurry depth, the gas releases associated with the initial RT instabilities in 23-in. and 70-in. vessel tests were relatively small, decreased with decreasing α_{RT} , and the observed motion was consistent with the general expectations for in-sediment buoyancy-induced flow. In addition, the observed motion was similar to numerical simulation predictions for RT instabilities. [Note that the numerical simulations were performed to obtain data that are considered to be For Information Only.] This subset of test results was selected for estimating gas releases in full-scale DSTs. The gas releases trended downward and became negligible at \leq ~15% void, and in the range of 14 to 16% void, there are test results for both the 23-in. and 70-in. vessels.

Extrapolation of these 23-in. and 70-in. vessel test gas-release data gives a predicted near zero gas release for a full-scale DST at ~15% void. More conservatively, including the uncertainty in the released gas measurements with the average of the results for repeat 23-in. vessel tests gives an estimated release of ~3% of the retained gas inventory. This is the best estimate for gas release in a full-scale DST should an RT event occur at α_{RT} of ~0.15 (e.g., a gas-free upper layer over a lower layer at ~15% void).

The For Information Only numerical simulation results were used to better understand RT instability behavior and to support extrapolation of gas-release estimates to full-scale DSTs. Simulations were completed for 23-in., 70-in., and 900-in. (75-ft, full-scale) diameter vessels for α_{RT} values of 8, 12.5, and 18.5 vol%. The dimensionless correlation for the onset of RT instabilities was used to estimate the strengths of sediment in the three vessels at each specified α_{RT} value. Subsequently, simulant property vs. solids content correlations developed in this study were used to estimate Bingham yield stress and consistency and slurry density, which are important input parameters for the simulation scaleup estimates. The simulation results showed decreasing gas release with increasing vessel diameter, which suggests that the small-scale experiment-based extrapolations should over estimate gas releases.

The test data also suggest a simple α_{RT} criterion for determining when RT instabilities give low gas releases. Experimental results in both the 23-in. and 70-in. vessels for geometrically-scaled total sludge depth of $1\times$ or less show that gas releases are small to negligible for $\alpha_{RT} \leq \sim 0.15$ (15 vol%), and, therefore, this value of α_{RT} is the suggested screening criterion. [$\alpha_{RT} \sim 0.15$ is, because of availability of multiple data points, the same gas fraction used for the extrapolation discussed above.] Note that the experimentally determined α_{RT} is both the absolute retained gas fraction in the lower slurry layer and the difference in retained gas fraction between the lower and upper slurry layers, which have the same gas-free density. From the perspective of full-scale tank operations, waste “layers” that have the same gas-free density would need to have differences in retained gas on the order of α_{RT} to be RT unstable. For example, a lower sludge layer would need a retained gas fraction of 0.25 (25 vol%) to become unstable if the layer above it has a steady-state retained gas fraction of 0.10 (10 vol%) and the waste properties (e.g., density and shear strength) are such that α_{RT} is 0.15 (15 vol%).

A modified energy ratio model was developed with the goal of finding a relationship between the volume of gas released and the ratio of the buoyant energy in a volume of gaseous sludge to the energy required to yield the volume of sludge and allow it to rise from the lower sediment layer into the upper sediment layer. This energy ratio approach has been successful as a predictor for the magnitudes of gas releases from buoyant-displacement events in which gas-containing sediment became buoyant in a supernatant liquid layer. However, this study found that there are no clear trends in the relationship between the size of gas releases in classic in-sediment buoyancy RT instabilities and the calculated modified energy ratios. Therefore, this is not a useful screening tool for RT instability gas releases.

Finally, using the experiment-based gravity yield parameter correlations for the onset of RT instability at an α_{RT} of 8 vol%, which is the estimated void fraction in AN-101 and AN-106, RT motion will not occur unless the waste (simulant) shear strength is less than 430 Pa (dimensional Y_G correlation) or 230 Pa (dimensionless Y_G correlation). This indicates that for the waste strengths measured in tanks AN-101 and AN-106 (on the order of 1000 Pa) that an 8% void fraction (difference between layers) is not high enough to initiate RT motion.

Acknowledgments

The authors would like to thank Joe Meacham of Washington River Protection Solutions and Beric Wells, Phil Schonewill, and Richard Daniel of Pacific Northwest National Laboratory for helpful technical discussions and suggestions on this topic area. The authors would also like to thank Sarah Suffield and Quality Engineer Bill Dey for careful reviews of calculations and the document, Kathy Neiderhiser and Cary Counts for document preparation, and the many others who contributed to preparation of the experimental systems and conducting the Rayleigh-Taylor instability gas-release tests including Leo Fifield, Mac Zumhoff, Kent Parker, Dave Heldebrant, Craig Lukins, Monte Telander, Stan Owsley, and Tom Loftus.

Acronyms and Abbreviations

APEL	Applied Process Engineering Laboratory
ASO	Analytical Support Operations
ASTM	ASTM International (formerly the American Society for Testing and Materials)
BDGRE	buoyant-displacement gas release event
DSGRE	deep-sludge gas release event
DSGREP	DSGRE Project
DST	double-shell tank
FIO	For Information Only
GRE	gas release event
HASQARD	Hanford Analytical Services Quality Assurance Requirements Document
H ₂ O ₂	hydrogen peroxide
HCl	hydrochloric acid
M&TE	measuring and test equipment
M30	Min-U-Sil [®] 30 (fine crystalline silica)
M30:B	Min-U-Sil [®] 30 mixed with bentonite clay and the mass ratio of these
MSA	Mission Support Alliance
PNNL	Pacific Northwest National Laboratory
QA	quality assurance
RT	Rayleigh-Taylor (instability)
SL	single layer (of slurry in single-slurry-layer tests)
SR	spontaneous release (of gas in single-slurry-layer tests)
TP	Test Plan
vol%	volume percent
WRPS	Washington River Protection Solutions LLC
wt%	weight percent
WWFTP	WRPS Waste Form Testing Program

Nomenclature

A	cross-sectional area (plan view) of vessel; or pre-exponential constant in an exponential equation (in context)
$b_{V/L}$	intercept of a linear vessel level-volume correlation, L
c_1, c_2, \dots, c_n	curve-fitting constants used in RT instability gas fraction (α_{RT}) correlations
C_D	coefficient of drag
c_e	exponential constant in an exponential equation
D	vessel or tank diameter
d_b	diameter of a bubble
d_{crit}	critical diameter for bubble motion in a stagnant yield stress fluid
d_{max}	maximum depth below which gas-release channels are closed off in a sludge bed
E_b	buoyant energy of a gob of sediment
E_y	energy required to yield at the periphery of a gob of sediment
ER_S	modified energy ratio (this is the ratio for buoyant sediment rising through an upper layer of sediment in a DSGRE, and is not the same as the energy ratio defined for buoyant sediment rising through an upper layer of liquid in a BDGRE)
f_{exp}	expansion factor between in situ pressure and atmospheric pressure
g	gravitational acceleration, 9.8 m/s^2
H_L	thickness of supernatant liquid layer
H_{res}	measurement resolution for the level measurement
H_S	thickness of total sediment (solids)
H_{S0}	thickness of lower solids layer at the time supernatant loading is completed
H_{S1}	thickness of upper solids layer
H_{S2}	thickness of lower solids layer
$H_{S2,0}$	thickness of lower solids layer at the time supernatant loading is completed
k_S	a gas fraction ratio used in calculating ER_S
L	characteristic length of a Rayleigh-Taylor (RT) instability; a level (height) measured in a test vessel after gas has begun to accumulate
L_0	the supernatant level at initial gas-free condition
ΔL_{optic}	the correction for the combined parallax/refraction error for level measurements made from camera images
$m_{0,low}$	mass of lower sediment layer at initial gas-free condition
$m_{0,up}$	mass of upper sediment layer at initial gas-free condition
$m_{0,sup}$	mass of supernatant layer at initial gas-free condition
\dot{m}_{evap}	the average mass loss rate from evaporation
n	shear strength vs. time power-law exponent
\hat{n}	specific acid demand for pH 3 to 5 target, mol HCl/kg bentonite

P_A	atmospheric pressure
Re_b	Reynolds number of a bubble
$s_{V/L}$	slope of a linear vessel level-volume correlation, L/cm
t	time or elapsed time
t_u	time that slurry is left undisturbed after mixing
U	bubble rise velocity
V	volume of material contained in a vessel
$V_{0,low}$	volume of lower sediment layer at initial gas-free condition
$V_{0,up}$	volume of upper sediment layer at initial gas-free condition
$V_{0,sup}$	volume of supernatant layer at initial gas-free condition
V_{rel}	volume of gas release at atmospheric pressure
V_g	retained gas volume (at in situ pressure)
V_{RT}	volume of in situ gas just before a RT release
V_S	volume of gas-free sediment
$V_{S,0}$	total volume of gassy sediment at the time supernatant loading is completed
V_{S2}	volume of gas-free lower-layer sediment
V_t	total volume of gassy sediment
x_B	weight fraction as-received bentonite clay in the mixed solid phase of a simulant
x_{M30}	weight fraction as-received Min-U-Sil [®] 30 silica in the mixed solid phase of a simulant
x_S	weight percent total solid phase in a slurry or wet solids layer
x_w	weight fraction water in a simulant
Y	critical yield number for bubble motion in a static yield stress fluid
Y_G	gravity yield parameter for RT instability
$\Delta\alpha$	difference between gas volume fractions of the layers (upper minus lower)
α	gas volume fraction (at local conditions)
α_{NB}	gas volume fraction in the lower sediment layer that makes it neutrally buoyant in the liquid
α_{NBS}	gas volume fraction in the lower sediment layer that makes it neutrally buoyant in the upper sediment layer
α_{Res}	gas volume fraction uncertainty that corresponds to H_{res}
α_{RT}	gas volume fraction in the lower sediment layer that produces RT instability between two solids layers
α_{SR}	gas fraction at the point of the initial spontaneous release in single-layer tests
α_0	initial gas volume fraction in the lower sediment layer
$\dot{\gamma}$	shear rate or strain rate
γ_S	a ratio of static pressures used in calculating ER_S
ϵ_y	the strain at failure for the sediment

μ_{app}	apparent viscosity, as determined from the Bingham plastic rheology model
$\Delta\rho$	difference between densities of the layers (upper minus lower)
ρ_B	dry intrinsic (not bulk) density of bentonite clay (reference value, not measured)
ρ_L	supernatant liquid density
ρ_{M30}	dry intrinsic density of Min-U-Sil [®] 30 silica (reference value, not measured)
ρ_S	gas-free density of both solids layers, if the two layers are of equal density
ρ_{s0}	density of the lower layer at the time supernatant loading is completed
ρ_{s1}	gas-free density of the upper layer
ρ_w	density of water
ρ_1	gas-free density of the upper layer
ρ_2	gas-free density of the lower layer
τ	shear stress
τ_c	shear strength vs. time power-law constant
τ_S	gas-free shear strength of both solids layers, if the two layers are of equal density
τ_0	yield stress constant in the Bingham plastic rheology model
τ_1	gas-free shear strength of the upper layer
τ_2	gas-free shear strength of the lower layer
ϕ_{RT}	specific gas volume fraction in the lower layer that produces RT instability between two solids layers (gas volume/gas-free lower-layer sediment volume)
$\phi_{post-RT}$	specific gas volume fraction (in situ gas volume/gas-free lower-layer sediment volume) after an RT instability gas release

Contents

Executive Summary	iii
Acknowledgments.....	vii
Acronyms and Abbreviations	ix
Nomenclature.....	xi
1.0 Introduction.....	1.1
2.0 Objectives.....	2.1
3.0 Quality Assurance	3.1
4.0 Technical Approach	4.1
4.1 Theory	4.1
4.1.1 RT Scoping Study	4.1
4.1.2 Energy Ratio Considerations.....	4.2
4.2 Test Approach	4.3
4.2.1 Geometric Scaling	4.3
4.2.2 Targeting Appropriate Gas Release Events.....	4.5
4.3 Test Matrix and Extrapolation Concepts.....	4.6
4.3.1 Identifying Tests for Extrapolation	4.6
4.3.2 Selecting the Test Matrix	4.8
4.4 Assumptions	4.12
5.0 Simulant Selection and Target Properties	5.1
5.1 Simulant Selection.....	5.1
5.1.1 Shear Strength and Density	5.1
5.1.2 Gas Generation.....	5.3
5.1.3 Gas Release Mechanism.....	5.6
5.2 Target Simulant Properties	5.7
6.0 Experimental Methods, Systems, and Data Analysis.....	6.1
6.1 Test Facilities and Equipment	6.1
6.1.1 Laboratories.....	6.2
6.1.2 Test Vessels.....	6.3
6.1.3 Measuring and Test Equipment.....	6.4
6.1.4 Mixers and Containers.....	6.6
6.1.5 Slurry Pumps and Distributors	6.7
6.2 Simulant Preparation	6.8
6.2.1 Materials.....	6.8
6.2.2 Recipes	6.9
6.2.3 Preparation	6.10
6.3 Simulant Characterization	6.11

6.4 Conducting RT and SL Tests 6.12

 6.4.1 Test Requirements and Acceptance Criteria 6.12

 6.4.2 Test Steps 6.12

6.5 RT and SL Test Data Analysis 6.15

 6.5.1 Quantitative Data Analysis and Uncertainty 6.16

7.0 RT Test Simulant Properties 7.1

 7.1 Test Batch Characterization Results..... 7.1

 7.1.1 Density of RT Test Batches..... 7.1

 7.1.2 Shear Strength 7.2

 7.1.3 Non-Newtonian Rheological Properties..... 7.8

 7.2 Comparison of Simulant and Hanford Tank Waste Rheology 7.10

8.0 Rayleigh-Taylor Instability Test Results..... 8.1

 8.1 Equal Slurry Layer Thickness Tests..... 8.1

 8.1.1 Test Matrix, Equal Layer Depths 8.1

 8.1.2 Visual Characteristics of an RT Instability Event 8.6

 8.1.3 Test Results, Equal Layer Depths 8.9

 8.2 Varying Relative Slurry Layer Depth Tests in the 23-in. Vessel 8.19

 8.2.1 Test Matrix, Varying Relative Layer Depths 8.20

 8.2.2 Test Results, Varying Relative Layer Depths 8.22

 8.3 Single-Slurry-Layer Tests 8.27

 8.3.1 Test Matrix, Single Slurry Layers 8.27

 8.3.2 Test Results, Single Slurry Layers 8.31

 8.4 Interpretation of High Void Fraction Releases..... 8.38

 8.5 Summary of RT Test Results 8.40

 8.5.1 RT Instability Gas Releases 8.41

 8.5.2 Modified Energy Ratio..... 8.43

 8.5.3 RT Stability Criterion..... 8.46

9.0 Modeling of Rayleigh-Taylor Events..... 9.1

 9.1 Modeling Approach..... 9.1

 9.2 Selecting Input Parameters for Simulations 9.3

 9.3 Simulation Results for Selected Equal Slurry Layer Thickness Tests 9.5

 9.3.1 Results for Gas Release..... 9.12

 9.3.2 Results for Strain Rate and Gas Release Rate vs. Time 9.15

 9.4 Results for Varied Slurry Layer Thickness Ratios 9.18

 9.5 Conclusions 9.19

10.0 Extrapolation of Results 10.1

 10.1 Extrapolation from Experimental Results 10.1

 10.2 Relationship to Numerical Results 10.3

 10.3 Overall Estimate of Gas Release in Full-Scale DSTs..... 10.5

11.0 Summary and Conclusions..... 11.1
12.0 References 12.1
Appendix A Modified Energy Ratio Derivation..... A.1
Appendix B Slurry Simulant Properties.....B.1
Appendix C Detailed Test ResultsC.1

Figures

1.1	Evolution of an RT Instability of a Less-Dense Waste Layer Rising in a More-Dense Layer and Subsequent GRE Scenarios.....	1.3
4.1	Diagram of an Expected Waste/Simulant Configuration in a Vessel with Reference Dimensions	4.4
4.2	Conceptual Example of Extrapolation to Full Scale.....	4.7
4.3	Conceptual Example of Extrapolation at Constant Vessel Size	4.8
4.4	Scatterplot Illustrating the Target Conditions of the Originally Planned Test Matrix Found in the TP.....	4.9
4.5	Scatterplot Comparing the Target Conditions of the Planned Test Matrix to Scaling at Constant τ_y/D for Three Assumed Sludge Strengths in the DST.....	4.11
5.1	Gas Generation Rates from H ₂ O ₂ Decomposition in 47 to 48 wt% 90:10 M30:B Slurries	5.5
6.1	Schematic Drawing of an RT Instability Gas-Release Test Setup.....	6.2
6.2	Preparation of ~110-gal Batches of Naturally Colored Lower-Layer Slurry and Dyed Upper-Layer Slurry by Two Teams Manning Double-Auger Mixers	6.7
6.3	Slurry Distributor Being Used for Spreading Dyed Upper-Layer Slurry Over the Gas-Generating Lower Layer in a 70-in. Vessel Test.....	6.8
7.1	Multi-Sample Average Shear Strength Data for RT Test Batches and Corresponding Exponential Correlations as a Function of Slurry Solids Content	7.3
7.2	Shear Strength Data for Simulant Samples Diluted with Water and Pre-Dilution Samples.....	7.4
7.3	Shear Strength Data as a Function of Time Undisturbed for Four RT Test Samples.....	7.6
7.4	Shear Strength Data as a Function of Time Undisturbed for a Lower-Layer Slurry Sample and a Water-Diluted Sample.....	7.7
7.5	Correlations for Bingham Model Parameters Developed from Select RT Test Simulant Batches of Varying Solids Content and Comparison (of Yield Stress) to Shear Strength Correlations.....	7.9
7.6	Comparison of Bingham Model Parameters for Hanford Tank Waste to a Variety of Chemical and Physical Waste Simulants, Including the Type Used in RT Tests.....	7.11
8.1	Time Sequence of Images Surrounding the RT Instability Gas-Release Event in RT Test 70-22	8.7
8.2	Retained Gas Volume Fraction vs. Time for RT Test 23-06	8.10
8.3	Gas Volume Fraction vs. Time for Replicate Tests in the 23-in. Vessel.....	8.11
8.4	Gas Volume Fraction vs. Time for Simulants of Different Shear Strength in the 23-in. Vessel at 1× Total Slurry Depth	8.12
8.5	Gas Volume Fraction vs. Time for Three Depths of Slurry in the 23-in. Vessel at ~15-Pa Shear Strength	8.13
8.6	Summary of Retained Gas Fractions and RT Instability Gas Releases for Equal Slurry Layer Thickness and Varying Total Depth of Slurry in the 23-in. Vessel.....	8.14
8.7	Gas Volume Fraction vs. Time for Simulants of Different Shear Strength in the 70-in. Vessel at 1× Total Slurry Depth	8.16

8.8. Summary of Retained Gas Fractions and the Gravity Yield Parameter for Simulants of Different Shear Strength in the 70-in. Vessel	8.17
8.9 Gas Volume Fraction vs. Time for Three Depths of ~45-Pa Shear Strength Slurry in the 70-in. Vessel	8.18
8.10 Summary of Retained Gas Fractions and RT Instability Gas Releases for Equal Slurry Layer Thickness and Varying Total Depth of Slurry in the 70-in. Vessel	8.19
8.11 Gas Volume Fraction vs. Time for Varying Relative Depths of ~15-Pa Shear Strength Slurry in the 23-in. Vessel	8.23
8.12 Gas Volume Fraction vs. Time for Varying Relative Depths of ~22-Pa Shear Strength Slurry in the 23-in. Vessel	8.24
8.13 Summary of Retained Gas Fractions and RT Instability Gas Releases for Varying Relative Slurry Layer Thicknesses at Constant Total Depth of Slurry in the 23-in. Vessel	8.25
8.14 Gas Volume Fraction vs. Time for Constant Lower-Layer Depth (0.33×) and Varying Total Depths of ~15-Pa Shear Strength Slurry in the 23-in. Vessel.....	8.26
8.15 Summary of Retained Gas Fractions and RT Instability Gas Releases for Constant Lower-Layer Depth and Varying Total Depths of Slurry in the 23-in. Vessel.....	8.27
8.16 Comparison of Gas Volume Fraction vs. Time for Single-Layer and Two-Layer RT Tests at 0.5× Lower-Layer Depth of ~22-Pa Shear Strength Slurry in the 23-in. Vessel	8.32
8.17 Gas Volume Fraction vs. Time for Single-Layer Tests in the 23-in. Vessel Using Simulants of Different Shear Strength.....	8.33
8.18 Comparison of Gas Volume Fraction vs. Time for Single-Layer and Two-Layer RT Tests at 0.5× Lower-Layer Depth of ~45-Pa Shear Strength Slurry in the 70-in. Vessel	8.34
8.19 Comparison of Gas Volume Fraction vs. Time for Single-Layer and Two-Layer RT Tests at 0.5× Lower-Layer Depth of ~95-Pa Target Shear Strength Slurry in the 70-in. Vessel.....	8.35
8.20 Comparison of Gas Fraction vs. Time for Single-Layer Tests in the 23-in. and 70-in. Vessels Using the Same ~30-Pa Target Shear Strength Slurry.....	8.36
8.21 Summary of Retained Gas Fractions and Spontaneous Gas Releases in Single-Slurry-Layer Tests in the 23-in. and 70-in. Vessels	8.37
8.22 Effect of Vessel Size on Gas Release Characteristics in Single-Layer Tests Using the Same ~87-Pa Estimated Shear Strength Slurry	8.40
8.23 Fraction of Gas Released as a Function of the Ratio of α_{RT} to α_{NB} for Completed RT Tests.....	8.41
8.24 Fraction of Gas Released as a Function of the Modified Energy Ratio for Completed RT Tests.....	8.45
8.25 Comparison of Measured α_{RT} from RT Tests to Predicted Values Using a Dimensional Correlation Determined for a Limited Data Set.....	8.47
8.26 Comparison of Measured α_{RT} from RT Tests in Three Scale Vessels to Predicted Values Using a Dimensional Correlation and a Dimensionless Correlation	8.50
8.27 Comparison of Experimentally Determined Y_G Values to Predictions for a Full-Scale Vessel (1× Depth, 1:1) at Three Assumed α_{RT} Levels Using a Dimensional Correlation and a Dimensionless Correlation.....	8.52
9.1 Apparent Viscosity as a Function of Local Strain Rate and Weight Percent Solids.....	9.2
9.2 Density and Gas Void Fraction for Smallest Bubbles at the 23-in. Mid-Plane at Time = 0 s	9.5
9.3 Density, Gas Void Fraction for Smallest and Largest Bubbles, z-Direction and y-Direction Velocities, and Strain Rate at the 23-in. Mid-Plane at Time = 200 s	9.6

9.4 Density, Gas Void Fraction for Smallest and Largest Bubbles, z-Direction and y-Direction Velocities, and Strain Rate at the 23-in. Mid-Plane at Time = 350 s 9.7

9.5 Density, Gas Void Fraction for Smallest and Largest Bubbles, z-Direction and y-Direction Velocities, and Strain Rate at the 23-in. Mid-Plane at Time = 700 s 9.8

9.6 Final Distributions for the Density and Gas Void Fraction for the Smallest and Largest Bubbles at the 23-in. Mid-Plane. 9.9

9.7 Final Distributions for the Density and Gas Void Fraction for the Smallest and Largest Bubbles at the 70-in. Mid-Plane. 9.11

9.8 Final Distributions for the Density and Gas Void Fraction for the Smallest and Largest Bubbles at Full Scale 9.11

9.9 Total Gas Release as a Function of Vessel Size and Initial Void Fraction..... 9.13

9.10 Total Gas Release as a Function of Vessel Size and Initial Void Fraction..... 9.14

9.11 Maximum Slurry Strain Rate as a Function of Time for $\alpha_{RT} = 18.5\%$ 9.15

9.12 Maximum Strain Rate as a Function of Vessel Diameter and Initial Void Fraction 9.16

9.13 Strain Rate at Location Near Slurry Surface as a Function of Time for $\alpha_{RT} = 18.5\%$ 9.17

9.14 Rate of Gas Release as a Function of Time for $\alpha_{RT} = 18.5\%$ 9.18

9.15 Comparison of Small-Bubble Void Fraction at $t = 10$ s After Initialization with Different Wavelength Perturbations, 0.8 (a) and 0.57 (b) times the Vessel Diameter 9.19

10.1 Fraction of Gas Released as a Function of α_{RT} for Completed RT Tests after Applying First-Cut Screening Criteria..... 10.3

10.2 Total Gas Release as a Function Initial Void Fraction α_{RT} Extrapolated to Full Scale with Comparison to Experiments..... 10.5

Tables

3.1	QA Implementing Procedures.....	3.2
4.1	Geometrically-Scaled Dimensions for the Test Vessels	4.4
6.1	Data Collection Requirements, M&TE Type, and Collection Methods	6.5
6.2	Test Requirements and Acceptance Criteria.....	6.13
8.1	Matrix of Completed Equal Slurry Layer Thickness RT Tests in the 10-in., 23-in., and 70-in. Vessels.....	8.3
8.2	Matrix of Completed Varying Relative Slurry Layer Thickness RT Tests in the 23-in. Vessel	8.21
8.3	Matrix of Completed Single-Slurry-Layer Tests in the 23-in. and 70-in. Vessels	8.30
8.4	Magnitude of Single-Layer Spontaneous Gas Releases	8.38
8.5	Magnitude of RT Instability Gas Releases	8.42
8.6	Modified Energy Ratios for Completed RT Tests	8.44
8.7	Gravity Yield Parameter Determined from RT Tests and Predicted for Full Scale.....	8.53
9.1	Input Values for Parametric ParaFlow Simulations.....	9.4
9.2	Input Parameters for Test Case ParaFlow Simulations.....	9.4
9.3	Gas Release as a Function of Vessel Size, Initial Void Fraction, and Bubble Size.....	9.10
9.4	Comparison of Simulation Results and Measured Gas Release	9.14

1.0 Introduction

This report is the second and final of a two-part series. The initial (Rev. 0) report described the results of approximately half of planned experiments to assess gas releases due to Rayleigh-Taylor (RT) instabilities using waste simulants in three reduced-scale test vessels,¹ as defined and described below. The conclusions drawn in the initial report from the limited available data and preliminary numerical simulations are refined and extended here based on a substantially broader range of test conditions.² Also, the current report covers an additional suite of experiments that were designed to assess spontaneous gas releases from the simulant used in the RT tests. These later tests were not planned at the time of the initial report, but were motivated by observations in many of the RT tests, as discussed below.

In the Hanford Site underground storage tanks, a typical waste configuration in the newer double-shell tanks (DSTs) is a settled bed of solid particles with interstitial liquid beneath a supernatant liquid layer. Because of chemical decomposition of the waste induced by radiation and elevated temperature, and to a lesser extent because of corrosion of the tank walls, gases (primarily hydrogen, nitrous oxide, and nitrogen) are slowly generated in both the supernatant and the settled solids. Gas produced in the supernatant layer can move freely and continuously to the tank headspace. Gas produced in the settled solids layer is trapped by mechanisms related to the waste's pore configuration and strength. At some point, the retained gas in the sediment bed may be released by one of several mechanisms that are rapid compared to the gas generation rate (Stewart et al. 1996, Meyer et al. 1997).

One such mechanism for gas release occurs when the sediment bed retains enough gas that it becomes sufficiently less dense than the supernatant liquid to allow the strength of the sediment to be overcome. Buoyant sediment "gobs" containing gas rise into the supernatant fluid, and much of the retained gas in the gobs and in other disturbed regions of the sediment bed is released to the tank headspace. The largest Hanford historical gas releases are attributed to this type of instability, which is known as a buoyant-displacement gas release event (BDGRE). This instability has been studied extensively (see, for example, Meyer et al. 1997, Meyer and Stewart 2001, Stewart et al. 2005). Stewart et al. (2005) provides an empirical model based on historical tank farm gas release data to predict the hydrogen concentration in a tank's headspace resulting from a spontaneous gas release event depending on the waste characteristics, including variation in the waste sediment's yield stress in shear with depth. This and related models developed in these studies have been applied to managing waste storage in underground storage tanks at Hanford (Weber 2009).

Because waste management operations may lead to transfers resulting in sludge depths in DSTs that are greater than in historical practice, consideration is being given to an additional mode of gas retention and a gas release mechanism that has not yet been quantified. The postulated gas retention-release scenario is referred to as a deep-sludge gas release event (DSGRE). It is predicated on the work of

¹ Rassat SD, PA Gauglitz, LA Mahoney, DR Rector, RP Pires, JA Fort, GK Boeringa, DN Tran, MR Elmore, and WC Buchmiller. 2013. Gas Release Due to Rayleigh-Taylor Instability within Sediment Layers in Hanford Double-Shell Tanks: Results of Scaled Vessel Experiments, Modeling, and Extrapolation to Full Scale, PNNL-23060 (DSGREP-RPT-002, Rev. 0), Pacific Northwest National Laboratory, Richland, Washington. Rev. 0 of the report addresses a portion of the planned RT tests in which the two slurry layers have equal thickness.

² This Rev. 1.0 of the report addresses all completed RT tests including additional (since Rev. 0) equal slurry layer thickness tests and new varying relative slurry layer thickness experiments. Also, numerical simulations of RT instability gas release events have been revised to use what are thought to be more representative simulant and waste physical properties, in addition to other refinements.

van Kessel and van Kesteren (van Kessel 1999; van Kessel and van Kesteren 2002), who are concerned about gas retention and release in sludge depots in the Netherlands. They provided a model and analysis suggesting that below a certain maximum depth, referred to as d_{max} , the network of channels for the release of in situ generated gas to the surface would be closed off because of slumping of the overburden due to its depth and the physical properties of the sediment. According to their models for the sludge depots, d_{max} would be less than the maximum depth of waste (~310 in. [7.87 m]) proposed for storage in Hanford waste tank 241-AN-101 (Uytioco 2010; see Section 4.2.1). While the hypothesis of van Kessel and van Kesteren suggests that d_{max} exists and is quantifiable, it has not been demonstrated experimentally, including their own work, or observed in practice, based on our review of available information. Of concern in Hanford waste tanks is the possible increased retention of gas in waste at depths exceeding d_{max} , in particular when the depths and gas fractions are greater than current operational experience, and the possible subsequent release of this gas.

Pacific Northwest National Laboratory (PNNL) has been contracted by and is working with Washington River Protection Solutions LLC (WRPS) to investigate d_{max} and the plausibility of DSGREs in Hanford waste storage tanks. There are multiple elements to the strategy for investigating DSGREs and the potential risk should such an event occur. Work was conducted on several fronts in parallel with an ultimate goal of integrating the results into a cohesive story. The parallel paths included modeling and analysis and experimental studies.

First, in a somewhat independent part of the WRPS/PNNL deep-sludge gas release event project (DSGREP), the previously developed BDGRE model of Stewart et al. (2005) was applied to define a maximum sludge depth in these tanks that would limit the potential peak hydrogen concentrations to safe levels, should gas be released by a mechanism of that type. The results of those BDGRE model applications to DSTs 241-AN-101 and 241-AN-106 are described in Wells et al. (2013). They are not related to the experimental study described in this report.

Also independent of this report were experimental studies whose purpose was to demonstrate that retained gas fractions do not increase with added waste depth greater than d_{max} . According to the d_{max} theory, d_{max} should increase with increasing strength (e.g., shear strength¹) provided that other relevant physical properties are constant. Experiments with waste simulant (e.g., kaolin clay/water) of varying strength in columns loaded to different depths exceeding the calculated d_{max} were completed. These included studies using ~350-Pa shear strength simulant in a 7.25-in. (0.18-m) inside-diameter column loaded to an “intermediate” sludge depth of ~14 ft (4.3 m) (Powell et al. 2014), and “tall-column” studies in a 5-ft (1.5-m) diameter column loaded with ~500- or ~1000-Pa simulant to the maximum fill depth in a DST (~26 ft [7.9 m]) (Schonewill et al. 2014). These studies concluded that channels for gas release remained open in deep sludge, including at depths greater than the calculated d_{max} , and that there was no appreciable increase in retained gas with increasing depth in the sludge. Another set of small-scale experiments reported by Powell et al. directly probed open channel depths using kaolin simulants by creating small-diameter channels and observing the depth at which they closed due to slumping.

¹ Specific “strength” quantities stated in this report, e.g., 1000 Pa, are shear strengths unless noted otherwise (e.g., Bingham yield stress discussed in Section 7.1.3). For a given sludge or slurry type (e.g., fixed solid and liquid components, but with potentially varying relative amounts of the two), all pertinent measures of strength, such as shear and tensile strength and yield stress, will increase or decrease together. Therefore, the relative terms strong and weak, which are also used throughout this report, are applicable to any particular strength metric for a given material.

Although the parallel project activities described in this report were motivated by the potential of enhanced gas retention below d_{max} and associated DSGREs, potentially unstable waste configurations may exist or be created in other ways. The settled sludge bed in a Hanford waste tank is typically composed of layers, and these layers can have different physical and chemical properties. One postulated configuration within the settled bed is a more-dense layer lying atop a less-dense layer. The different densities can be a result of different quantities of retained gas in the layers, different degrees of settling and compaction in the layers, or different solid particle compositions. Such a configuration can experience an RT instability, in which the less-dense lower layer of solids rises into the upper layer. This motion may cause a release of retained gas. Until the recent preliminary study of Gauglitz et al. (2013), studies of gas retention and release in Hanford waste had not considered potential buoyant motion within a settled bed of solids.

Figure 1.1 schematically depicts a storage tank containing a settled bed with two layers where the lower layer has a lower density than the upper layer due to a larger volume of trapped gas bubbles. Figure 1.1 also shows a plausible evolution of the interface between the layers as the less-dense material rises into the upper sediment layer followed by three gas release event (GRE) scenarios of increasing magnitude. The “negligible GRE” and “small GRE” pathways are the result of in-sediment buoyant motion. The pathway to BDGREs is crossed out (X) because in-sediment buoyant motion is the focus of this work, not because BDGREs are infeasible, should sufficient gas be retained. It was also correctly assumed in planning the RT studies that the companion DSGREP studies (e.g., Powell et al. 2014 and Schonewill et al. 2014) would demonstrate that the retained void fraction is not sufficient to cause a buoyant rise of sediment through the supernatant for most sludge-waste sediment and liquid densities.

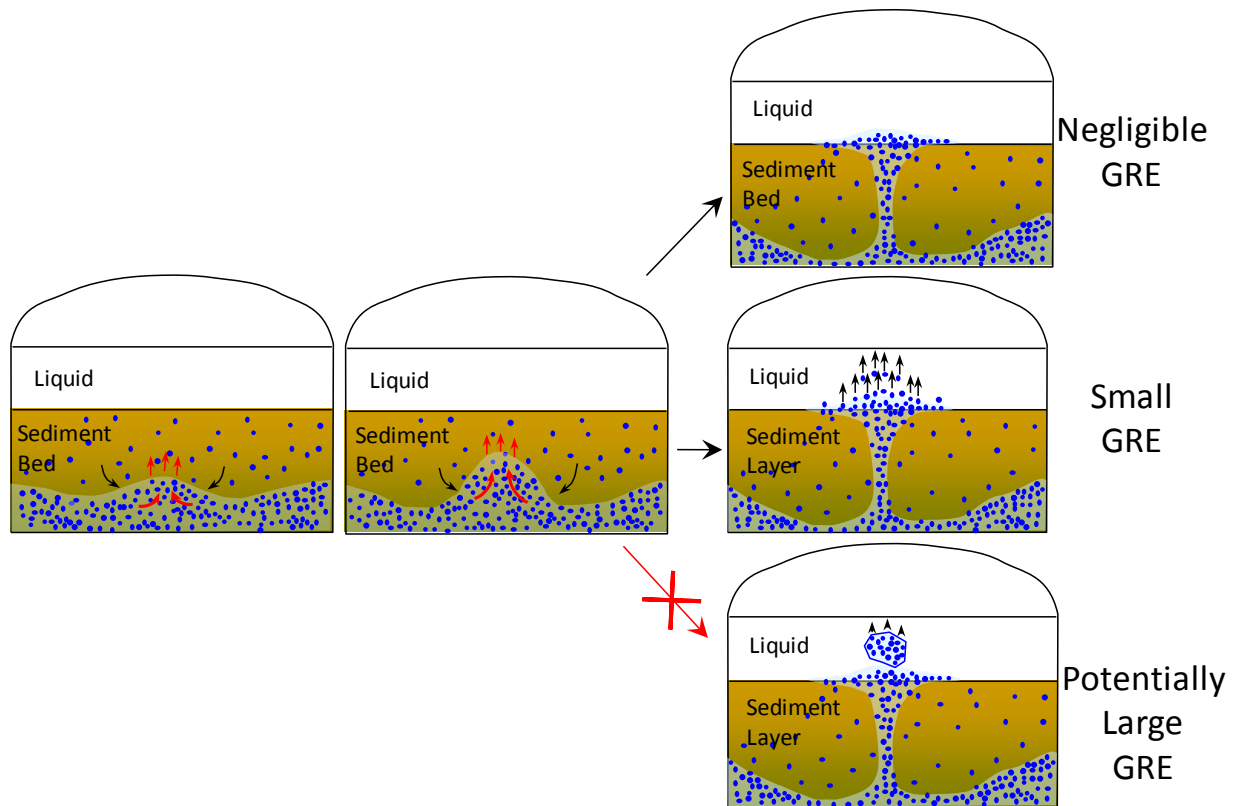


Figure 1.1. Evolution of an RT Instability of a Less-Dense Waste Layer, due to Retained Gas Bubbles (depicted as blue spheres), Rising in a More-Dense Layer, and Subsequent GRE Scenarios

The goal of the present work is to provide quantitative information for 1) predicting the conditions under which an RT instability might occur in waste stored in DSTs and 2) estimating the size of the DSGRE should an RT instability occur. The study is directed in particular at the sludge layer configurations that would result from proposed transfers to DSTs 241-AN-101 and 241-AN-106 (Uytioco 2010).

This report describes scaled experiments and models developed to quantify gas release due to potential DSGREs, as laid out in the governing Test Plan (TP).¹ In particular, the focus is on quantifying gas released when the RT instability occurs at void fractions where the layer of sediment simulant does not undergo a BDGRE and float in the supernatant. This is because the likelihood and significance of floating gobs could (potentially) be operationally limited in the Hanford tank farms by removing supernatant liquid. Also, as noted above, other experimental efforts seek to demonstrate that gas retention behavior will not change below d_{max} , and therefore, the sediment will not retain sufficient gas to become neutrally buoyant in the liquid.

The results of experiments that supplement RT instability gas-release tests² also are described in this report. To characterize the magnitudes of gas retention in and spontaneous gas release from the RT test simulants, in the absence of an in-sediment RT instability event, a series of tests was conducted in the 23-in. and 70-in. diameter vessels without an overlying gas-free upper slurry layer. A primary purpose of these “single-layer” (SL) tests is to evaluate the gas retention/release characteristics in simulants having shear strengths that span those used in completed RT tests. The SL test results are compared, in particular, to bubble-cascade-like gas release behavior in the subset of RT tests in which the initial gas release was relatively large, and to secondary GREs typical of most RT tests.

The scaled RT experiments in this work build on those in the preliminary study (Gauglitz et al. 2013) with experimental configurations now including 10-in., 23-in., and 70-in. diameter vessels in which the bottom gas-generating layer and the upper higher-density layer have the same thickness. Completed tests in the 23-in. vessel with varying relative slurry layer thicknesses further extend our understanding of RT instability scaling.

The specific objectives for this study are listed in Section 2.0. Section 3.0 describes the quality assurance program under which the work was conducted. The technical approach, including theory behind RT test design, test vessel scaling, concepts for extrapolation to full scale, and the original test matrix are presented in Section 4.0; key assumptions also are summarized in that section. Section 5.0 describes considerations that led to the selection of a Min-U-Sil[®]30 silica and bentonite clay slurry simulant and the important physical and chemical properties of the simulant. Section 6.0 addresses RT test experimental methods, including simulant preparation; facilities and equipment used in RT tests, and the use of collected RT test data, including quantitative data analysis and estimation of uncertainty. The measured physical properties for simulant batches prepared for RT and SL tests are summarized and rheological properties are briefly compared to Hanford tank waste in Section 7.0. Test matrices for completed RT and SL experiments are tabulated and test results and analysis are provided in Section 8.0. Numerical model development and For Information Only (FIO) computer simulation of selected scaled RT experiments and full-scale tank conditions are described in Section 9.0. Extrapolations of test and model results to full-scale tank configurations are included in Section 10.0, leading to a report summary

¹ The TP number and versions are TP-DSGREP-001, Rev. 0.0, 1.0, 2.0, 3.0, and 4.0.

² These single slurry layer tests were identified in Rev. 4.0 of TP-DSGREP-002.

and conclusions in Section 11.0. Following a listing of report references (Section 12.0), the modified energy ratio model is derived in Appendix A, test-by-test simulant batch characterization results are given in Appendix B, and additional data for each RT test is provided in Appendix C.

2.0 Objectives

The overall objective of this study is to quantify gas release when an RT instability occurs in experimental vessels and use the resulting data to estimate the size of GREs in DSTs. The technical approach discussed in Section 4.0 describes how the studies are being used to satisfy the overall objective. The overall objective is subdivided into five primary objectives as listed below:

1. Measure the gas releases caused by RT instability in experiments with waste simulants in which RT instabilities are initiated by the retention of gas generated in situ.
2. Quantify how the onset of RT instabilities and gas releases are affected by the absolute and relative depths of gaseous (lower) and gas-free (upper) slurry layers.
3. Characterize gas retention and spontaneous gas releases from RT test simulants when gas release is not initiated by an in-sediment RT instability event (i.e., single gas-generating slurry layer tests).
4. Develop a modified energy ratio to describe the ratio of buoyant energy and the energy required to yield a gas-bearing gob when RT instabilities occur in the experiments.
5. Evaluate the gas releases predicted by models by comparison with experimental data obtained from testing.

Testing and analysis to meet the objectives above were performed at the quality assurance (QA) technology level of Applied Research (see Section 3.0).

3.0 Quality Assurance

Work performed by Deep-Sludge Gas Release Event Project staff was done in accordance with the Support to Evaluation of Gas Release Mechanisms in Deep Sludge Project Quality Assurance Plan (64405-QA-001). The DSGREP uses the Washington River Protection Solutions LLC Waste Form Testing Program (WWFTP) QA program (QA-WWFTP-001) at the Applied Research level as the basis for performing work. The WWFTP QA program implements an NQA-1-2000 Quality Assurance Program, graded on the approach presented in NQA-1-2000, Part IV, Subpart 4.2. This QA program and implementing procedures meet the Quality Requirements of NQA-1-2004, NQA-1a-2005, and NQA-1b-2007 as provided in the Statement of Work authorizing Pacific Northwest National Laboratory to conduct these studies.¹ When needed, analyses performed by the Analytical Support Operations (ASO) organization are conducted under the ASO QA Plan, which complies with the requirements of Hanford Analytical Services Quality Assurance Requirements Document (HASQARD) and NQA-1.

Table 3.1 lists the implementing procedures identified in the WWFTP QA Plan (QA-WWFTP-001) that govern the work conducted under this study. Listed below is a summary of key procedures.

- All staff members contributing to the work described in this report received proper technical and QA training prior to commencing quality-affecting work in accordance with QA-NSLW-0201, *Training*.
- The planned studies were conducted in accordance with QA-NSLW-1102, *Scientific Investigation for Applied Research*.
- The studies were planned and conducted in accordance with QA-NSLW-1104, *Test Plans*, and QA-NSLW-1107, *Test Instructions*.
- Test materials and samples were identified and controlled in accordance with QA-NSLW-0801, *Item Identification and Sample Control*.
- Measuring and testing equipment used to generate quality-affecting data was properly procured, controlled, calibrated, handled, and maintained in accordance with QA-NSLW-1201, *Calibration and Control of M&TE*.
- All data and calculations used in this report were reviewed in accordance with QA-NSLW-1108, *Data Entry and Data Review*, QA-NSLW-0301, *Management of Electronic Data*, and QA-NSLW-0304, *Calculations*.
- This technical report was generated in accordance with QA-NSLW-1109, *Reporting*, and was peer reviewed in accordance with QA-NSLW-0601, *Document Preparation and Change*, and QA-NSLW-0603, *Independent Technical Review*.

¹ This program has been independently evaluated by Acquisition Verification Services (AVS) of Mission Support Alliance (MSA) to specified requirements of NQA-1:2004 (including NQA-1a-2005 and NQA-1b-2007 Addenda) and is operating under a WRPS-approved Supplier Quality Assurance Program Implementation Plan (SQAPIP) (QA-WWFTP-002).

Table 3.1. QA Implementing Procedures (from QA-WWFTP-001)

Document Number	Title
QA-NSLW-0201	Training
QA-NSLW-0202	Surveillances
QA-NSLW-0203	Management Assessments
QA-NSLW-0301	Management of Electronic Data
QA-NSLW-0302	Software Control – Applied Research
QA-NSLW-0304	Calculations
QA-NSLW-0305	Safety Software
QA-NSLW-0401	Control of Procurements
QA-NSLW-0501	QA Implementing Procedures
QA-NSLW-0601	Document Preparation and Change
QA-NSLW-0602	Document Control
QA-NSLW-0603	Independent Technical Review
QA-NSLW-0801	Item Identification and Sample Control
QA-NSLW-0901	Special Processes
QA-NSLW-1001	Inspections
QA-NSLW-1102	Scientific Investigation for Applied Research
QA-NSLW-1104	Test Plans
QA-NSLW-1106	Operating Procedures
QA-NSLW-1107	Test Instructions
QA-NSLW-1108	Data Entry and Data Review
QA-NSLW-1109	Reporting
QA-NSLW-1110	General Documents
QA-NSLW-1201	Calibration and Control of M&TE
QA-NSLW-1301	Handling and Storage
QA-NSLW-1401	Status and Tagging
QA-NSLW-1501	Nonconformance
QA-NSLW-1502	Deficiency Reporting
QA-NSLW-1601	Significant Quality Issues
QA-NSLW-1602	Trending
QA-NSLW-1701	Record System
QA-NSLW-1801	Project Audits

4.0 Technical Approach

This section provides the details of the technical approach, including theoretical background, testing and modeling approaches, details of the planned RT test matrix, and concepts for extrapolation to full scale. It also summarizes key assumptions in the technical approach.

The focus is on the technical approach of RT experiments and the tie to analytical models that were used to characterize the results, and with varying degrees of success, used to estimate gas release behavior in full-scale tanks. Comparisons of the experimental results to the analytical models and concepts presented in this section (4.0) are made in Section 8.5 and in the discussion of Extrapolation of Results (Section 10.0). In addition to the analytical modeling, Section 9.0 describes FIO numerical computer simulations that were developed and used to better understand the physical mechanisms that influence DSGREs.

4.1 Theory

Theoretical background and development for this study is included in the following sections. Section 4.1.1 recaps developments in the scoping study of Gauglitz et al. (2013) and Section 4.1.2 presents a newly developed model for a modified energy ratio relevant to RT stability.

4.1.1 RT Scoping Study

The RT instability scoping studies of Gauglitz et al. (2013) provide a framework to design similar tests at multiple vessel geometric scales and to interpret the results. In the earlier work, an RT instability criterion at constant gravity yield parameter, Y_G (e.g., 0.09), was proposed. For a primary wavelength of instability L , the instability criterion can be written in a number of equivalent forms:

$$Y_G = \frac{(\tau_1 + \tau_2)}{(\rho_1 - \rho_2)gL} = \frac{2\tau_s}{\Delta\rho gL} = \frac{2\tau_s}{\rho_s \Delta\alpha gL} = \frac{2\tau_s}{\rho_s \alpha_{RT} gL} \quad (4.1)$$

where g is the gravitational acceleration, and the shear strength and the gas-free density, τ_s and ρ_s , respectively, are assumed equal in lower (subscript 2) and upper (subscript 1) settled solids layers. Also assuming that the upper layer is gas-free, the difference in gas fraction $\Delta\alpha$ in the two layers necessary for the system to become RT unstable is equal to the gas fraction in the lower layer at RT instability, α_{RT} . Generally, an absolute retained gas volume fraction α is the ratio of the retained gas volume (V_g) to the total volume (V_t) of gas and gas-free slurry (V_s): $\alpha = V_g/(V_s + V_g) = V_g/V_t$. Here, α and α_{RT} are defined with respect to the volume of gas-free lower-layer slurry, V_{S2} .

As in Gauglitz et al. (2013), it was assumed, initially, that the longest length scale of a system is the least stable. In the case of a DST and geometrically-scaled RT test vessels, the maximum proposed depth of sediment is approximately one-third the vessel diameter, D (see Section 4.2.1). Therefore, the characteristic dimension of the system for RT instability is expected to be D . Assuming this and for a constant Y_G at a target (constant) α_{RT} , the quantity $\tau_s/(\rho_s D)$ from Equation (4.1) is also constant:

$$\alpha_{RT} = \left(\frac{\tau_s}{\rho_s D} \right) \frac{2}{Y_G g} \quad (4.2)$$

And, at constant density difference in the two layers ($\Delta\rho = \rho_s \alpha_{RT} = \text{constant}$), the quantity τ_s/D is constant:

$$\Delta\rho = \rho_s \alpha_{RT} = \left(\frac{\tau_s}{D} \right) \frac{2}{Y_G g} \quad (4.3)$$

One approach to extrapolating the gas release results to full-scale DSTs is to select (or interpolate) test results at constant values of either of these forms of the RT instability criterion for each of the different test vessel sizes. This approach is discussed further below, and constant α_{RT} (Equation (4.2)) was one of the key considerations in development of the test matrix.

4.1.2 Energy Ratio Considerations

Consistent with the goals identified in Section 2.0, a modified energy ratio model was developed to describe the ratio of buoyant energy and the energy required to yield a gas-bearing gob when RT instabilities occur. This was done to support the design of the experimental test matrix and is a consideration for extrapolation to full scale. It is discussed in more detail in Section 8.5.2 and Appendix A.

The ratio between the buoyant energy, E_b , and the energy required to yield the gas-bearing gob participating in the buoyant displacement within the sediment layer, E_y , is termed the “modified energy ratio” to distinguish it from the energy ratio for a gob rising through the supernatant liquid (e.g., Stewart et al. 2005). The expression for the modified energy ratio, ER_S , is

$$ER_S = \frac{E_b}{E_y} = \frac{\alpha_{RT} \rho_{s1} g H_{s1}}{(1 - \alpha_{RT}) \varepsilon_y \tau_s} \left[\left(1 + \frac{1}{\gamma_s} \right) \ln(1 + \gamma_s) - k_s \right] \quad (4.4)$$

where ε_y is the strain at failure (assumed to be 1 in calculations here) and ρ_{s1} and H_{s1} are, respectively, the density and height of the upper sediment layer. A ratio of static pressures, γ_s , and the gas fraction ratio, k_s , are defined as

$$\gamma_s = \frac{\rho_{s1} g H_{s1}}{P_A + \rho_L g H_L} \quad k_s = \frac{\alpha_{NBS} (1 - \alpha_{RT})}{\alpha_{RT} (1 - \alpha_{NBS})}$$

where P_A is the atmospheric pressure and ρ_L and H_L are the density and height of the supernatant liquid. In k_s , α_{NBS} is the gas void fraction for neutral buoyancy between two sediment layers (subscript S), not

between a sediment layer and a liquid layer.¹ Likewise, the subscript S nomenclature is applied to the modified energy ratio ER_S , γ_S , and k_S to distinguish these terms from preceding tank farm gas release modeling work for buoyant sediment rising into liquid.

4.2 Test Approach

The method used to construct the test matrix has several distinct elements, namely:

- Defining the geometric parameters of the test vessels
- Eliminating physically unrealistic gas release scenarios
- Selecting an appropriate set of simulants (settled solids and supernatant liquid)
- Considering tests that span a range of the modified energy ratio (defined in Section 4.1.2)
- Identifying tests that provide data to extrapolate to larger scales.

These elements are discussed in more detail in the following pages, leading to a description of the originally planned test matrix in Section 4.3. Adjustments to the particular test conditions to satisfy the objectives of the test matrix, necessitated by initial experimental results, are discussed in Section 8.1.1. The specifics of simulant selection and properties are described in Section 5.0.

4.2.1 Geometric Scaling

A common method to conduct scaled experiments is to preserve geometric similarity. Figure 4.1 shows a conceptual schematic of a vessel and the reference dimensions that characterize the expected in-tank physical configuration of the various waste layers. In the majority of the RT experiments, a sediment bed composed of two layers, each having a height of $1/2 \times H_S$ (i.e., 1:1 lower-to-upper layer depth ratio), was used. The layers initially had the same target shear strength and density, and gas generation occurred only in the bottom slurry (sediment) layer (layer 2). In later tests, the relative depths of the two slurry layers were varied.

The reference dimensions in Figure 4.1 can be scaled to the smaller-scale experiments by holding the ratios H_L/D and H_S/D constant at the values for the full-scale vessel (i.e., geometric scaling). The full-scale values for the supernatant liquid height (depth), H_L , and the total sediment depth, H_S , are based on expected waste retrievals into tank 241-AN-101, which is scheduled to have a deeper sludge depth than tank 241-AN-106 (Uytioco 2010).² The physical dimensions resulting from geometric scaling of 10-in., 23-in., and 70-in. diameter test vessels are shown in Table 4.1.

Ideally, geometric similarity would be preserved in the experiments. However, the geometrically-scaled dimensions are relatively small, particularly for the 10-in. vessel. It was expected that they would challenge the resolution of the primary method for determining gas release (measurement of level changes). To improve the resolution of the measurement, the baseline configuration used an H_S that is

¹ For the RT tests described in this report, the densities of the gas-free lower-layer and the upper-layer slurries were equal, in which case α_{NBS} and k_S are zero.

² The reference states a maximum final (post-additions) sediment depth of 303 in. and a supernatant depth of 83 in., the latter being set at its upper limit according to the buoyant-displacement gas-release event energy ratio. The scaling in these tests assumes 310 in. of sediment, rounding up from 303 in., along with the 83-in. liquid depth from the reference.

two times the geometrically-scaled dimension (2×) for the 10-in. vessel, or equal to the geometrically-scaled dimension (1×) for the two larger test vessel sizes. The liquid height did not have the factor of two applied, but was nominally geometrically scaled as shown in Table 4.1.¹

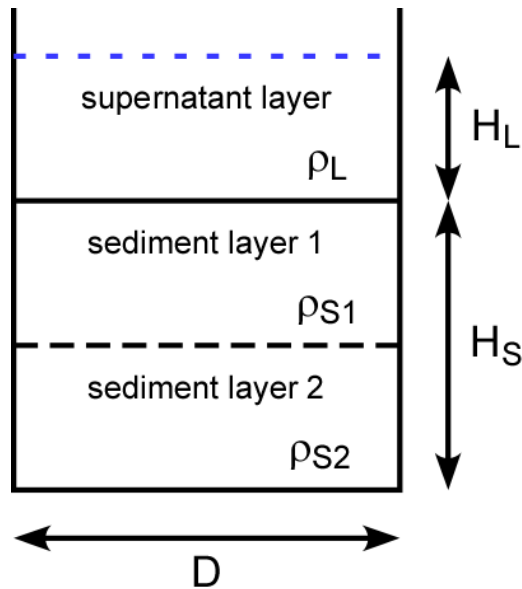


Figure 4.1. Diagram of an Expected Waste/Simulant Configuration in a Vessel with Reference Dimensions (not to scale)

Table 4.1. Geometrically-Scaled Dimensions for the Test Vessels

Dimension	Full Scale (DST)	10-in. Vessel	23-in. Vessel	70-in. Vessel
D (m)	22.86	0.254	0.584	1.778
H_S (m)/ H_S (in.) ^(a)	7.87/310	0.087/3.44	0.20/7.92	0.61/24.1
H_L (m)/ H_L (in.) ^(a)	2.11/83	0.023/0.92	0.05/2.12	0.16/6.46

(a) Based on $H_S/D = 0.34$ and $H_L/D = 0.09$.

¹ An additional ~5-cm (~2-in.) depth of supernatant liquid was used in scaled-vessel RT testing for the 10-in. and 23-in. vessels to ensure that any dome formed by deformation of the solids layer, as a result of gas retention, does not extend above the supernatant layer and cause underestimation of the retained gas fraction. This is addressed further in Section 4.3.2. The adjustment was anticipated to be necessary in the smaller vessels, for which the geometrically-scaled liquid layer thickness is only 2 to 5 cm, because the doming observed in some past tests was about 1 to 2 cm. In the 70-in. vessel, the geometrically-scaled liquid layer is 16 cm, which was (expected to be) deep enough to prevent any sediment dome from reaching the liquid surface.

In all but the first single slurry layer (SL) test in the 23-in. vessel, the liquid depth in the 23-in. and 70-in. vessels was reduced by a factor of 4. This was done to minimize the distance that (potentially) neutrally buoyant slurry could rise through the liquid, which could enhance gas release. Like the RT tests, the purpose of the SL spontaneous gas release tests was to investigate gas release from the slurry without buoyant displacement in the supernatant. Unlike the RT tests, the retained gas fractions at the point of instability in the spontaneous release tests were typically near those needed for neutral buoyancy in water.

Experimental results showed that the scaling of slurry depth was a significant factor in α_{RT} and the sizes of gas releases. This was particularly noted in comparison of tests at 1× and 2× slurry depths in the 23-in. vessel; see, for example, the summaries of results in Section 8.5.1 and Section 10.1.

4.2.2 Targeting Appropriate Gas Release Events

The RT instability mechanism results in a situation where at least a portion of sediment layer 2 (lower layer) achieves a gas void fraction that is sufficient to initiate motion of the sediment of layer 2 into the sediment of layer 1 (upper layer). More than one kind of gas release behavior may occur once the instability-driven motion has initiated. One possibility is that a portion of sediment layer 2, which is already buoyant in sediment layer 1, has generated and retained sufficient gas to be buoyant in the liquid layer as well (at or above a buoyant gas volume fraction α_{NB}). In this scenario, the material from sediment layer 2 would likely rise rapidly to the liquid surface and be sheared apart by the motion, potentially leading to a significant BDGRE. Other experiments in the overall DSGREP effort (not described here) demonstrated that retained gas void fractions in deep sludge were relatively low (e.g., Powell et al. 2014, Schonewill et al. 2014)¹ and are not expected to become sufficiently high to allow BDGREs for sediment and supernatant liquid densities of the sludge waste in AN-101 and AN-106 (Meacham and Kirch 2013). In addition, tank farm operations could possibly remove the liquid layer to essentially eliminate the potential for buoyant rise in it. For these reasons, this experimental study focused on configurations where an RT instability gave rise to motion between the sediment layers but where the gas-laden sediment layer did not have a buoyant rise through a liquid layer.

Gas release is also dependent on the characteristics of the generated gas, particularly on the bubble size. Small bubbles are less likely to coalesce and produce releases familiar in Hanford watch list tanks. The RT scoping studies (Gauglitz et al. 2013) found that very small bubbles were generated in kaolin clay-based simulants. Simulants in the current study were selected to produce larger bubbles and more prototypic gas release behavior. This is more fully discussed in Section 5.1.3. For the purpose of investigating gas releases due to in-sediment motion due to RT instabilities, it is also important to choose a combination of simulant properties and operating conditions to avoid spontaneous bubble-cascade releases. Such self-propagating gas releases are possible using relatively weak materials. For example, Gauglitz et al. (1996) observed spontaneous releases in <4-Pa shear strength bentonite slurry with retained gas fractions of ~10 vol% and at higher gas fractions in somewhat stronger material (e.g., >25 vol% at ~30 Pa). This topic is addressed for simulants used in RT tests in discussion of the companion single-slurry-layer tests (Section 8.3) and the related discussion in Section 8.4.

¹ These other experimental activities were completed in parallel with the RT instability studies, and therefore, the results were not known *a priori*.

4.3 Test Matrix and Extrapolation Concepts

This section discusses concepts for extrapolating gas release data obtained in scaled-vessel RT experiments to full-scale tanks and the planned test matrix to provide the data.

4.3.1 Identifying Tests for Extrapolation

The gravity yield parameter Y_G has been specified to be 0.09 based on past work (see Epstein and Gauglitz 2010; Gauglitz et al. 2013), and this value was used to define target experimental conditions. However, one component of the testing was to obtain a better estimate of the Y_G parameter (see Section 8.5.3). Selecting the simulant solids concentration x_S specifies the shear strength for the prepared slurry batches (e.g., Equation (5.2)) and it specifies the initial sediment density as given, for example, by Equation (5.3). Together, Equations (5.2) and Equation (5.3) constrain the value of α_{RT} given by Equation (4.2).

The planned experiments were chosen to satisfy the overall objective of the testing: obtaining a basis for estimating the point at which gas is released and the quantity released in a full-scale vessel during an RT instability event. A planned extrapolation method was to use smaller-scale vessels (10-in., 23-in., and 70-in. diameters) and keep the void fraction in each vessel constant at the onset of RT instability (or interpolate to constant α_{RT}). This would allow the gas release results to be scaled with vessel diameter, thereby facilitating extrapolation using constant α_{RT} data to a prediction for the full-scale vessel (see Section 10.0). This is shown conceptually in Figure 4.2. Note that it was anticipated that an extrapolation approach of this type could also be applied to gas release data using other metrics such as constant difference in sediment layer density ($\Delta\rho$, Equation (4.3)), as a function of sediment shear strength, and at constant (or near-constant) modified energy ratio (Equation (4.4)). Modified energy ratio extrapolation is also considered in concept in Figure 4.2. Like the dependence of gas release on α_{RT} (Section 8.5.1), the relationship between ER_S and gas release was determined empirically as part of the testing (Section 8.5.2).

The dashed lines in Figure 4.2 are examples of how the data might be extrapolated to full scale (the solid vertical line), and the trends shown are hypothetical extremes (without the benefit of knowledge gained in these studies). The upward trending line through circles represents the scenario where gas release increases with scale, whereas the downward trending line joining the triangles shows the opposite. Note that extrapolation of results from RT instability experimental and modeling studies shows constant or decreasing gas releases with increasing vessel scale [see Section 10.0].

In practice, extrapolation at constant α_{RT} is complicated by the imprecision in predicting when RT instabilities will occur. Thus, to obtain data sets of constant α_{RT} , the conceptual approach was to perform experiments that permitted interpolation to the same α_{RT} at multiple vessel scales. This can be done, for example, by performing experiments at similar expected α_{RT} in both scales and using vessel-specific measured α_{RT} vs. shear strength curves to interpolate to gas release behavior at constant α_{RT} . Originally planned tests to implement this strategy are discussed in Section 4.3.2, and the matrix of and results for completed tests are discussed in Section 8.1.

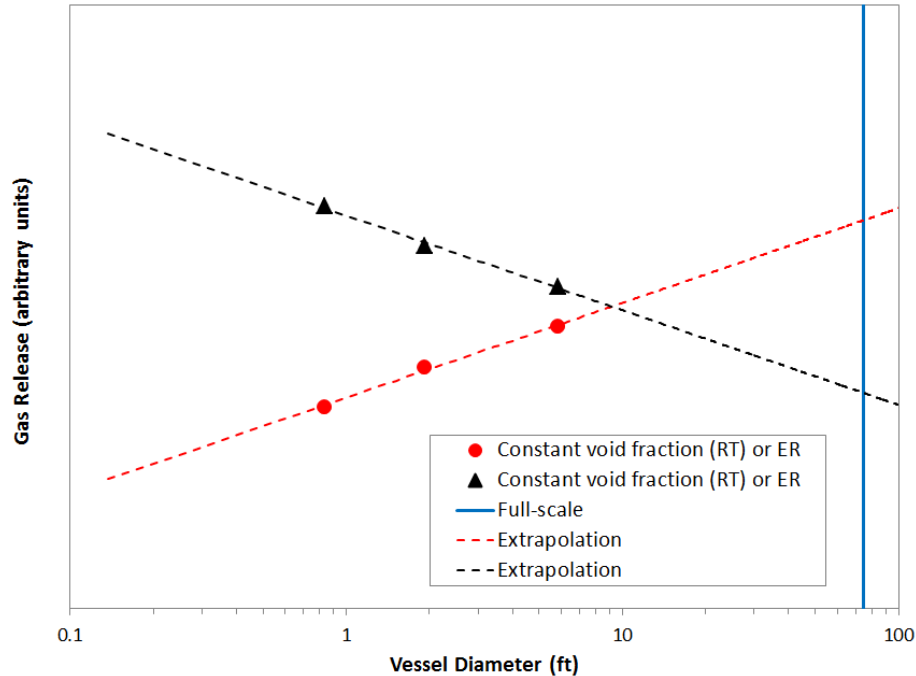


Figure 4.2. Conceptual Example of Extrapolation to Full Scale. The dashed lines represent possible curves of gas release with either constant void fraction at RT instability (α_{RT}) or modified energy ratio (ER_S , shown as ER in the legend).

Another conceptual approach considered for scaling gas release is shown in Figure 4.3. The curves in the figure depict extrapolation of gas release behavior to full-scale shear strength along lines of constant vessel size. As before, the curves in Figure 4.3 are hypothetical and should not be construed as expected or observed behavior. Three types of potential data sets are shown for illustrative purposes: 1) gas release increasing with τ_S (blue squares), 2) gas release decreasing with τ_S (red triangles), and 3) gas release approximately constant (due to some scatter in the data) with τ_S (green diamonds). Note that, because of coupling of τ_S and α_{RT} (e.g., Effect of Shear Strength in Section 8.1.3.3), the need to use lower than expected shear strength slurry to obtain α_{RT} in the target range (e.g., Section 8.1.3.1), and the more apparent dependence of gas release on α_{RT} (Sections 8.5.1 and 10.1), direct extrapolation along lines of increasing strength proved not to be applicable.

While these theoretical approaches for extrapolation are all valid, the options in the RT studies described here were in practice much more limited than anticipated. This is primarily due to the need to use considerably weaker slurry simulant than planned, which effectively made the third vessel (10-in.) too small for meaningful experiments and the results from the few tests in it essentially unusable for extrapolations. See Section 8.1 for an explanation of the experimental limitations and Section 10.0 for a discussion of extrapolation approaches that were pursued.

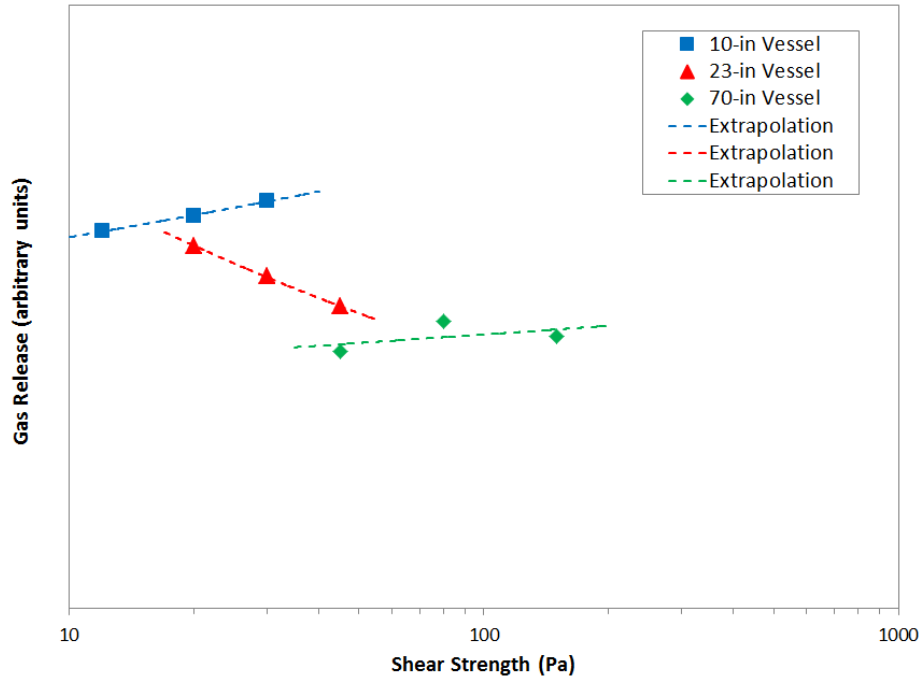


Figure 4.3. Conceptual Example of Extrapolation at Constant Vessel Size. Each data set represents tests at various shear strengths for a different vessel – the trends shown are for illustration purposes only.

4.3.2 Selecting the Test Matrix

The equal lower and upper slurry layer depth tests originally planned for the 10-in., 23-in., and 70-in. vessels to implement the strategy for extrapolation of gas release behavior to full scale are defined here. Updates to the matrix are addressed in Section 8.1.1, and matrices for varying relative slurry layer thickness RT tests and SL tests are discussed in Section 8.2.1 and Section 8.3.1, respectively. The slurry simulant shear strength and density correlations used in development of the original test matrix are discussed in the Target Simulant Properties section (Section 5.2).

Equation (5.2) and Equation (5.3)) were used in conjunction with Equation (4.2) to develop 90:10 M30:B simulant recipes for planned testing conditions. In a typical application, a target α_{RT} value was specified, and the weight fraction solids was determined such that $\tau_s(x_s)$ and $\rho_s(x_s)$ simultaneously satisfied the gravity yield parameter at the point of RT instability according to Equation (4.2) with Y_G set to 0.09. The original test matrix for tests of equal slurry layer thickness in the 10-in., 23-in. and 70-in. vessels, shown in detail in two tables of the TP¹, was developed using this approach. In each vessel, tests targeting α_{RT} values of 8, 12.5, and 18.5 vol% retained gas were defined. The slurry shear strength increases with the α_{RT} target, and therefore, tests were planned for a minimum of three strengths in each vessel. Additional tests were planned in which the same simulant recipe (target τ_s) is used in RT tests in both the 10-in. and 23-in. vessels or in both the 23-in. and 70-in. vessels. This results in additional τ_s and α_{RT} targets in the larger of each pair of vessels.

¹ Table 3.4 for 10-in. and 23-in. vessels and Table 3.5 for the 70-in. vessel in TP-DSGREP-001, Rev. 1.0 and later versions (2.0, 3.0, and 4.0).

A method to visualize the planned test matrix in the 10-in., 23-in., and 70-in. diameter vessels is the scatter plot shown in Figure 4.4. The figure shows the planned tests plotted as a function of the two primary test parameters of interest from Equation (4.2): shear strength of the sediment layer and the target void fraction at RT instability. The figure visually demonstrates how the formulated test matrix proposes tests at three α_{RT} values across three vessel scales and duplicates tests at the same shear strength across two scales. It is not practical to have tests at the same shear strength across all three scales because either α_{RT} would be too close to α_{NB} in the 10-in. vessel or, using relatively weak simulant in the 70-in. vessel, α_{RT} would be too low to get the vessel filled before the RT instability occurred and/or too close to the minimum detection limit. Test numbers shown in Figure 4.4 correspond to the Test IDs in the test matrix tables of the TP.

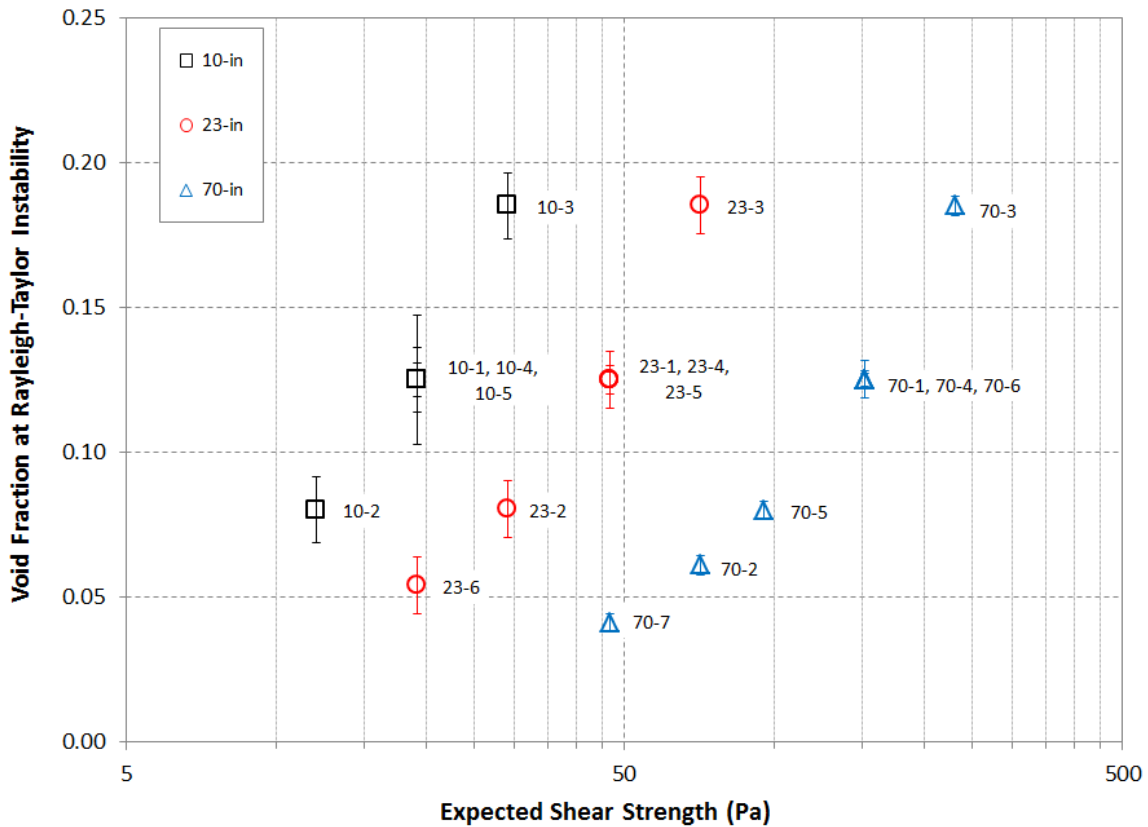


Figure 4.4. Scatterplot Illustrating the Target Conditions of the Originally Planned Test Matrix Found in the TP

The vertical error bars in Figure 4.4 represent the nominal level measurement resolution (e.g., 1 mm) in terms of the corresponding maximum uncertainty in gas fraction in the bottom slurry layer.¹ In cases where tests at multiple slurry depths were planned (e.g., 10-1, 10-4, and 10-5), the relative error decreases

¹ A more comprehensive definition of experimental uncertainty in gas fraction measurements is discussed in the RT Test Data Analysis section (Section 6.5.1). For planning purposes, it was correctly assumed that a level measurement resolution H_{res} of 1 mm could be attained. Noting that changes in volume and retained gas volume fraction for a vessel of constant cross-section can be calculated equivalently from changes in height (depth), a gas fraction uncertainty, α_{res} , based on level resolution can be defined approximately in terms of H_{res} . The maximum uncertainty in gas fraction calculated for the test matrix is defined in terms of the initial depth of the bottom slurry, $H_{s2,0}$: $\alpha_{res} = H_{res} / (H_{s2,0} + H_{res})$.

with increasing depth. For this reason, the most tests in the 10-in. vessel were planned and conducted with 2× the geometrically-scaled settled solids depth, while the base set of tests in the 23-in. and 70-in. vessels specify 1× scaled depth. Using level measurement resolution alone, the estimated α uncertainty is ~1 vol% at most in the 23-in. and 70-in. vessels, and geometrically-scaled conditions provide a more direct means of extrapolating to full scale.

In addition to gas fraction uncertainty considerations, varying slurry depths in multiple tests at a constant α_{RT} target (e.g., 12.5 vol%) is a means to: 1) probe the effect of layer thickness on the gravity yield parameter Y_G and the RT instability criterion (Equation (4.1)); and 2) establish test conditions having a range of modified energy ratios to investigate the effect of ER_S on gas releases. For slurry depth of 1×, 2×, and 4× geometrically scaled in the 10-in. and 23-in. vessels, the ER_S calculated from Equation (4.4) using the target α_{RT} values and the corresponding slurry properties also varies by a factor of approximately four, from ~4.4 to ~18. The ER_S range is lower for the 70-in vessel, being ~2 to ~7 for 0.5×, 1×, and 1.5× geometrically-scaled slurry depth. (The slurry depth in the 70-in. vessel is limited by the vessel height.) The direct relationship of ER_S with slurry depth is predicated on α_{RT} being independent of layer depth. This is not supported by the test results (see Section 8.1.3), which made extrapolations to full-scale DSTs more difficult than originally anticipated. The calculated ER_S for each of the planned tests is shown in the test matrix tables of the TP.¹

For reference, ER_S was calculated for the full-scale DST (AN-101) using 1000- and 2000-Pa shear strength and a density of 1600 kg/m³, which are typical values for waste parameters (Uytioco 2010). The corresponding estimated α_{RT} values for these waste properties range from ~6 to ~12 vol%. The ER_S for these cases is ~5, assuming that the sludge depth (Section 4.2.1) is equally split into a gas-free upper layer over a gaseous lower layer. The DST parameters also demonstrate that the target α_{RT} values for the planned tests are similar to those calculated for full scale, assuming a Y_G of 0.09. Comparison of experimental ER_S results to full scale is addressed further in Section 8.5.2, and differences between the assumed and experimentally determined Y_G are discussed in Section 8.5.3.

Figure 4.5 provides another view into the relationship of DST and scaled-vessel test conditions. The figure compares target conditions of the originally planned test matrix (e.g., Figure 4.4), which are primarily derived from constant α_{RT} targets, to scaling at constant τ_s/D (= constant $\Delta\rho$, Equation (4.3)). Results are shown for three assumed sludge shear strengths in the DST: 1000, 1750, and 2500 Pa; the corresponding calculated α_{RT} values in the DST are 6.2, 10.8, and 15.5 vol%, respectively ($Y_G = 0.09$; $\rho_s = 1600$ kg/m³). The constant τ_s/D lines in the figure indicate decreasing α_{RT} with increasing strength, in contrast to the planned constant α_{RT} test conditions. However, the breadth of the planned α_{RT} test targets effectively bounds the constant τ_s/D cases for 1000- to 2500-Pa sludge in the DST.

¹ Table 3.4 and Table 3.5 of TP-DSGREP-001, Rev. 1.0 and later versions (2.0, 3.0, and 4.0).

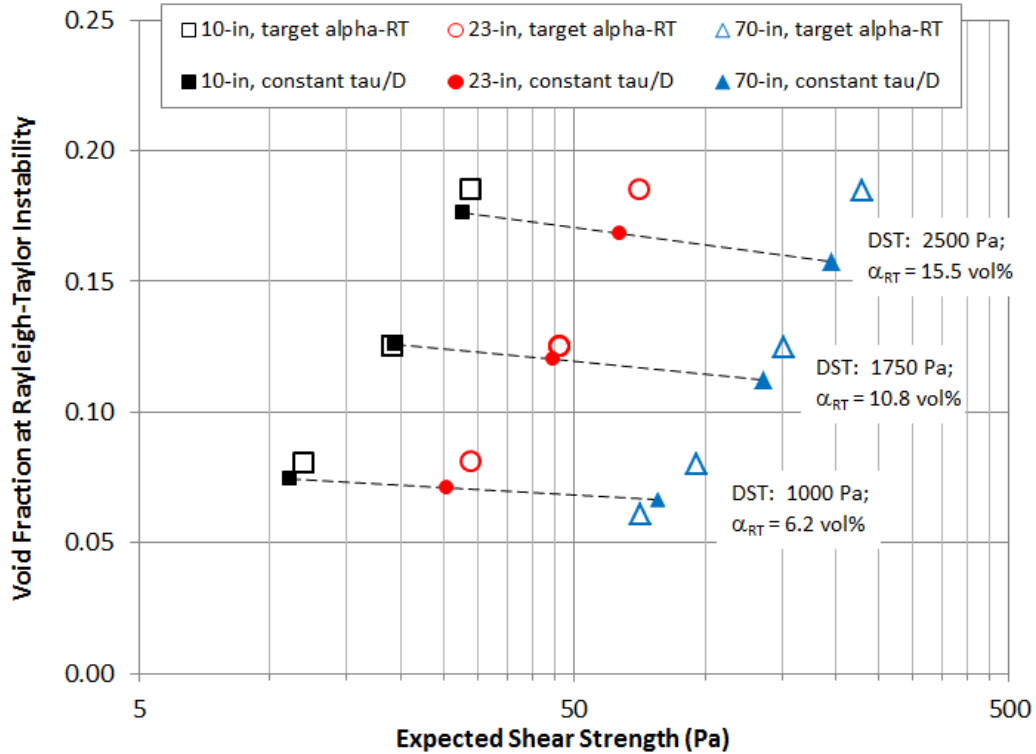


Figure 4.5. Scatterplot Comparing the Target Conditions of the Planned Test Matrix (open symbols) to Scaling at Constant τ_s/D for Three Assumed Sludge Strengths in the DST (filled symbols and dashed lines)

Note that water is used as the supernatant liquid in the experiments and that its depth is the geometrically-scaled value plus ~ 5 cm (~ 2 in.) in the 10-in. and 23-in. vessels to ensure that any dome formed by deformation of the solids layer, as a result of gas retention, does not extend above the supernatant layer and cause an underestimation of the retained gas fraction.¹ Because a low-density liquid is used as supernatant, the void fraction in the slurry at neutral buoyancy is relatively high. The TP test matrix includes α_{NB} for each of the originally planned tests to demonstrate that the expected void fraction at RT instability was well below (e.g., at least 8 vol% less than) the void fraction range where buoyancy in the supernatant liquid is possible, thereby minimizing the potential for floating gobs.

¹ Compared to calculations using geometrically-scaled liquid depth, the addition of ~ 5 cm of water in the 10-in. and 23-in. scaled test vessels changes the modified energy ratio values by <0.1 .

4.4 Assumptions

There are a number of important assumptions in the planned technical approach that were identified in the governing TP.¹ The key assumptions that are being evaluated as part of the RT and SL tests described in this report are listed below:

- The onset of RT instabilities, in different size vessels, can be quantified with a dimensionless gravity yield parameter.
- Gas releases from RT instabilities, in different size vessels, will have an orderly change in behavior that allows extrapolating the small-scale results to full-scale tanks.
- The retained gas fraction at the onset of an RT instability is less than the gas fraction at which gas would spontaneously release from the slurry in the absence of an RT instability or other disturbance.
- In-sediment motion due to RT instabilities does not result in bubble-cascade gas releases.²
- The upper slurry layer in RT tests remains sufficiently uniform (flat) while gas is retained such that the liquid surface is not disturbed and the overall liquid level (volume) can be measured (e.g., a slurry dome does not form and crest the liquid before the initial instability occurs).
- The actual water layer thickness does not affect the RT instability and gas release in the absence of floating gobs.
- In RT tests, gas bubbles are generated and primarily retained in the bottom slurry layer and are not appreciably present in or releasing through the upper slurry layer.
- No vessel-spanning bubbles are formed.

There are a number of technical limitations of the planned approach to extrapolate the results to full-scale DSTs. These limitations include the use of simulants rather than actual tank waste, the heterogeneity of actual waste in the DSTs is not represented, and the absence of tank internals and instrument trees in the current test vessels. The future use of extrapolated results will need to recognize the uncertainty caused by these limitations.

¹ TP-DSGREP-001, Rev. 0.0, 1.0, 2.0, 3.0, and 4.0.

² Although not stated in the TP, this assumption and the need to evaluate it were identified during RT tests.

5.0 Simulant Selection and Target Properties

The rationale for selection of a slurry simulant for use in RT tests is described in this section. Some of the physical and chemical properties of the selected silica-bentonite clay sediment simulant, as determined in an FIO simulant development and characterization effort that preceded the RT tests described in later sections of this report,¹ are also summarized. This development effort provided target simulant property information that was used in preparation of the original test matrix described in Section 4.0. The slurry simulants prepared for and used in the RT experiments were also routinely characterized as part of testing, and results are discussed in Section 7.0.

5.1 Simulant Selection

The simulant selection process, which followed the guidelines set in ASTM C1750-11 (2011), is briefly summarized here. The main limits on the scope of simulant used are 1) matching the range of gas volume fractions estimated for RT instability at full scale in tank AN-101, while 2) using smaller-scale vessels. The selection criteria for the simulant were as follows:

- The shear strength of the material could be controlled by changing solids concentration
- The supernatant liquid density was low enough and/or the bulk density of the sediment simulant was sufficiently large that the sediment with retained gas would not be neutrally buoyant ($\alpha_{NB} > \alpha_{RT}$) in the liquid layer
- Gas could be generated in the sediment simulant in sufficient quantity and rate to conduct the experiments in a practical amount of time, but slow enough that a test vessel could be filled before a significant volume of gas was generated and retained
- The sediment simulant releases gas when disturbed or sheared, presumably with more gas released when the simulant has a lower yield stress and an equivalent amount of retained gas
- The bubble-release mechanism was qualitatively the same as for observed in-tank releases (large bubbles released when disturbed).

A detailed discussion of simulant requirements and of simulant design and preparation is given below.

5.1.1 Shear Strength and Density

Equation (4.1) shows that the RT instability yield criterion is a function of both τ_s and the gas-free slurry density, ρ_s . Both τ_s and ρ_s increase with increasing solids fraction for clay-water slurry simulants. Higher solids fractions and slurry densities mean that the slurry can become neutrally buoyant in the supernatant liquid (e.g., water) of density ρ_L only at relatively high gas fractions α_{NB} , as shown by the relationship

¹ The FIO simulant development effort and results are first discussed in the Revision 0.0 of the governing Test Plan, TP-DSGREP-001. The shear strength vs. solids content correlation was updated in Rev. 1.0 of the TP and was retained in later versions (2.0, 3.0, and 4.0). The correlations shown in the TP are superseded by those determined for simulant batches prepared for RT tests, as discussed in Section 7.0.

$$\alpha_{NB} = 1 - \frac{\rho_L}{\rho_S} \quad (5.1)$$

This is a desirable characteristic in experiments in which the goal is to study gas release associated with motion within the settled solids layer(s) due to an RT instability, such as might be experienced in a DSGRE in a waste tank. If the gas fractions retained in the settled solids at the time an RT instability occurs are close to those for neutral buoyancy, gobs of slurry could rise and float in the supernatant liquid, which would be more representative of a BDGRE scenario. Quantifying gas release associated with DSGREs rather than BDGREs is the focus of the current investigation. Therefore, it is preferable that there is a large difference between α_{NB} and the gas fraction at RT instability, α_{RT} , to avoid the creation of floating gobs. To this end, slurries with higher ρ_S are beneficial, as is a supernatant with lower ρ_L .

Pure bentonite-water slurries develop significant shear strength at relatively low solids concentration (>100 Pa at 15 wt% solids; Gauglitz et al. 1996) and density (e.g., $\rho_S \sim 1.1$ g/mL; see Equation (5.3) below). In this example, α_{NB} would be <10 vol% retained gas for the slurry to become neutrally buoyant in water (Equation (5.1)). This is too low to prevent floating gobs for planned tests in which the target α_{RT} ranges up to 18.5 vol% retained gas (see Section 4.3.2). Additionally, the rate of O₂ gas generation from the decomposition of hydrogen peroxide (H₂O₂) in bentonite-water slurries is known to be very fast (see, for example, Gauglitz et al. 1996). Control of gas generation rates in RT instability gas-release tests is discussed below.

Combining Big Horn[®] BH 200 bentonite (B)¹ with fine-ground crystalline silica such as Min-U-Sil[®] 30 (M30)² allows the slurry density to be increased compared to that for pure bentonite, because a higher solids concentration is required to achieve a given τ_S . FIO simulant development scoping tests were conducted with 80:20, 85:15, and 90:10 ratios of M30:B (without pH adjustment; see next section).³ At a given solids loading (wt% total solids), τ_S increased with increasing fraction of bentonite, indicating that strength is substantially derived from the cohesive properties of bentonite. Lower theoretical densities (Equation (5.3)) in the 80:20 and 85:15 ratio slurries result in reduced α_{NB} relative to 90:10 ratio formulations. Given the uncertainty in the actual α_{RT} under test conditions and to alleviate concerns of floating gobs in tests with high target α_{RT} (e.g., 18.5 vol%), it is preferred to have α_{NB} at least 5 vol% higher than the α_{RT} target. Considering further increases in τ_S and decreases in solids loading and ρ_S when pH is reduced in the simulants, the 90:10 M30:B is preferred over the formulations with higher bentonite content. The 90:10 M30:B slurries were expected to provide at least 8 vol% difference in α_{NB} and α_{RT} under all planned RT test conditions (see Section 4.3.2). In addition, the higher density of the 90:10 M30:B simulants provides a better match to the sediment density in AN-101 and AN-106 (Uytioco 2010).

¹ Big Horn BH 200 bentonite (previously sold under the CH 200 label) is supplied by Wyo-Ben, Inc. A May 2013 Rev. of the Technical Data Sheet shows a Specific Gravity of 2.55 ± 0.1 .

² Min-U-Sil[®]30 is produced by Brenntag Specialties, Inc. and distributed by U.S. Silica. A Product Data sheet issued October 2007 and revised December 2011 shows that Min-U-Sil[®]30 is typically 99.5% SiO₂, has a Median Particle Size of 8.2 microns, and a (particle) Specific Gravity of 2.65.

³ These scoping tests generated FIO simulant data that was used for planning purposes only.

5.1.2 Gas Generation

In an RT test, gas is generated in a bottom slurry layer to create a density inversion with respect to a nominally gas-free upper slurry layer. The rate at which gas is generated directly affects the time it takes to reach an RT unstable condition. In 70-in. vessel RT tests, approximately 400 gal of simulant split into the gas-generating and gas-free layers, plus a supernatant liquid layer, must be added to the vessel to start a test. Depending on the strength of the slurry, it takes ~1 to 2 hours to make final simulant preparations (e.g., add H₂O₂) and fill the 70-in. vessel. This practical experimental consideration limits the maximum acceptable rate of gas generation. If it is too fast, the bottom slurry layer can be RT unstable at the time filling is completed or shortly thereafter. This concern also applies to 10-in. and 23-in. vessel tests, but to a lesser extent because the slurry volumes are much smaller and the fill times shorter.

Note that experimental gas generation rates must also be orders of magnitude faster than in the Hanford sludge waste tanks in order to complete tests in ~1 day (target) after filling the vessel, as dictated by experimental practicality. Gas generation rates may affect the bubble size distribution, with higher generation rates tending to nucleate more small bubbles and lower rates producing fewer, larger bubbles. The size distribution, like the bubble shape, may depend on the strength of the material in which the bubbles are generated. As shown in Gauglitz et al. (1996), for example, bubble shape progresses from spherical bubbles in weak materials (e.g., <100-Pa bentonite), to distorted, oblate spheres at moderate strength, to channels and cracks in relatively strong materials (e.g., >500 Pa). Generation rate may have a more pronounced impact on the number and size of round bubbles in weak materials than it does on the channel structure in strong materials. Variation in bubble size distribution, and bubble morphology itself, may affect the quantity of gas released in a release event (also see Section 5.1.3). However, the onset of a buoyant in-sediment RT instability event, which is driven by the difference in bulk density of adjacent slurry layers, is not expected to be affected appreciably by the bubble size distribution (or morphology), assuming that the gas is uniformly distributed in the layer. Bulk density is a function of the total retained gas fraction and not the size or shape of the retained bubbles.

Experimentally, the decomposition of H₂O₂ to liberate oxygen gas and liquid water has long been used in the study of gas retention and release in bentonite, kaolin, and kaolin-bentonite physical simulants representing various Hanford wastes and associated waste streams (e.g., Gauglitz et al. 1996, 2012a). The corrosion of zero-valent iron (Fe) powder to generate hydrogen gas in kaolin simulants of Hanford K-Basin waste has also been used successfully to investigate gas retention behavior (Gauglitz et al. 2012a). In FIO tests, it was observed that bentonite-water and M30:B-water slurries mixed with Fe powder did not generate gas even after standing a week or so, presumably due at least in part to pH differences in the bentonite-based slurries (alkaline) and kaolin slurries (acidic). There may be additional surface chemistry effects which promote Fe corrosion with kaolin. Several M30:B slurries were acidified with hydrochloric acid solutions to different pH targets. At pH ~3 and above, gas generation was minimal or nonexistent, whereas at pH ~2.4 and below, 15 vol% or more gas was generated in the Fe-containing slurry in <<1 hr. More moderate gas generation rates were observed at a relatively narrow range of pH (e.g., ~2.6 to 2.9), but it was concluded that this level of pH control for RT tests was experimentally impractical.

A number of FIO tests were conducted to assess the rate of O₂ generation in M30:B slurries of varying composition, with and without candidate additives to help control the rate of gas generation. Common to each of these tests, nominally 3 wt% H₂O₂ solution in water was added to a prepared slurry a few minutes prior to partially filling volumetrically graduated glassware, e.g., a beaker or a graduated

cylinder. Completion of filling defined elapsed time zero, and changes in volume due to gas retention were tracked over time to assess gas generation rates and retained gas volume fractions, α (= retained gas volume/total gaseous slurry volume). The quantity of H₂O₂ solution was specified to achieve target mass fractions of neat H₂O₂ in the slurry; 0.1 wt% H₂O₂ was typical. Figure 5.1 shows the results of three tests conducted in 500-mL graduated cylinders. The upper plot shows a reference case for a 47 wt% solids 90:10 M30:B slurry prepared with tap water without any additives or pH adjustment to control the gas generation rate. A gas fraction of 25 vol% was generated and retained in <2 hr, which is much too fast for RT tests in the 70-in. vessel, as discussed above.

Acetanilide is a stabilizer that is commonly added to H₂O₂ solutions in relatively low concentration (e.g., 200 ppm) to improve the shelf life. The H₂O₂ solutions used to generate the results shown in Figure 5.1 were supplied by the manufacturer with ~200 ppm acetanilide. Tests were conducted with increased concentrations of acetanilide in the slurry that were obtained by dissolving solid acetanilide (Aldrich, labeled 97% purity) in either the H₂O₂ solution or in the tap water used in slurry preparation.

Even with significantly increased acetanilide concentration using the latter approach, there was no apparent reduction in the O₂ gas generation rate. However, acidification of the M30:B slurries with hydrochloric acid (HCl) solutions to reduce the pH from >8 (as prepared with tap water) to pH ≤ 5 did reduce the gas generation rate. This is shown in Figure 5.1 for 48 wt% 90:10 M30:B slurries adjusted to pH ~4. At an equivalent H₂O₂ concentration (0.1 wt%, upper plot), the gas generation rate was reduced to <3 vol% in 2 hr, which is acceptable for RT tests in 70-in. (and smaller) vessels. The lower plot in Figure 5.1 shows that the gas generation rate can be adjusted by changing the concentration of H₂O₂ at a constant pH (e.g., increased rate at 0.15-wt% vs. 0.10-wt% H₂O₂). The lower plot also shows, for reference, α_{RT} targets of 8, 12.5, and 18.5 vol% retained gas. For the given pH and H₂O₂ concentrations, the minimum α_{RT} target gas fraction is reached in ~8 hr or longer and the maximum target is reached in ~2 days or more. At a fixed pH target of 4.4,¹ the H₂O₂ concentration was in some cases set at values other than those shown here to complete RT testing in a preferred maximum ~1-day window (see Section 8.1.1). The laboratory and simulant temperatures, and likely the concentration (solids loading) of bentonite, are factors affecting the gas generation rate that can be compensated by adjustments in the H₂O₂ concentration.

¹ It was found in simulant development scoping tests using materials acquired for RT tests that the acid demand for 90:10 M30:B simulants to achieve a target pH in the 3 to 5 range is given approximately by $\hat{n} = -0.125pH + 1.066$, where \hat{n} is the specific acid demand in units mol HCl/kg bentonite.

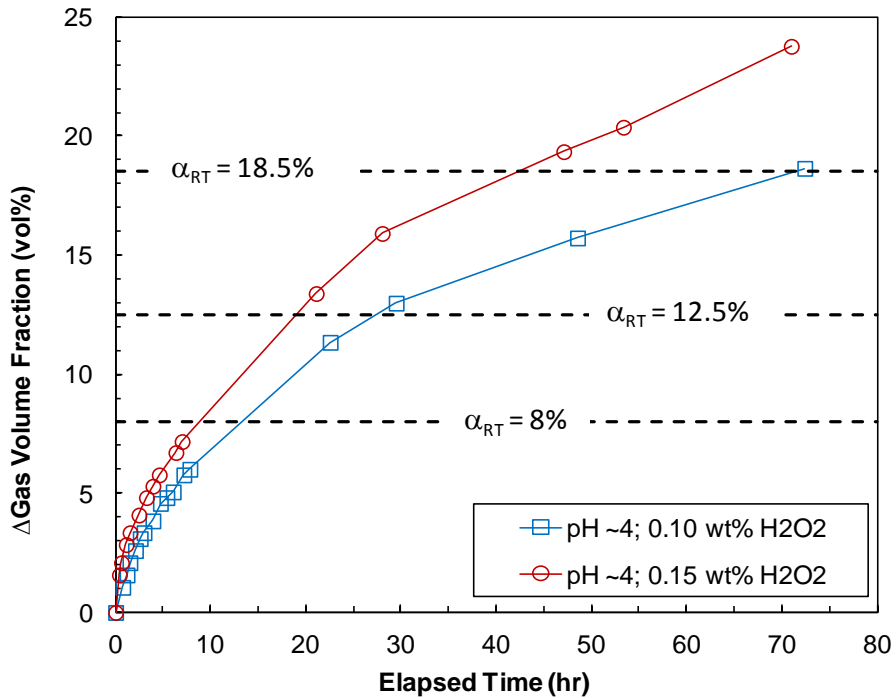
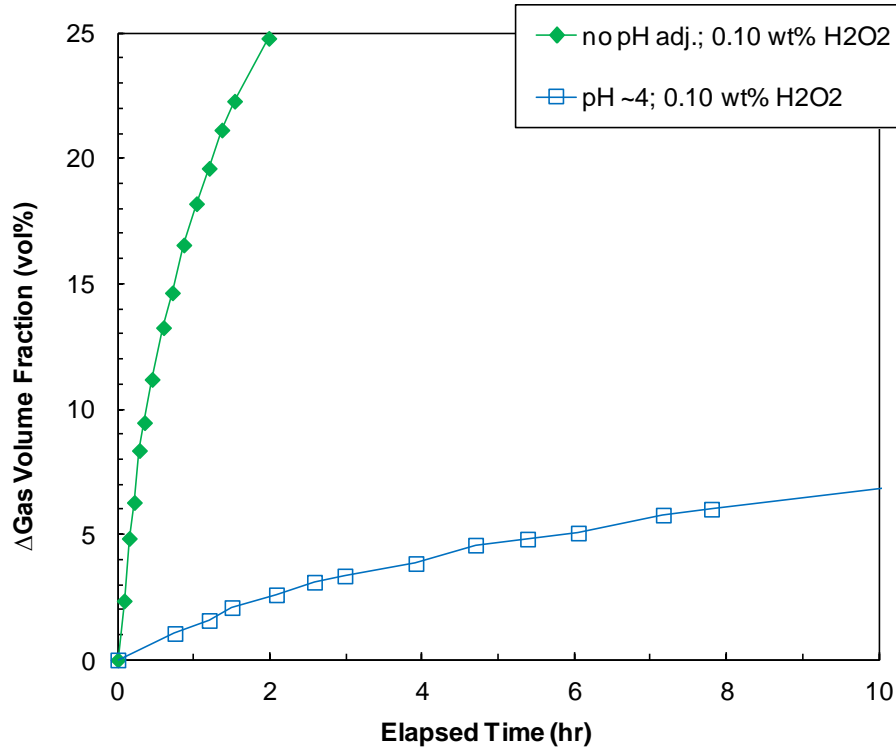


Figure 5.1. Gas Generation Rates from H₂O₂ Decomposition in 47 to 48 wt% 90:10 M30:B Slurries (upper – comparing initial rates with (pH ~4) and a reference case without pH adjustment; lower – effect of H₂O₂ concentration on initial and long-term O₂ generation in pH ~4 slurries with reference to α_{RT} targets of 8, 12.5, and 18.5 vol% gas fraction)

5.1.3 Gas Release Mechanism

Gas release behavior is an important aspect of simulant selection, and the simulant selection criteria above noted: 1) the importance of simulant releasing gas when sheared, and 2) that the bubble-release mechanism should be qualitatively similar to in-tank gas releases from actual waste. Videotape of a few GREs in DST 241-SY-101 provides the limited visual observations of in-tank gas releases. Qualitatively, the bubbles were perhaps a few centimeters in diameter, suggesting significant coalescence, and they released rapidly once motion was initiated during a BDGRE. FIO simulant development tests in which gas-retaining slurry was stirred showed slow, incomplete release with significant frothing in kaolin slurries versus relatively larger apparent bubble sizes at the point of release and higher gas release rates with bentonite and M30:B slurries. The latter behavior is more consistent with the tank 241-SY-101 visual observations of bubble release. It is also conservative from the perspective of bounding the quantity of gas released in an RT instability event and scaling the gas release to a full-scale DST. It may not be conservative, however, in the sense that slurry motion without gas release (e.g., using kaolin slurry) might lead to greater accumulation prior to a subsequent instability and potential gas release. The M30:B simulant was chosen over kaolin-containing simulants to obtain the conservatively higher gas release rates and quantities and because the visual bubble-release behavior of the M30:B simulant was closer to the limited bubble-release observations in 241-SY-101 during a BDGRE.¹

During the course of conducting the RT gas release studies reported here, an additional study (Daniel et al. 2014) was initiated to provide a more quantitative evaluation of gas release behavior in the three slurry simulants (kaolin, bentonite, and M30:B) that had been evaluated in the FIO simulant development tests. For these tests, a single shear strength target value of 30 Pa (vane method) was selected. Gas bubbles were generated by decomposition of H₂O₂ over about a 16-hr period or by applying a vacuum over a 3- to 15-minute period to nucleate and grow bubbles from dissolved gas in the test slurry. The testing also used two methods of inducing gas release. One method for causing gas release was hand-stirring similar to that used in the FIO simulant development tests. A second method was developed for potential use in a hot cell with actual Hanford tank waste². This method used a laboratory vibrator with adjustable settings to provide repeatable shearing to waste or simulants with retained gas bubbles that had been generated either by application of a vacuum or H₂O₂ decomposition. The results showed that the method of bubble generation substantially affected the gas release behavior in simulants. For bubbles generated by H₂O₂ over relatively long periods (about 16 hours), the kaolin slurry had incomplete and comparatively slow release while the releases from bentonite and M30:B simulants were faster, more extensive, and comparable to each other. These results, using both hand-mixing and vibrator gas-release methods, are similar to observations in the FIO simulant development tests and support the selection of the M30:B simulant as having conservative (comparatively fast) release that appears qualitatively consistent with tank 241-SY-101 visual observations. For bubbles generated over a 3-minute period by application of vacuum, bentonite slurry exhibited a slow, incomplete release whereas kaolin and RT simulant showed a more rapid, relatively complete gas release. The gas release behavior observed for vacuum tests, at least with respect to kaolin and bentonite slurries, is opposite of that observed when testing with H₂O₂. The RT testing reported here uses bubble generation from H₂O₂ that occurs over time

¹ In the companion tall-column tests (Schonewill et al. 2014), which were completed to evaluate gas retention and release in relation to d_{max} predictions (see Section 1.0), kaolin was selected as the simulant because it was considered the best simulant for bubble behavior in strong (>500-Pa) layers.

² A project decision was made to stop planned actual waste activities after the gas-release method was developed, but before hot cell testing was started.

periods similar to the 16-hr periods used in the simulant evaluation tests by Daniel et al. (2014). Based on these considerations, selection of the M30:B simulant for RT gas release testing is still appropriate.¹

5.2 Target Simulant Properties

For the purposes of generating the TP test matrix (see report Section 4.3.2) and providing simulant recipes for RT tests (see report Section 6.2.2 and Section 8.0), slurry shear strength and density are key properties. The relationship between these properties and total solids content (weight fraction or weight %) was determined in FIO simulant development tests, as described below.

The shear strengths of pH-adjusted (4.4 target) 90:10 M30:B slurries having a range of solids content were measured. Simulant make-up and mixing procedures were conducted at two different scales: ~2-L batches, which were mixed with a KitchenAid® mixer, and ~15-L batches, which were mixed with a power-driven double auger. The smaller batches were only prepared during the simulant development phase of the project, and not in any of the RT tests described in the remainder of this report. At both batch scales, the strengths at about 1 hr after remixing were about two-thirds of those measured on samples that stood undisturbed overnight (~18 to 23 hr).² Considering the target gas fractions at α_{RT} and the gas generation rates for pH-adjusted slurries at relatively low H₂O₂ concentrations (Figure 5.1), it was anticipated that slurry would attain strength, τ_S , closer to that of the overnight measurements than that of the ~1-hr post-mixing values due to the RT test durations. Therefore, the overnight (“18-hr”) shear strength values were used in planning tests.

A practical consideration of the time-dependent shear strength of the M30:B simulant for RT testing is that slurry batch recipes based on 18-hr τ_S values will be considerably weaker at the time when the test vessel is first filled. In turn, the gas fraction at RT instability would expectedly be lower than the α_{RT} target. This further emphasizes the need to control the gas generation rate in RT tests such that strength develops before the slurry layers become RT unstable.

Slurry simulants for RT tests in the 10-in. and 23-in. vessels described in this report were prepared in ~15-L batches using double-auger mixers (with only one of the two mixing paddles in place); the same mixers (with both mixing paddles) were used to prepare larger “trough” batches of simulant for 70-in. vessel tests. Therefore, shear strength correlations developed from the larger batch (~15-L) preparation method were used as a basis for planning tests. The FIO τ_S results for four ~15-L slurry batches prepared with 42 to 58 wt% solids were fit to exponential functions of the form

$$\tau_S = A \exp(c_e x_S) \quad (5.2)$$

where the solids fraction x_S is typically expressed in weight % and τ_S is in Pa, and A and c_e are the fit pre-exponential and exponential constants, respectively. For the range of solids content used in the RT tests,

¹ Because only the M30:B simulant was used in the RT tests discussed in Section 8.0, it is not possible to validate its choice relative to other simulants. However, like the limited bubble-release observations in 241-SY-101 during a BDGRE (as noted above), gas releases from the M30:B simulant in RT tests were rapid, and generally large, when the retained gas fraction approached the gas fraction required for neutral buoyancy in the supernatant liquid (for example, see Sections 8.3.2.3 and 8.5.1).

² See, for example, Figure 3.3 of TP-DSGREP-001, Rev. 1.0 and later versions (2.0, 3.0 and 4.0).

both 1-hr and 18-hr undisturbed shear strengths were well correlated by this exponential function, as shown in Section 7.1.2 for completed RT test batches.

A consistent relationship between the 1-hr and 18-hr τ_s values allows a 1-hr undisturbed measurement to be used as a batch acceptance criterion for the simulant (see Table 6.2). Otherwise, RT testing would be delayed while waiting for an 18-hr measurement. The transient in τ_s with time after mixing has been more fully characterized for slurry batches used in RT tests and is discussed in Section 7.1.2.

FIO slurry density measurements were also made on many pre-RT test batches of slurry within minutes of remixing (to facilitate transfer to graduated cylinders). Analogous to methods used previously for clay simulants, a theoretical slurry density can also be estimated from the weight fractions (not weight percent as above) of the components and individual component densities (obtained from references):

$$\rho_S = \left(\frac{x_{M30}}{\rho_{M30}} + \frac{x_B}{\rho_B} + \frac{x_w}{\rho_w} \right)^{-1} = \left(\frac{0.9x_S}{\rho_{M30}} + \frac{0.1x_S}{\rho_B} + \frac{1-x_S}{\rho_w} \right)^{-1} \quad (5.3)$$

where x_w and ρ_w are the weight fraction and density of water, respectively. The rightmost form of Equation (5.3) is applicable, for example, to slurries having a 90 wt% to 10 wt% ratio of M30 and B solids. Using 2.65, 2.55, and 0.998 g/mL for the densities of M30 (ρ_{M30}), B (ρ_B), and water, respectively, theoretical slurry densities calculated with Equation (5.3) were <2% and typically $\leq 1\%$ higher than the FIO measurement values. The slight discrepancy may be due to experimental error and/or uncertainty in the solid component densities (which may be lower than reference values due to moisture content, for example), or to small amounts of entrained air in the samples. Measured densities for RT test batches were also typically within 1% of the theoretical density values (see Section 7.1.1).

The liquid layer simulant was chosen to be water to reduce the probability that gas-laden sediment will be neutrally buoyant in the liquid, as discussed above.

6.0 Experimental Methods, Systems, and Data Analysis

The RT tests are depicted schematically in Figure 6.1. Tests are conducted in a cylindrical, open-topped, clear-plastic test vessel that is placed on a scale to record the mass of simulant added and liquid lost due to evaporation, if significant. Simulant is added in layers: the bottom sediment (slurry) layer contains H_2O_2 to generate oxygen gas; dyed slurry having no gas-generating components is carefully layered on top of the naturally colored bottom sediment (except in single-slurry-layer tests); and supernatant liquid (e.g., water) is added on top of the upper sediment layer. Oxygen bubbles that are generated and retained in the lower simulant layer as a test progresses in time cause the overall liquid level to increase. The retained gas reduces the bulk density of the lower layer, in comparison to the upper layer, until the layers become unstable (RT instability or spontaneous gas release). The wave-like RT instability grows with time and some portion of the lower layer rises upwards (for example, see Section 8.1.2). If this motion causes gas bubbles to be released, the overall liquid level decreases.¹ A number of measuring tapes are attached to the vessel to track changes in simulant level and retained gas volume during the course of a test. Test progress is continuously recorded using digital video cameras. One camera (e.g., Camera 1 in Figure 6.1), is dedicated to recording surface level changes, and the other cameras provide more macroscopic views of motion along the side of the vessel (panorama Camera 2) and at the top surface (overhead Camera 3).

The following subsections describe experimental systems and methods used in RT testing: 6.1) Test Facilities and Equipment; 6.2) Simulant Preparation; 6.3) Simulant Characterization; and 6.4) Conducting RT and SL Tests. Summary information on RT test data collection requirements, data collection methods, and instrument types and accuracy are tabulated in Section 6.1.3. Likewise, overall RT Test Requirements and Acceptance Criteria are tabulated in Section 6.4.1. The use of RT and SL test data is described in the RT Data Analysis section (6.5), which includes a discussion of calculation methods and experimental uncertainty.

6.1 Test Facilities and Equipment

Test facilities and equipment used in the RT tests are described in this section: 6.1.1) Laboratories; 6.1.2) Test Vessels, including level-volume correlations; 6.1.3) key measuring and test equipment, including balances and weigh scales, the simulant level measurement system, and video cameras; and 6.1.4 and 6.1.5) equipment used in simulant preparation and vessel loading.

¹ An exception, observed in some 70-in. vessel tests, is that the water level may increase due to expansion of the gas as slurry in the lower layer moves upward and “switches places” with the dense upper layer. Expansion effects may dominate over gas release, if gas release is small.

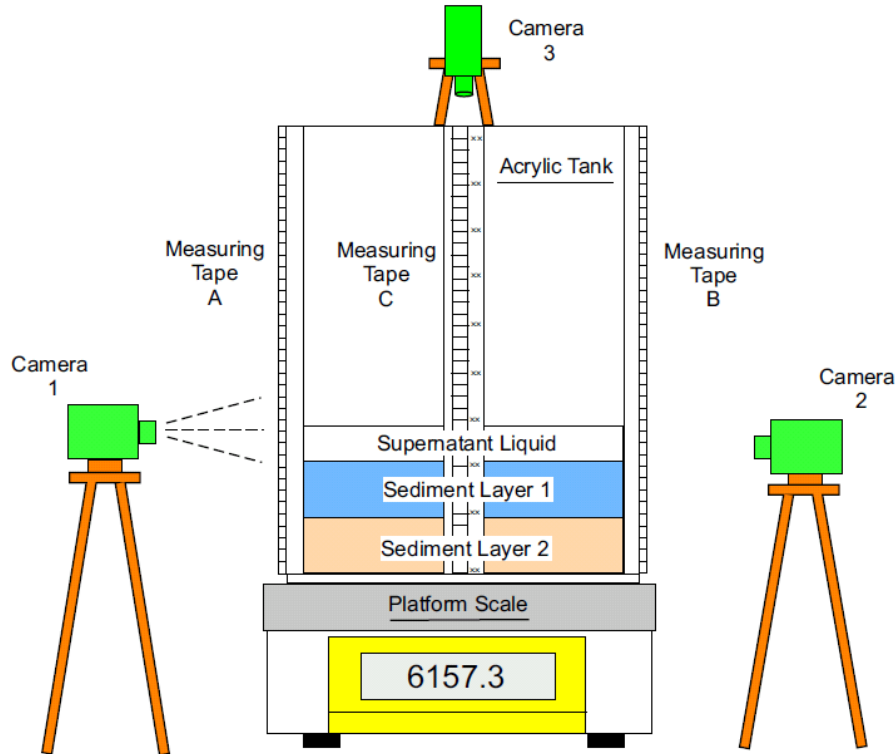


Figure 6.1. Schematic Drawing of an RT Instability Gas-Release Test Setup (not to scale). Note that Camera 1 (of 3), zoomed in on Measuring Tape A (of 3), is used for primary liquid surface level measurements. (Also note that the ordering of measuring tapes in the figure, A-C-B from left to right, and the positioning of cameras with respect to the tapes, are different than on the actual test vessels. The relative and absolute sediment layer depths may also vary, with exclusion of the upper Sediment Layer 1 in some tests.)

6.1.1 Laboratories

The vessel RT tests were conducted in PNNL laboratories, primarily in Applied Process Engineering Laboratory (APEL) 184 high bay space. Two rheometers located in APEL 111 were used to evaluate simulant batch properties (Section 6.3). Although climate controlled to varying degrees, each of these spaces is subject to seasonal and sometimes daily temperature fluctuations. RT Test Requirements and Acceptance Criteria established in the TP allow simulant batch and laboratory temperatures in the range of $24 \pm 8^\circ\text{C}$ (see Section 6.4.1). These acceptance temperatures are measured in the laboratory in which simulant is prepared and RT tests are conducted (e.g., APEL high bay space). Further, APEL 184 temperatures were measured and logged periodically during RT tests, and they ranged from $\sim 16^\circ\text{C}$ to $\sim 22^\circ\text{C}$ during the tests reported in Section 8.0. The simulant characterization laboratory temperature is also logged routinely at the time of analyses, and measured values were within, but generally on the warmer end of, the range of the RT test laboratory temperatures.

These temperature fluctuations slightly impact gas generation rates from H_2O_2 decomposition and slurry rheology, but are not adverse to conduct of tests or test results. The α_{RT} and gas release results are not expected to depend explicitly on the gas generation rate, although slurry strength varies with test duration (see Section 7.1.2.3). Further, adjustments to the H_2O_2 concentration used in simulant

preparation can be made to help control the gas generation rate and test duration (see Section 5.2). In addition, the simulant physical properties (density and shear strength) should not be significantly affected within the modest temperature range experienced based on an examination of the temperature stability of kaolin slurries (Gauglitz et al. 2012b).

6.1.2 Test Vessels

The nominally 10-in. (0.25-m), 23-in. (0.58-m), and 70-in. (1.78-m) inside-diameter test vessels share the following characteristics: 1) they are clear, transparent acrylic; 2) they are nominally cylindrical and oriented vertically; 3) the horizontal bottoms are flat; and 4) the tops are open.

The 10-in. vessel used in testing described in this report has 0.5-in. (1.27-cm) thick walls and is ~20-in. (~0.5-m) tall. It is similar in dimensions and fabrication to the vessel used in earlier RT scoping tests (Gauglitz et al. 2013).

The 23-in. vessel (0.375-in. [0.95-cm] wall), available from previous PNNL project work, consists of two sections, with a gasket-sealed flange at ~30 in. (0.76 m) from the bottom; the overall height is ~48 in. with the upper section in place. A level-volume correlation (next section) was established for the full vessel height in anticipation of a deep-slurry test, but only the bottom section of the vessel was used in RT tests because of a change from original plans.

The nominal 70-in. inside-diameter vessel has 1-in. (2.5-cm) thick walls, is affixed to a 2-in. (5.1-cm) thick flat bottom, and is 45-in. (1.14-m) tall. The vessel height limits the depth of slurry in RT tests to ~1.5× geometrically scaled. It was fabricated by California Quality Plastics, Inc. (CAL Aquaria Division) for these studies.

During testing, the vessels were placed in secondary containment to isolate unexpected spills.

6.1.2.1 Vessel Level-Volume Correlations

The volume contained in each RT test vessel was correlated to fill height (level), nominally as follows. Aliquots of tap water of a known temperature, measured using a calibrated digital thermometer (e.g., thermocouple with readout), were added to or removed¹ from the vessel. The mass of the aliquot of water was measured by change in mass of the partially water-filled vessel that was placed directly on a calibrated scale, and the corresponding fill height was read at each level measurement position (ruler) on the vessel (e.g., 10-A, 10-B, and 10-C).

Level-volume correlations for each vessel were established using more than ten approximately equal increments covering a range from below the lowest height of the bottom slurry layer to be used in testing and ending above the supernatant liquid level anticipated for a test using the thickest slurry and supernatant liquid layers and the maximum expected retained gas fraction (e.g., <35 vol% of the bottom slurry layer). The mass of water contained in the vessel at each fill level was converted to volume using a handbook value for the density of water at the measured water temperature. The level data, measured at the primary (“A”) rulers on each vessel, were subsequently correlated to water volume. The linear level (L)-volume (V) correlations having slopes in liters per centimeter and intercepts in liters are:

¹ In the 70-in. vessel, the vessel was first filled with water, which was then removed incrementally.

- 10-in. vessel: $V = 0.5123L + 0.005$
- 23-in. vessel: $V = 2.7324L + 0.305$
- 70-in. vessel: $V = 24.691L + 1.682$.

Non-zero intercepts account for offsets in the rulers from the bottom of the vessel and other non-uniformities near the bottom.

The average (effective) vessel diameters D were also determined from the analyses: “10-in.”, $D = 10.055$ in.; “23-in.”, $D = 23.22$ in.; and “70-in.”, $D = 69.8$ in.

6.1.3 Measuring and Test Equipment

RT test data collection requirements and collection methods identified in the TP are summarized in Table 6.1. The table provides information on the specific and/or generic types of instruments used, the target (minimum) accuracy of the instruments, and the calibration requirements, as defined by the measuring and test equipment (M&TE) category. Details of selected systems are provided below.

6.1.3.1 Balances and Weigh Scales

Calibrated balances and weigh scales (scales) of sufficient range and resolution/accuracy for the intended measurement were used for a variety of purposes, including simulant batch preparation, determining simulant density (see Simulant Characterization, Section 6.3), and tracking mass additions to (and mass losses from) the RT test vessels. Balances and scales used for each of these processes had greater accuracy than the minimum targets defined in Table 6.1. Each test vessel was placed on a scale for the primary purpose of weighing the mass of simulant added upon filling.¹ The data were used to estimate the initial volume of each simulant layer and the gas fraction in the bottom layer (see RT Test Data Analysis, Section 6.5). Changes in mass over the course of the experiment were used to estimate mass loss due to evaporation of water.

6.1.3.2 Level Measurement System

Adhesive-backed metal tape measures (rulers) reading in cm and marked to 0.1 cm (1 mm) were permanently affixed to the outer surface of each vessel in a vertical orientation for level measurement (three on the 10-in. vessel and four on each of the 23-in. and 70-in. vessels). The locations of the rulers were uniquely identified, for example, positions A, B, and C on the 10-in. vessel. Commercial-off-the-shelf rulers are considered Category 3 M&TE and do not require calibration, because they already provide the needed accuracy. However, as noted in Section 6.1.2.1, vessel level-volume correlations were established for the tape measures affixed to the vessels.

¹ Balances with the following specifications were used for the vessels: 1) 10-in. – Sartorius Model CP 34001 S having a 34-kg range, 0.1-g resolution (readability), and a calibrated uncertainty of ± 0.15 g or less (95% confidence level); 2) 23-in. – Fairbanks Model 748x1000 with a Cardinal readout having a 1000-lb range, 0.1-lb or 0.05-kg resolution (readability), and a calibrated uncertainty of ± 0.12 lb or less (95% confidence level); and 3) 70-in. – Rice Lake Floor Scale Model 6X6HP-5000, 72-in.×72-in. RoughDeck[®] with a Model IQ-355-2A Readout having a 5000-kg range, 0.5-kg readability, and a calibrated uncertainty of ± 0.5 kg or less (95% confidence level).

Table 6.1. Data Collection Requirements, M&TE Type, and Collection Methods

Required Measurement	Instrument (General and/or Specific Examples)	M&TE Category ^(a)	Target Accuracy (meets or exceeds minimum accuracy requirements)	Data Collection Method
Simulant Component Masses for Preparation	Scale	1	±1% of mass	Recorded manually by test operator
Simulant Mass in Test Vessel	<u>10-inch Vessel Scale:</u> Sartorius CP 34001 S <u>23-inch Vessel Scale:</u> Fairbanks Model 748×1000 w/ Cardinal Readout <u>70-inch Vessel Scale:</u> Rice Lake Floor Scale Model 6X6HP-5000, 72 in.× 72in. RoughDeck [®] , w/ Model IQ-355-2A Readout	1	<u>10-inch vessel:</u> ±5 g <u>23-inch vessel:</u> ±0.1 kg <u>70-inch vessel:</u> ±1 kg	Recorded manually by test operator
Simulant Mass for Density	Scale or Balance	1	± 0.1% of mass	Recorded manually by test operator
Time	Commercial clocks, watches, and video camera time stamps	3	Accuracy of ±5 s Synchronize before start of test	Recorded manually by test operator (nearest minute) or recorded on video image (nearest second)
Level (Height or Depth)	Ruler	3	±1 mm	Recorded manually by test operator or recorded on video image
Video Images	Video Camera	NA	NA	Video recorded on SD memory cards
Temperature of Water, Simulant, and Laboratory	Thermocouple and Readout	1	±2 °C	Recorded manually by test operator
Shear Strength (Vane Method)	HAAKE VT550 with Shear Vane	2	Torque within ±10% or ±15% depending on selected certified viscosity standard	Recorded by instrument software
Rheogram	Anton-Paar Physica CR301	2	Torque within ±10% or ±15% depending on selected certified viscosity standard	Recorded by instrument software
pH	pH meter	2	±0.1 pH unit using certified pH buffer solutions	Recorded manually by test operator
Volumetric Glassware for Density	Kimax Class A Graduated Cylinder	3	±0.5% of glassware volume; ±1.0% of measurement volume	Recorded manually by test operator

(a) M&TE Categories:

Category 1 – M&TE that is calibrated with traceability to a nationally recognized standard or physical constant, performed under controlled conditions and by an evaluated and accepted calibration laboratory, agency, or metrology facility.

Category 2 – M&TE that can be calibrated prior to and verified prior to and after use, by the user, with certified standards traceable to a nationally recognized standard or physical constant. The calibration frequency shall be called out in the associated instrument operating procedure.

Category 3 – Commercial devices procured as normal commercial equipment that provide adequate accuracy, such as rulers, tape measures, graduated glassware.

6.1.3.3 Video Cameras

At least three stably mounted (e.g., tripod) digital video cameras (Brinno TLC200 Pro time lapse cameras) were used to provide continuous recording of the RT tests: 1) Side View, Level – the primary level measurement camera was relatively tightly focused on one of the affixed rulers near the liquid surface (e.g., ~12-cm field of view at position A); 2) Side View, Panorama – this camera provided a macroscopic (panoramic) view to capture motion visible along the wall in the slurry layers, at the slurry-liquid interface, and the liquid surface; and by placing it with one of the rulers in view, it also served as secondary level measurement camera (with lower expected height resolution); and 3) Overhead View – this camera provided qualitative information on surface motion at the liquid surface and the slurry-liquid interface, depending on clarity of the liquid. The video cameras have internal clocks that were synchronized at the start of the test to within 5 seconds of each other, and typically to within 1 to 2 seconds. Camera images were recorded at one frame per second (1 Hz) to SD memory cards (e.g., 32 Gb capacity sufficient for approximately three days recording, depending on the amount of visual action). Data on memory cards were uploaded to a personal computer for processing, including preparation of videos to show events of interest and review of individual frames for surface level vs. time data. The latter capability was used for subsequent quantification of gas retention and release.

6.1.4 Mixers and Containers

Approximately 15-L batches of slurry simulant for 10-in. and 23-in. vessel tests were prepared in 5-gal plastic buckets. The buckets were used for both dry blending of solids and mixing of solids with water and other liquids (see Section 6.2). A double-auger mixer was used for the slurry mixing steps (Northern Industrial Tools Double Auger Mortar Mixer; 2-speed, 800 rpm maximum; 22-in. long shaft with ~6-in. long mixer paddle). Only one of the two included mixing paddles was used in the 5-gal bucket batches (i.e., effectively a single-auger mixer, but the term “double-auger” is used throughout this report). For 70-in. vessel tests, two of the double-auger mixers were typically used simultaneously in the preparation of each ~110-gal to ~120-gal batch of slurry in a ~120-gal plastic, rectangular trough (2-ft H × 2-ft W × 4-ft L) or in up to ~150-gal plastic feed troughs. Solids for these large batches were dry blended in other plastic feed troughs, also using the double-auger mixers. Figure 6.2 shows two two-man mixing teams preparing a batch of dyed upper-layer slurry in one trough and a batch of lower-layer slurry (natural color, pre-H₂O₂) in another, shortly after solids addition.



Figure 6.2. Preparation of ~110-gal Batches of Naturally Colored Lower-Layer Slurry (foreground) and Dyed Upper-Layer Slurry (background) by Two Teams Manning Double-Auger Mixers with Additional Staff Support

6.1.5 Slurry Pumps and Distributors

Slurry was added to the 10-in. and 23-in. vessels using conventional peristaltic pumps with large-bore flexible tubing (e.g., 0.625-in. O.D. \times 0.125-in. wall). A 1-in. diaphragm pump and reinforced transparent plastic tubing with metal quick-disconnect fittings were used to fill the 70-in. vessel. In all the vessels, the bottom slurry layers were added directly from the tubing. The upper slurry layers were added through a vertically oriented section of steel tubing (e.g., 1-in. O.D.) that terminated a few inches above attached, shop-built distributor plate assemblies. The assemblies incorporate a horizontally-oriented solid metal plate that is centrally located beneath the down tube and transfers vertical slurry momentum to radial, horizontal flow. A larger diameter circular perforated metal plate (or stiff mesh) is attached to and extends radially outward from the central plate. The slurry spreads across and through these distributor openings. The distributor used in 10-in. and 23-in. vessel tests has a diameter of ~5 in. (~13 cm) and for 70-in. vessel filling it is ~18 in. (0.46 m) across. The down tube and distributor are mounted to a horizontal metal framework (or plate for the smaller vessels) that straddles the upper rim of the vessel, even when the assembly is pushed to an edge of the vessel. This allows the slurry distributor to cover the vessel surface while maintaining horizontal flow. The vertical down tube passes through a standard bulkhead fitting (e.g., Swagelok) that is rigidly fixed to the framework and uses nylon or Teflon ferrules to allow the elevation of the distributor to be adjusted during filling. The distributor assembly and layering process during an RT test in the 70-in. vessel are shown in Figure 6.3.



Figure 6.3. Slurry Distributor Being Used for Spreading Dyed Upper-Layer Slurry Over the Gas-Generating Lower Layer in a 70-in. Vessel Test¹

6.2 Simulant Preparation

Batches of simulant for RT testing were prepared to established recipes with the expectation of achieving target simulant properties, consistent with those necessary to complete the goals of the RT test program (see Section 2.0 and Section 4.3). Prior to make-up of a batch of simulant, adjustments in the solids weight fraction were made, as necessary, to achieve target simulant properties, but no in-process adjustments to simulant formulations were permitted or made (consistent with TP requirements). During simulant preparation, shear strength and density of representative batches were tested and compared to expected values to determine whether the simulant was within the acceptance range given in Table 6.2 (Section 6.4.1). To complete the characterization, shear strength/rheology and pH were also measured in the course of testing (see Simulant Characterization, Section 6.3, and RT Test Simulant Properties, Section 7.0).

Acidified (pH-adjusted) 90:10 Min-U-Sil 30:Bentonite was used for RT testing, and the original Test Matrix described in Section 4.3.2 was developed with FIO simulant property data for this simulant. Other than allowed adjustments in solids content (see above) and H₂O₂ concentration,² no revision in the simulant formulations was made in the course of RT testing addressed in this report.

6.2.1 Materials

The following materials were used in simulant preparation:

- Min-U-Sil[®] 30³ – A quantity of M30 fine-ground crystalline silica sufficient to complete the first twelve 10-in. and 23-in. vessel tests described in this report was acquired from a single lot. This material lot was also used in FIO simulant development testing to establish the previously noted τ_s and ρ_s vs. weight percent solids correlations for test planning purposes (Section 5.2). Additional

¹ Photos are courtesy of Robert E. Frank of WRPS and are shown in Quality Surveillance Report TF-13-QSR-107, Rev. 0, December 13, 2013.

² Adjustments in the pH target are also allowed, but were not made.

³ Min-U-Sil 30 is produced by Brenntag Specialties, Inc. and distributed by U.S. Silica.

pallets of M30 were acquired for 70-in. vessel and later 23-in. vessel tests. All the M30 was used as-received.

- Bentonite – A quantity of Big Horn[®] BH 200 bentonite clay sufficient to complete the testing described in this report was acquired in a single pallet purchase.¹ This material was also used in FIO simulant development testing to establish the previously noted τ_s and ρ_s vs. weight percent solids correlations for test planning purposes. It was used as-received.
- H₂O₂ – A quantity of nominally 3 wt% H₂O₂ sufficient to complete the first twelve 10-in. and 23-in. vessel tests described in this report was acquired in a single purchase, and additional quantities were acquired from the same source for 70-in. and later 23-in. vessel tests.² This material was used in FIO simulant development to assess gas generation rates, including those shown in Figure 5.1.
- Hydrochloric Acid – Certified NIST Traceable 2.0 M HCl in water or 6.0 M HCl diluted to 2.0 M was used in slurry batch preparation.³
- Water – Richland City tap water was used as-is for simulant preparation and supernatant liquid.
- Dye – A dye (e.g., blue) was added in low concentration to a portion of the simulant to distinguish lower and upper (dyed) slurry layers in the test vessel. The dye was dissolved in the batch water prior to addition of other simulant components.

6.2.2 Recipes

In each RT test, the final solids concentration was the same in the lower and upper slurry layers (see x_s in Table 8.1 of Section 8.1.1 and Table 8.2 in Section 8.2.1). However, the recipes for the two slurry layers differ, because the lower layer, or the only layer in SL tests, contains H₂O₂ to generate gas, and the upper layer contains dye but no H₂O₂. Simulant batch recipes for each slurry layer specified the following:

- the target total solids mass fraction, x_s
- the proportions (90:10 M30:B in all cases) and masses of M30 and bentonite
- the mass of water to achieve the final target solids concentration, reduced by the water content that was added with other components (i.e., HCl and H₂O₂)
- the concentration and mass of HCl solution for a final slurry pH target of 4.4⁴
- the type, final concentration, and mass of dye; 150 ppm of blue dye was used in each batch of upper-layer slurry

¹ Big Horn BH 200 bentonite, previously sold as CH 200, is supplied by Wyo-Ben, Inc.

² Ricca Chemical Company 4-L jugs indicate that the peroxide solution has a Certified Traceable to NIST Standard Reference Material Manufacturing Specification of 3.3 ± 0.1 wt% H₂O₂ (Cat. No. 3819-1). However, certification of the concentration is not required for this testing.

³ Because the HCl is used for gross adjustment of pH to approximate target values and not for analytical purposes, it is not necessary to know the concentration precisely (e.g., $\pm 5\%$ is acceptable) or to purchase it with QA clauses and certification. Label concentration of newly purchased stock is sufficient.

⁴ It was found in simulant development scoping tests with the materials acquired for these RT tests that the acid demand for 90:10 M30:B simulants to achieve a target pH in the 3 to 5 range is given approximately by $\hat{n} = -0.125pH + 1.066$, where \hat{n} is the specific acid demand in units mol HCl/kg bentonite.

- the mass and H₂O₂ solution concentration (nominally 3 wt%) to achieve an overall target H₂O₂ concentration in the bottom slurry layer; 0.10 wt%, 0.15 wt%, and 0.20 wt% concentrations were used in RT tests, as shown in Table 8.1 of Section 8.1.1 and Table 8.2 in Section 8.2.1.

6.2.3 Preparation

Vessel filling and RT testing started on the day following the start of simulant preparation. The delay allows the solids to hydrate and the pH to approach an equilibrium value (e.g., for ion exchange of H⁺ for Na⁺ in bentonite to approach equilibrium). The quantity of simulant needed for a test dictated the number of “identical” batches that needed to be prepared (e.g., in multiple 5-gal buckets or 120-gal troughs), either in parallel or series, minimizing the difference in age of the batches as much as possible. The standard simulant preparation process and the data obtained for each batch are as follows.

1. Target simulant component masses were specified in recipes.
2. Actual masses of all components used in the batch were weighed and recorded, along with the component concentrations and lot numbers, where applicable.
3. The solid materials (M30 and bentonite) were weighed and pre-mixed dry either by shaking (e.g., in 5-gal buckets) or using mechanical agitators such as the double-auger mixers described in Section 6.1.4. This step was often completed a day prior to the start of hydration and, therefore, two days before vessel filling.
4. Solids were added slowly to the specified quantity of water (and dissolved dye, if applicable, but without HCl and H₂O₂) while mixing with double-auger mixer(s).¹ This step typically took 5 to 10 min. for ~15-L bucket batches and approximately a half-hour for >100-gal batches prepared in troughs.
5. Once the water and solids were thoroughly mixed, mixing ceased and “pre-hydration” started. A pre-hydration period of 4 ± 1 hr was specified and used for all batches.
6. The pre-hydrated slurry was remixed, the time was noted, and the HCl solution was added slowly while mixing. This step typically took 10 min. or less.
7. The thoroughly mixed acidified slurry was allowed to hydrate/equilibrate (with optional intermittent remixing) for a specified duration of ≥24 hr (and <48 hr). In all tests reported here, the equilibration time was 24 hr or a few hours longer.
8. Approximately 1.5 to 2 hr before the slurry was added to the RT test vessel, at least one batch each of the upper- and lower-layer simulants was remixed and sampled for Simulant Characterization (Section 6.3).
9. After verifying that the measured shear strength and density of slurry samples from both layers met Acceptance Criteria (Section 6.4.1), and shortly before filling the RT test vessel, final simulant preparation steps were completed. The bottom-layer slurry was remixed, and the pre-weighed H₂O₂ solution was added while mixing with double-auger mixer(s), noting the time that addition started. The slurry was mixed with H₂O₂ for ~5 min. (or less in small batches), being thorough while avoiding

¹ Mechanical mixing was typically supplemented with manual mixing steps using spatulas and/or paddles to scrape the container walls and corners.

entrainment of air bubbles. To further reduce the amount of entrained air, final mixing was done by hand with spatulas and/or paddles to dislodge larger bubbles.

10. Upper-layer slurry batches were remixed prior to or during the addition of the lower slurry layer to the vessel. Again, effort was made to reduce the amount of entrained air.

6.3 Simulant Characterization

The key properties of slurries used as settled solids simulants in RT and SL tests were characterized and documented following the RPL-COLLOID-02 procedure, which is in accordance with the project QA program.¹

1. Each RT test – The following methods were applied to determine the physical (density, rheology) and chemical (pH) properties of ~600 mL or larger samples of the slurry simulants used in the lower layer or single layer (natural color, pre-H₂O₂ addition) and upper layer (dyed, gas-free):
 - a. Density, ρ_s , was determined by measuring the mass and volume of a sample placed in commercial off-the-shelf volume-calibrated 500 mL graduated cylinder. The measurement method and equipment were selected to give a typical density measurement accuracy of $\pm 2\%$ (and typically less than $\pm 1\%$).
 - b. The pH of slurries was measured using a pH meter that was user-calibrated and performance-checked using certified pH buffer solutions. The pH electrode was directly immersed in freshly mixed slurry, usually on the day following vessel filling and after measurement of the 18-hr shear strength (see Item c).
 - c. Shear strength, τ_s , was determined by the shear vane method using an instrument (e.g., Thermo Fisher Scientific HAAKE Viscotester 550) that was qualified with certified viscosity standards. The shear vane used has a cross-pattern (viewed from the end) and is 16-mm diameter \times 32-mm height. The shear strength was measured on thoroughly mixed samples that were allowed to stand undisturbed for ~1 hr (for Acceptance Criteria checks, see Section 6.4.1) and ~18 hr (basis of TP test matrix, Section 4.3.2).
 - d. The non-Newtonian simulant rheology was further characterized by obtaining rheograms with a rotational viscometer (e.g., Anton-Paar Physica MCR301 with concentric cylinder sample geometry and qualified with certified viscosity standards). Using software provided with the instrument, the data were fit to a two-parameter Bingham plastic model (e.g., defined by a yield stress, τ_0 , and a consistency (apparent viscosity at infinite shear rate), μ_∞); see Section 7.1.3.
2. Two RT tests – Using the protocols described in 1c), the shear strength of the slurry simulants used in the lower and upper layers in two RT tests (four slurry batches total) were measured on samples that had been allowed to stand undisturbed for varying durations to assess the transient development of shear strength. Seven measurements, including the standard 1-hr and 18-hr readings, were made on each sample covering a time period longer than the initial RT instability in each test. Large samples (e.g., 2 L) were used so that each shear strength measurement was made in an undisturbed region at least two vane diameters from other measurement locations. Results are discussed in Section 7.1.2.3.

¹ The analytical simulant characterization data were obtained following the guidelines of the most current version of the RPL-COLLOID-02 Procedure (Daniel 2011), “Measurement of Physical and Rheological Properties of Solutions, Slurries, and Sludges.” The current Revision Number is 2, effective March 11, 2011.

3. Water-dilution samples – In the single-slurry-layer tests, in which there is no upper layer, small portions of pre-H₂O₂ “lower-layer” slurry batches were diluted with water proportionate to the amount of H₂O₂ that would eventually be added (i.e., to give the same final solids concentration x_3). All the water-dilution samples were subjected to the suite of analyses described in 1) above. One of the dilution samples and another sample from the same batch that was not diluted (i.e., pre-H₂O₂ addition) were also used in a shear strength vs. time study like 2) above. Shear strength results for the water-dilution samples are discussed in Section 7.1.2.

6.4 Conducting RT and SL Tests

This section provides details of the approach and methods used in conducting RT and SL tests (Section 6.4.2). First, specific Test Requirements and Acceptance Criteria are summarized in Section 6.4.1.

6.4.1 Test Requirements and Acceptance Criteria

Specific Test Requirements and Acceptance Criteria that were applied and achieved in each RT and SL test are summarized in Table 6.2. These may be categorized as: a) simulant batch properties and quality; b) operating and test conditions; and c) test characteristics. Several of the items listed have no specific requirements, but they were measured for later evaluation of test consistency and possible modification of test parameters (e.g., revised H₂O₂ concentration based on measured gas generation rates and RT test duration). The remaining Requirements and Acceptance Criteria in Table 6.2 were evaluated prior to and during vessel filling, as is discussed further in the following subsection.

6.4.2 Test Steps

Single-slurry-layer tests are analogous to two-layer RT tests except that the upper dyed sediment layer is absent (i.e., the single layer is equivalent to a lower layer in RT tests). Therefore, SL tests can be conducted in the same manner as RT tests by deleting the steps associated with the upper slurry layer (e.g., no upper-layer slurry is prepared or analyzed, and the upper-layer thickness is set to zero). In the following, SL tests are treated as a subset of RT tests and, in general, are not called out separately unless differences, besides the absence of the upper layer, are noteworthy.

Each RT and test was assigned a unique test number, as outlined in Section 8.0. The procedure and specifications for conducting the tests were given in approved Test Instructions that referenced this test number. As with simulant recipes, target simulant batch properties and layer-by-layer simulant filling targets (level and mass) consistent with the test matrix conditions were provided in formally reviewed calculations. Data and other test information were recorded on test-specific bench or data sheets or in Laboratory Record Books. The following are representative test steps and summarize data that were acquired.

Table 6.2. Test Requirements and Acceptance Criteria

Quantity (Purpose of Measurement)	Requirement or Acceptance Criterion
Simulant Solids Content (Batch Quality)	As-made-up solids content within ± 1.0 wt% of recipe; determined by calculation.
Simulant Density (Batch Quality and Property)	Measured density within $\pm 3\%$ of the theoretical density calculated for the recipe (e.g., using Equation (5.3)).
Simulant Shear Strength (Batch Property)	After slurry acidification and equilibration, the shear strengths of the slurry for the two layers ^(a) measured one hour after mixing and sampling will be within 50% of the value determined in the previously established shear strength vs. solids content correlation (e.g., using Equation (5.2)).
Simulant Rheology, e.g., Bingham Yield Stress and Consistency (Batch Property)	No requirement; measurement only.
Simulant pH (Batch Property)	No requirement; measurement only.
Temperature (Operating Condition)	Simulant and laboratory temperature (at start of RT or SL test) in the range of 24 ± 8 °C.
Simulant Layer Thicknesses (Test Condition/Quality)	Individual and overall (gas-free) simulant layer thicknesses within $\pm 10\%$ of test matrix targets, as determined by fill mass and simulant density.
Gas Generation Rate (Test Characteristic)	No requirement; measurement only.

(a) For the bottom slurry layer, the shear strength was measured on a sample taken before H₂O₂ addition. Therefore, the sample had higher solids content and a higher shear strength target than the upper layer.

Slurry simulant for an RT or SL test was prepared as described in Section 6.2. As noted in step (9) of Preparation (Section 6.2.3), H₂O₂ addition to the lower-layer slurry and vessel filling could not proceed until it was determined that the slurry shear strength and density for both lower and upper layers met the Acceptance Criteria listed in Table 6.2. Additionally, the calculated simulant solids content, simulant temperature, and laboratory temperature had to satisfy Acceptance Criteria prior to starting the RT test.

Other preparatory steps were completed prior to starting the test. These included:

- Synchronizing camera clocks and other reference time-pieces to within 5 seconds or less
- Preparing time-lapse cameras, including labeling and installing memory cards and locating cameras in final (or near final) positions (Section 6.1.3.3)
- Placing the cleaned and dried vessel on the tared (zeroed) scale in a repeatable, earth-level position and recording the vessel tare weight (except for the 70-in. vessel, which was not removed from its floor scale between tests)
- Taring (zeroing) the scale with the vessel in place in preparation for slurry filling.

Once these steps and the pre-test Acceptance Criteria checks noted above were completed, vessel filling proceeded as follows:

- In many tests, one or more of the cameras were turned on to record the filling process.
- H₂O₂ Addition – H₂O₂ was added and mixed in the containers of lower-layer slurry (see step (9) of Section 6.2.3).

- Lower Slurry Layer Filling – As soon as practical after H₂O₂ addition was completed, lower-layer slurry was pumped into the vessel (Section 6.1.5) to a specified target mass (i.e., gas-free volume equivalent). For the strengths of materials used in these tests (Section 8.1.1), the slurry was sufficiently self-leveling that mechanical means were not necessary to flatten and smooth the lower-layer surface. Where beneficial and practical, small amounts of simulant smeared or splashed on the vessel wall above the fill level were removed (e.g., using a damp towel). The lower-layer slurry addition process typically took ~10 to 15 min. in the 10-in. and 23-in. vessels and ~20 min. in the 70-in. vessel.
- Lower Slurry Layer Acceptance Criterion – The final mass of lower-layer slurry added to the vessel was recorded and checked against the Simulant Layer Thickness Acceptance Criterion (Table 6.2) prior to proceeding to addition of the upper slurry layer to the vessel. The lower-layer slurry surface level at each ruler on the vessel was also recorded.
- Upper Slurry Layer Filling (not applicable to SL tests) – As soon as practical after the lower slurry layer was added, the upper-layer slurry filling process started. Slurry was pumped onto the lower-layer slurry using a distributor assembly (Section 6.1.5) to a specified target mass (i.e., gas-free volume equivalent). The distributor was positioned ~0.5 to ~2 cm above the lower-layer surface at the start of the filling process. Typically, a thin initial layer (e.g., ~0.5 to ~1 cm) of upper slurry was distributed “uniformly” across the lower slurry surface by continuously walking the distributor around the perimeter of the vessel and then spiraling toward the center. The distributor assembly was raised intermittently to keep it from submerging in the already added slurry, and filling proceeded by continually moving the distributor across the surface. As with the lower-layer slurry, the upper layer was relatively self-leveling and no mechanical flattening was required. Again, where warranted, small amounts of simulant that smeared or splashed on the vessel wall above the fill level were removed (e.g., using a damp towel). The upper-layer slurry addition process typically took ~10 to 20 min. in the 10-in. and 23-in. vessels and no longer than ~45 min. in the 70-in. vessel.
- Upper Slurry Layer Acceptance Criterion (not applicable to SL tests) – The final cumulative mass of slurry added to the vessel was recorded and the mass of upper slurry (determined by difference) was checked against the Simulant Layer Thickness Acceptance Criterion (Table 6.2) prior to proceeding to addition of the supernatant water to the vessel. The upper-layer slurry surface level at each ruler on the vessel was also recorded.
- Supernatant Water Filling – As soon as practical after the upper slurry layer (or single layer in SL tests) was added, the supernatant water filling process started. Much like the upper slurry layer filling process, water was pumped onto the upper-layer slurry using the same distributor assembly, which was cleaned after slurry addition was completed. Approximately 5 to 10 cm of water were spread across the slurry surface by walking the distributor around the vessel to minimize disturbance of the slurry. Subsequently it was possible to allow the distributor to remain stationary without disturbing the slurry surface. The distributor was raised intermittently, keeping it slightly above the liquid surface or slightly submerged to avoid splashing, and water was added to a specified target mass (i.e., volume equivalent). Water addition typically took ~10 to 15 min. in the 10-in. and 23-in. vessels and no longer than ~25 min. in the 70-in. vessel.
- Supernatant Water Layer Acceptance Criterion – The final cumulative mass of simulants added to the vessel was recorded and the mass of water (determined by difference) was checked against the Simulant Layer Thickness Acceptance Criterion (Table 6.2) as the last step in the filling process. The water surface level at each ruler on the vessel was also recorded.

- Fill Data, All Layers – As noted above, the mass of simulant added and surface level were recorded after filling each layer was completed. Additionally, the start and stop times of each layer addition were noted.

Effectively, the RT test started once the labor-intensive filling process¹ was finished. Test progress was monitored and tests were completed as follows:

- Cameras – If cameras were not located in their final positions before the filling process and/or the filling process was not recorded, the cameras were properly placed and recording was started. The cameras were operated throughout the test, except when stopped to check remaining storage capacity or to switch out memory cards. See Video Cameras, Section 6.1.3.3.
- Staff Operations – One or more staff monitored the test progress intermittently, recording the liquid surface level/time and other observations (e.g., slurry-liquid and bottom-upper slurry interface levels/time). Around-the-clock staff coverage of the experiment was not required or used, because the cameras monitored test progress continuously. Staff also periodically documented the lab temperature and the mass of simulant remaining in the vessel to assess evaporative losses, and they checked camera operations.
- Duration and Completion – The duration of an experiment varied due to numerous factors such as the gas generation rate and the retained gas fraction at the point of the initial RT instability (e.g., α_{RT}). Test completion was typically defined by the time of the first instability/GRE (if known) plus an additional period (e.g., 8 hr or more). This continued monitoring was used to track potential follow-on gas-release events.
- Cleanup – At the completion of a test, the vessel contents were emptied into a large volume plastic storage tote for future waste disposal, and the vessel was cleaned with water. Other than to meet test schedule demands, there was no driver for the timing of vessel cleaning.

6.5 RT and SL Test Data Analysis

Both qualitative and quantitative data were acquired in the vessel RT and SL tests. Qualitative data of interest include the nature and extent of slurry motion during an RT instability and the characteristics/mechanisms of gas release (e.g., relatively large coalesced bubbles readily released vs. small bubbles forming stable froths) in both RT and SL tests. The qualitative data were visual, observed directly by staff and/or recorded by video cameras. Additionally, key assumptions (Section 4.4) pertaining to vessel-spanning bubbles (none observed) and doming of the sediment surface above the liquid surface were evaluated based on the qualitative visual data.

Supernatant liquid level vs. time data were used to quantify changes in the volume of retained gas in periods of gas retention and resulting from gas-release events. Using these data in conjunction with the initial fill data, the gas volume changes can be expressed in terms of changes in retained gas volume fraction in a slurry layer, $\Delta\alpha$. These were the primary quantitative data derived from RT and SL test measurements. Initial fill data were also used to estimate the initial gas volume fraction retained in the lower (single) slurry layer, which allowed estimation of the absolute retained gas volume fraction, α , not

¹ A minimum of three and preferably four staff were engaged in preparing and filling the 10-in. and 23-in. vessels. About eight staff contributed to the similar activities for the 70-in. vessel tests.

just $\Delta\alpha$. In addition to direct application of gas volume fractions to the assessment of α_{RT} (or the gas fraction at the point of the initial spontaneous release in SL tests, α_{SR}) and the magnitude of gas releases (Section 8.0 in general and summarized in Section 8.5.1), these data are used to assess the modified energy ratio (Section 8.5.2), evaluate the RT instability criterion and the gravity yield parameter (Section 8.5.3), and extrapolate gas releases to full scale (Section 10.0).

More specific information on data sources, quantification, and use follow:

- Camera Level Data – Individual frame images obtained from the primary level measurement camera recordings were the main source of supernatant liquid level vs. time data. Staff reviewed video footage and recorded the data electronically (e.g., in a Microsoft Excel[®] spreadsheet) for subsequent gas fraction calculations. The frequency of recorded level data was commensurate with the rate of change of level, and it was also relatively high around events of interest, regardless of level change. Level was measured to the nearest 1 mm, and in many cases, changes of fractions of a millimeter were discerned and recorded.
- Other Level Data – Level measurements logged by staff during the test were used to supplement the camera data. For example, measurements made by eye were compared with by-camera measurements made at the same time to develop a parallax/refraction correction. In analysis of later tests (e.g., after the 12th test), only theoretical parallax corrections were made, with no by-eye modification.

6.5.1 Quantitative Data Analysis and Uncertainty

Use of these and other data in quantitative data analysis and estimation of uncertainty is described in the following. The description is geared toward RT tests, but is also applicable to SL tests. Variables with subscript RT, for example, α_{RT} , can be swapped with equivalent variables having subscript SR (spontaneous release) in an SL test.

The absolute gas volume fraction in the lower-layer sediment was calculated using several measurements:

- The mass of each layer that is loaded into the vessel
- The gas-free density measured on a sample of the upper layer (chosen because the upper layer is sampled at a time when the solids concentration is at the final value, whereas the lower layer is at a higher-than-final concentration because it is sampled before the H₂O₂ solution has been added) or measured on the water-dilution sample in SL tests
- The water (supernatant) density determined from a reference handbook for the system temperature
- The supernatant surface level measured by eye on the rulers at the fill-completion time and infrequently at later times (for by-eye compensation to the parallax/refraction correction, where used)
- The supernatant surface level measured at frequent intervals by viewing videos of the vessel and the primary ruler, with images recorded by a camera at a fixed elevation that is generally above or below the supernatant surface
- The level measurement camera working distance and visible range, along with vessel wall thickness, for theoretical parallax/refraction correction

- The linear correlation for volume of contents versus supernatant surface level (Section 6.1.2.1)
- The mass of the vessel and its contents, measured infrequently during the test.

The combination of layer masses and layer densities, together with the level-volume correlation, provided a baseline value for the total system volume at zero gas.

$$V_0 = V_{0,up} + V_{0,low} + V_{0,sup} = \frac{m_{0,up} + m_{0,low}}{\rho_S} + \frac{m_{0,sup}}{\rho_L} \quad (6.1)$$

In Equation (6.1), V_0 is the total volume at zero gas, the other V_0 variables are the gas-free volumes of the upper (subscript “up”), lower (subscript “low”), and supernatant (subscript “sup”) layers, the m_0 variables are the initial masses of the upper, lower, and supernatant layers, ρ_S is the sediment density (as measured on the upper-layer sample), and ρ_L is the density of water at the system temperature at fill time. The time at which the fill of the lower layer was completed was used as $t = 0$ for all elapsed-time computations because it is the time after which there was no bulk disturbance of the gas-generating layer, although this was not exactly the same as the time at which the retained gas in the system was zero.

The supernatant surface level at zero gas was found using the level-volume correlation for the vessel (see Section 6.1.2.1):

$$L_0 = \frac{V_0 - b_{V/L}}{s_{V/L}} \quad (6.2)$$

where $s_{V/L}$ and $b_{V/L}$ are the slope and intercept of the linear relation for volume (V) versus level (L), $V = s_{V/L}L + b_{V/L}$.

The change in level from this gas-free baseline is proportional to the volume of retained gas. However, the measured levels generally could not be used as-is, but required correction for two sources of error, optical and evaporative.

Nearly all of the supernatant surface level measurements came from reading camera images, which were close-up views of the primary ruler on the outside of the vessel and the supernatant interface inside the vessel. Because the camera level is not the same as the surface level and the ruler is separated from the meniscus by the wall thickness, a parallax error was introduced into the level measurement read from the images. In addition, there is a refraction error because the meniscus is viewed through the transparent acrylic wall, whose refractive index is not the same as that of air.

The combined parallax/refraction error was assumed to be a linear function of the difference between the meniscus level and the camera level, a reasonable assumption for small differences in level. For the first 12 tests, the combined error was estimated by comparing measurements made by eye, which have no parallax or refraction error because the line of sight is perpendicular to the vessel wall, with by-camera measurements made at the same time. The comparison provided a ratio of the optical error to the distance of the meniscus above/below the camera level, with the error being zero at the camera level. For analysis of later tests, a theoretical parallax/refractive index correction was made using information about camera position and visible range along with the measured vessel wall thickness.

Evaporative volume loss was estimated using measurements of vessel mass at various times during the test. The mass loss rate was calculated for each increment of mass loss, and the average of the mass loss rates was used to represent the mass loss rate over the entire test.

The level change from the gas-free level, after corrections, was used to determine the volume fraction of gas, α , in the gas-containing lower layer.

$$\alpha = \frac{\Delta L}{\Delta L + L_{0,low}} = \frac{L + \Delta L_{optic} + \frac{\dot{m}_{evap}t}{A\rho_L} - L_0}{L + \Delta L_{optic} + \frac{\dot{m}_{evap}t}{A\rho_L} - L_0 + \frac{V_{0,low} - b_{V/L}}{s_{V/L}}} \quad (6.3)$$

In Equation (6.3), ΔL_{optic} is the correction for the combined parallax/refraction error, \dot{m}_{evap} is the average mass loss rate from evaporation, t is the elapsed time, and A is the vessel cross-sectional area.

The gas was assumed to be present only in the lower layer, an assumption that allows the calculation of the gas volume fraction in the lower layer (gas volume/gassy layer volume) and the specific gas ratio (gas volume/gas-less layer volume). In practice, there were some observations of bubbles at the wall in the lower part of the upper layer. These are believed to have been present because the gradual compaction of the lower layer forced a small amount of its gas-generating liquid up into the upper layer. The liquid is thought to have risen further near the wall than in the bulk of the upper layer.

A specific gas ratio ϕ , which is the retained gas volume per volume of gas-free lower layer, was also calculated as $\phi = \alpha / (1 - \alpha)$. Using the specific gas ratio, the volume of gas released by the RT event per volume of gas-free lower layer was

$$\frac{V_{rel}}{V_{0,low}} = f_{exp}(\phi_{RT} - \phi_{post-RT}) \quad (6.4)$$

The difference term in parentheses is the difference between the maximum ϕ_{RT} corresponding to the release time observed on the video and the minimum subsequent $\phi_{post-RT}$. The factor f_{exp} converts a gas volume at in-situ pressure (taken to be the pressure halfway up the bottom layer) to a gas volume at atmospheric pressure:

$$f_{exp} = 1 + \frac{(m_{0,sup} + m_{0,up} + 0.5m_{0,low})g}{AP_A} \quad (6.5)$$

where g is gravitational acceleration and P_A is atmospheric pressure (assumed to be 1 atm). Although the expression above is precisely accurate only when evaporation and the motion of liquid out of the gas-retaining layer have not taken place, its error at later times is not significant.

The fraction of gas inventory released during the RT event is

$$\frac{V_{rel}}{V_{RT}} = \frac{\phi_{RT} - \phi_{post-RT}}{\phi_{RT}} \quad (6.6)$$

The uncertainties of the gas fraction and specific gas ratios were calculated using linearized error-propagation methods, where the error σ_y of a dependent variable y is related to the errors σ_{x_i} of a set of independent non-correlated variables x_i by the expression

$$\sigma_y = \sqrt{\sum_i \left(\frac{\partial y}{\partial x_i} \sigma_{x_i} \right)^2} \quad (6.7)$$

The measurement uncertainties used in this report were set equal to the resolution of measurements - for example, between 0.5 mm and 1 mm for the supernatant surface level measurements. The overall uncertainty in the absolute gas fraction at the time of release was between 1 and 2 vol% gas, often about 10% of the total gas fraction. Taking RT Test 23-05 as an example (see Section 8.1.3.2), the uncertainty in α_{RT} was 0.015 volume fraction. Zeroing the uncertainty assumed for the sample density (0.01 g/mL) reduced the gas fraction uncertainty by about one-third, and zeroing the uncertainties in the parallax correction and in the level measurements themselves reduced it by another one-third. Based on this assessment, significant uncertainty is contributed both by determination of the baseline (gas-free) level and by the subsequent level measurements.

Calculated gas release volumes do not depend on the baseline (gas-free) level, which reduces the uncertainty of releases as compared to the uncertainty of absolute gas fractions. Further decrease in the uncertainty of gas release volumes can result if the level change is small (giving the same parallax correction before and after release, so that the uncertainty of the change in parallax correction is small), and if the time over which release occurs is short (such that the evaporation during release is small and the uncertainty in evaporative loss can be disregarded).

7.0 RT Test Simulant Properties

As a precursor to discussion of the RT tests, the results of simulant characterization completed on slurries prepared for the tests are discussed in this section. Measured physical properties for the RT simulants and key correlations are discussed in Section 7.1. The RT test simulant rheological characteristics are compared to the properties of Hanford tank waste, chemical tank waste simulants, and other physical waste simulants in Section 7.2.

7.1 Test Batch Characterization Results

Equation (4.2) in Section 4.1.1 expresses the expected dependence of α_{RT} on the slurry simulant shear strength and density. Further, the original TP test matrix described in Section 4.3.2 was established on the basis of achieving target τ_S and ρ_S values for defined simulant recipes. Given the significance of these properties to the interpretation of RT test results, the measured τ_S and ρ_S values and other rheological properties for the slurry batches prepared for the RT and SL tests are discussed in this section. Except for intentional differences in recipes and target properties, 15-L batches prepared exclusively for 10-in. and 23-in. vessel tests are not distinguishable from the 110- to 120-gal batches prepared for 70-in. vessel tests. Therefore, RT simulant properties are treated as a whole, rather than distinguishing them by batch size. Slurry density is addressed briefly in Section 7.1.1. Shear strength data for samples collected from RT test batches are presented in Section 7.1.2. This includes discussion of the dependence of shear strength on the time that the slurry is left undisturbed and the effects of water dilution associated with the addition of H_2O_2 solution. Non-Newtonian simulant rheology is discussed in Section 7.1.3. More detailed measured property data for RT and SL test simulant samples are provided in Appendix B.

Note that the general RT test numbering scheme is described in Section 8.0. Test conditions and results for specific numbered RT Tests are also discussed in Section 8.0.

7.1.1 Density of RT Test Batches

The densities of slurry samples taken from batches prepared for each of the RT and SL tests were measured. They were all within ~1% of, and tended to be lower than, the theoretical density calculated using Equation (5.3). This is consistent with FIO measurements made on simulant development batches, as discussed in Section 5.2. Details of the density data for RT and SL test batch samples (and a plot) are provided in Appendix B (Section B.3.1). The most likely explanations for low slurry densities are: 1) residual moisture on the solid components, which would reduce the individual component and theoretical slurry densities; and 2) retention of small gas bubbles in samples, despite efforts to remove them by stirring before loading the graduated cylinder for the density measurement. A residual gas content of ~1 vol% due to entrainment during batch preparation, for example, is quite plausible and would fully account for a low slurry density of magnitude comparable to the retained gas fraction. Note, however, that density samples did not contain H_2O_2 , and, therefore, gas was not being generated during measurements.

7.1.2 Shear Strength

In each RT test, representative samples of slurry batches were taken before the test vessel was filled. The simulant characterization sample for the lower-layer slurry was taken before H₂O₂ was added, and therefore, it had higher solids content than the corresponding upper-layer slurry sample. The shear strength of each sample was measured post-mixing and standing undisturbed for ~1 hr and ~18 hr. For the RT tests in the three test vessels, the solids fractions in upper and lower-layer slurry samples ranged from ~42 wt% to ~54 wt%. For several tests, a portion of pre-H₂O₂ lower-layer slurry was diluted with water equivalent to the amount of H₂O₂ solution that would be added to the slurry just before filling the RT test vessel. These samples were prepared to assess the effect of H₂O₂ dilution on physical properties compared to upper-layer slurry batches that were already at the same final solids concentration. Dilution with water instead of H₂O₂ allowed the dilution effect to be investigated without further potential impact to properties due to changing quantities of retained gas. For a few RT test simulant batches and a water-dilution sample, the shear strength was measured as a function of time undisturbed after last mixing. In addition to the standard 1-hr and 18-hr shear strengths, these time studies provided information on the transient development of strength. Summary results of the various shear strength analyses are presented in this section.

7.1.2.1 Routine 1-hr and 18-hr Measurements

The results of the 1-hr and 18-hr shear strength measurements are shown in Figure 7.1 along with the exponential curve fits. The fits were made to a subset of the data obtained in the following way. There were 13 solids concentrations for which more than one measurement of shear strength had been made. At each concentration, the averages of all 1-hr and 18-hr shear strength measurements were calculated. Because these 13 averages were expected to be closer to the true mean than any individual measurement, they were used as the points to which exponential curve fits were made.

The final correlations of τ_S (Pa) with the solids fraction x_S ,¹ expressed in weight percent, are as follows:

Undisturbed for 1 hr:

$$\tau_S = 1.06 \times 10^{-2} \exp(1.59 \times 10^{-1} x_S) \quad (7.1)$$

Undisturbed ~18 hr:

$$\tau_S = 1.84 \times 10^{-2} \exp(1.56 \times 10^{-1} x_S) \quad (7.2)$$

¹ In TP-DSGREP-001 Rev. 4.0 (and earlier versions 1.0, 2.0, and 3.0), the shear strength correlations that were used for test planning purposes were based on four 15-L batches of slurry. The FIO correlations for these 15-L batches corresponding to Equation (7.1) and Equation (7.2) were:

$$1 \text{ hr: } \tau_S = 4.88 \times 10^{-3} \exp(1.72 \times 10^{-1} x_S)$$

$$18 \text{ hr: } \tau_S = 1.83 \times 10^{-2} \exp(1.54 \times 10^{-1} x_S)$$

Shear strengths calculated with these “planning” correlations are lower than the values determined with the final correlations (e.g., 40.4 Pa vs. 44.9 Pa at 18 hr for 50-wt% solids, or ~10% lower).

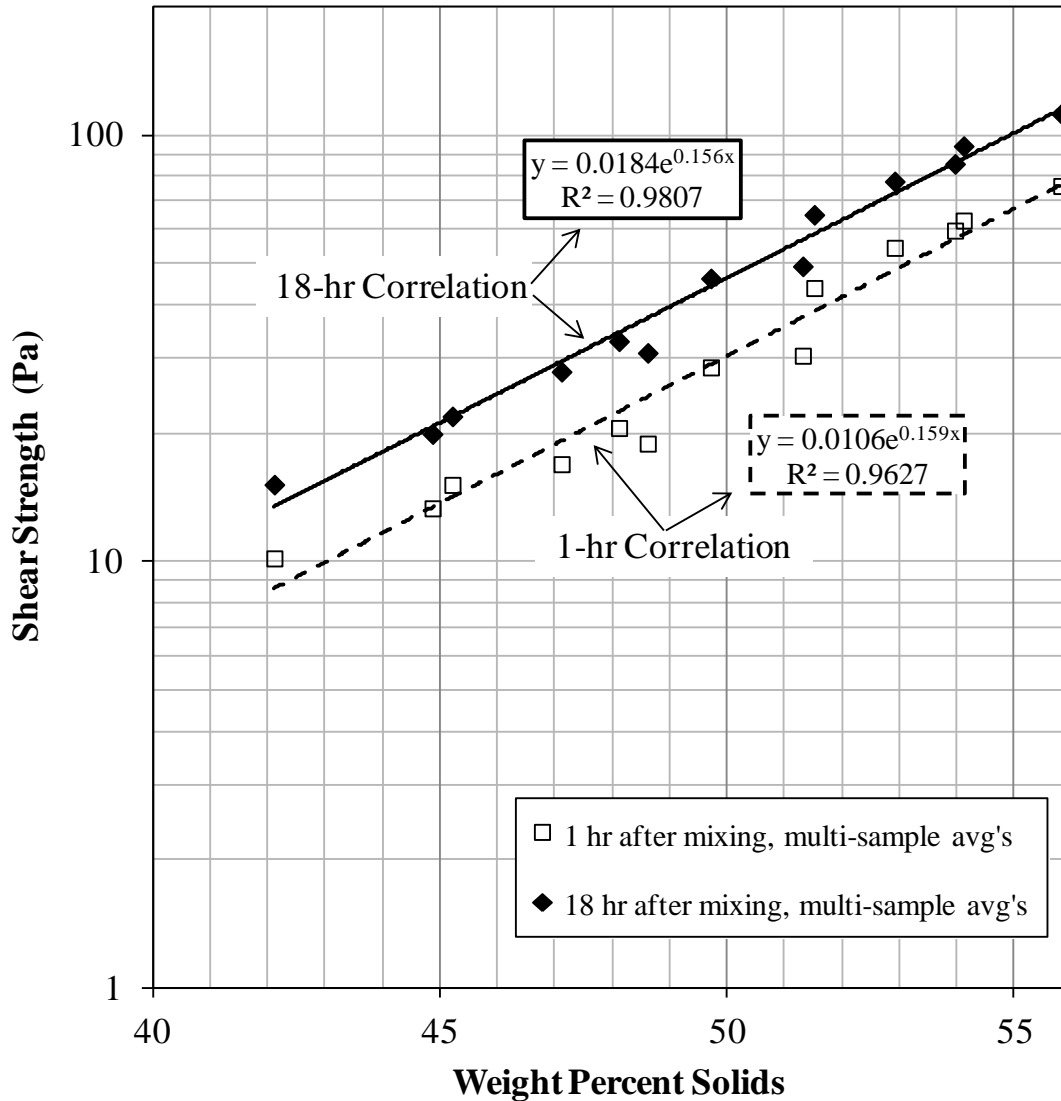


Figure 7.1. Multi-Sample Average Shear Strength Data for RT Test Batches and Corresponding Exponential Correlations as a Function of Slurry Solids Content (1-hr and 18-hr τ_s)

7.1.2.2 Effect of Dilution

In several of the later RT tests, pre- H_2O_2 lower-layer slurry samples were diluted with water equivalent to the amount of H_2O_2 solution that would be added, thereby giving a final solids content equivalent to a typical upper-layer slurry. Results for shear strength measurements taken ~1 hr and ~18 hr after dilution and standing undisturbed are shown in Figure 7.2.

Figure 7.2 compares the shear strengths of water-diluted samples (x and + symbols) to the 1-hr and 18-hr τ_s correlations (lines) developed for undiluted (upper layer) and pre-dilution (lower-layer) slurry samples and shown in Figure 7.1 (discussed in Section 7.1.2.1). Figure 7.2 also shows the shear strengths for pre-dilution slurry samples (squares and diamonds) for the same batches from which the water-diluted

samples were prepared. For clarification, note that the pre-dilution sample for a given test has a solids concentration 3-4 wt% greater than that of the water-diluted sample. The data indicate that the water-diluted sample shear strengths tend to track at lower values than the general τ_s correlations and the trend for the five pre-dilution batch samples. The latter also tend to trend below the correlation line for undiluted samples.

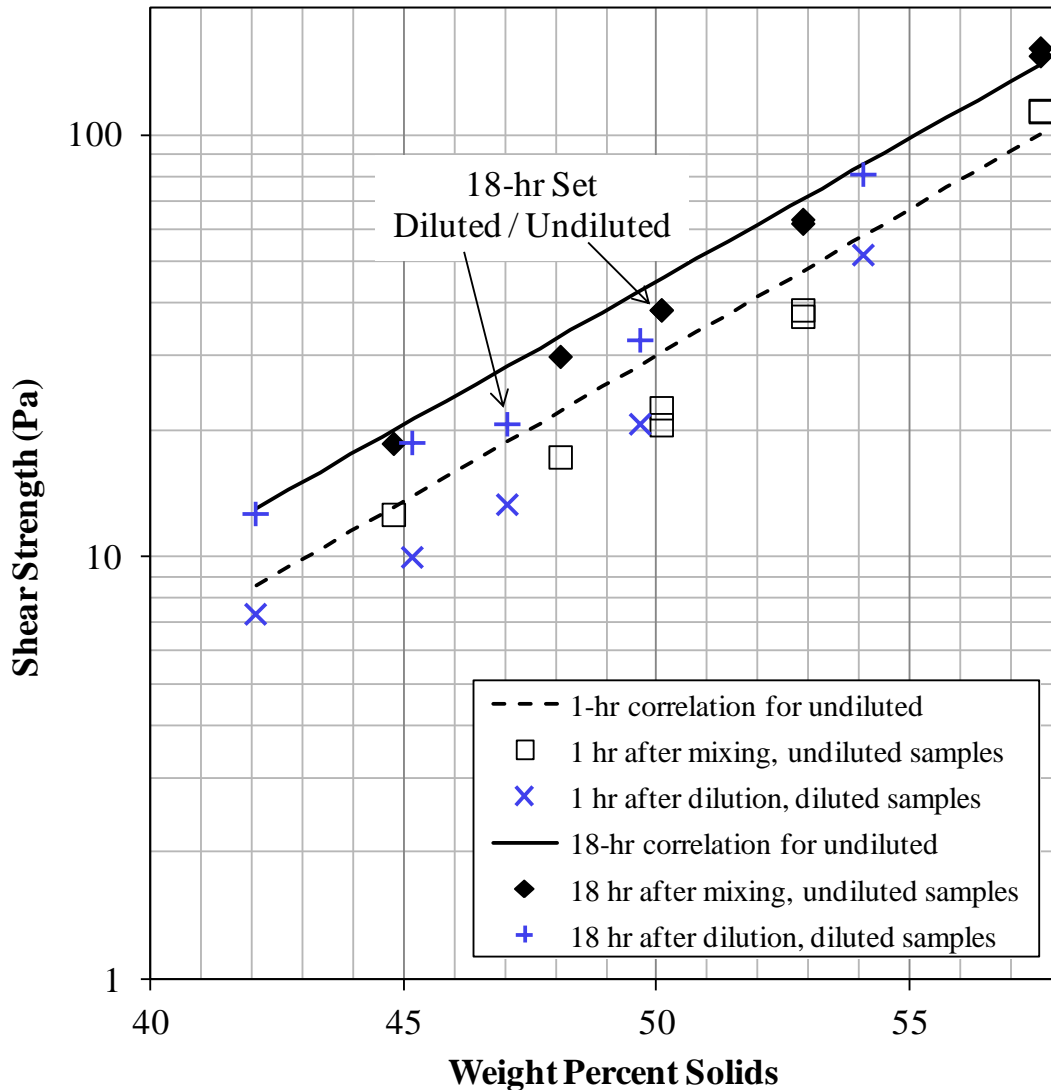


Figure 7.2. Shear Strength Data for Simulant Samples Diluted with Water and Pre-Dilution (Undiluted) Samples from the Same Batches Compared to Correlations for Undiluted Sample Averages (Arrows mark the 47.1 wt% [21 Pa, 18 hr] water-diluted sample and the undiluted 50.1 wt% [39 Pa, 18 hr] batch sample from which it was prepared.)

In the worst 18-hr case, the τ_s for the 47.1-wt% water-diluted sample (21 Pa) is 25% lower than the correlation at the same solids content (28 Pa). However, note that the 18-hr τ_s for the corresponding pre-dilution sample (50.1 wt%), is also lower than the correlation, in this case by 16% (39 Pa measured vs. 46 Pa correlation). In general, there is a decrease of roughly 20% in shear strength that is due to dilution alone (i.e., not including the variability in the pre-dilution sample). This difference is for samples

that were diluted with water to the same extent as batches whose target H₂O₂ concentration was 0.2 wt% (as it typically was in the 23-in. tests). A target concentration of 0.1 wt% H₂O₂, which was used in most of the 70-in. tests, would have corresponded to half that dilution and likely half the effect. The implication of these results is that during RT testing the shear strength of the H₂O₂-diluted lower layer could have been 10-20% less than that of the undiluted upper layer, the strength of whose samples was used to characterize both the upper and lower layers. Based on Equation (4.1), when two layers have different shear strengths the average of the two strengths should be used in calculations (such as calculations of Y_G or expected α_{RT}). Had this been done, the shear-strengths in calculations would have been 5-10% lower than the ones that were actually used. To put this in context, the relative standard deviation (RSD) of shear-strength measurements, based on measurements for multiple samples all at the same solids concentration, could be anywhere from 2% to 14%. The difference between the two-layer average shear strength (accounting for dilution) and the upper-layer shear strength (actually used in calculations) is less than the measurement variability.

7.1.2.3 Time Dependence of Shear Strength

For a few RT tests, shear strength was measured as a function of time undisturbed after last mixing, t_u . Multiple τ_s measurements were made in between and beyond the standard 1-hr and 18-hr characterization times. Results for four slurry samples collected in two RT tests (70-09 and 23-10, see Section 8.1.1) are shown in Figure 7.3. The two samples in each test are for higher solids content lower-layer slurry obtained prior to addition of H₂O₂ (52.9 wt% in 70-09 and 44.8 wt% in 23-10), and the fully-prepared and lower solids content upper-layer slurry (49.7 wt% in 70-09 and 42.1 wt% in 23-10). The 23-10 simulant recipe was used in several of the reported RT tests, and it has the lowest solids content and shear strength target used in all the RT tests. The solids content of the 70-09 simulant bounds the upper end of that used in all the 23-in. tests, and it is in the middle of the range for tests conducted in the 70-in. vessel. Therefore, the time dependence of the development of shear strength shown in Figure 7.3 should be representative of the behavior for the RT tests that are reported.

Figure 7.3 shows that the shear strength of the M30:B simulant continues to increase well beyond 18 hr. In the case of the 70-09 samples, τ_s measured after ~70 hr were approximately 40% higher than the values measured at ~18 hr. The continued development of strength is likely due to a number of time-dependent physical and chemical processes, including compaction (settling), hydration and physico-chemical bond formation, and pH changes due to ion exchange (e.g., H⁺ for Na⁺ on bentonite). The figure shows that the data can be well represented by an empirical power-law model of the form

$$\tau_s = \tau_c t_u^n \quad (7.3)$$

where τ_c is a constant, which is essentially the fit τ_s at $t_u = 1$ hr. The power-law exponent n varies from 0.166 to 0.202 in the four curve fits shown in Figure 7.3, with an average of 0.185, and it tends to be lower for the lower strength data and if the long-time data are excluded from the individual curve fits.

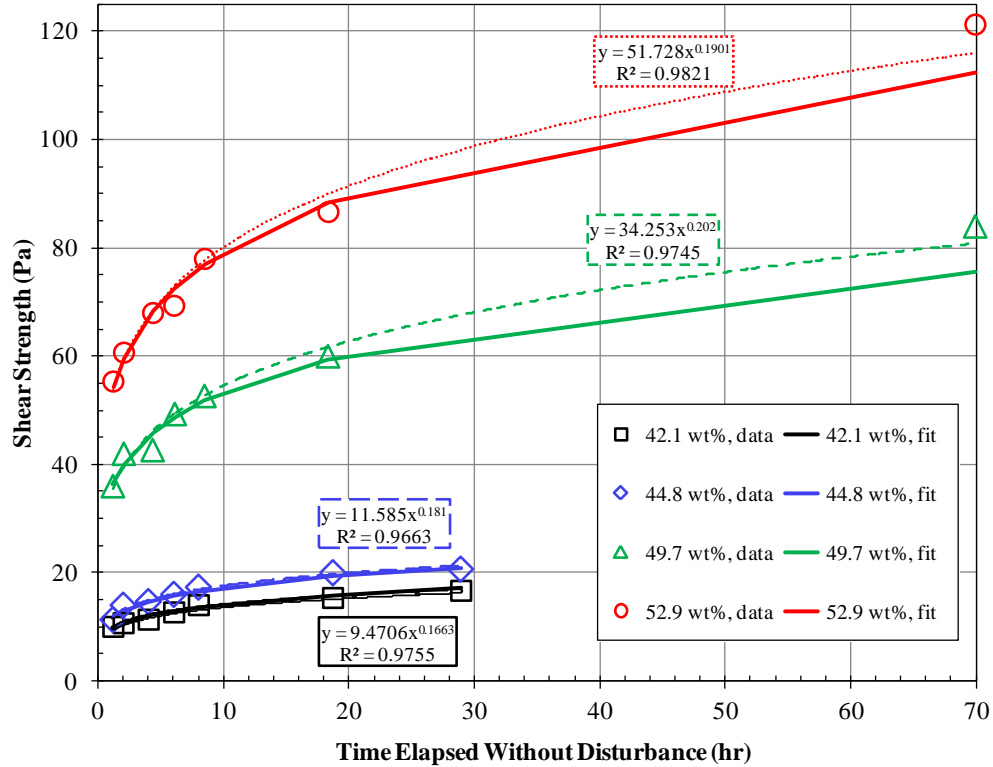


Figure 7.3. Shear Strength Data as a Function of Time Undisturbed for Four RT Test Samples. (Power law fits are shown by thin lines and equations; and universal fits using $n = 0.18$ are the thicker solid lines shown in the legend.)

For the purpose of estimating the shear strength of slurry at the time of RT instability events in experiments in which only 1-hr and 18-hr τ_S data are available, Equation (7.3) can be used as a “universal” model by setting n to a constant value, e.g., 0.18 (the average rounded to 2 digits). The shear strength constant τ_c varies from test to test due to formulation and variability in batch preparation, but it is nominally the measured 1-hr τ_S value. For constant n , τ_c can also be estimated by rearranging Equation (7.3) and applying it to data obtained at any t_u

$$\tau_c = \frac{\tau_S}{t_u^n} \quad (7.4)$$

An average τ_c can be determined by applying Equation (7.4) separately to the 1-hr and 18-hr τ_S data in each RT test and taking the mean of the results. In this way, the 1-hr and 18-hr τ_S data are equally weighted. The universal curve fits shown in Figure 7.3 were obtained using this τ_c averaging approach and $n = 0.18$. Like the individual power-law curve fits, the universal model tends to underestimate the lone long-time shear strength in the higher solids slurries, but the fit through the 18-hr data is very good in all four cases. This method of providing best-estimate τ_S values was used in the calculation of Y_G and ER_S that are discussed below (Section 8.5).

As shown in Figure 7.4, limited shear strength time-dependence studies were also conducted on a high solids content pre- H_2O_2 lower-layer slurry sample (SL Test 70-30; 57.6 wt% solids, red circles) and a water-diluted sample (54.1 wt% solids, green triangles) prepared from a portion of the same batch. The

solids content of the diluted sample was equal to that of the lower-layer slurry after H₂O₂ had been added to it. The data series for this undiluted/diluted sample pair in Figure 7.4 (circles and triangles) are not expected to overlay, in the same way that upper and lower-layer sample results for a given RT test do not coincide in Figure 7.3. The lines in Figure 7.4 show the strength expected for each of these samples based on the power-law correlation developed above. The correlation seems to give reasonable results, even though it was developed for samples with lower solids concentrations and no dilution effect.

Figure 7.4 also shows the 1-hr and 18-hr τ_s data for an undiluted upper-layer slurry sample (RT Test 70-20; 54.1 wt% solids, blue diamonds) with the same solids content as the diluted SL Test 70-30 sample. The difference between these data and the diluted 70-30 slurry (triangles) is caused partly by sample-to-sample variability and partly by dilution. The diluted 70-30 sample has shear strength about 15% less than that of the undiluted 70-20 sample with the same concentration at 18 hr. This is consistent with the results that were shown in Figure 7.2. At 96 hr, the measured shear strength for the diluted 70-30 sample is nearly equal to the correlation prediction for the undiluted 70-20 sample. It seems reasonable that at a sufficiently long time after dilution the effect of dilution would vanish.

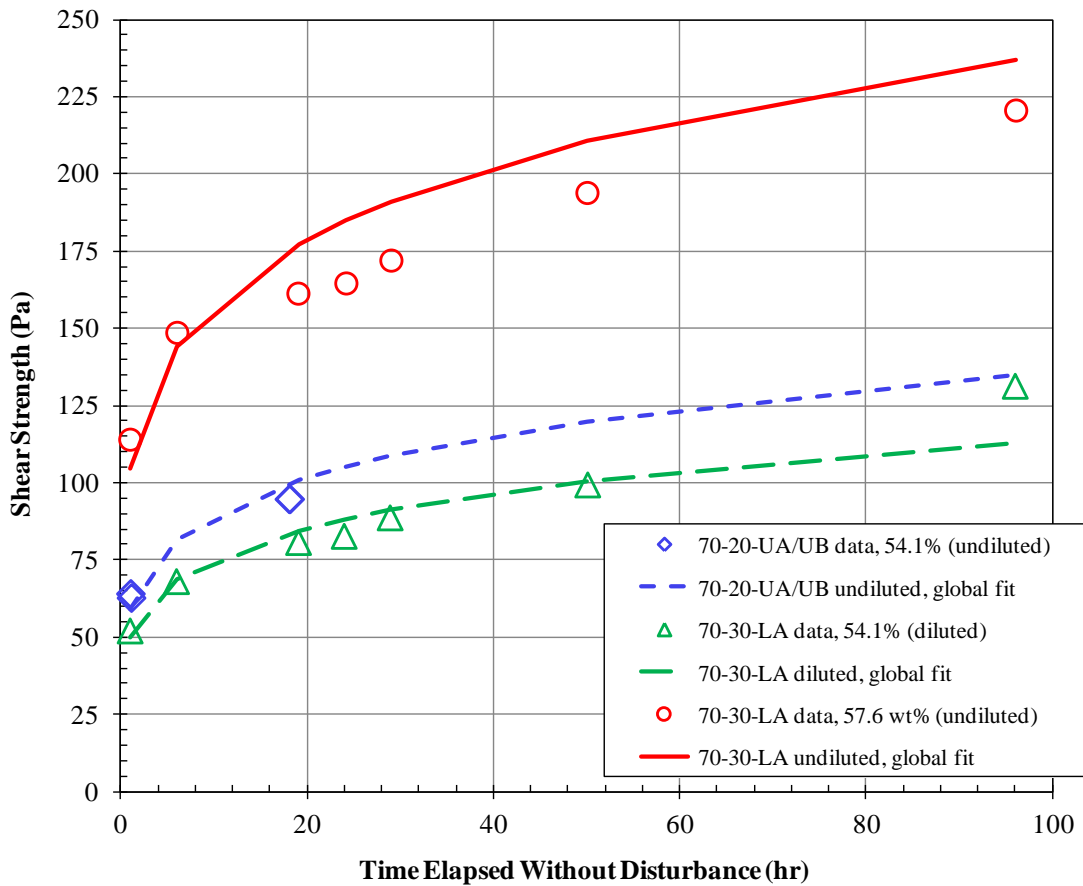


Figure 7.4. Shear Strength Data as a Function of Time Undisturbed for a Lower-Layer Slurry Sample and a Water-Diluted Sample

7.1.3 Non-Newtonian Rheological Properties

Using a rotational viscometer, as described in Section 6.3, rheograms were obtained for simulant samples taken from RT test batches. Rheograms for 13 representative samples from RT test batches are shown in Appendix B (Section B.3.1). They show the measured shear stress, τ , as a function of the shear rate, $\dot{\gamma}$ (typically in units s^{-1}), applied by the instrument. The non-Newtonian rheology of the slurry can be represented by a number of empirical models, including the two-parameter Bingham plastic model, which is given by

$$\tau = \tau_0 + \mu_{\infty} \dot{\gamma} \quad (7.5)$$

The Bingham parameters are the yield stress, τ_0 , and the consistency, μ_{∞} .

The consistency is also the viscosity of the non-Newtonian material in the limit of infinite shear rate, as determined from the Bingham model. The apparent viscosity, μ_{app} , at any shear rate is the shear stress divided by the shear rate. Using Equation (7.5), the apparent viscosity at a given shear rate can be estimated from the Bingham model parameters

$$\mu_{app} = \mu_{\infty} + \tau_0 / \dot{\gamma} \quad (7.6)$$

In this form, it is clear that the apparent viscosity equals the consistency as the shear rate tends toward infinity. Conversely, μ_{app} is dominated by the Bingham yield stress term at low shear rates (e.g., $< 1 \text{ s}^{-1}$).

Appendix B shows measured rheograms for selected single samples at the same 13 solids concentrations for which averages of shear strengths and Bingham properties had been calculated. The samples were selected for having Bingham properties near the calculated average for the solids concentration. Each sample was run through two cycles, ramping the shear rate up from zero to $1,000 \text{ s}^{-1}$ and then back down to zero in each cycle. The Bingham properties of yield stress and consistency were obtained by fitting a line to the shear rate and shear stress (y-axis) data in the second down-ramp between 150 and 850 s^{-1} ; this fitting calculation was performed by the rheometer software. The Bingham yield stress was the y-intercept of the line, and the consistency was the slope.

Figure 7.5 compares the Bingham yield stress of RT test simulants to the 1-hr and 18-hr shear strengths for varying solids content. The dependence on solids concentration is similar for the Bingham yield stress and the 18-hr shear strength, with the ratio of yield stress to 18-hr shear strength being approximately one-third (~ 0.35). The Bingham consistency in units of centiPoise ($\text{cP} = \text{mPa}\cdot\text{s}$) is also plotted. The lines in the figure represent fits of the 13 selected data points to an exponential function of the form used to correlate shear strength vs. solids data (e.g., Equation (5.2)). The correlations are

Bingham yield stress:

$$\tau_0 = 2.63 \times 10^{-3} \exp(1.75 \times 10^{-1} x_S) \quad (7.7)$$

Bingham consistency:

$$\mu_{\infty} = 1.88 \times 10^{-1} \exp(9.96 \times 10^{-2} x_S) \tag{7.8}$$

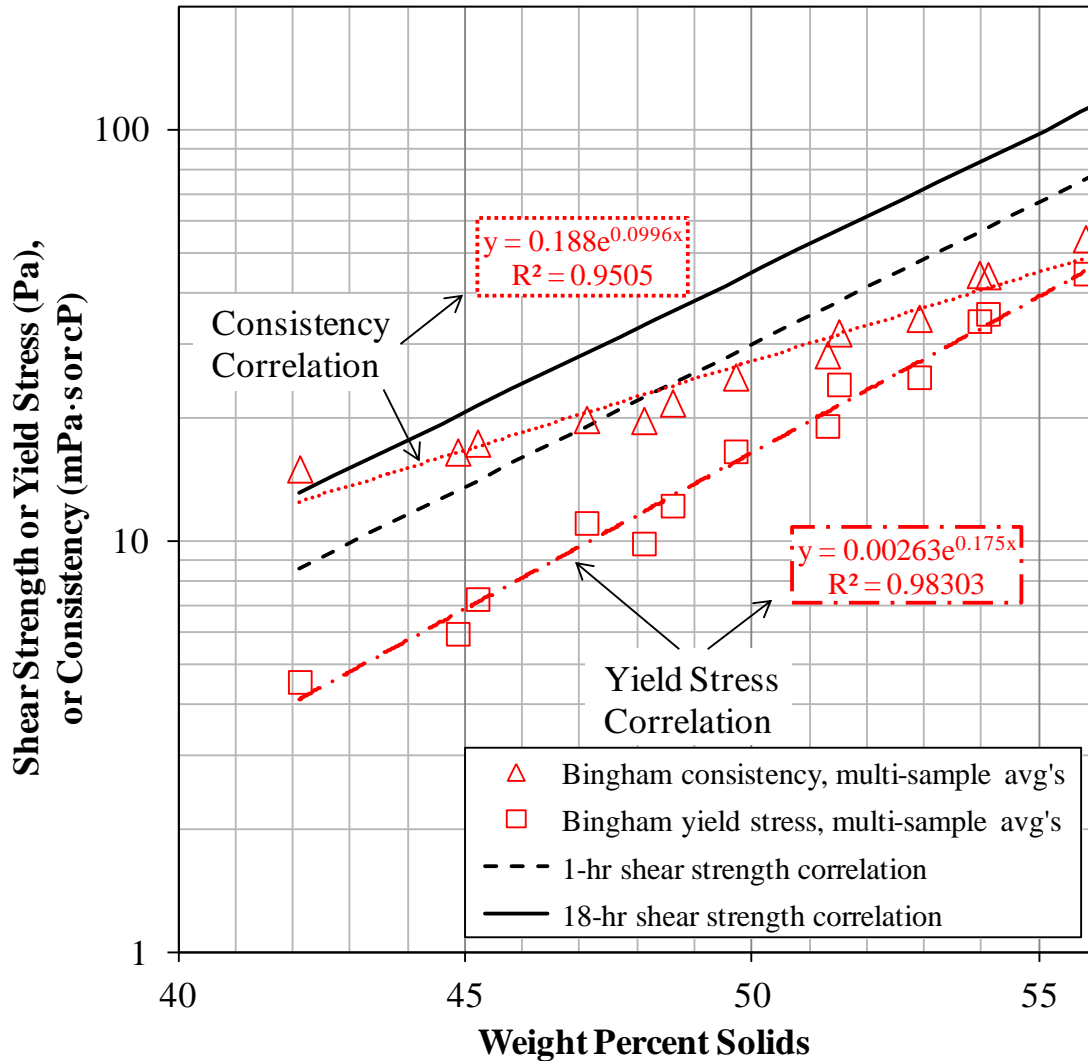


Figure 7.5. Correlations for Bingham Model Parameters Developed from Select RT Test Simulant Batches of Varying Solids Content and Comparison (of Yield Stress) to Shear Strength Correlations

The 13 averages of measured Bingham parameters for RT test simulant are compared to Hanford tank waste properties in Section 7.2, and the Bingham parameter correlations are used to support the full-scale tank RT instability gas-release simulations described in Section 9.0.

7.2 Comparison of Simulant and Hanford Tank Waste Rheology

Measured values of the Bingham model parameters for batches of M30:B simulant used in RT tests (see previous section) are compared to the rheological properties of a large number of Hanford tank waste samples in Figure 7.6. The figure and actual waste data shown in it are adapted from Wells et al. (2011b).¹ Also shown in the plot are FIO data for relatively strong kaolin and bentonite clay physical waste simulants² and previously reported data for chemical simulants at a number of concentrations and strengths, reproduced from Wells et al. (2010). The two chemical simulants are CBM-3, which has been used in filtration and dissolution tests, and a simulant representing the composition of a mixture of wastes from Hanford tanks 241-AN-101, C-104, C-111, and C-112. The data show that the relationship and trend of Bingham yield stress to consistency in the RT test simulant is consistent with Hanford waste and a variety of simulants often used to represent it.

The shear strength of the highest-viscosity (most concentrated) CBM-3 simulant shown in Figure 7.6 was 921 Pa immediately after stirring and 1383 Pa at 24 hr after stirring. The more concentrated AN-101/C-tank simulant also had high shear strength, 775 Pa immediately after stirring and 1133 Pa at 24 hr. The Bingham yield stresses of these chemical simulants are not greatly different from the yield stress of the most concentrated RT simulant, but the shear strengths of the chemical simulants are considerably greater than that of the RT simulant that has about the same Bingham yield stress (i.e., for the chemical simulants, the ratios of shear strength to yield stress are higher). Reported measurements for Hanford tank waste indicate variability in the shear strength / yield stress relationship (see, for example, Gauglitz et al. (2009)).

If waste in tanks AN-101 and AN-106 has properties like the chemical simulants, the shear strength to yield stress ratios could be much higher than the ratio for RT simulant (approximately 3). This implies that waste having shear strength of ~1000 Pa could have lower yield stress than the RT simulants. In turn, this would lead to lower apparent viscosities in the waste (at low shear rate) that could increase gas releases associated with events in which the waste is sheared. The expected mechanism of increased gas release is a lower effective viscosity, primarily produced by lower yield stress, which would allow faster rise of bubbles through the yielded slurry.

¹ Note that the actual waste and chemical simulant data shown in the Figure 7.6 from cited sources were not all originally obtained with an NQA-1 documentation pedigree. However, the values shown in this report are traceable to the original values and transcription accuracy has been reviewed and documented under the QA Program described in Section 3.0.

² The FIO Bingham parameter data for kaolin and bentonite were obtained using a parallel plate rheometer and were provided in a personal communication from Richard Daniel (e-mail of 1/28/14 at 10:21am). The e-mail has been included in the DSGREP Records.

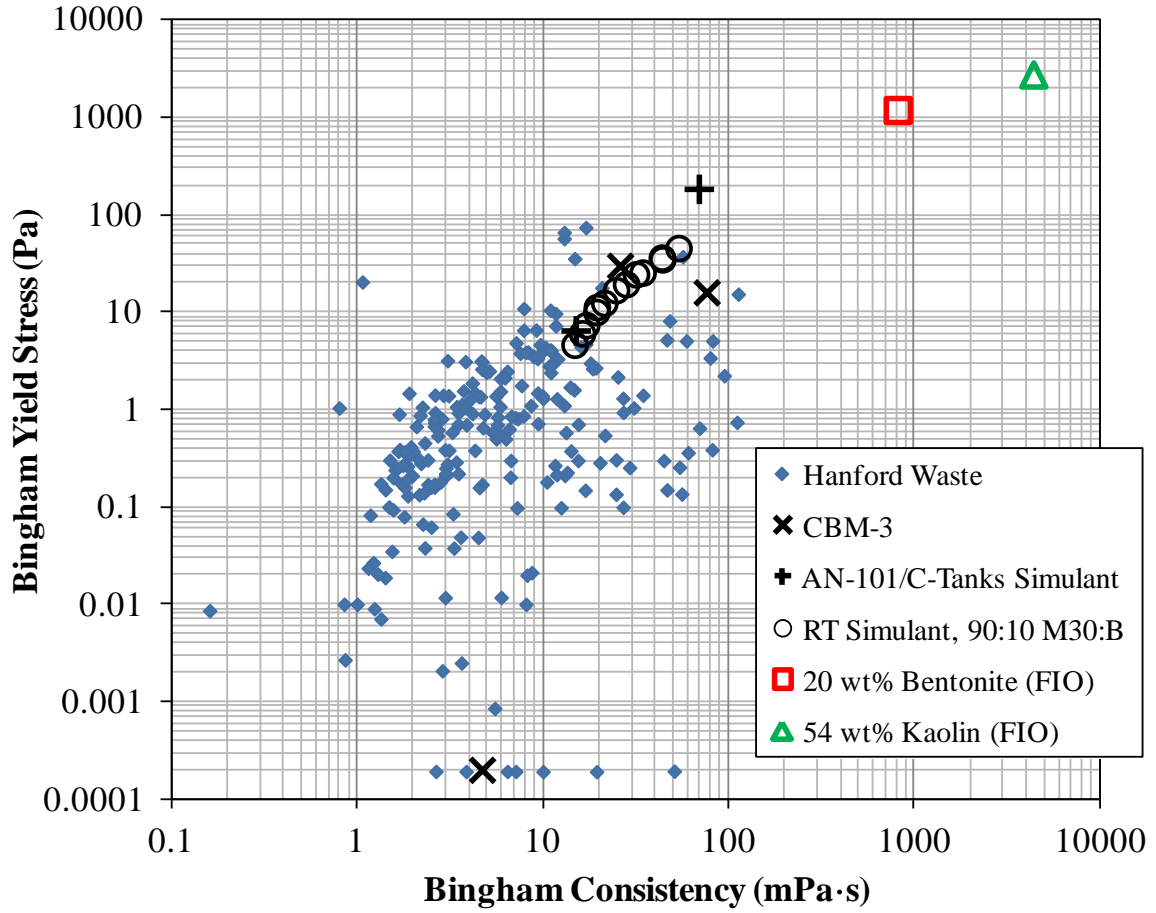


Figure 7.6. Comparison of Bingham Model Parameters for Hanford Tank Waste to a Variety of Chemical and Physical Waste Simulants, Including the Type Used in RT Tests

8.0 Rayleigh-Taylor Instability Test Results

The results of RT instability gas release tests in the 10-in., 23-in., and 70-in. vessels are summarized in this section and are the primary focus. This section also summarizes the results of complementary single-slurry-layer spontaneous gas release tests in the 23-in. and 70-in. vessels. See the previous section for an overview of the physical and rheological properties of slurry simulants used in all these tests. RT tests using lower and upper slurry layers of equal thickness are discussed in Section 8.1, RT tests with varying relative slurry layer depths are presented in Section 8.2, and SL tests are covered in Section 8.3. Each of these experimental result sections begins with a matrix summarizing completed tests and relates them to the TP. Discussion of spontaneous gas releases in SL tests (Section 8.3) is a natural lead-in to the dedicated discussion in Section 8.4 of interpretation of relatively high void fraction releases that were observed in the initial instability events in a subset of the RT tests and in secondary GREs typical of most RT tests. Finally, a Summary of Tests Results is given in Section 8.5. It includes a tabulation of the magnitude of gas releases from RT instabilities, an assessment of the modified energy ratio for each RT test, and re-evaluation of the RT stability criterion as a scaling tool.

Throughout the report, the completed RT and SL tests are identified by a unique test number, which includes a two-digit vessel code corresponding to the vessel diameter (“10-”, “23-”, or “70-”) and a two-digit sequence number starting at “01”. The sequence number reflects the order in which all tests were conducted and is independent of the vessel used. For example, RT Test 23-01 was the first test in the series of 32 tests and it was in the 23-in. vessel, and RT Test 70-09 in the 70-in. vessel was the ninth test overall. The RT and SL test numbers are generally different than the corresponding test numbers in the TP.¹

8.1 Equal Slurry Layer Thickness Tests

The RT test matrix quickly evolved when behavior in the initial planned equal slurry layer thickness tests described in Section 4.3.2 differed from expected. Specifically, it was found that slurry shear strength had to be much weaker than the planned values to get α_{RT} in the target range of 8 to 18.5 vol%. The modified RT Test Matrix for the equal slurry layer depth cases that were completed is summarized in Section 8.1.1, a visual example of an RT instability GRE in the 70-in. vessel is shown in Section 8.1.2, and the RT Test Results are covered in Section 8.1.3.

8.1.1 Test Matrix, Equal Layer Depths

The conditions used in the RT tests in the 10-in., 23-in., and 70-in. vessels in which the depth of the lower and upper slurry layers were nominally equal (1:1, lower:upper) are described in this section and summarized in Table 8.1. The information in Table 8.1 is listed in test sequence order, not by vessel size. The table also provides a map to TP test numbers. Because of a change in test strategy needed to meet the

¹ The TP test numbers are shown in Tables 3.4, 3.5, 3.6, 3.7, and 3.8 of TP-DSGREP-001 Rev. 4.0 (some of these tables also appear in Revisions 1.0, 2.0, and 3.0 of the TP).

project objectives (Section 2.0), which will be discussed briefly below, the conditions used in completed RT tests do not in all cases track tests identified in the original TP test matrix presented in Section 4.3.2.¹

In addition to vessel diameter, Table 8.1 summarizes other key test conditions, including the solids fraction (as wt%) in the final prepared slurry simulant for both layers, which effectively defines τ_S and the gas-free ρ_S , the concentration of H₂O₂ in the lower-layer slurry, and the total depth of slurry, represented as a factor \times of the geometrically-scaled value (Section 4.2.1). The relative depth of upper and lower slurry layers was 1:1 in all of these tests. Where applicable, Table 8.1 also shows the original TP targets or expected values of 18-hr τ_S and α_{RT} . For comparison and subsequent analysis, the table includes the experimentally determined values of τ_S , ρ_S , α_{RT} , and the elapsed time from the start of the RT test² to the RT instability event. The table also shows the retained gas fraction necessary for the settled slurry to be neutrally buoyant in the supernatant water (α_{NB}), and notes some important characteristics and relationships of the tests.

As shown in Table 8.1, the retained gas fractions measured at RT instability for the first four RT tests, two each in the 10-in. and 23-in. vessels, all exceeded 22 vol%, were ~3-times or more higher than the α_{RT} targets, and approached or exceeded α_{NB} . These results were the basis of shifting to lower-shear-strength simulants than originally identified in the TP test matrix to obtain α_{RT} values in the target range of ~8 vol% to ~18.5 vol% in later RT tests. The shear strengths of the slurry in the first three tests, in particular, were somewhat higher than the TP targets owing to an early shift in the τ_S vs. solids loading correlation and the long duration of the tests (~2 to >3 days). However, as discussed in Section 7.1, the magnitude of the effect of these factors on τ_S is expected to be on the order of a 50% increase (e.g., ~10% from a shift in planning to final τ_S vs. x_S correlations and ~40% or less from aging beyond 18 hr). The basis of the original RT test design, Equation (4.2), shows that α_{RT} is directly proportional to τ_S for constant slurry density and constant gravity yield parameter. Therefore, shear strength would have to be ~3 \times higher than the target to account for the very high measured α_{RT} values. As noted in Section 4.3.2, the original TP test matrix was developed under the assumption that RT instability is governed by Equation (4.2) with Y_G constant at 0.09 and a characteristic dimension equal to the vessel diameter. Analysis of the RT test results presented in Section 8.5.3 suggests that Y_G is typically closer to ~0.03 and that the depths of the slurry (sediment) layers, in addition to the vessel diameter, are critical dimensions. Each of these conditions is consistent with the need for reduced τ_S to achieve target α_{RT} values in geometrically-scaled RT tests.

¹ The “original” TP test matrix is shown in Tables 3.4 and 3.5 of TP-DSGREP-001 Rev. 4.0 (and Revisions 1.0, 2.0, and 3.0). Table 3.6 was added to Rev. 3.0 of the TP to summarize completed and proposed RT tests in the 23-in. and 70-in. vessels having conditions different than in the original test matrix. Table 3.7 was also added to Rev. 3.0 of the TP to define proposed tests of varying relative slurry layer thicknesses, which included a complementary equal layer thickness test in the 23-in. vessel. Tables 3.4, 3.5, 3.6, and 3.7 of Rev. 4.0 of the TP cover all proposed equal slurry layer thickness tests that are discussed in this section (8.1) of the report.

² The start of the RT test is defined here as the time at which filling the lower slurry layer in the test vessel was completed.

Table 8.1. Matrix of Completed Equal Slurry Layer Thickness RT Tests in the 10-in., 23-in., and 70-in. Vessels (test sequence order; shaded by vessel size)

RT Test No.	TP Test No. ^(a)	Total Depth, H_S	Lower: Upper Depth	H_2O_2 (wt%)	x_s (wt%)	18-hr τ_S (Pa)		Meas. ρ_S (g/mL)	Time to RT (hr)	α_{RT} (vol%)		α_{NB} (vol%)	Notes
						TP ^(b) Target	Meas.			Meas.	TP ^(b) Target		
23-01	23-2	1	1:1	0.1	47.9	29	38.6	1.422	59	27.3	8.0	29.8	original low and new very high τ_S for 23-in.
10-02	10-2	2	1:1	0.1	42.1	12	16.0	1.345	52	22.2	8.0	25.8	lowest practical τ_S ; 0.1 wt% H_2O_2
23-03	23-6	1	1:1	0.1	45.2	19	21.3	1.385	82	29.6	5.4	27.9	original very low τ and new mid-to-high τ_S for 23-in.; 0.1 wt% H_2O_2
10-04	10-2	2	1:1	0.2	42.1	12	14.6	1.353	41	29.5	8.0	26.2	repeat of RT Test 10-02 using 0.2 wt% H_2O_2
23-05	23-B (N/A)	1	1:1	0.2	42.1	10-16 (12)	14.0	1.348	15	14.6	~12.5 (<5.4)	26.0	same (new low) τ_S and H_{S2} as RT Tests 23-12 and 23-13; 1× total slurry depth
23-06	23-A (23-6)	1	1:1	0.2	45.2	17-26 (19)	22.0	1.39	21	21.4	~18.5 (5.4)	28.2	repeat of RT Test 23-03 using 0.2 wt% H_2O_2 ; same (mid-to-high) τ_S and H_{S1} as RT Test 23-23; same τ_S and H_{S2} as RT Test 23-24
23-07	23-C (N/A)	2	1:1	0.2	42.1	10-16 (12)	15.3	1.34	9.2	10.5	~8 (<5.4)	25.5	low τ_S for 23-in.; 2× total slurry depth
10-08	10-5 (alt. τ_S)	4	1:1	0.2	42.1	12	13.3	1.346	24	23.0	8.0	25.9	4× total slurry depth like TP No. 10-5, but using τ_S of TP No. 10-2
70-09	70-A (~70-7)	1	1:1	0.2	49.7	40-59 (47)	51.1	1.44	7.4	12.6	~12.5 (4.1)	30.7	new mid τ_S for 70-in.; 1× total slurry depth; essentially TP No. 70-7 (original very low τ_S)
23-10	23-D (N/A)	0.67	1:1	0.2	42.1	10-16 (12)	15.3	1.34	19	18.3	~18.5 (<5.4)	25.5	same (low) τ_S and H_{S2} as RT Tests 23-15 and 23-17; 0.67× total slurry depth
70-11	70-C (~70-2)	1	1:1	0.15	51.5	60-80 (71)	67.3	1.464	10	14.7	~18.5 (6.1)	31.8	new mid-to-high τ_S for 70-in.; 1× total slurry depth; essentially TP No. 70-2 (original low τ_S)
23-12	23-E (N/A)	1	1:1	0.2	42.1	10-16 (12)	15.3	1.342	15	15.7	~12.5 (<5.4)	25.6	repeat of RT Test 23-05 (TP No. 23-B) to evaluate reproducibility of the test method; also same τ_S and H_{S2} as RT Test 23-13
70-14	70-B	1	1:1	0.1	47.1	17-26/27-39	28.0	1.410	12	10.3	8	29.2	new low τ_S for 70-in.; 1× total slurry depth
70-16	70-D	0.67	1:1	0.1	49.7	40-59	45.0	1.446	29	18.5	18.5	31.0	mid τ_S for 70-in.; 0.67× total slurry depth

83

RT Test No.	TP Test No. ^(a)	Total Depth, H_S	Lower: Upper Depth	H_2O_2 (wt%)	x_s (wt%)	18-hr τ_S (Pa)		Meas. ρ_S (g/mL)	Time to RT (hr)	α_{RT} (vol%)			Notes
						TP ^(b) Target	Meas.			Meas.	TP ^(b) Target	α_{NB} (vol%)	
70-18 ^(c)	70-A	--	--	--	--	--	--	--	--	--	--	--	intended to be a repeat of RT Test 70-09 (TP No. 70-A) using 0.1 wt% H_2O_2 ^(c)
70-20 ^(d)	N/A	1	1:1	0.1	54.1	N/A	94.6	1.501	22	20.5	N/A	33.5	new high τ_S for 70-in., targeting α_{RT} of ~18-19 vol% based on preceding tests; 1× total slurry depth
23-21	23-K	2	1:1	0.2	45.2	17-26	24.7	1.379	14	16.1	8-12.5	27.6	mid-to-high τ_S for 23-in.; 2× total slurry depth
70-22 ^(e)	70-E	1.5	1:1	0.1	49.7	40-59	42.4	1.439	13	12.1	8	30.6	mid τ_S for 70-in.; 1.5× total slurry depth

Key:	× Geo-Scaled	Relative Depth	Total Solids	Shear Strength	Density	Initial Event	RT Gas Fraction	NB in water
------	--------------	----------------	--------------	----------------	---------	---------------	-----------------	-------------

- (a) TP test numbers are given in test matrix Tables 3.4, 3.5, 3.6, and 3.7 of TP-DSGREP-001 Rev. 4.0. Not all the simulant formulations and/or slurry depths used in completed tests are explicitly addressed in the TP, in which case N/A is indicated for the TP number. The “original” test matrix (Tables 3.4 and 3.5 of the TP) had numeric TP test numbers (e.g., 23-2 for RT Test 23-01). TP test numbers ending with letters, e.g., 23-B for RT Test 23-05, were introduced with updated test matrices in Tables 3.6 and 3.7 of the TP (starting with Rev. 3.0). The later test matrices were based on understanding developed in the initial RT tests and, therefore, more accurately reflect the required simulant properties and expected outcomes. The transition from original to the later test matrices occurred in the course of completing the first twelve tests (ending with RT Test 23-12). For cases where there is overlap in TP test numbers and matrix conditions in these twelve tests, the original number from Table 3.4 or 3.5 of the TP is shown in parentheses below the newer number from Table 3.6.
- (b) In cases where multiple TP test numbers are indicated, TP Targets from, or based on concepts used to develop, the original test matrix (Tables 3.4 and 3.5 of TP-DSGREP-001 Rev. 4.0) are shown in parentheses below the more refined values from the updated test matrix (Table 3.6 of the TP).
- (c) RT Test 70-18 was a planned repeat of RT Test 70-09, the only difference being a lower H_2O_2 concentration in the latter (0.1 wt% instead of 0.2 wt%, consistent with all 70-in. RT tests after test 70-11). Following completion of test 70-18, it was determined through analysis of multiple batch samples and review of the Test Instruction data sheets that two errors had occurred in slurry batch preparation affecting solids concentration and physical properties. Note, however, that analyses of selected batch samples used for Test Acceptance had met Acceptance Criteria (Section 6.4.1), which allowed the RT test to proceed. The batch preparation discrepancies were subsequently documented in Deficiency Report DR-64405-002 Rev. 0. Because of these issues, the RT Test 70-18 results are excluded from this technical report.
- (d) For RT Test 70-20, there are no (not) applicable (N/A) TP test number and TP Target values for τ_S and α_{RT} .
- (e) In the process of filling the vessel in RT Test 70-22, the upper slurry depth was intentionally reduced by ~5% of target (~2.4 cm less) and the initial depth of supernatant water was reduced from a typical 16 cm to 10 cm, both to allow for gas retention and level growth without overflowing the vessel in this 1.5× slurry depth test. These changes are not believed to have had any significant impact on the test results. Following the initial RT instability event, in which essentially no gas was released, a further quantity of water was carefully siphoned off to allow for continued growth.

Observations in the first three tests also prompted increasing the H_2O_2 concentration in the lower-layer slurry to generate gas faster and reduce the test duration from several days to a day or less, consistent with the use of the 18-hr τ_s in development of the test matrix. The results of RT Tests 10-02 and 10-04 also led to a decision to deemphasize use of the 10-in. vessel in favor of more tests in the larger vessels. All the 10-in. vessel tests used relatively weak slurry ($\sim 15\text{-Pa}$ τ_s at 18 hr), which would need to be reduced by at least a factor of two to obtain α_{RT} near the middle of the target range. Using less than 10-Pa slurry, which is weaker still when sheared for vessel loading, is experimentally impractical. Issues include enhanced solids settling in more dilute slurry and greater difficulty in creating a uniform interface between lower and upper slurry layers during filling.

With the shifts noted above, RT tests were completed to address the project objectives (Section 2.0). Brief descriptions of the purposes and specific (pre-test) assumptions for some of the key series of equal slurry layer depth tests are given below. Refer to Table 8.1 for test conditions of the identified RT Test numbers.

- By varying slurry shear strength at fixed total geometrically-scaled slurry depth and equal slurry layer depths (1:1), assess the relationship of α_{RT} and the quantity of gas released in different diameter vessels. Pertinent tests, in order of increasing strength within each group, include:
 - 23-05 (and repeat 23-12), 23-06, and 23-01: $\tau_s \sim 15$ to ~ 40 Pa (~ 22 Pa excluding 23-01, one of the suspect initial tests), $H_S = 1\times$;
 - 23-07 and 23-21: $\tau_s \sim 15$ to ~ 25 Pa, $H_S = 2\times$;
 - 70-14, 70-09, 70-11, and 70-20: $\tau_s \sim 30$ to ~ 95 Pa, $H_S = 1\times$.
- Holding the slurry shear strength (recipe) constant and maintaining equal individual slurry layer depths (1:1), assess the effect of total geometrically-scaled slurry depth (H_S) on α_{RT} and the quantity of gas released at multiple vessel scales. It was initially assumed that α_{RT} would be constant with variation in slurry depth (for 1:1 layers), in which case varying depth was considered a direct means to assess the relationship of modified energy ratio ER_S and gas release. Pertinent tests, in order of increasing total depth within each group, include:
 - 23-10, 23-05 (and repeat 23-12), and 23-07: $0.67\times$, $1.0\times$, and $2.0\times$ with $\tau_s \sim 15$ Pa;
 - 23-06 and 23-21: $1.0\times$ and $2.0\times$ with $\tau_s \sim 22$ Pa;
 - 70-16, 70-09, and 70-22: $0.67\times$, $1.0\times$, and $1.5\times$ with $\tau_s \sim 45$ Pa.
- Evaluate repeatability of the RT test approach:
 - 23-05 and 23-12: $\tau_s \sim 15$ Pa, $H_S = 1.0\times$ (1:1).

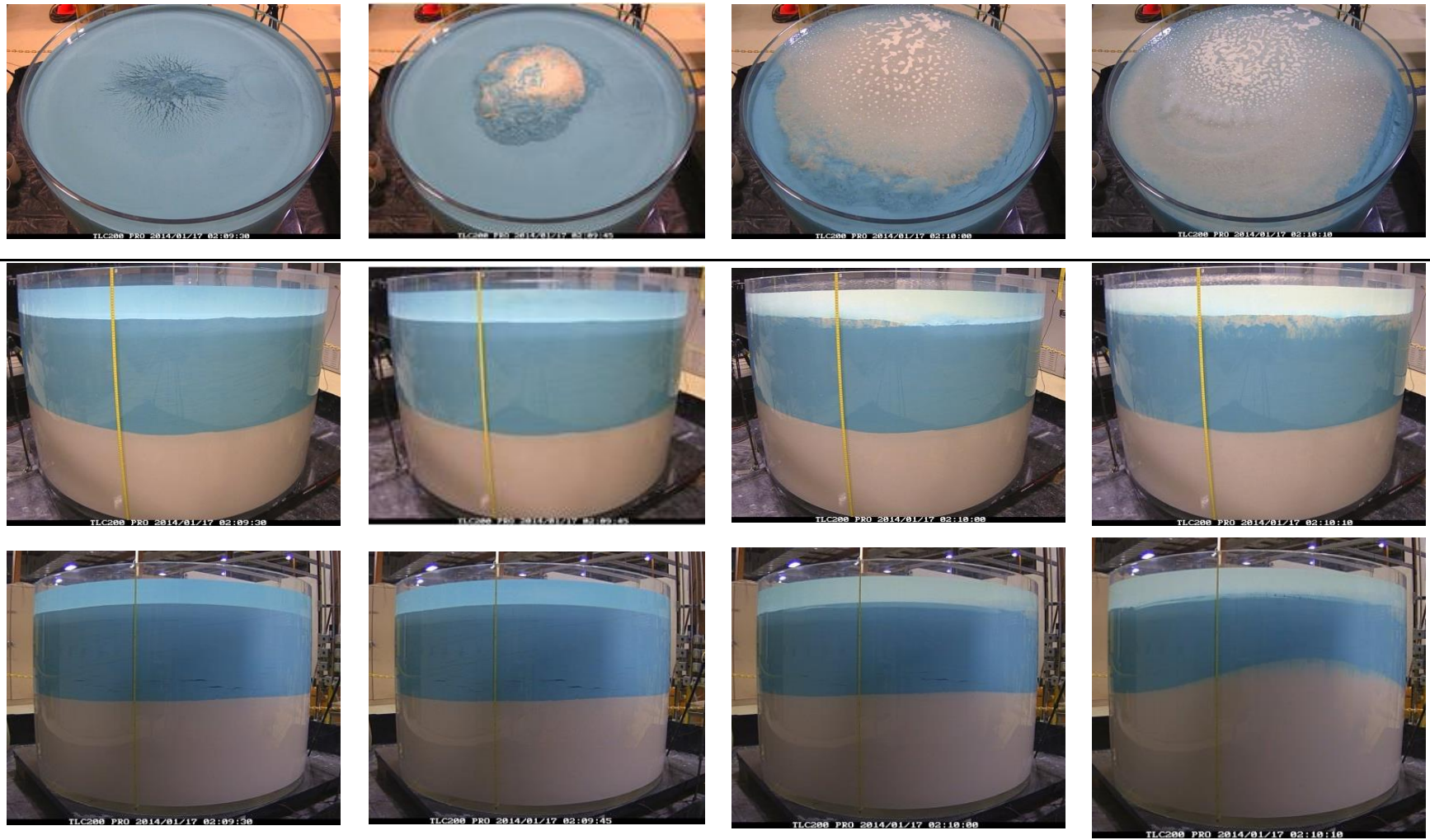
8.1.2 Visual Characteristics of an RT Instability Event

Prior to presentation of RT test results, this section shows visually a representative RT instability GRE. The example is for a 70-in. vessel test, but similar characteristics were also seen in 23-in. vessel tests. A 70-in. vessel case is shown not only because it is the largest vessel, but also because more cameras were used to capture images from multiple perspectives. The specific RT test (70-22: $1.5\times$ total depth, equal layer depths, $\sim 45\text{-Pa}$ τ_s , and $\alpha_{RT} = 12.1$ vol%) shown in Figure 8.1 was selected to illustrate a “classic” wavy RT instability with in-sediment buoyant motion that is visible around the vessel. The figure shows a time sequence of the RT instability event from 15 s before until 35 s after, when the event was substantially complete. Photos from three cameras at eight elapsed times measured from the start of the RT instability event (elapsed time 0 s) are shown in Figure 8.1: the top row shows an overhead (top) view looking down on the slurry surface; the middle row shows a side (panorama) view from a point that roughly corresponds to the upper left corner of the top view; and the bottom row provides a side view from the opposite side of the vessel that equates approximately to the lower right corner of the overhead view.

Although the pre-event camera images in Figure 8.1 (first column of first page) are shown only 15 s beforehand, they are representative of images from much earlier. The cracked-surface, squat volcano-like feature seen off-center in the overhead view is typical of most of the RT tests and it generally developed over hours. In some cases, an initial slight upwelling in the eventual location of this feature was seen within a few hours of loading the vessel. The start of the RT instability (second column of first page), which is defined in this case by observation of natural-colored lower-layer slurry solids flowing through this feature onto the (blue) upper slurry surface, occurred ~ 13 hr after adding the lower layer¹. At 15-s elapsed time (third column of first page), a cloud of solids continues to spread across the surface, which is seen in the overhead view and evidenced by the presence of natural clay at the slurry surface along the vessel wall (middle row). The third overhead image also shows a very light froth and a few small bubbles popping in the vicinity of the plume. The lower side-view image at +25 s (fourth column of first page) shows large wave-like motion as observed at the slurry layer interface by a substantial upwelling of lower-layer material. The overhead-view and lower side-view images 2 s later (+27-s elapsed time, first column of second page) show bulk slurry pushing into the supernatant liquid, although no (appreciable) gas is released, as is also seen in the +28-s and +30-s top-view images. The sequence of images from +27-s to +35-s elapsed time (all columns on the second page) shows substantial slurry motion as noted by the continued distortion of the lower-upper layer slurry interface on both sides of the vessel and mixing of dyed and natural simulant. Although not shown in Figure 8.1, bulk motion had essentially stopped within ~ 45 s of the start of the RT event.

Although bulk motion of the sediment is extensive and visually impressive in this RT instability event, gas release was negligible. The visual evidence is supported by the quantitative results. A slight water level increase was observed, indicating negative gas release ($+\sim 0.5$ mm within ~ 2 min. of the RT event time). This can be explained by expansion of gas bubbles as lower-layer slurry moves upward, replaced below by more-dense upper-layer slurry. This phenomenon was more pronounced in the relatively deep sediment bed in RT test 70-22 ($1.5\times$ depth). As will be shown below (Section 8.1.3.3 and Section 8.5.1), near zero gas release was observed in all 70-in. vessel RT tests in which the difference in retained gas fraction between the two slurry layers, α_{RT} , was ~ 0.15 (~ 15 vol%) or less.

¹ As noted in the discussion of the test matrix above (Section 8.1.1), the start of the RT test, for data analysis purposes, is defined as the time at which filling the lower slurry layer in the test vessel was completed.



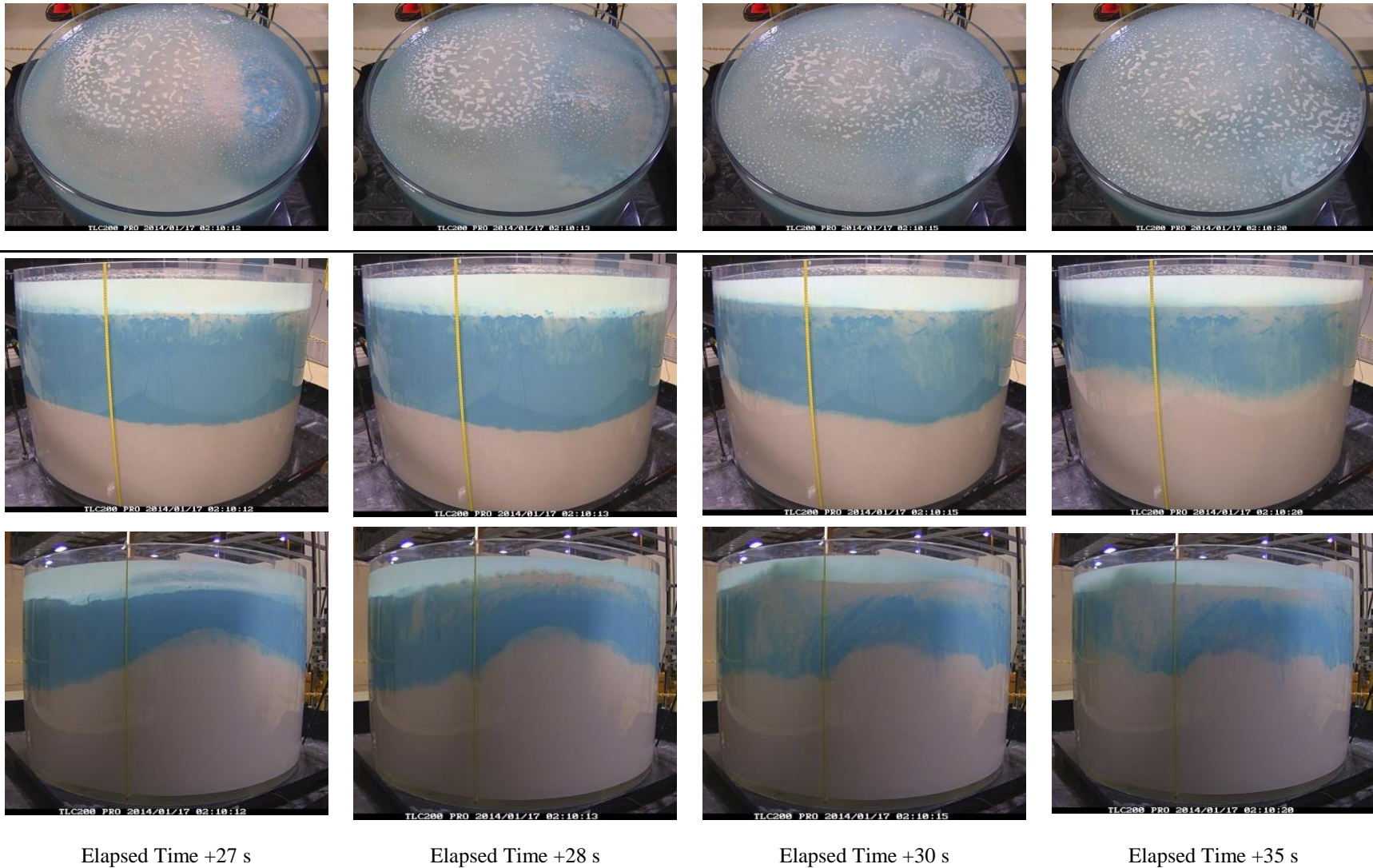
Elapsed Time -15 s

Elapsed Time 0 s

Elapsed Time +15 s

Elapsed Time +25 s

Figure 8.1. Time Sequence of Images Surrounding the RT Instability Gas-Release Event in RT Test 70-22 (~45 Pa, 1.5× depth, 1:1 lower:upper; middle row = upper left of top (overhead) view and bottom row = lower right of top view)



Elapsed Time +27 s

Elapsed Time +28 s

Elapsed Time +30 s

Elapsed Time +35 s

Figure 8.1. (cont.) Time Sequence of Images Surrounding the RT Instability Gas-Release Event in RT Test 70-22 (~45 Pa, 1.5× depth, 1:1 lower:upper; middle row = upper left of top (overhead) view and bottom row = lower right of top view)

8.1.3 Test Results, Equal Layer Depths

Individual RT test results for completed experiments identified in Table 8.1 are provided in Appendix C, and quantitative gas release results are summarized in Table 8.5 (Section 8.5.1). Select results from these tests, primarily from the 23-in. and 70-in. vessel tests that were completed after a series of initial tests in the 10-in. and 23-in. vessels, are the focus of this section.

8.1.3.1 Initial 10-in. and 23-in. Vessel Tests

The gas fractions at RT instability in the first two 10-in. experiments (RT Tests 10-02 and 10-04) and the first two 23-in. tests (23-01 and 23-03) were well above the 8 to 18.5 vol% target range. In RT Tests 23-03 and 10-04 in particular, α_{RT} exceeded the gas fraction for the slurry to become neutrally buoyant in water, α_{NB} . In the other two initial tests, α_{RT} was greater than 85% of α_{NB} , i.e., approaching neutral buoyancy. As summarized in Section 8.5.1, >75% of the retained gas was released in the initial instability in tests in which $\alpha_{RT} > \alpha_{NB}$ and in some other near neutral buoyancy cases. For example, the releases were relatively large in RT Test 23-01 ($\alpha_{RT}/\alpha_{NB} = 0.92$) and in a later 10-in. vessel test 10-08¹ in which $\alpha_{RT}/\alpha_{NB} = 0.89$. These data clearly suggest that approaching or exceeding neutral buoyancy gas fractions in the small-scale vessels is a primary factor in the size of gas releases.

The objective of these RT tests was to investigate gas releases due to in-sediment buoyant motion, not BDGREs in which the slurry is buoyant in the supernatant liquid. The test conditions in and results of all three of the 10-in. vessel tests and the first two 23-in. vessel tests were not conducive to this goal. As was discussed in Section 8.1.1 in conjunction with the progression of the test matrix beyond the initial four tests, the simulant shear strength needed to be reduced by a factor of $\sim 3\times$ to have α_{RT} in the target range and avoid neutral buoyancy in water. As was also noted in the test matrix discussion, it was deemed experimentally impractical to reduce the shear strength (appreciably) below the (original) 12-Pa target used in the 10-in. tests. Therefore, only the three 10-in. vessel tests were completed, and attention shifted exclusively to tests in the 23-in. and 70-in. vessels.

8.1.3.2 23-in. Vessel Tests

RT Test 23-06 was essentially a repeat of test 23-03 at twice the H_2O_2 concentration, 0.2 wt% vs. 0.1 wt%. Each had a target shear strength (based on the original correlation) of 19 Pa and a measured 18-hr τ_S of 21 to 22 Pa. As discussed in Section 8.1.3.1 and shown in Table 8.1, α_{RT} exceeded α_{NB} in test 23-03 ($\alpha_{RT} = 29.6$ vol%; $\alpha_{NB} = 27.9$ vol%), but it did not in test 23-06 ($\alpha_{RT} = 21.4$ vol%; $\alpha_{NB} = 28.2$ vol%). This can be explained, at least in part, by the relatively long duration of Test 23-03 (~ 82 hr to instability) compared to test 23-06 (~ 21 hr) and corresponding differences in the best-estimates of shear strength at the time of the initial RT instability (32 Pa and 25 Pa, respectively). Figure 8.2 shows the retained gas fraction versus time for RT Test 23-06. The point of RT instability, at an elapsed time of ~ 21 hr, as determined from video observations similar to those shown in the previous section, is marked

¹ The rationale for RT Test 10-08 in light of the results of the initial 10-in. tests (10-02 and 10-04) is as follows. A series of 23-in. vessel tests in which the slurry depth was varied indicated that α_{RT} decreased with increasing depth (see Section 8.1.3.2). The slurry depth in test 10-08 was $4\times$ geometrically scaled, twice the depth used in the other two 10-in. vessel tests, in an attempt to achieve an RT instability at a gas fraction significantly lower than α_{NB} . This was not observed and was a consideration in not conducting additional 10-in. vessel tests.

on the figure by an arrow and the filled (red) symbol. While α_{RT} of ~21 vol% is still slightly above the target range (18.5 vol% maximum), the relatively small release event of $\Delta\phi \sim 0.022$ L gas/L gas-free bottom slurry ($\Delta\alpha \sim 1.3$ vol%; $\sim 7.8\%$ of retained gas) is consistent with expected RT behavior for in-sediment buoyant motion. The latter conclusion is also supported by video observations of slurry motion.

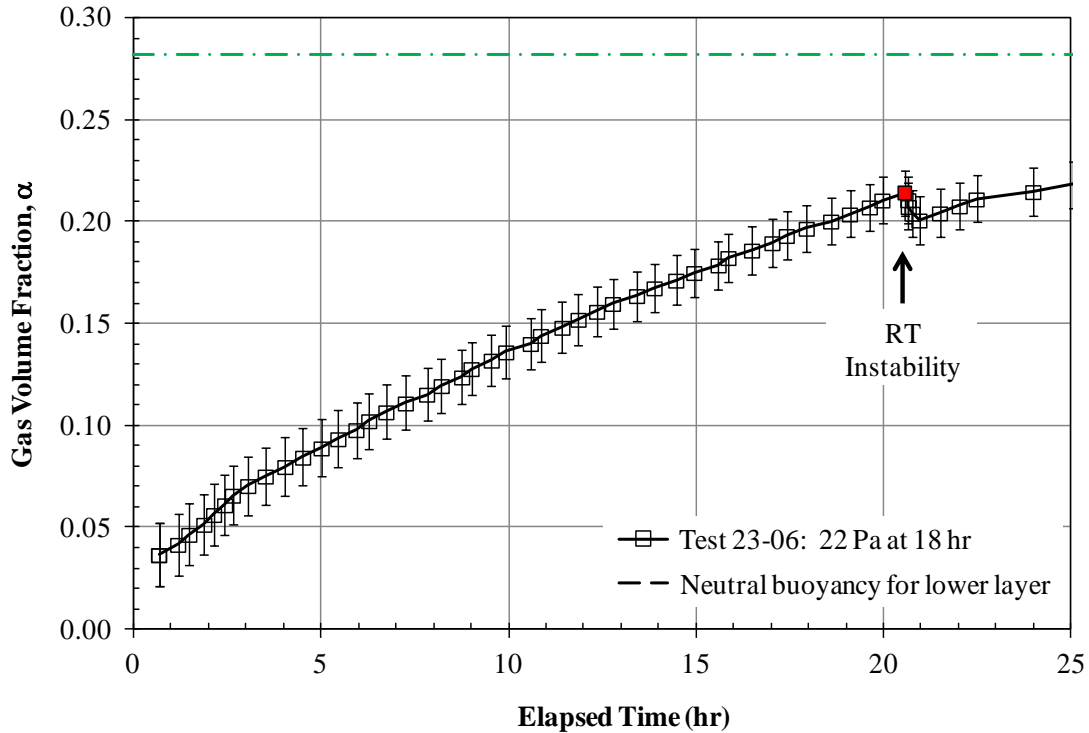


Figure 8.2. Retained Gas Volume Fraction vs. Time for RT Test 23-06

Figure 8.2 is also representative of measurement uncertainty in the 23-in. vessel tests. The error bars in the plot show the calculated uncertainty in the absolute gas volume fraction, using the calculation method described in Section 6.5.1. The uncertainty in the α values range from $\sim \pm 1.6$ vol% at the beginning of the test to $\sim \pm 1.1$ vol% around the time of the RT instability. The uncertainty in the quantity of gas released when calculated directly from the small (~ 2 -mm) level change is less than one-half of the uncertainty in absolute gas fractions shown by the error bars.

In Figure 8.2 and gas retention plots to follow, elapsed time is measured from the time that filling of the lower slurry layer in the RT test vessel was completed. Therefore, apparent trajectories of gas volume fractions to non-zero values at elapsed time zero may be due to gas retained in the slurry in the period from the start of H_2O_2 addition to the completion of the lower-layer slurry addition.

The simulant used in RT Tests 23-03 and 23-06 had the lowest target shear strength (19 Pa, original correlation¹) of all tests originally planned for the 23-in. vessel, and α_{RT} was expected to be very low, ~ 5 vol%. Because α_{RT} in test 23-06 was still greater than the 8 to 18.5 vol% target range, the (original)

¹ The 45.2-wt% solids formulation was later identified with a 17 to 26 Pa 18-hr τ_s target range (see Table 8.1) and throughout the report is often cited as the ~ 22 -Pa slurry recipe.

12-Pa target τ_s formulation¹ used in the 10-in. vessel tests became the primary simulant of choice for the series of 23-in. vessel tests described below.

RT Test 23-05 was the first to use the ~15-Pa (original 12-Pa) simulant recipe in the 23-in. vessel. As shown in Figure 8.3, the RT instability occurred at ~15-hr elapsed time with a retained gas fraction just under 15 vol%. The gas released during the RT event was negligible (quantitatively 0). Following several other tests in the 23-in. vessel (discussed below), conditions nominally identical to those of test 23-05 were used in test 23-12 to assess the repeatability of the RT test method. Figure 8.3 shows that the time to RT instability was almost exactly the same and α_{RT} was slightly higher, ~16 vol%. However, while still small, non-zero gas release was observed in test 23-12 ($\Delta\phi \sim 0.006$; $\Delta\alpha \sim 0.4$ vol%; ~3.3% of retained gas). Conservatively, from a gas release standpoint, repeat RT Test 23-12 is used as a basis of comparison to other 23-in. vessel tests rather than test 23-05.

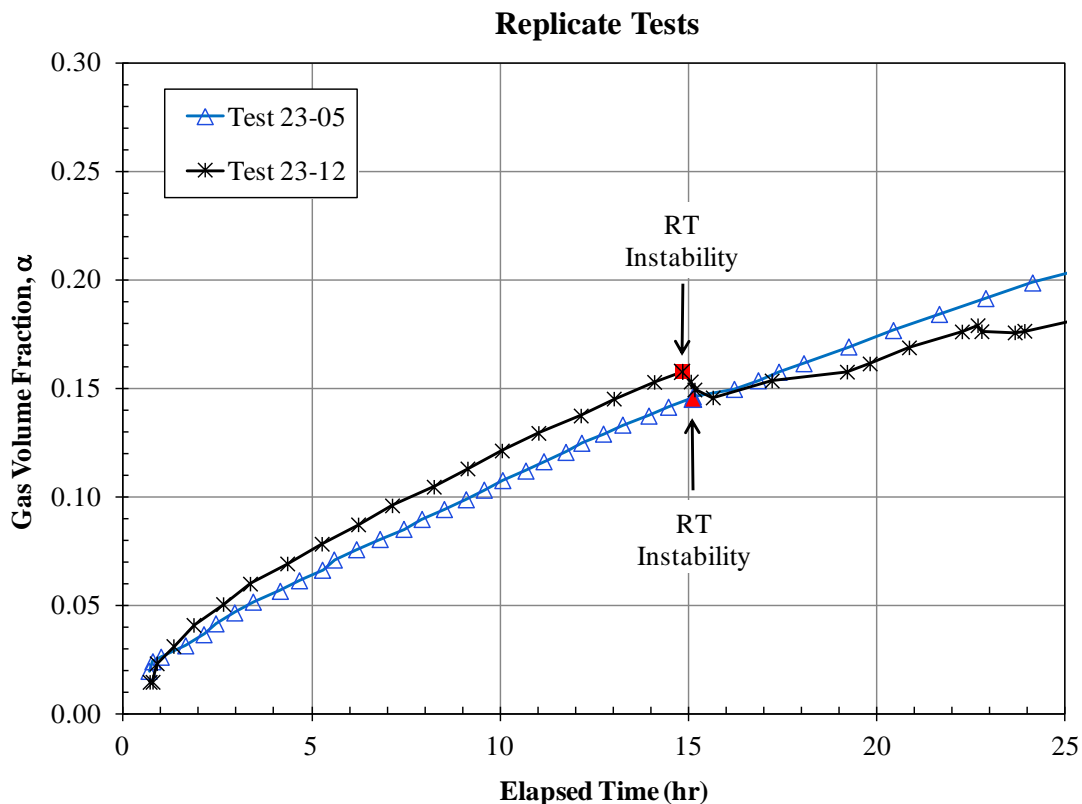


Figure 8.3. Gas Volume Fraction vs. Time for Replicate Tests in the 23-in. Vessel (~15-Pa shear strength)

¹ The 42.1-wt% solid formulation was later identified with a 10 to 16 Pa 18-hr τ_s target range (see Table 8.1) and throughout the report is often cited as the ~15-Pa slurry recipe.

Effect of Shear Strength

Figure 8.4 provides a head-to-head comparison of test 23-06 (Figure 8.2) and test 23-12 (Figure 8.3). Consistent with the RT stability criterion at constant Y_G (Equation (4.2)), Figure 8.4 shows that α_{RT} increases with increasing strength (~ 16 vol% at 17 Pa and ~ 21 vol% at 25 Pa, using best-estimate τ_s values). The limited data also suggest that the magnitude of the gas releases associated with initial RT instabilities also increases with increasing α_{RT} ($\Delta\phi \sim 0.006$ and ~ 0.022 in tests 23-12 and 23-06, respectively).

The same two simulant formulations were used in 1:1, $2\times$ total depth RT tests 23-07 and 23-21 (15-Pa and 24-Pa best-estimate τ_s , respectively). Again, both α_{RT} (10.5 vol% vs. 16.1 vol%) and $\Delta\phi$ (0.011 vs. 0.090) increased with increasing strength. While the strength dependence on the gas fraction at RT instability holds, there is an apparent effect of slurry depth on both α_{RT} and the quantity of gas released, as discussed next.

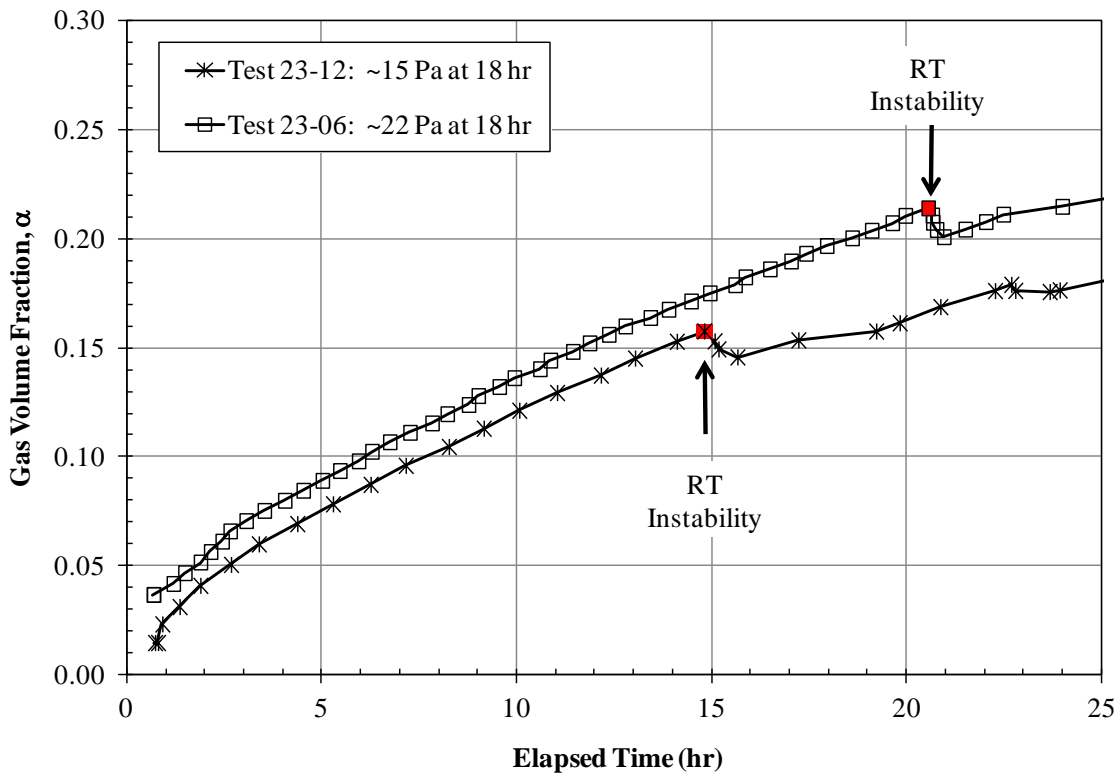


Figure 8.4. Gas Volume Fraction vs. Time for Simulants of Different Shear Strength in the 23-in. Vessel at $1\times$ Total Slurry Depth (1:1 lower:upper)

Effect of Depth

A series of three tests using the ~ 15 -Pa simulant formulation at different slurry depths was completed. The geometrically-scaled total slurry depths were $0.67\times$ in RT Test 23-10, $1\times$ in test 23-12 (and 23-05), and $2\times$ in test 23-07. The retained gas volume plots for the tests are shown in Figure 8.5. It shows that both the time to RT instability and α_{RT} increase with decreasing depth (~ 9 hr to $\alpha_{RT} \sim 10\%$ at $2\times$, 15 hr to

~16% at 1×, and 19 hr to ~18% at 0.67×). The gas releases in the three tests shown in Figure 8.5 are consistently small. However, there is no clear trend with α_{RT} or depth ($\Delta\phi \sim 0.011$, ~ 0.006 , and ~ 0.011 at 0.67×, 1×, and 2×, respectively). The best estimates of τ_S based on time to the RT instabilities range from 15 to 17 Pa, and therefore, differences in shear strength alone do not explain the differences in α_{RT} . The RT instability criterion given in Equation (4.2) suggests that α_{RT} should be constant for sediment of equal strength and density in a vessel of diameter D . The results shown in Figure 8.5 suggest that slurry depth, H_S , is a factor in the RT stability criterion in addition to D . This is discussed further in Section 8.5.3.

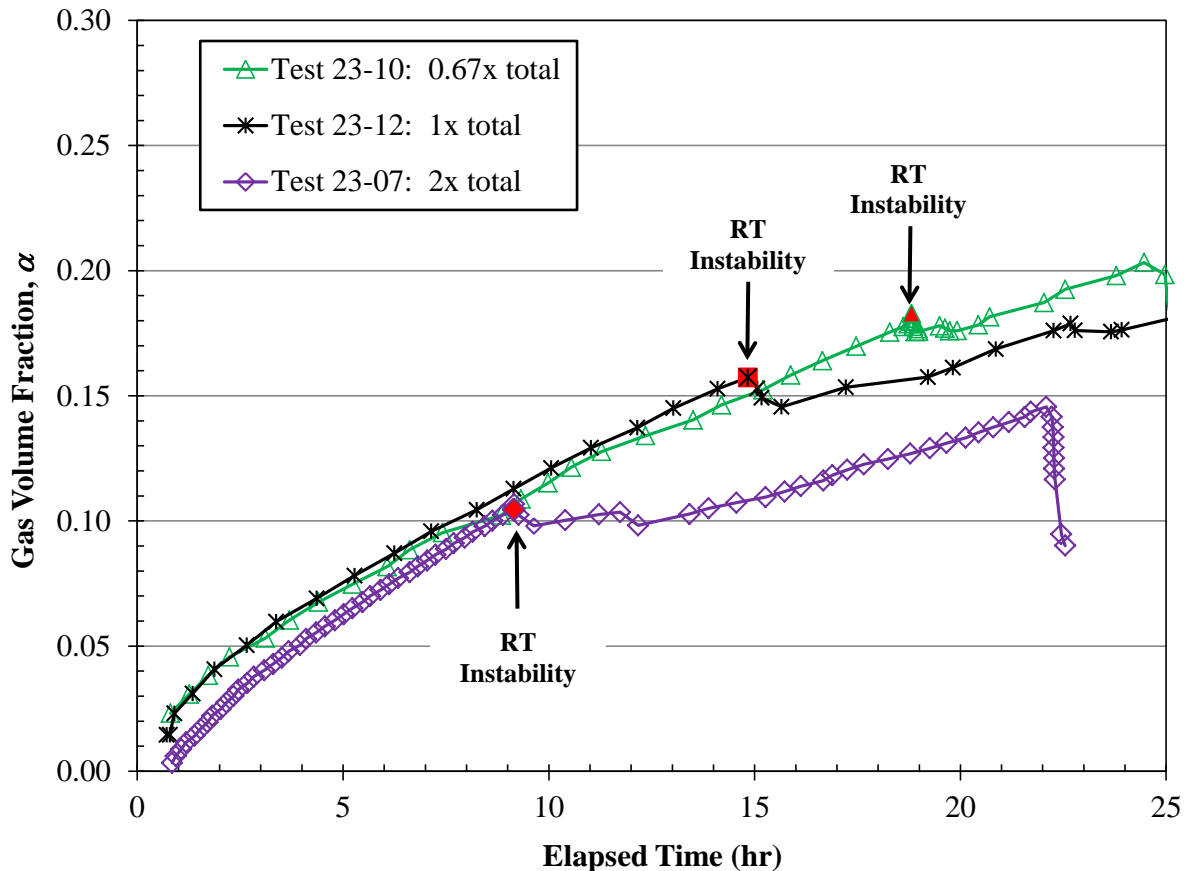


Figure 8.5. Gas Volume Fraction vs. Time for Three Depths of Slurry in the 23-in. Vessel at ~15-Pa Shear Strength (1:1 lower:upper)

Depth was also varied in a pair of equal slurry layer thickness tests using the ~22-Pa shear strength simulant recipe, both of which were discussed in the preceding discussion on Effect of Strength. In the 1× geometrically-scaled total depth test (23-06) α_{RT} was ~21%, and in the 2× depth test (23-21) α_{RT} was ~16%, showing again the trend for decreasing α_{RT} with increasing total slurry depth (1:1 cases). However, the specific gas release increased with increasing depth ($\Delta\phi \sim 0.022$ and ~ 0.090 at 1× and 2×, respectively), even though α_{RT} decreased.

Gas retention and release results for these varying total depth and equal layer thickness RT tests in the 23-in. vessel using ~15-Pa and ~22-Pa τ_S simulant formulations are summarized in Figure 8.6. As noted above, the figure shows decreasing α_{RT} with increasing slurry depth and decreasing slurry strength (filled

symbols and solid lines, left y-axis). The fraction of gas inventory released¹ (open symbols and dashed lines, right y-axis) tends to increase with increasing depth at a given strength, which is most apparent with the ~22-Pa slurry, but is also true for the 1× and 2× data for ~15-Pa slurry.

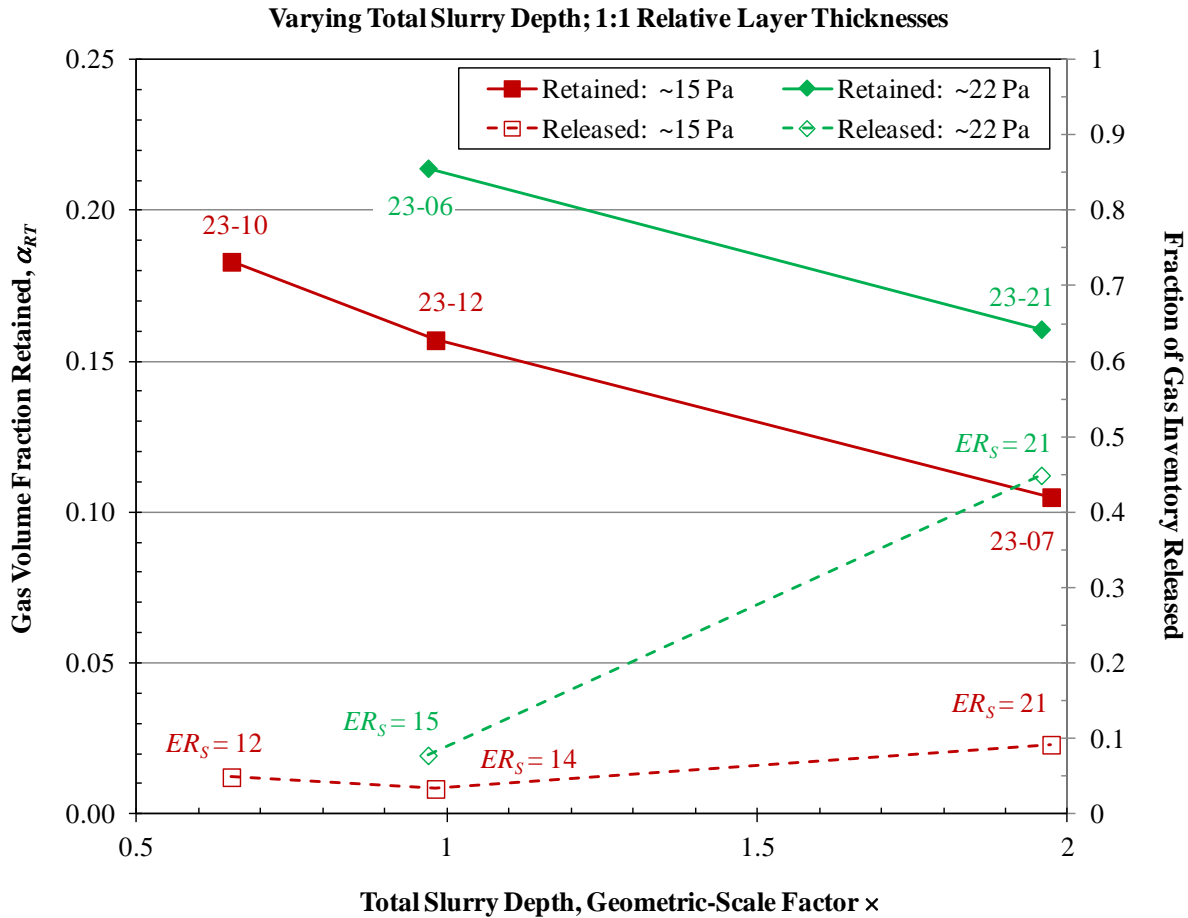


Figure 8.6. Summary of Retained Gas Fractions (left y-axis) and RT Instability Gas Releases (right y-axis) for Equal Slurry Layer Thickness and Varying Total Depth of Slurry in the 23-in. Vessel (~15-Pa and ~22-Pa cases; labels on the retained gas data points show RT test number, and labels in the gas release points show the calculated modified energy ratio, ER_S .)

The gas release data points in Figure 8.6 have labels indicating the modified energy ratio ER_S that is calculated from the test conditions and data using Equation (4.4). The equation shows that ER_S is expected to increase with the upper slurry layer depth H_{Sl} and α_{RT} , while it should decrease with τ_S , all else being equal. In test planning it was originally assumed that α_{RT} would be independent of total depth for 1:1 lower:upper layer depth cases, and therefore, varying total depth with a given simulant recipe would be a direct means to study the relationship of gas release and the modified energy ratio. With this assumption, doubling the slurry depth at a given τ_S would double ER_S . In the test cases shown in Figure 8.6, however, the modified energy ratio increases by a factor of ~1.4 ($ER_S = 15$ vs. 21 at ~22 Pa) and ~1.5 ($ER_S = 14$ vs. 21 at ~15 Pa) in going from 1× to 2× total depth. In these cases, the effect of

¹ The fraction of inventory released is the volume of gas released divided by the volume of gas retained at the start of the release event. The specific gas release $\Delta\phi$ is the volume of gas released per unit volume of gas-free lower-layer slurry.

depth on ER_S is countered to some extent by the experimentally observed decrease in α_{RT} with depth. Nonetheless, the experimental results show the expected trend of increasing modified energy ratio with increasing upper-layer sediment depth. Other RT test data do not provide a consistent picture of this relationship, as summarized in Section 8.5.2.

8.1.3.3 70-in. Vessel Tests

Effect of slurry layer strength and effect of slurry depth on RT instability gas-release characteristics were investigated in six 1:1 lower:upper slurry layer tests in the 70-in. vessel (see Table 8.1 in Section 8.1.1). Results are discussed in this section.

Effect of Shear Strength

Four RT tests in the 70-in. vessel were completed at $1\times$ geometrically-scaled total depth and equal layer thicknesses using different simulant formulations. The gas retention results for RT Tests 70-14, 70-09, 70-11, and 70-20, in order of increasing solids content and shear strength,¹ are shown in Figure 8.7. Like the results for 23-in. vessel tests (e.g., Figure 8.4) and as is expected based on the RT stability criterion model, Figure 8.7 shows that α_{RT} increases with increasing shear strength, using best-estimate τ_S values at the time of the RT instabilities: 10.3 vol% at 26 Pa in test 70-14; 12.6 vol% at 45 Pa in test 70-09; 14.7 vol% at 63 Pa in test 70-11; and 20.5 vol% at 104 Pa in test 70-20. Note that differences in void fraction growth rates, i.e., gas generation rates at 100% retention, are due in part to variation in the H_2O_2 concentration (0.2 wt% in test 70-09, 0.15 wt% in test 70-11, and 0.1 wt% in later 70-in. RT tests; see Table 8.1). Increasing solids content x_S , and the bentonite mass fraction in particular, with increasing shear strength also appears to contribute significantly to differences in the gas generation rates in these tests (e.g., compare tests 70-14 and 70-22, both at 0.1-wt% H_2O_2).

Videos around the RT instability events in these tests show lower-layer slurry reaching the upper slurry surface and subsurface motion of the two slurry layers, as viewed from the side wall (see, for example, the photos in Section 8.1.2). Except for test 70-20, a relatively small number of gas bubbles were observed popping at the liquid surface, and the gas releases were quantitatively negligible, or slightly negative, as shown in Figure 8.7. An apparent negative release can be explained, for example, by expansion of gas as the lower slurry layer moves upward, as noted previously in the discussion of photos from RT test 70-22 ($1.5\times$ total depth). Within measurement uncertainty, the gas releases in 70-in. vessel tests 70-09, 70-11, and 70-14 having α_{RT} of ~ 15 vol% or less are effectively 0. Comparing 23-in. vessel tests at similar α_{RT} (e.g., replicate RT Tests 23-05 and 23-12, ~ 15 to ~ 16 vol%) shows similar gas releases in the smaller vessel (although it was non-zero for test 23-12). Extrapolation of these limited 23-in. and 70-in. vessel data along lines of constant α_{RT} to full scale suggests that a gas release due to an RT instability in a DST could be small, possibly zero, for α_{RT} of ~ 15 vol% or less. Extrapolation is considered further in Section 10.0.

¹ The 47.1-wt%, 49.7-wt%, and 54.1 wt% solids formulations used in tests 70-14, 70-09, and 70-20 are cited throughout the report as the ~ 30 -Pa, ~ 45 -Pa, and ~ 95 -Pa slurry recipes, respectively. These values, rounded to the nearest 5 Pa, are based on a combination of the target and typical measured 18-hr shear strengths as well as the best-estimate τ_S values at the time of RT instabilities in various tests.

Note, however, that the gas release characteristics and quantities were significantly different in test 70-20 using the strongest simulant. At a retained gas fraction of ~ 20 vol%, approximately 57% of the retained gas was released ($\Delta\phi \sim 0.16$) immediately following the RT instability event, as seen in the steep drop in retained gas in Figure 8.7. This release is more characteristic of the secondary releases in the other tests shown in the figure, which occur many hours after and at higher retained gas fractions than the initial RT instabilities. These secondary releases, and the primary release in test 70-22, are similar to spontaneous, bubble-cascade gas releases observed in SL tests, as will be discussed further in Section 8.3.2.2. Insight into the gas release characteristics of the simulant was also attained in another way. Following completion of test 70-09, a few days after filling, the undisturbed (by human or machine) gaseous settled simulant in the 70-in. vessel was mixed by hand with a paddle. Retained gas was readily and essentially quantitatively released by the low-shear-rate mixing action: the pre-mix and post-mix void fractions were ~ 14 vol% and $\sim 0\%$, respectively. That gas is readily released when the M30:B slurry is sheared with relatively gentle shearing by hand further demonstrates that the simulant is a conservative choice in studies of the quantitative analysis of gas releases due to RT instabilities.

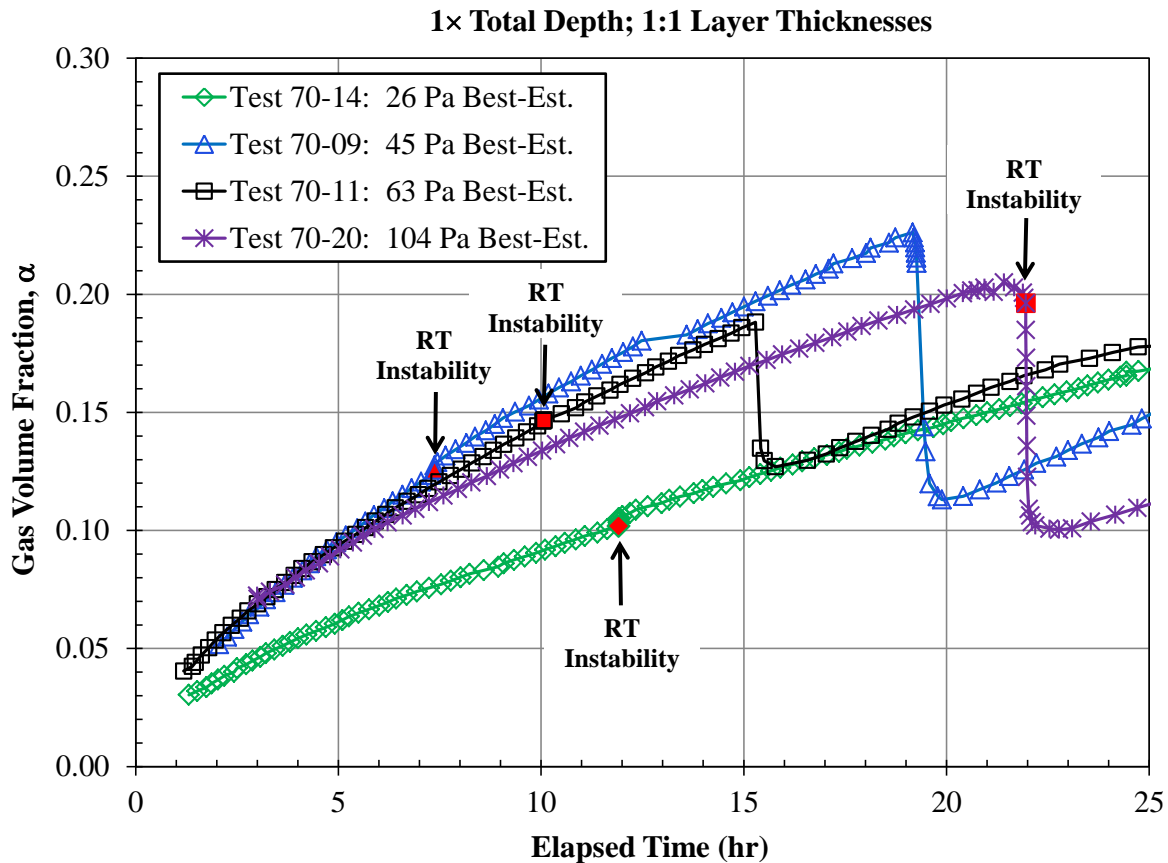


Figure 8.7. Gas Volume Fraction vs. Time for Simulants of Different Shear Strength in the 70-in. Vessel at $1\times$ Total Slurry Depth (1:1 lower:upper)

The effect of strength on the retained gas fraction at the onset of RT instability in the four equal layer thickness and $1\times$ total depth 70-in. vessel tests is summarized in Figure 8.8 (left plot). The data show an essentially linear relationship between α_{RT} and the best-estimate τ_S at the time of the RT event. Data for two 23-in. vessel tests (23-06 and 23-12) are also shown on the plot. The gravity yield criterion in the form given in Equation (4.2) shows that α_{RT} should have a linear dependence on $\tau_S/(\rho_S D Y_G)$ and have an

intercept of zero (i.e., the void fraction to initial RT motion should be zero for layers with no strength). At constant length scale D , a non-zero intercept (such as seen in Figure 8.8) might be explained, at least in part, by a non-constant gravity yield parameter Y_G . The plot on the right in Figure 8.8 shows that Y_G calculated from Equation (4.1) (with $L = D$) for the 23-in. and 70-in. tests varies from ~ 0.02 to ~ 0.04 , with a trend toward increasing Y_G with increasing strength within each vessel. The non-constant Y_G and its non-linear dependence on τ_s , or more properly, on $\tau_s/(\rho_s D)$, is addressed further in Section 8.5.3.

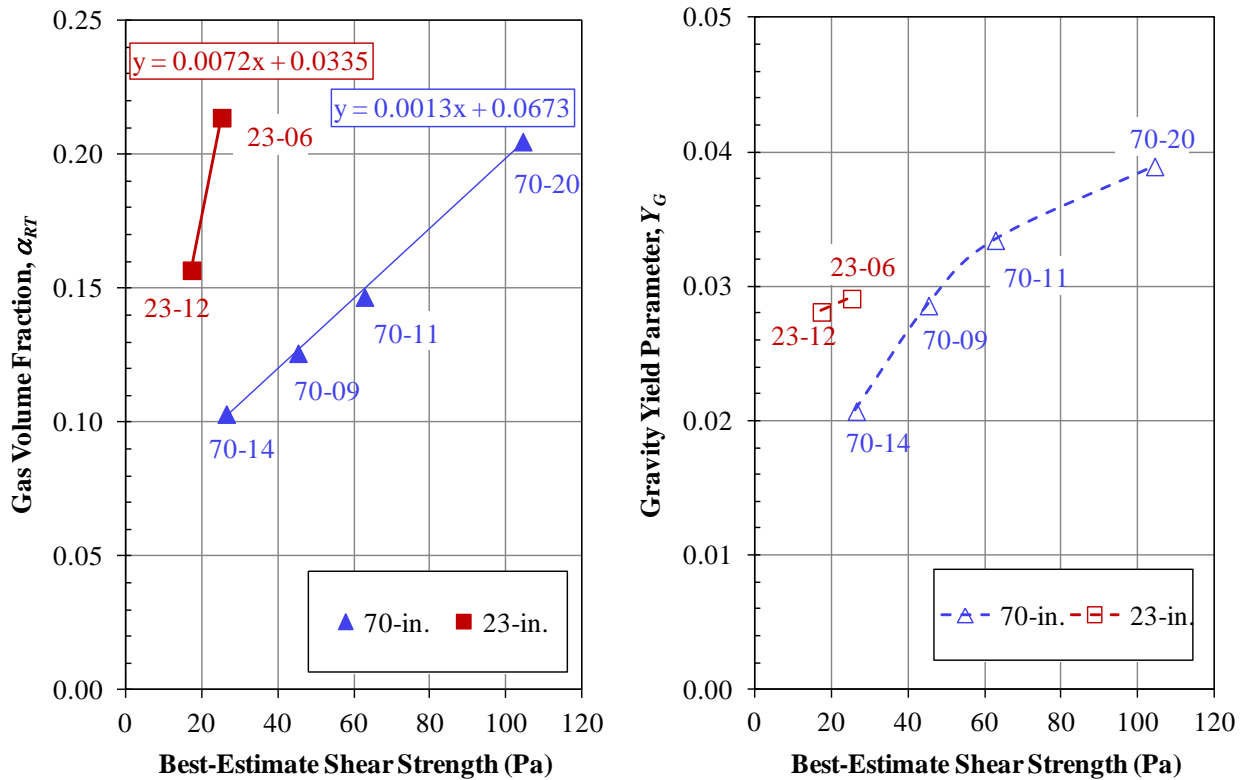


Figure 8.8. Summary of Retained Gas Fractions (left) and the Gravity Yield Parameter (right) for Simulants of Different Shear Strength in the 70-in. Vessel (1 \times total depth and 1:1 lower:upper)

Effect of Depth

Three tests using the ~ 45 -Pa simulant formulation at different slurry depths were completed in the 70-in. vessel (all 1:1 lower:upper). The geometrically-scaled total slurry depths were $0.67\times$ in RT Test 70-16 (50-Pa estimated τ_s at event time), $1\times$ in test 70-09, and $1.5\times$ in test 70-22 (see photos in Section 8.1.2). The retained gas volume plots for the tests are shown in Figure 8.9. The higher growth rate in test 70-09, which was the first completed in the 70-in. vessel, is due to the use of 0.2-wt% H_2O_2 compared to 0.1 wt% in the later tests. Consistent with the 23-in. vessel tests discussed previously (Effect of Depth in Section 8.1.3.2), Figure 8.9 shows that α_{RT} decreases with increasing depth from $0.67\times$ ($\alpha_{RT} = 18.5$ vol%, 50-Pa estimated τ_s at event time) to $1\times$ (12.6 vol%, 45-Pa estimated τ_s). However, the trend does not appear to continue to $1.5\times$, in which case $\alpha_{RT} = 12.1$ vol% (at 41-Pa estimated τ_s) and is the same as the $1\times$ depth test within experimental error. The gas releases at $1.0\times$ and

1.5× depth were both effectively zero, although quantitatively they were negative. This is most pronounced in the 1.5× depth test, for which the potential for gas expansion when the lower-layer sediment rises due to buoyancy is maximized. A relatively small but measurable gas release was observed in the 0.67× depth test ($\Delta\phi \sim 0.014$ or $\sim 5.8\%$ of the retained gas).

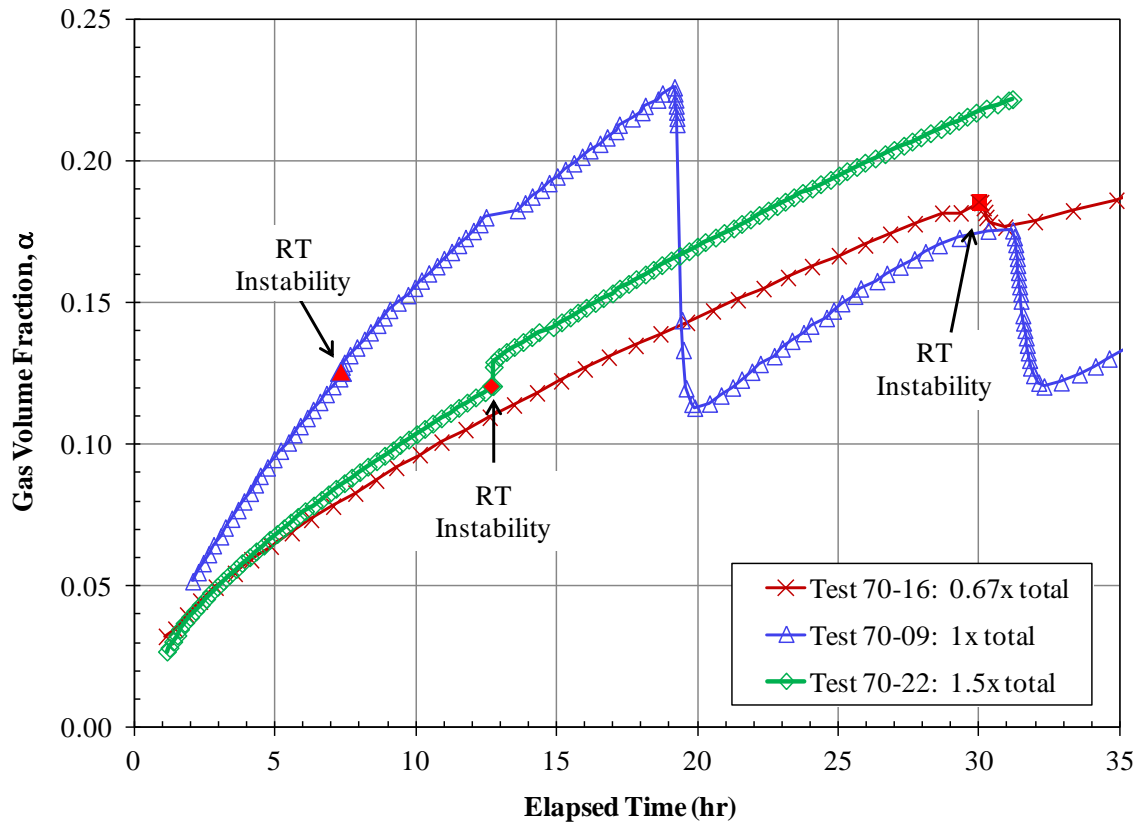


Figure 8.9. Gas Volume Fraction vs. Time for Three Depths of ~ 45 -Pa Shear Strength Slurry in the 70-in. Vessel (1:1 lower:upper)

Gas retention and release results for the three varying total depth tests in the 70-in. vessel are summarized in Figure 8.10. As noted above, the figure shows initially decreasing α_{RT} with increasing slurry depth before leveling out (filled symbols and solid line, left y-axis). The retained gas fraction at the point of RT instability decreased essentially monotonically with depth from 0.67× to 2× in the 23-in. vessel tests. The apparent plateau at ~ 12 to 13 vol% in the 70-in. tests may suggest that there is a finite depth beyond which there is no further effect of layer depth on α_{RT} .

Figure 8.10 also shows the fraction of gas inventory released (open symbols and dashed line, right y-axis) as a function of total slurry depth. As noted above, only the 0.67× depth test showed any measurable gas release. In comparison, gas releases tended to be larger with increasing slurry depth in the 23-in. vessel tests even though α_{RT} decreased with depth. However, the trend was most apparent in the ~ 22 -Pa slurry tests at 1× and 2× depth in which α_{RT} was ~ 16 vol% and greater. The 70-in. vessel 0.67× data also support a conclusion that gas releases tend to be smaller or negligible when α_{RT} is ~ 15 vol% or less, regardless of depth.

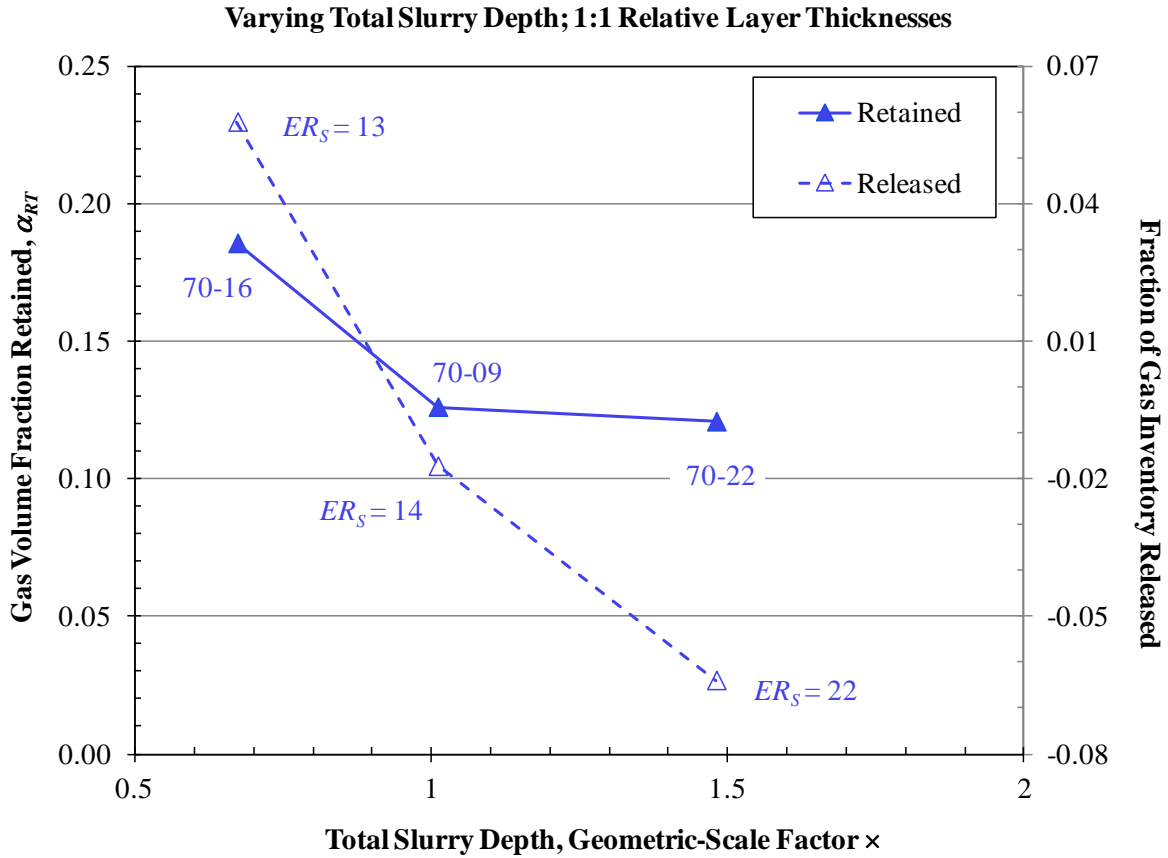


Figure 8.10. Summary of Retained Gas Fractions (left y-axis) and RT Instability Gas Releases (right y-axis) for Equal Slurry Layer Thickness and Varying Total Depth of Slurry in the 70-in. Vessel (~45-Pa cases; labels on the retained gas data points show RT test number, and labels in the gas release points show the calculated modified energy ratio, ER_S .)

The gas release data points in Figure 8.10 have labels indicating the modified energy ratio ER_S that is calculated using Equation (4.4). The ER_S values increase with increasing depth from 13 at 0.67 \times to 22 at 1.5 \times . The trend in ER_S with depth is expected. However, having the largest gas release in conjunction with the lowest ER_S does not bode well for a universal modified energy ratio criterion, applicable to any vessel scale, for discriminating conditions that would lead to gas releases of concern. Correlation of ER_S and RT instability gas releases is discussed further in Section 8.5.2.

8.2 Varying Relative Slurry Layer Depth Tests in the 23-in. Vessel

The varying relative slurry layer thickness tests described in this section were designed to support the RT test objectives (Section 2.0) pertaining to understanding the effects of slurry depth on the magnitude of gas releases associated with RT instability in the sediment and to help develop models (e.g., modified energy ratio) to predict behavior at full-scale. The matrix of varying relative slurry layer depth tests in the 23-in. vessel that were completed is summarized in Section 8.2.1, and the test results are discussed in Section 8.2.2.

8.2.1 Test Matrix, Varying Relative Layer Depths

The conditions used in the varying relative slurry layer depth tests in the 23-in. vessel are described in this section and summarized in Table 8.2. Note that two originally planned 70-in. vessel tests were not completed, in favor of the SL spontaneous gas release tests that are discussed in the next section (8.3).¹ Of the six completed tests, the extremes in lower:upper slurry ratios ranged from 1:5 (0.33× lower, $H_{S2} + 1.67\times$ upper, $H_{S1} = 2\times$ total depth, H_S) to 3:1 (1.5× lower to 0.5× upper).

A seventh test, RT Test 23-21 in Table 8.1, was also run as part of the suite of tests shown in Table 8.2. It is a 1:1, 2× total depth companion test that completes a relative slurry depth series progression (e.g., 1:3, 1:1, and 3:1). Likewise, a number of other equal slurry layer thickness tests shown in Table 8.1 are coupled with the varying relative depth tests for the purposes of analyzing and interpreting the data. Tests can be grouped in multiple ways to probe various hypotheses and effects. Some of the more important sets of tests and the specific assumptions and objectives are as follows.

- Assuming that α_{RT} is constant for a given lower slurry layer depth (H_{S2}) and shear strength (τ_S), varying the upper-layer slurry depth (H_{S1}) allows the relationship of gas release and modified energy ratio (ER_S) to be investigated independent of the effect of depth on α_{RT} . ER_S is a strong function of H_{S1} , as shown by Equation (4.4). Pertinent test groups, in order of increasing relative and absolute depth of the upper layer, include:
 - 23-10, 23-17, and 23-15: $\tau_S \sim 15$ Pa, $H_{S2} = 0.33\times$, and $H_{S1} = 0.33\times$ (1:1), $0.67\times$ (1:2), and $1.67\times$ (1:5)
 - 23-05 (and repeat 23-12) and 23-13: $\tau_S \sim 15$ Pa, $H_{S2} = 0.5\times$, and $H_{S1} = 0.5\times$ (1:1) and $1.5\times$ (1:3)
 - 23-06 and 23-24: $\tau_S \sim 22$ Pa, $H_{S2} = 0.5\times$, and $H_{S1} = 0.5\times$ (1:1) and $1.5\times$ (1:3).
- At constant overall sediment depth (H_S) and constant τ_S , investigate the effect of relative layer thicknesses on gas releases while spanning the target range of α_{RT} values (changing H_{S2}) and varying ER_S (changing H_{S1} , primarily). Pertinent test groups, in order of decreasing relative and absolute depth of the lower layer, include:
 - 23-17 and 23-05 (and repeat 23-12): $\tau_S \sim 15$ Pa, $H_S = 1\times$, and $H_{S2}:H_{S1} = 1:2$ and $1:1$
 - 23-15, 23-13, 23-07, and 23-19: $\tau_S \sim 15$ Pa, $H_S = 2\times$, and $H_{S2}:H_{S1} = 1:5$, $1:3$, $1:1$, and $3:1$
 - 23-24, 23-21, and 23-23: $\tau_S \sim 22$ Pa, $H_S = 2\times$, and $H_{S2}:H_{S1} = 1:3$, $1:1$, and $3:1$.

¹ Two proposed varying relative thickness tests in the 70-in. vessel are shown in Table 3.7 of the TP, TP-DSGREP-001, Rev. 4.0 and an earlier version (3.0). The tests were to be 1:2 and 2:1 layer ratios and 1× total slurry depth. Alternate (revised) scope, SL spontaneous gas release tests, was introduced in Rev. 4.0 of the TP.

Table 8.2. Matrix of Completed Varying Relative Slurry Layer Thickness RT Tests in the 23-in. Vessel (test sequence order)

RT Test No.	TP Test No.	Total Depth, H_S	Lower: Upper Depth	H_2O_2 (wt%)	x_s (wt%)	18-hr τ_S (Pa)		Meas. ρ_S (g/mL)	Time to RT (hr)	α_{RT} (vol%)			Notes
						TP ^(a) Target	Meas.			Meas.	TP ^(a) Target	α_{NB} (vol%)	
23-13	23-I	2	1:3	0.2	42.1	10-16	14.7	1.342	18	15.3	~12.5	25.6	Same τ_S and H_{S2} as RT Tests 23-05 and 23-12; 2× total slurry depth
23-15	23-H	2	1:5	0.2	42.1	10-16	18.7	1.345	28	24.1	~18.5	25.8	Same τ_S and H_{S2} as RT Tests 23-10 and 23-17; 2× total slurry depth
23-17	23-F	1	1:2	0.2	42.1	10-16	15.3	1.343	22	19.5	~18.5	25.7	Same τ_S and H_{S2} as RT Tests 23-10 and 23-15; 1× total slurry depth
23-19	23-J	2	3:1	0.2	42.1	10-16	16.0	1.352	12	13.2	<8	26.2	Same τ_S and H_{S1} as RT Tests 23-05 and 23-12; 2× total slurry depth
23-23	23-M	2	3:1	0.2	45.2	17-26	22.0	1.376	12	15.7	~8	27.5	Same τ_S and H_{S1} as RT Test 23-06; 2× total slurry depth
23-24	23-L	2	1:3	0.2	45.2	17-26	20.0	1.372	31	27.6	~18.5	27.3	Same τ_S and H_{S2} as RT Test 23-06; 2× total slurry depth

Key: × Geo- Relative Total Shear Strength Density Initial RT Gas Fraction NB in

 Scaled Depth Solids Event water

(a) Targets or expected values given in the test matrix, Tables 3.7 of TP-DSGREP-001 Rev. 4.0 (and initially shown in Rev. 3.0 of the TP).

- Proposed tests provide additional opportunities to investigate the effect of τ_S and varying α_{RT} values on the magnitude of gas releases at constant absolute and relative layer thicknesses and nearly constant ER_S . Pairs of tests for comparison include:
 - 23-13 and 23-24: $H_S = 2x$, $H_{S2}:H_{S1} = 1:3$, and $\tau_S \sim 15$ Pa and ~ 22 Pa
 - 23-07 and 23-21: $H_S = 2x$, $H_{S2}:H_{S1} = 1:1$, and $\tau_S \sim 15$ Pa and ~ 22 Pa
 - 23-19 and 23-23: $H_S = 2x$, $H_{S2}:H_{S1} = 3:1$, and $\tau_S \sim 15$ Pa and ~ 22 Pa.

The majority of tests shown in Table 8.2 have unequal lower and upper slurry layer depths, with emphasis on tests having thinner lower layers than the upper layers, which, as a result of equal layer depth tests, was anticipated to result in relatively higher α_{RT} values.

8.2.2 Test Results, Varying Relative Layer Depths

Individual RT test results for the six completed experiments identified in Table 8.2 are provided in Appendix C, and quantitative gas release results are summarized in Table 8.5 (Section 8.5.1). Varying relative slurry layer depth tests in the 23-in. vessel are evaluated from two perspectives in the following sections. First, for cases of constant total slurry depth, the relative depths of the lower and upper slurry layers are varied. Second, for a fixed lower slurry layer depth, the total slurry depth is varied, which thereby affects the lower:upper layer ratio. In each of these approaches, results from applicable equal layer thickness tests described in Section 8.1 are included.

8.2.2.1 Varying Relative Layer Depths at Constant Total Depth

Figure 8.11 shows retained gas volume plots for four $2\times$ total slurry depth tests in the 23-in. vessel at varying lower:upper slurry layer depth ratios, all using the ~ 15 -Pa simulant formulation. In order of increasing geometrically-scaled lower-layer depth H_{S2} , the tests and the retained gas fractions at RT instability shown in the figure are: i) test 23-15, $H_{S2} = 0.33\times (1:5)$, and $\alpha_{RT} = 24.1$ vol%; ii) test 23-13, $H_{S2} = 0.5\times (1:3)$, and $\alpha_{RT} = 15.3$ vol%; iii) test 23-07, $H_{S2} = 1.0\times (1:1)$, and $\alpha_{RT} = 10.5$ vol%; and iv) test 23-19, $H_{S2} = 1.5\times (3:1)$, and $\alpha_{RT} = 13.2$ vol%. With the exception of the last test in the series (3:1), α_{RT} and the size of gas releases increase with increasing upper slurry layer depth and decreasing lower-layer depth. Additionally, the larger gas releases tend to be more rapid with relatively steep drops in the retained gas fraction in shorter periods. The gas release rate characteristics and quantity in the $1.5\times$ depth bottom-layer test are consistent with its intermediate α_{RT} (13.2 vol%), even though α_{RT} is out of line with respect to the trend of decreasing α_{RT} with decreasing upper-layer depth.

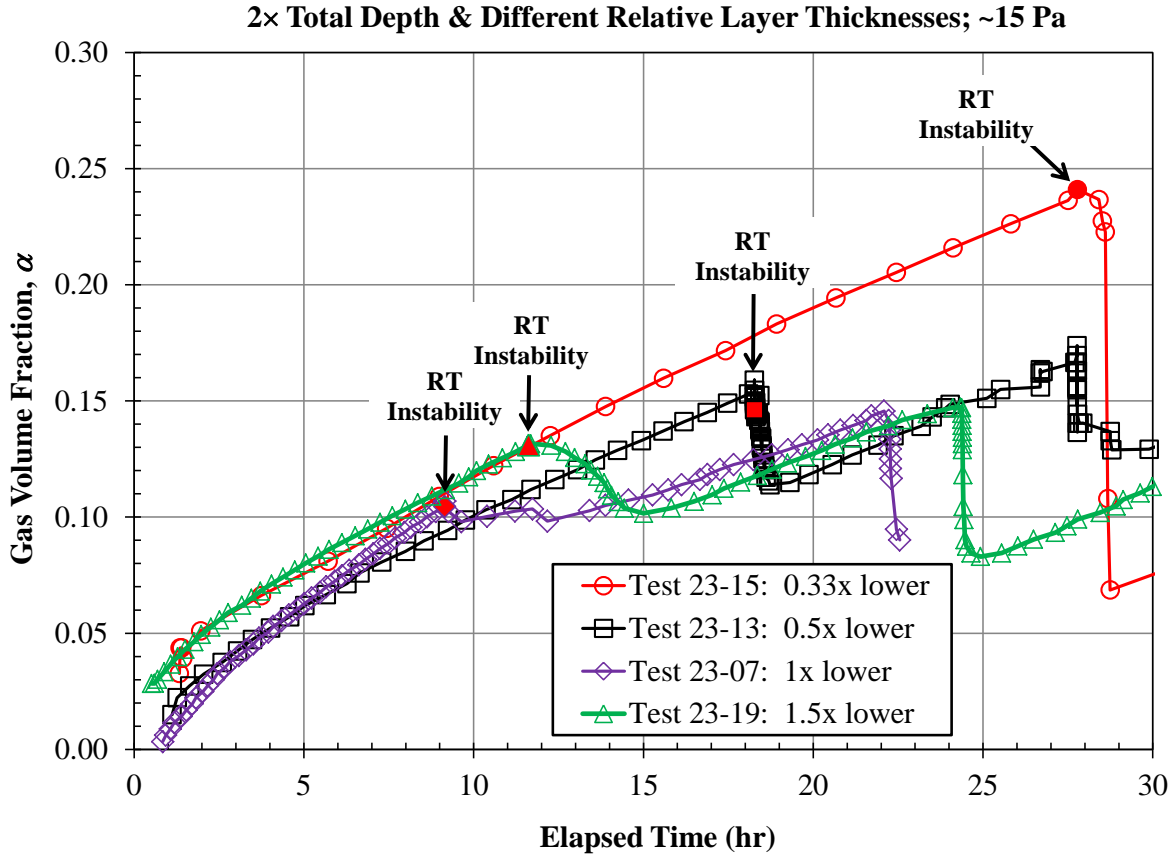


Figure 8.11. Gas Volume Fraction vs. Time for Varying Relative Depths of ~15-Pa Shear Strength Slurry in the 23-in. Vessel (2× total slurry depth)

Figure 8.12 shows a comparable three-test series at 2× total slurry depth using the ~22-Pa simulant formulation. In order of increasing lower slurry layer depth, the tests and the retained gas fractions at RT instability shown in the figure are: i) test 23-24, $H_{S2} = 0.5\times (1:3)$, and $\alpha_{RT} = 27.6 \text{ vol}\%$ ($\approx \alpha_{NB}$); ii) test 23-21, $H_{S2} = 1.0\times (1:1)$, and $\alpha_{RT} = 16.1 \text{ vol}\%$; and iii) test 23-23, $H_{S2} = 1.5\times (3:1)$, and $\alpha_{RT} = 15.7 \text{ vol}\%$. Again there is a trend of decreasing α_{RT} and decreasing size of gas releases with increasing bottom-layer depth up to 1×. In this series, however, the 1.5× and 1× bottom depth tests both had α_{RT} of ~16 vol%, but whereas essentially no gas was released in the $H_{S2} = 1.5\times$ test, a significant fraction of the retained gas inventory (~45%) was released from the shallower bottom-layer case. This is consistent with a higher modified energy ratio for the latter ($ER_S = 21$ vs. 12), which is driven by twice the upper slurry layer depth (1× vs. 0.5×) and a corresponding increase in gas expansion potential following in-sediment buoyant motion. The very large gas release in the 0.5× bottom-layer case (test 23-24) shown in Figure 8.12 is typical of other RT tests having retained gas fractions near or exceeding those required for neutral buoyancy in water (see Section 8.1.3.1).

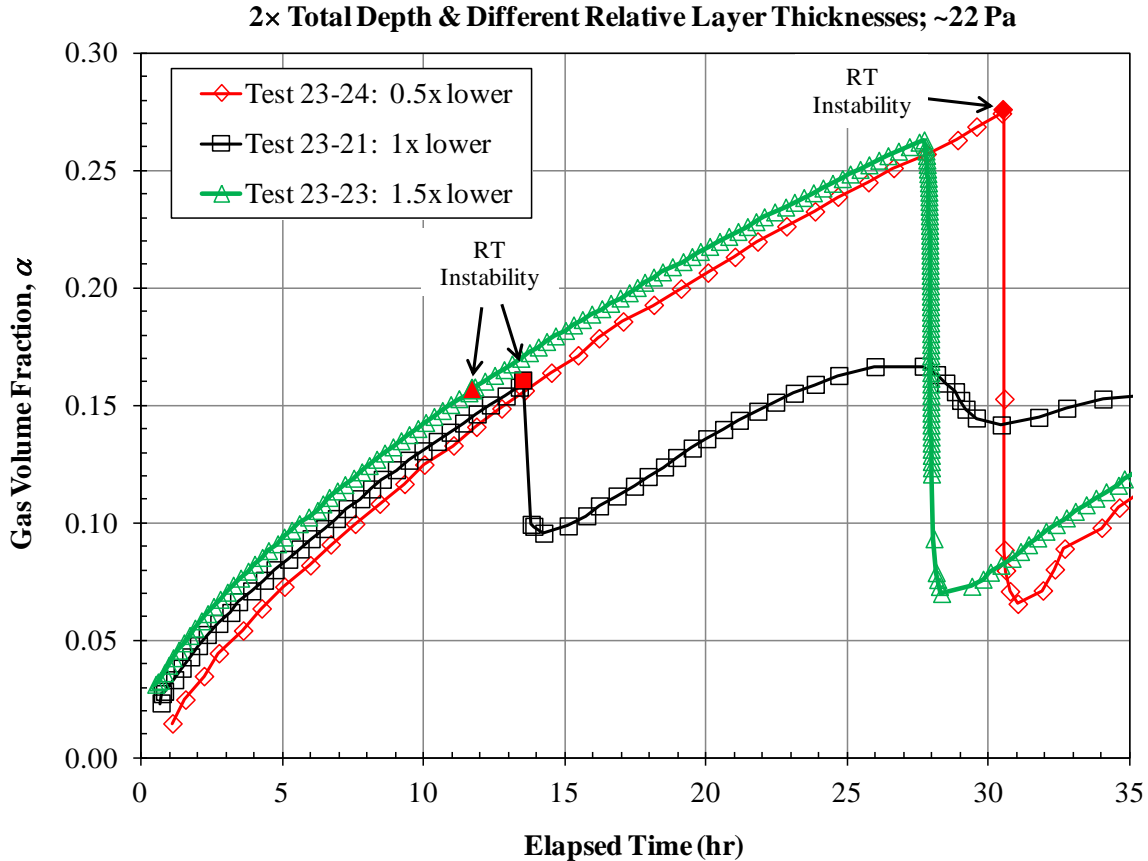


Figure 8.12. Gas Volume Fraction vs. Time for Varying Relative Depths of ~22-Pa Shear Strength Slurry in the 23-in. Vessel (2× total slurry depth)

The gas retention and release data for the tests included in Figure 8.11 and Figure 8.12 are summarized in Figure 8.13 as a function of the geometrically-scaled lower-layer depth. Results for a two-test series at 1× total slurry depth using the ~15-Pa simulant recipe are also shown in the summary figure; the two additional tests and their retained gas fractions at RT instability are: i) test 23-17, $H_{S2} = 0.33 \times (1:2)$, and $\alpha_{RT} = 19.5$ vol%; and ii) test 23-12, $H_{S2} = 1 \times (1:1)$, and $\alpha_{RT} = 15.7$ vol%. Figure 8.13 shows expected decreases in α_{RT} with decreasing τ_S at equivalent layer depths. It also shows the previously noted general trend of increasing α_{RT} and increasing gas release quantities with decreasing lower-layer depth (H_{S2}), which is equally applicable to the newly introduced 1× total depth tests. (Again, RT test 23-19 with $H_{S2} = 1.5 \times$ is an unexplained exception.) As is also discussed in Section 8.2.2.2 and shown in Figure 8.15, deeper upper layers at a given lower-layer depth appear to stabilize against RT instability, requiring larger α_{RT} to overcome the greater apparent τ_S resulting from increased lithostatic load. In conjunction with this, greater upper slurry layer depth increases the potential for gas expansion when the lower layer rises as a result of RT motion and may lead to larger releases.

Comparison of the 1× and 2× depth series using ~15-Pa shear strength slurry shows equal or lower α_{RT} and considerably smaller gas release at a given lower-layer depth. This is consistent with arguments made in the previous paragraph regarding upper-layer depth effects. Overall, the data in Figure 8.13 suggest that the α_{RT} threshold for small gas releases is, in general, reduced in 2× total slurry depth tests (e.g., to <~15 vol%).

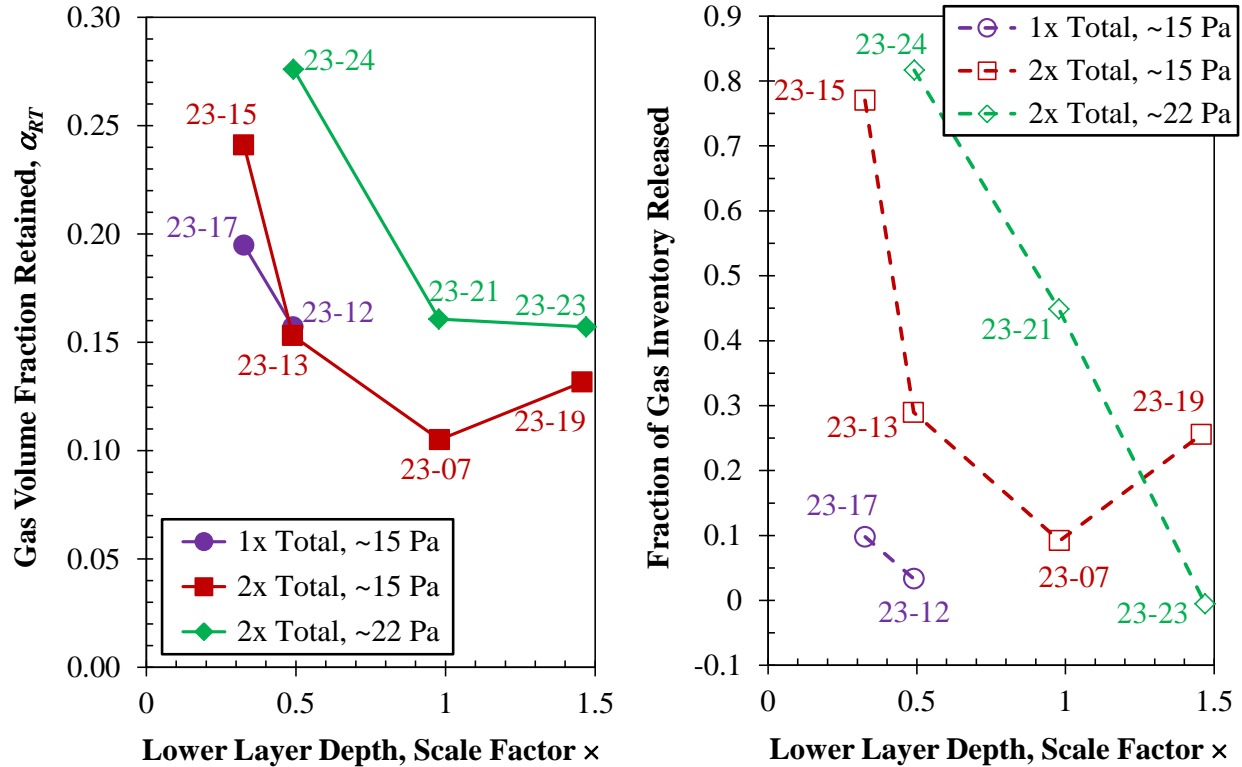


Figure 8.13. Summary of Retained Gas Fractions (left plot) and RT Instability Gas Releases (right plot) for Varying Relative Slurry Layer Thicknesses at Constant Total Depth of Slurry in the 23-in. Vessel (1 \times and 2 \times at ~15-Pa τ_S and 2 \times at ~22-Pa τ_S ; RT test numbers are as labels.)

8.2.2.2 Varying Relative Layer Depths at Constant Lower-Layer Depth

Another view to the effects of varying relative layer thicknesses is from the perspective of constant lower-layer depth with differing upper-layer and total (H_S) slurry depths. Figure 8.14 shows retained gas volume plots for three 0.33 \times lower-layer depth tests in the 23-in. vessel using the ~15-Pa simulant: i) test 23-10, $H_S = 0.67\times$ (1:1), and $\alpha_{RT} = 18.3$ vol%; ii) test 23-17, $H_S = 1\times$ (1:2), and $\alpha_{RT} = 19.5$ vol%; and iii) test 23-15, $H_S = 2\times$ (1:5), and $\alpha_{RT} = 24.1$ vol%. All these data, except for the test 23-17 gas retention vs. time data shown in Figure 8.14, have been shown in previous compilation plots and the gas retention/release data have been discussed. However, this grouping provides direct indication of the increase of α_{RT} and the magnitude of gas releases with increasing upper-layer depth at constant H_{S2} .

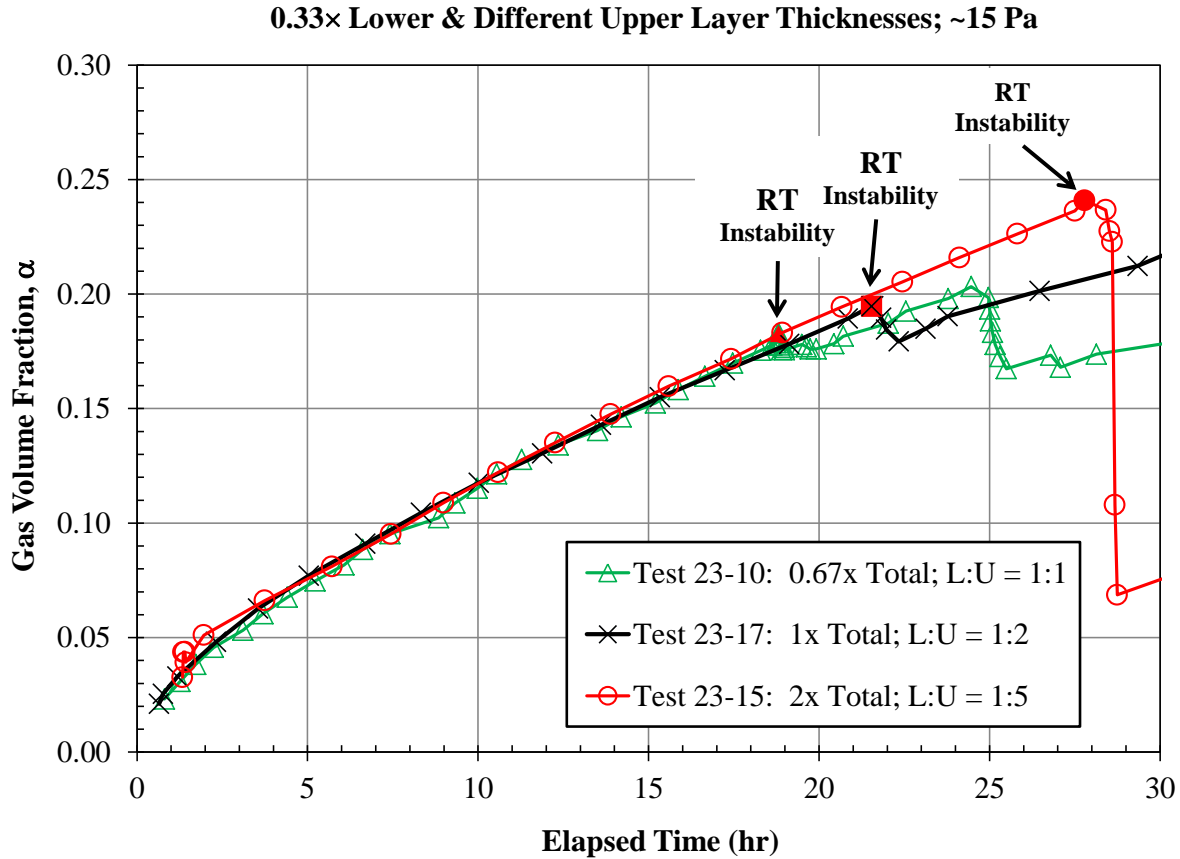


Figure 8.14. Gas Volume Fraction vs. Time for Constant Lower-Layer Depth (0.33×) and Varying Total Depths of ~15-Pa Shear Strength Slurry in the 23-in. Vessel

The gas retention and release data for the tests included in Figure 8.14 are summarized in the left and right plots, respectively, of Figure 8.15 as a function of the geometrically-scaled total slurry depth. Results for two other two-test series at $H_{S2} = 0.5\times$, one using the ~15-Pa simulant recipe (tests 23-12 and 23-13) and the other the ~22-Pa formulation (tests 23-06 and 23-24), are also shown in the summary figure. These additional tests have been discussed previously in either Section 8.1.3.2 or in Section 8.2.2.1. Figure 8.15 shows more directly (than Figure 8.13, for example) increasing (or ~equal) α_{RT} and increasing quantities of gas released with increasing upper-layer and total slurry depth at fixed lower-layer depth. In particular, note that the magnitude of gas releases is significantly smaller in the 0.67× and 1× total depth tests than for 2× cases.

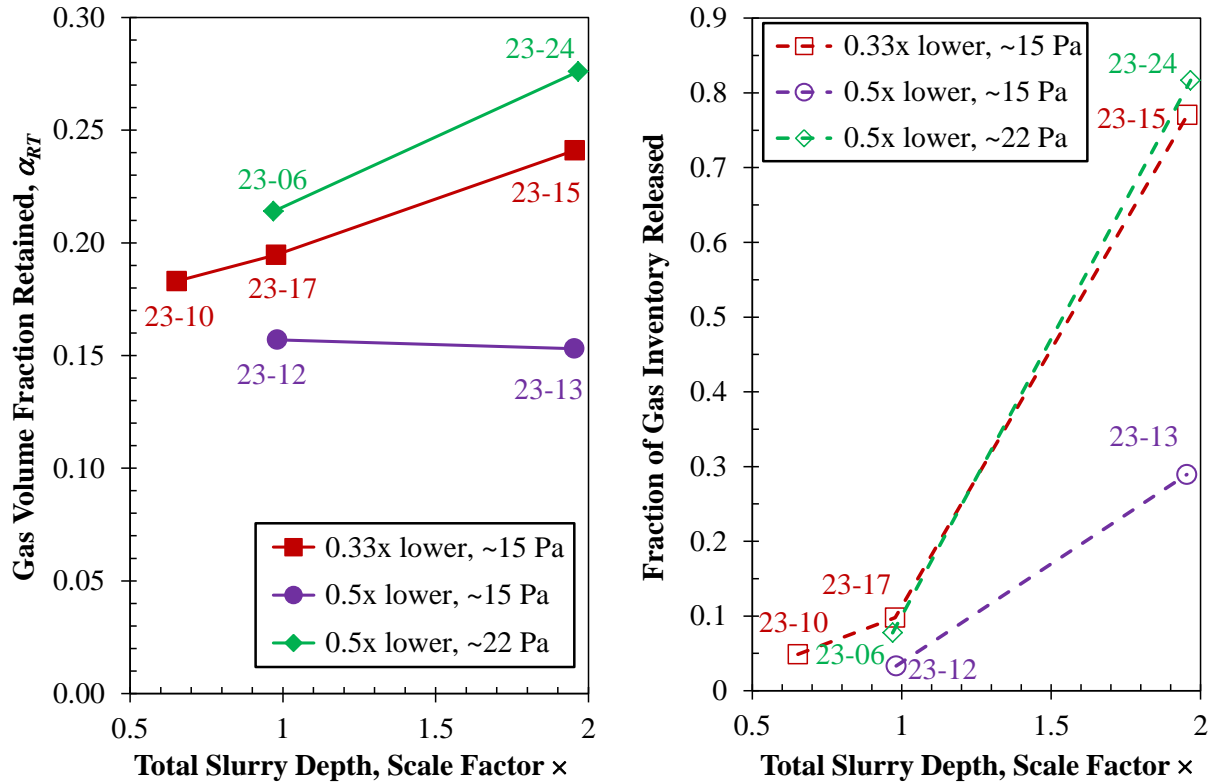


Figure 8.15. Summary of Retained Gas Fractions (left plot) and RT Instability Gas Releases (right plot) for Constant Lower-Layer Depth and Varying Total Depths of Slurry in the 23-in. Vessel (RT test numbers are shown as labels.)

8.3 Single-Slurry-Layer Tests

The single-slurry-layer tests described in this section were designed to support the test objective (Section 2.0) to characterize gas retention and spontaneous gas releases from RT test simulants when gas release is not initiated by an in-sediment RT instability event. It is related to assessment of the following key assumptions, which are repeated from Section 4.4:

- The retained gas fraction at the onset of an RT instability is less than the gas fraction at which gas would spontaneously release from the slurry in the absence of an RT instability or other disturbance.
- In-sediment motion due to RT instabilities does not result in bubble-cascade gas releases.

The matrix of SL tests in the 23-in. and 70-in. vessels that were completed is summarized in Section 8.3.1, and the SL test results are discussed in Section 8.3.2. These results are insightful for the interpretation of high void fraction releases in some RT tests, which is discussed further in Section 8.4.

8.3.1 Test Matrix, Single Slurry Layers

The conditions used in the SL spontaneous gas release tests in the 23-in. and 70-in. vessels are described in this section and summarized in Table 8.3. These tests were conducted with slurry simulant recipes having typical shear strength that spans that used in completed RT tests. Because these

spontaneous release tests do not pre-suppose a gas fraction at the point of instability and there is no need to control conditions such that the gas fraction at the initial spontaneous release, α_{SR} , is in the target range of α_{RT} in RT tests (e.g., 8 to 18.5 vol%), much stronger materials can be used in SL tests than were used in RT tests. This allowed for a portion of a large trough batch of slurry prepared for a 70-in. SL test to be used simultaneously in the 23-in. vessel. Such parallel 23-in. tests were completed with each of the three 70-in. tests shown in Table 8.3.

The gas-generating slurry layer in the SL tests is equivalent in function and solids concentration to lower-layer slurry in RT tests, and, therefore, the single layer is often referred to as “lower”. In this context, and in the absence of an upper slurry layer, the lower-to-upper slurry layer ratio in SL tests is 1:0. A geometrically-scaled slurry layer depth of $0.5\times$ (lower, $H_{SI} = \text{total}, H_S$) was used in all the SL tests. This depth is equivalent to the lower layer in all the equal slurry layer (1:1) $1\times$ total depth tests (Table 8.1 in Section 8.1.1).

The initial approach in the SL tests was to maintain the supernatant water depth the same as used in RT instability tests. However, it was anticipated that α_{SR} could exceed α_{NB} in water, and this was observed in the first SL test (23-25). Because of potentially enhanced gas release from the slurry due to buoyant rise through the “thick” liquid layer, the water depth was reduced in subsequent tests in the 23-in. and 70-in. vessel tests by a factor of 4 from the depths used in RT tests (e.g., ~ 2.5 cm instead of ~ 10 cm in the 23-in. vessel and ~ 4 cm instead of ~ 16 cm in the 70-in. vessel). A relatively thin water layer was retained in the later SL tests to allow for potential doming of the slurry without cresting the water and to provide accurate level measurements.

A few other distinctions from RT tests that are summarized in Table 8.3 are noteworthy. First, a final H_2O_2 concentration of 0.2 wt% in the slurry was used in all SL tests, which is the same as 23-in. RT tests after test 23-03. However, only the first 70-in. RT test (70-09) used 0.2 wt% H_2O_2 ; most used 0.1 wt%¹. The higher concentration of H_2O_2 was used in SL tests to help ensure that sufficient oxygen gas could be generated to have the *a priori* unknown α_{SR} as high as ~ 50 vol%. Secondly, as a result of not having upper-layer slurry, shear strength and density measurements of undiluted slurry at the final solids content (after H_2O_2 addition to the lower-layer slurry) were not available for SL tests. Therefore, water-diluted samples at the noted final solids concentration x_S (starting with pre- H_2O_2 lower-layer slurry samples from the test batch) were prepared and characterized. The 18-hr τ_S and ρ_S for these samples are shown in Table 8.3. As discussed in Section 7.1.2, the shear strength of these water-diluted samples is estimated to be about 10% lower than undiluted slurry at the same x_S , and τ_S for several of the SL test batches already tended to be lower than correlation values (based on measurements of the pre- H_2O_2 slurry samples from the same batches). Finally, α_{SR} and the time to the initial spontaneous release event after completion of slurry filling are shown instead of the RT instability test equivalents.

The completed SL tests shown in Table 8.3 were selected, in part, to provide overlapping conditions in slurry simulant properties and absolute slurry layer depths with completed tests shown in Table 8.1 (Section 8.1.1) and Table 8.2 (Section 8.2.1), as highlighted in the Notes column of Table 8.3. Single-slurry layer tests can be grouped in multiple ways to probe various effects, as follows.

¹ Relatively higher solids content slurry, and correspondingly higher bentonite concentrations, used in 70-in. tests is thought to have increased generation rates compared to the weaker slurry used in 23-in. RT tests. Therefore, the H_2O_2 concentration was reduced in 70-in. RT tests so that RT instability events would occur closer to the 18 to 24 hr target.

- At a constant gas-generating lower (and total) slurry layer depth of $0.5\times$ geometrically scaled ($H_{S2} = H_S = 0.5\times$), investigate the effect of τ_S on the gas retention and spontaneous gas release characteristics. This can be evaluated from the results of the following sets of tests in 23-in. and 70-in. vessels using simulant recipes that spanned (and exceeded in the 23-in. vessel) the range of strengths used in completed RT tests. Pertinent test groups, in order of increasing shear strength within each series, include:
 - 23-25, 23-32, 23-29, 23-27, and 23-31: $H_{S2} = H_S = 0.5\times$ and τ_S ranging from ~ 15 Pa to ~ 90 Pa
 - 70-28, 70-26, and 70-30: $H_{S2} = H_S = 0.5\times$ and τ_S ranging from ~ 30 Pa to ~ 95 Pa.
- At a constant gas-generating lower (and total) slurry layer depth of $0.5\times$ geometrically scaled, investigate the effect of vessel size on the gas retention and spontaneous gas release characteristics at constant τ_S . Pertinent test groups include:
 - 23-29 and 70-28: $H_{S2} = H_S = 0.5\times$ and $\tau_S \sim 30$ Pa
 - 23-27 and 70-26: $H_{S2} = H_S = 0.5\times$ and $\tau_S \sim 45$ Pa
 - 23-31 and 70-30: $H_{S2} = H_S = 0.5\times$ and $\tau_S \sim 95$ Pa.
- At constant τ_S (simulant recipe), compare gas retention/release characteristics in SL and RT tests having the same geometrically-scaled lower-layer depth (H_{S2}) and varying total slurry depth (H_S). Test groups, in order of increasing upper-layer (H_{S1}) and total slurry depth within each series, include:
 - 23-25, 23-05 (and 23-12), and 23-13: $H_{S1} = 0, 0.5\times, \text{ and } 1.5\times$ with $\tau_S \sim 15$ Pa
 - 23-32, 23-06, and 23-24: $H_{S1} = 0, 0.5\times, \text{ and } 1.5\times$ with $\tau_S \sim 22$ Pa
 - 70-28 and 70-14: $H_{S1} = 0$ and $0.5\times$ with $\tau_S \sim 30$ Pa
 - 70-26 and 70-09: $H_{S1} = 0$ and $0.5\times$ with $\tau_S \sim 45$ Pa
 - 70-30 and 70-20: $H_{S1} = 0$ and $0.5\times$ with $\tau_S \sim 95$ Pa.

Table 8.3. Matrix of Completed Single-Slurry-Layer Tests in the 23-in. and 70-in. Vessels (test sequence order; shaded by vessel size)

SL Test No.	TP Test No.	Total Depth, H_S	Lower: Upper Depth	H_2O_2 (wt%)	x_s (wt%)	18-hr τ_S (Pa)		Meas. ^(b) ρ_S (g/mL)	Spontaneous Release			Notes
						TP ^(a) Target	Meas. ^(b)		Time to SR (hr)	α_{SR} Meas.	α_{NB}	
23-25	23-P	0.5	1:0	0.2	42.1	~15	13	1.339	36	0.301	0.255	Same τ_S and H_{S2} as RT Tests 23-05, 23-12, and 23-13; “thick”, ~10-cm deep water layer ^(c)
70-26	70-I	0.5	1:0	0.2	49.7	~45	33	1.437	27	0.271	0.305	Same τ_S and H_{S2} as RT Test 70-09
23-27	23-S	0.5	1:0	0.2	49.7	~45	33	1.437	30	0.290	0.305	Same H_{S2} as ~half of the 23-in. vessel tests and the same τ_S as RT Test 70-09
70-28	70-H	0.5	1:0	0.2	47.1	~30	21	1.395	30	0.281	0.285	Same τ_S and H_{S2} as RT Test 70-14
23-29	23-R	0.5	1:0	0.2	47.1	~30	21	1.395	36	0.311	0.285	Same H_{S2} as ~half of the 23-in. vessel tests and the same τ_S as RT Test 70-14
70-30	70-J	0.5	1:0	0.2	54.1	~95	81	1.494	14	0.237	0.332	Same τ_S and H_{S2} as RT Test 70-20
23-31	23-S	0.5	1:0	0.2	54.1	~95	81	1.494	14	0.234	0.332	Same H_{S2} as ~half of the 23-in. vessel tests and the same τ_S as RT Test 70-20
23-32	23-Q	0.5	1:0	0.2	45.2	~22	19	1.374	38	0.288	0.274	Same τ_S and H_{S2} as RT Tests 23-06 and 23-24
Key:		× Geo-Scaled	Relative Depth	Total Solids	Shear Strength	Density	Initial Event	Gas Frac.	NB in water			

(a) Targets or expected values given in the test matrix for SL tests, Table 3.8 of TP-DSGREP-001 Rev. 4.0.

(b) The 18-hr shear strength and density were measured on slurry samples that were diluted with water to the same final solids content as the slurry batches used in the vessel tests after H_2O_2 had been added (i.e., x_s shown in this table). The water-dilution samples were prepared ~2 hr before the H_2O_2 was added to the bulk of the batch and the vessel was filled. In the two-layer RT tests, measured 18-hr τ_S and ρ_S values shown in Table 8.1 and Table 8.2 are for upper-layer slurry batch samples that were previously prepared to the final solids concentration.

(c) In the first SL test in the 23-in. vessel (23-25), the “standard” water layer depth that had been used in other RT tests (~10 cm) was used. After observing potentially enhanced gas release from the slurry due to buoyant rise through the “thick” liquid layer, the water depth was reduced in subsequent tests in the 23-in. and 70-in. vessel tests by a factor of 4 from the depths used in RT tests (e.g., ~2.5 cm instead of ~10 cm in the 23-in. vessel and ~4 cm instead of ~16 cm in the 70-in. vessel). A relatively thin water layer was retained in the later SL tests to allow for potential doming of the slurry without cresting the water and to provide accurate level measurements.

8.3.2 Test Results, Single Slurry Layers

Individual single-slurry-layer test results for the eight completed experiments identified in Table 8.3 are provided in Appendix C. In the following, the five SL tests in the 23-in. vessel and the three in the 70-in. vessel are discussed in individual sections, before comparing and summarizing the results in a final section.

8.3.2.1 23-in. Vessel Tests

Figure 8.16 compares SL test 23-32 to two-layer RT tests (23-06 and 23-24) having the same 0.5× lower-layer depth. The ~22-Pa shear strength recipe was used in all three tests. In the SL test, the gas fraction at spontaneous release, $\alpha_{SR} = 28.8$ vol%, was ~5% higher than the gas fraction for the slurry to become neutrally buoyant in the supernatant water. Approximately 96% of the retained gas inventory was released spontaneously and rapidly in a bubble-cascade. Both α_{RT} (27.6 vol%) and the large, bubble-cascade-like gas release characteristics in RT test 23-24 (2× total depth, 1:3 lower:upper) are similar to the spontaneous release event in SL test 23-32. In this case, it could be argued that the release in RT test 23-24 was large either because α_{RT} approached α_{NB} or that it was nearly equal to α_{SR} . In 1× total depth, 1:1 lower:upper RT test 23-06, α_{RT} and the size of the gas release associated with the initial instability were smaller, which is attributed to the reduced total slurry depth and upper-layer depth in comparison to test 23-24 (e.g., see Section 8.2.2.2).

In RT test 23-06, both the reduced apparent gas fraction at the point of the secondary release (at ~29 hr) and the smaller size of the release shown in Figure 8.16 might be explained by redistribution of lower-layer slurry in the initial RT event. For example, a bulk portion of the lower-layer slurry may have remained intact (or stationary) during the initial RT event and continued to retain gas locally until it reached, e.g., the spontaneous release gas fraction. Because only a fraction of the original lower-layer slurry retained the higher gas fraction, the secondary release would be smaller. For lower-layer slurry that moved appreciably during the RT event, solids would be effectively diluted by (mixed with) upper slurry, so that even though gas continued to be generated, the local average retained gas fraction would be lower than that necessary to spontaneously release at the time of the first secondary-release event. The secondary-release hypothesis is perhaps also supported by the timing of the event in test 23-06 in comparison to the primary release in RT test 23-24 (~31 hr). Based on the consistency of the gas retention-vs.-time profiles for the tests (shown in Figure 8.16), it can be assumed that gas continued to be generated (and retained) at the same rate following the RT instability event at ~21 hr in test 23-06. Therefore, any undisturbed lower-layer slurry should have retained approximately the same gas fraction at ~30 hr as that in test 23-24 and had a spontaneous bubble-cascade at that time.

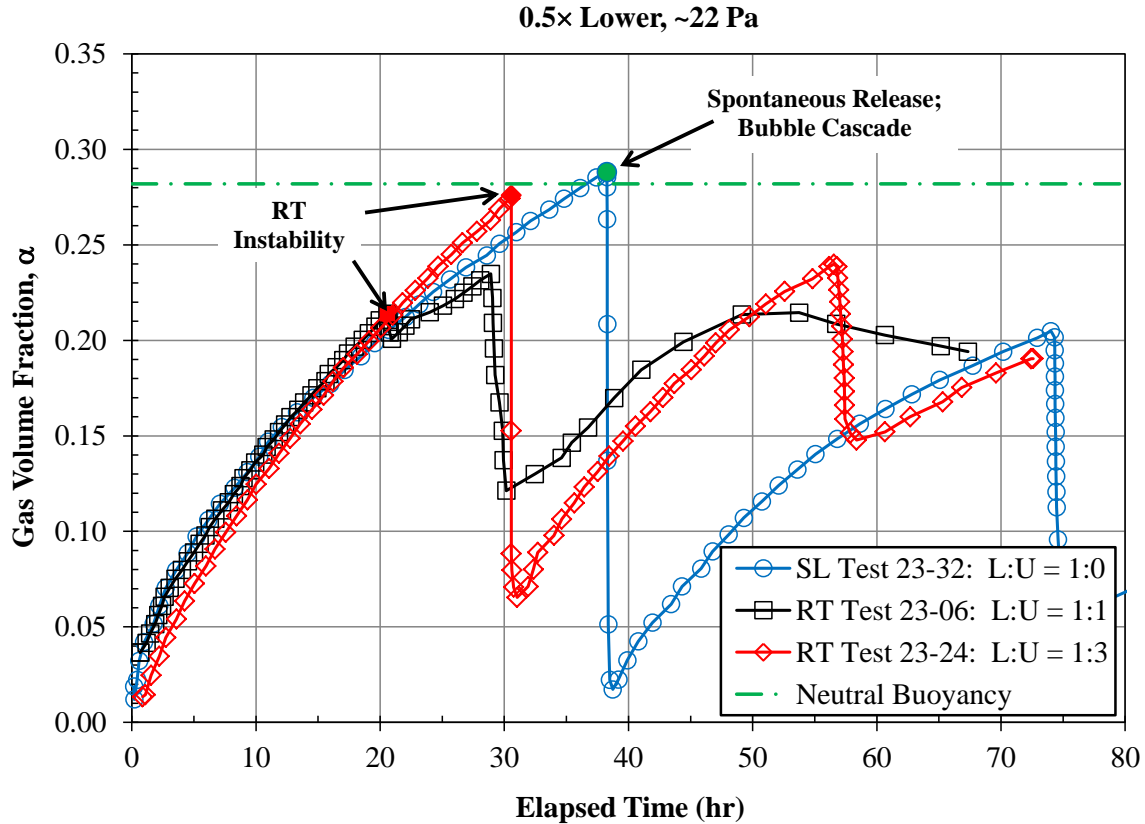


Figure 8.16. Comparison of Gas Volume Fraction vs. Time for Single-Layer and Two-Layer RT Tests at $0.5\times$ Lower-Layer Depth of ~ 22 -Pa Shear Strength Slurry in the 23-in. Vessel

Figure 8.17 shows the gas retention/release profiles for four other SL tests in the 23-in. vessel (all at $0.5\times$ lower = total slurry depth). These tests use simulant recipes that were also used in various RT tests in the 23-in. and 70-in. vessels. The recipes, noted by the typical formulation shear strength values (and the correlation-based estimate of τ_S at the time of the release event¹), and the gas fractions at spontaneous release shown in Figure 8.17 are: i) test 23-25, ~ 15 -Pa recipe (~ 16 Pa est.), and $\alpha_{SR} = 30.1$ vol%; ii) test 23-29, ~ 30 -Pa recipe (~ 34 Pa est.), and $\alpha_{SR} = 31.1$ vol%; iii) test 23-27, ~ 45 -Pa recipe (~ 50 Pa est.), and $\alpha_{SR} = 29.0$ vol%; and iv) test 23-31, ~ 95 -Pa recipe (~ 87 Pa est.), and $\alpha_{SR} = 23.4$ vol%. These data indicate a “peak” α_{SR} of ~ 30 vol% for the two weakest slurries and a trend of decreasing α_{SR} with increasing strength, which is clearly observed for the strongest material. The gas retention profiles in Figure 8.17 also show a direct correlation of increasing quantity of gas released with decreasing strength. In the weakest, essentially all the retained gas was released in a rapid bubble-cascade. The release event in the strongest slurry was both smaller and slower, progressing over ~ 5 hr. The effects of shear strength on spontaneous gas releases are further quantified and summarized in Section 8.3.2.3.

¹ These shear strength estimates are discussed in the section summarizing the SL test results (Section 8.3.2.3) and are shown there in Table 8.4.

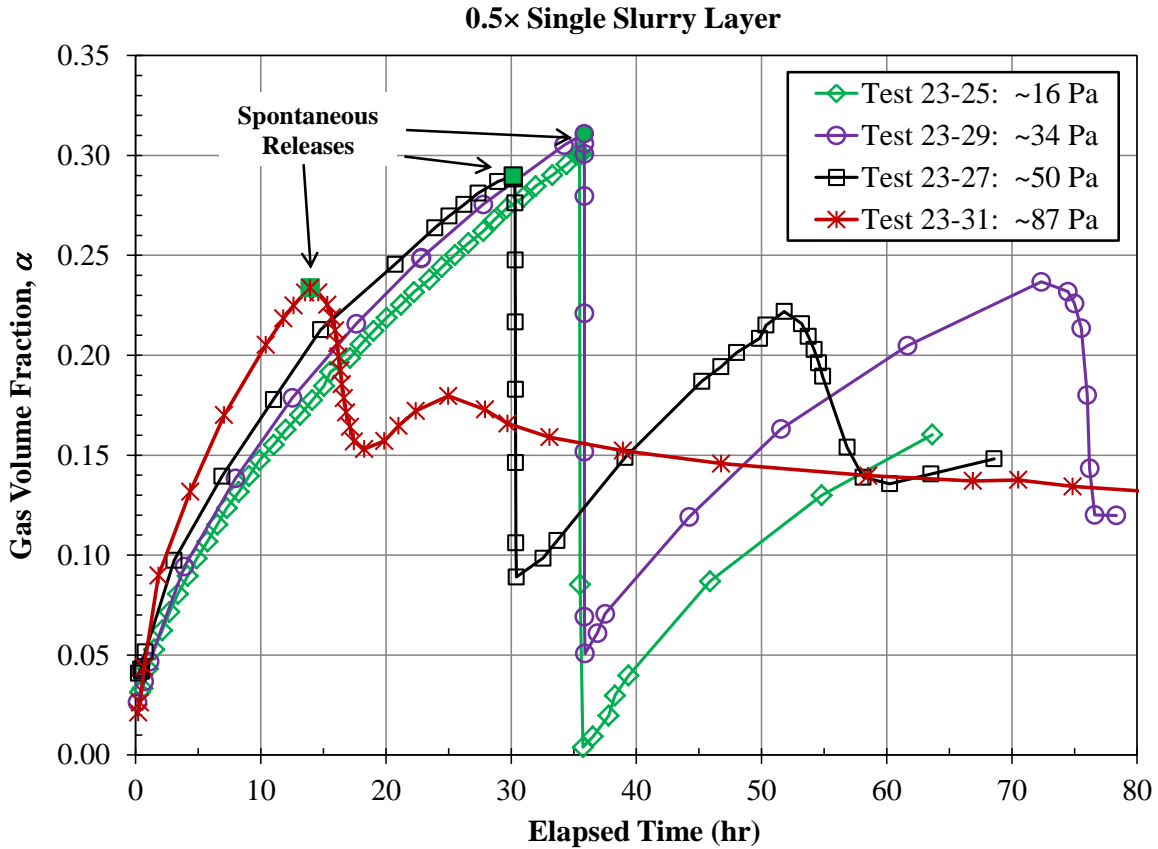


Figure 8.17. Gas Volume Fraction vs. Time for Single-Layer Tests in the 23-in. Vessel Using Simulants of Different Shear Strength

8.3.2.2 70-in. Vessel Tests

Figure 8.18 compares SL test 70-26 to RT test 70-09, both of which had 0.5× lower-layer depth and used the ~45-Pa shear strength simulant recipe with 0.2-wt% H₂O₂. The figure shows that α_{SR} in the SL test (27.1 vol%) was higher than the gas fraction of the secondary release in the RT test (~22 vol% at ~19 hr), but both demonstrate characteristically rapid, large gas releases. As noted in the previous section, lower gas fractions at the point of secondary releases in RT tests compared to spontaneous releases in SL tests may be due to mixing of some, but not all, of the lower and upper slurry layers during the initial RT instability.

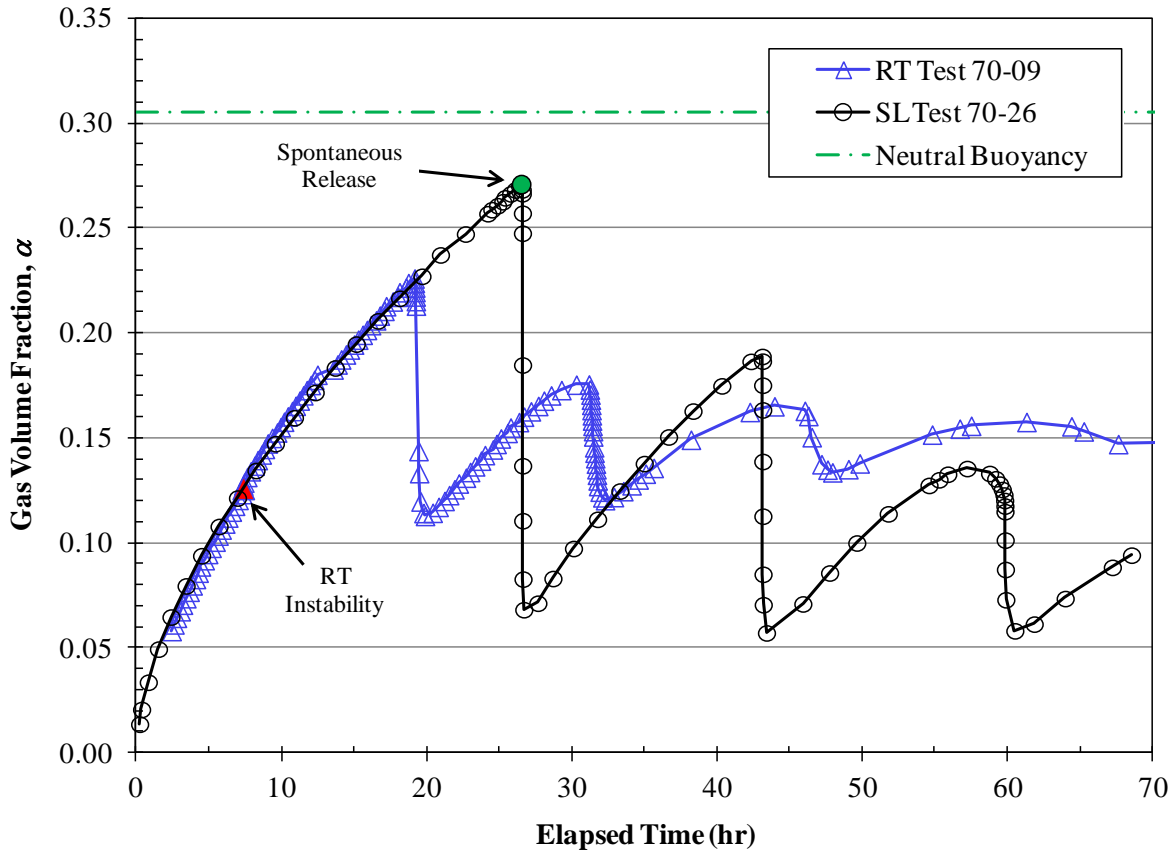


Figure 8.18. Comparison of Gas Volume Fraction vs. Time for Single-Layer and Two-Layer RT Tests at $0.5\times$ Lower-Layer Depth of ~ 45 -Pa Shear Strength Slurry in the 70-in. Vessel

SL test 70-30 and RT test 70-20, both using the highest strength simulant (~ 95 -Pa recipe), are compared in Figure 8.19. Differences in gas generation and growth rates in these tests are due to lower H_2O_2 concentration in the RT test (0.1 wt% vs. 0.2 wt%). The associated shift in the time to the release events is a factor in differences in shear strength, which are estimated to be 87 Pa in SL test 70-30 and 104 Pa in RT test 70-20. It is noted in the following section (8.3.2.3) that α_{SR} tends to decrease with increasing strength in this range of shear strength, and therefore, α_{SR} may be lower than shown at the conditions of the RT test. The measured gas fraction at spontaneous release in the SL test was 23.7 vol%, only a few percent higher than α_{RT} (19.6 vol% or $\sim 83\%$ of α_{SR}). As noted in Figure 8.19, release of numerous individual bubbles (e.g., approximately 2- to 4-cm diameter) was observed at a peak gas fraction of 20.5 vol% (or $\sim 86\%$ of α_{SR}) about an hour before the buoyant sediment motion characteristic of the RT instability was observed. The pre-release showed characteristics very similar to the bubble-cascade-like release of the SL test. The data suggest that when α_{RT} approaches α_{SR} that an RT instability gas release will take on the characteristics of a spontaneous release, consistent with the gas retention and release behavior of the simulant.

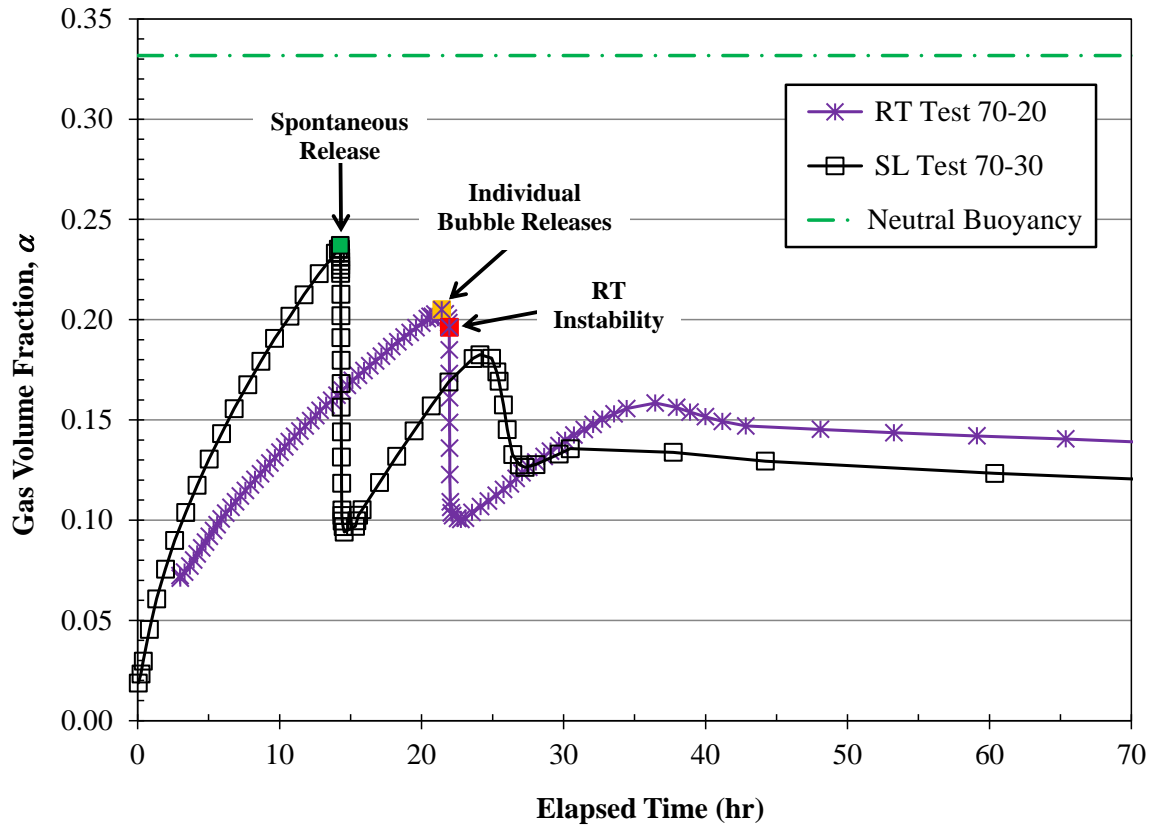


Figure 8.19. Comparison of Gas Volume Fraction vs. Time for Single-Layer and Two-Layer RT Tests at $0.5\times$ Lower-Layer Depth of ~ 95 -Pa Target Shear Strength Slurry in the 70-in. Vessel

8.3.2.3 Summary of 23-in. and 70-in. Single-Layer Test Results

Prior to summarizing gas retention and release in the SL tests, Figure 8.20 provides a head-to-head comparison of spontaneous gas release characteristics in the 23-in. and 70-in. vessels. Tests 70-28 and 23-29 were conducted in parallel using simulant (~ 30 -Pa recipe) in both vessels from batches that were nominally prepared for the 70-in. vessel test. Figure 8.20 shows that while α_{SR} was slightly higher in the 23-in. vessel (31.1 vol% vs. 28.1 vol%), both exhibited large and rapid release of approximately 90% of the retained gas inventory.

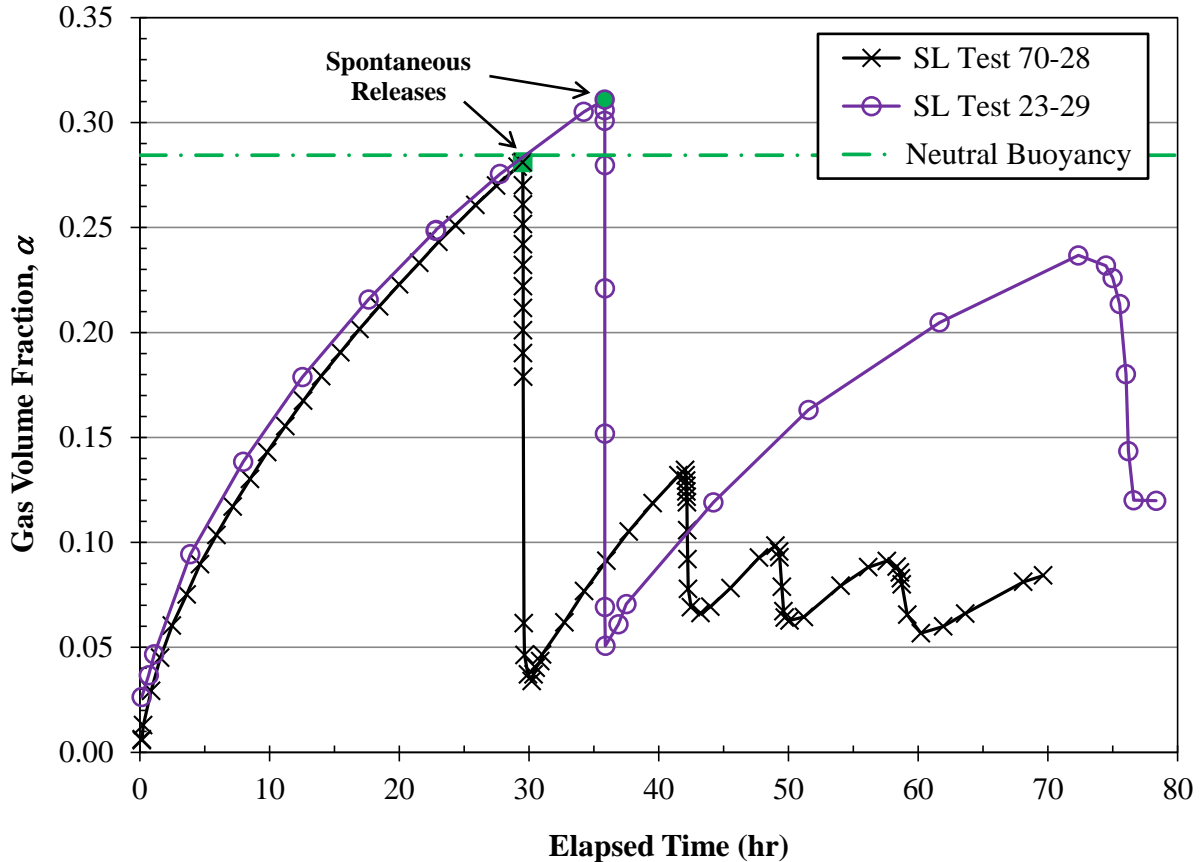


Figure 8.20. Comparison of Gas Fraction vs. Time for Single-Layer Tests in the 23-in. and 70-in. Vessels Using the Same ~30-Pa Target Shear Strength Slurry

Results for other parallel 23-in. and 70-in. SL tests show some strength-dependent differences in the gas retention and release behavior in the two vessels, but general trends of decreasing α_{SR} and decreasing quantities of gas released with increasing shear strength were observed at both vessel scales. This is shown in Figure 8.21 and summarized in Table 8.4. The 23-in. vessel gas retention data in the figure (left plot) suggest a peak in α_{SR} of ~31 vol% at ~34-Pa estimated shear strength. The figure and table also show that α_{SR} exceeds α_{NB} for each of the three simulants having strengths \leq ~34 Pa. Because the two-weakest simulants were not used in 70-in. vessel tests, it cannot be determined whether α_{SR} also peaks at ~30 Pa in the larger vessel. The gas release data in Figure 8.21 show a monotonic increase in release fraction with decreasing strength, suggesting more global bubble cascades in the lower shear strength and yield stress slurries. The most apparent difference in gas release behavior in the two vessels is noted for the highest shear strength slurry, estimated at ~87 Pa at the time of spontaneous release in both tests 70-30 and 23-31. About 67% of the gas inventory was released in the 70-in. test compared to ~41% released in the 23-in. test, even though α_{SR} was nearly equal in the experiments (23 to 24 vol%). A difference in release behavior is also demonstrated in the gas retention profiles for the tests, which are shown in Figure 8.19 (Section 8.3.2.2) for test 70-30, Figure 8.17 (Section 8.3.2.1) for test 23-31, and together in Figure 8.22 (Section 8.4 to follow). The release event in test 23-21 was slower, progressing over ~5 hr, compared to a relatively rapid release in the 70-in. test (e.g., in ~20 min.). The gas retention profiles suggest that the smaller vessel and/or reduced slurry depth may in some way restrain slurry motion and gas release. Another possibility is that the bubble size distribution differed in the two vessels

due to, for example, differences in effectiveness of degassing in the process of filling the vessels. However, estimated initial gas fractions after addition of the slurry layers in the two tests were comparable.

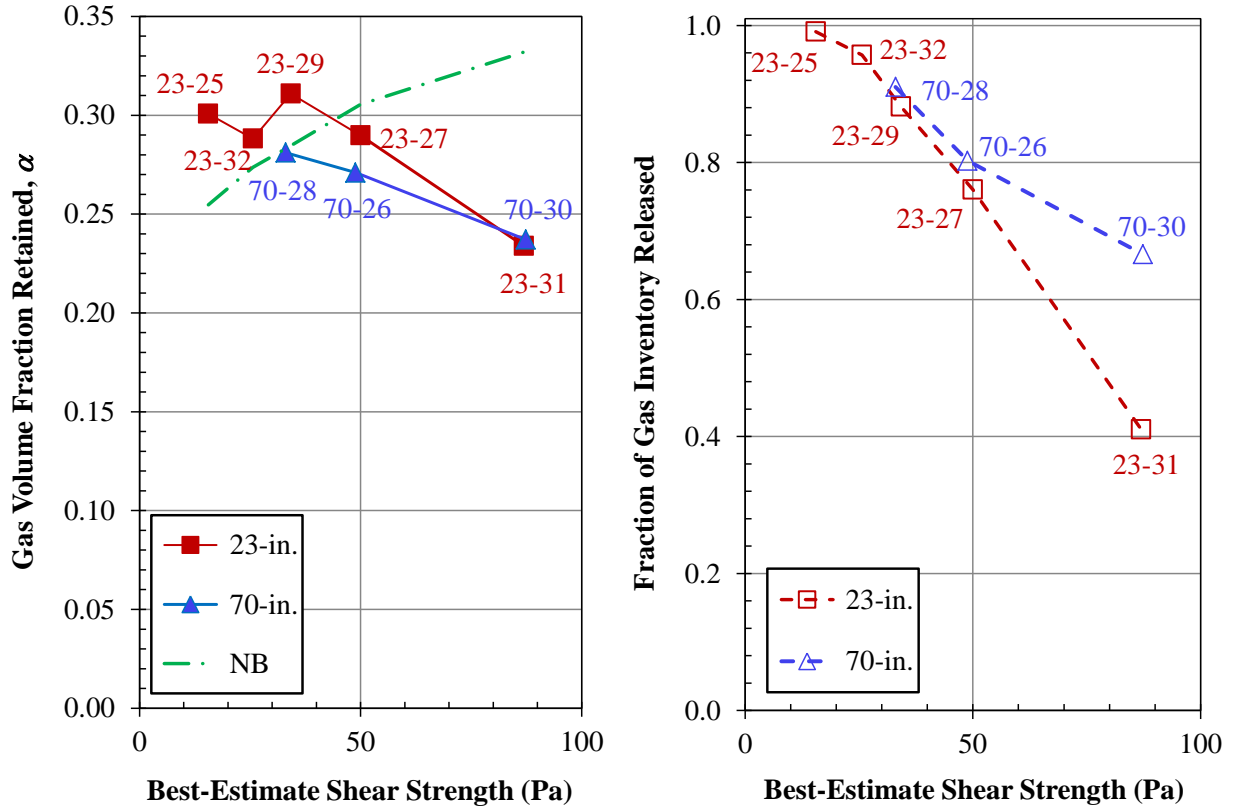


Figure 8.21. Summary of Retained Gas Fractions (left) and Spontaneous Gas Releases (right) in Single-Slurry-Layer Tests in the 23-in. and 70-in. Vessels (NB is the retained gas fraction required for neutral buoyancy in water; SL test numbers are shown as labels adjacent to data points.)

Table 8.4. Magnitude of Single-Layer Spontaneous Gas Releases (ordered by vessel and sequence)

SL Test	Depth vs. Geo-Scaled	L:U Depth	Dilution Sample ^(a)		Correlation τ_S ^(b)				Quantity of Gas Released		
			Density kg/m ³	Est'd τ_S Pa	18-hr Pa	Est'd Pa	α_{SR}	α_{SR}/α_{NB}	Void Frac. $\Delta\alpha$	Specific $\Delta\phi$	Fraction of Inventory
23-25	0.5	1:0	1339	14	13	16	0.301	1.181	0.297	0.433	0.991
23-27	0.5	1:0	1437	37	43	50	0.290	0.949	0.201	0.313	0.761
23-29	0.5	1:0	1395	24	29	34	0.311	1.093	0.260	0.401	0.882
23-31	0.5	1:0	1494	80	85	87	0.234	0.704	0.081	0.126	0.410
23-32	0.5	1:0	1374	20	21	26	0.288	1.053	0.271	0.391	0.957
70-26	0.5	1:0	1437	36	43	49	0.271	0.887	0.203	0.306	0.803
70-28	0.5	1:0	1395	24	29	33	0.281	0.988	0.247	0.365	0.910
70-30	0.5	1:0	1494	81	85	87	0.237	0.714	0.143	0.212	0.666

(a) The density and 1-hr and 18-hr (see Table 8.3) shear strengths were measured on a pre-H₂O₂ batch sample diluted with water to the same solids concentration as the slurry used in the SL test after H₂O₂ addition (which is also equivalent to upper- and lower-layer slurries that had been used in at least one RT test). The effect of dilution on shear strength and estimating the value at the gas-release event time from 1-hr and 18-hr τ_S values are addressed in Sections 7.1.2.2 and 7.1.2.3.

(b) In RT tests, the estimated shear strength at the gas-release event time (Section 7.1.2.3) is based on 1-hr and 18-hr shear strength for an upper-layer slurry sample, which has the same solids content as the lower-layer slurry after H₂O₂ addition. However, there is no “upper layer” in SL tests. Therefore, correlation-based estimates of shear strength were calculated for comparison to dilution-sample results, as follows: 1) using the final batch solids content x_S for the test (Table 8.3), the 1-hr and 18-hr τ_S values were calculated from Equations (7.1) and (7.2), respectively; and 2) these values and the time of the spontaneous release event (Table 8.3) were used in Equation (7.4) to obtain the best-estimate τ_S .

8.4 Interpretation of High Void Fraction Releases

Relatively high void fraction releases were observed in the initial instability events in a subset of the RT tests and in secondary GREs typical of most RT tests. This section offers interpretation of these events. First, and perhaps most importantly, several of the RT tests showed that gas releases tend to be relatively large if α_{RT} approaches or exceeds the gas fraction required for the slurry to become neutrally buoyant in water, α_{NB} . It turns out that the gas fraction for spontaneous gas release determined in SL tests is also close to α_{NB} for shear strength $< \sim 35$ Pa. Therefore, one could use proximity of α_{RT} to the spontaneous release gas fraction α_{SR} as a possible means to screen for the potential of high void fraction releases in addition to α_{NB} . For example, in RT Test 70-20, the retained gas fraction shortly before and at the point of RT instability was 83 to 86% of α_{SR} . Using an α_{RT}/α_{NB} screening criterion, 85% appears to be a line separating large and small releases (see Section 8.5.1).

The RT instability gas releases discussed in Section 8.1.3 and Section 8.2.2 were generally followed by later release events whose behavior was visibly different from that of the initial RT event. This was shown, for example, in numerous retained gas fraction vs. time plots in the noted sections, and it can be seen in most of the individual RT test gas retention profiles in Appendix C. As shown photographically in Section 8.1.2, the initial RT events were typically characterized by the rise of a “volcano” cone near the center of the vessel (or a semi-conical heap nearer the vessel wall in some 10-in. and 23-in. vessel tests),

followed by an “eruption” of gas bubbles and bottom-layer solids. The bottom layer did not undergo an overall displacement that was visible at the wall, although some inter-layer motion was typically observed. By contrast, the later post-RT events often occurred over a broad area, sometimes with successive releases from several spots in that area, and a wave of displacement could often be seen sweeping across the bottom layer at the wall. It was not unusual for post-RT, secondary events to recur several hours apart, producing a “saw-tooth” pattern in retained gas volume fraction versus time as gas retention alternated with gas release.

The characteristics of these secondary releases in RT tests (and initial RT event releases, if they were large,) are both visually and quantitatively similar to the primary and secondary spontaneous gas releases observed in SL tests. Direct comparison of RT and SL test gas retention profiles, such as Figure 8.16 in Section 8.3.2.1 for the 23-in. vessel and Figure 8.18 and Figure 8.19 in Section 8.3.2.2 for the 70-in. vessel, provides good examples. The gas fraction at the point of secondary-release events in RT tests was often higher than the gas fraction α_{RT} at the start of the RT event, though not as high as the gas fraction α_{SR} at start of a spontaneous release event in an SL test using the same simulant formulation; see, for example, RT Tests 23-06 in Figure 8.16 and 70-09 in Figure 8.18 along with their companion SL Tests 23-32 and 70-26. The same gas release mechanism may govern both types of releases even though gas fractions at the start of post-RT event releases are lower compared to α_{SR} . This could be explained, for example, by mixing of slurry layers in an RT event and secondary releases emanating from a relatively unmixed portion of the lower-layer slurry having a higher local gas fraction than the measured bulk average α . Spontaneous gas releases in SL tests were also visually similar to secondary (and large initial) RT test gas releases. Bubble-cascade releases were evident in the SL tests, especially in slurries with estimated shear strength of 50 Pa or less.

Saw-tooth gas retention-release cycles similar to those seen in RT and SL test gas retention profiles were also observed in previous experimental studies by Gauglitz et al. (1996), in which single layers of bentonite clay simulant were used with no supernatant. It was noted that the maximum gas retention at the point of release and the periodicity depended on slurry shear strength. Saw-tooth behavior was seen in clay in 2.5-cm tubes for shear strengths of 3.4 Pa, 6.4 Pa, and 31 Pa, with the saw-tooth behavior being absent, except for a single release, at a shear strength of 67 Pa. The peak retained gas volume fraction in these low-strength materials rose from near zero (for 3.4 Pa) to 0.4 (at 31 Pa). For the same tube diameter and stronger materials (147 Pa, 323 Pa, 656 Pa, and 1040 Pa), the retained gas fraction increased to a fixed constant value (between 0.3 and 0.4), beyond which further generated gas was released through established pathways. A similar network of connected channels was observed in kaolin in the DSGREP intermediate- and tall-column sludge studies (Powell et al. 2014, Schonewill et al. 2014) and is expected in Hanford sludge, which is relatively strong.

Gauglitz et al. (1996) also studied the gas release behavior of 67-Pa and 200-Pa clays in wider vessels. The maximum gas fraction showed little dependence on the vessel diameter, but the size of the release increased markedly with diameter for the 67-Pa clay. Otherwise, the release behavior was the same in character for larger vessels: the 67-Pa clay produced only a single release in vessels between 2.5-cm and 30.5-cm diameter, and the 200-Pa clay produced small or no release in vessels between 2.5 cm and 91 cm, leveling off at a high retained gas fraction (>0.4) with continuous release. Although little dependence of the magnitude of gas releases with vessel size was noted in SL tests using ~ 50 -Pa and weaker M30:B simulant, Figure 8.21 (Section 8.3.2.3) shows divergence when the 87-Pa τ_5 (estimated) slurry was used. This is also shown in Figure 8.22, a head-to-head comparison of gas retention profiles

for the two SL tests (70-30 and 23-31) using the 87-Pa simulant. Both had 23-24 vol% retained gas at the time of their initial spontaneous releases, but the release pattern was dampened in the 23-in. vessel in the sense that initial and later releases were smaller, and they were spread over much longer time. The results of Gauglitz et al. and the SL studies presented in the current report suggest that both vessel size and simulant shear strength affect the size of spontaneous gas releases. While the trends are consistent, the specific dependence of release characteristics with operating conditions (e.g., shear strength and vessel size) is likely to be a function of the type of slurry used. Shifts in the trends for bentonite and M30:B simulants might be expected, for example, based on differences in maximum gas retention profiles: Figure 8.21 in Section 8.3.2.3 shows that the M30:B simulant has a peak gas fraction of ~ 0.3 at ~ 34 -Pa estimated shear strength, whereas the maximum gas fraction for bentonite slurry of comparable strength is ~ 0.4 (Gauglitz et al. 1996).

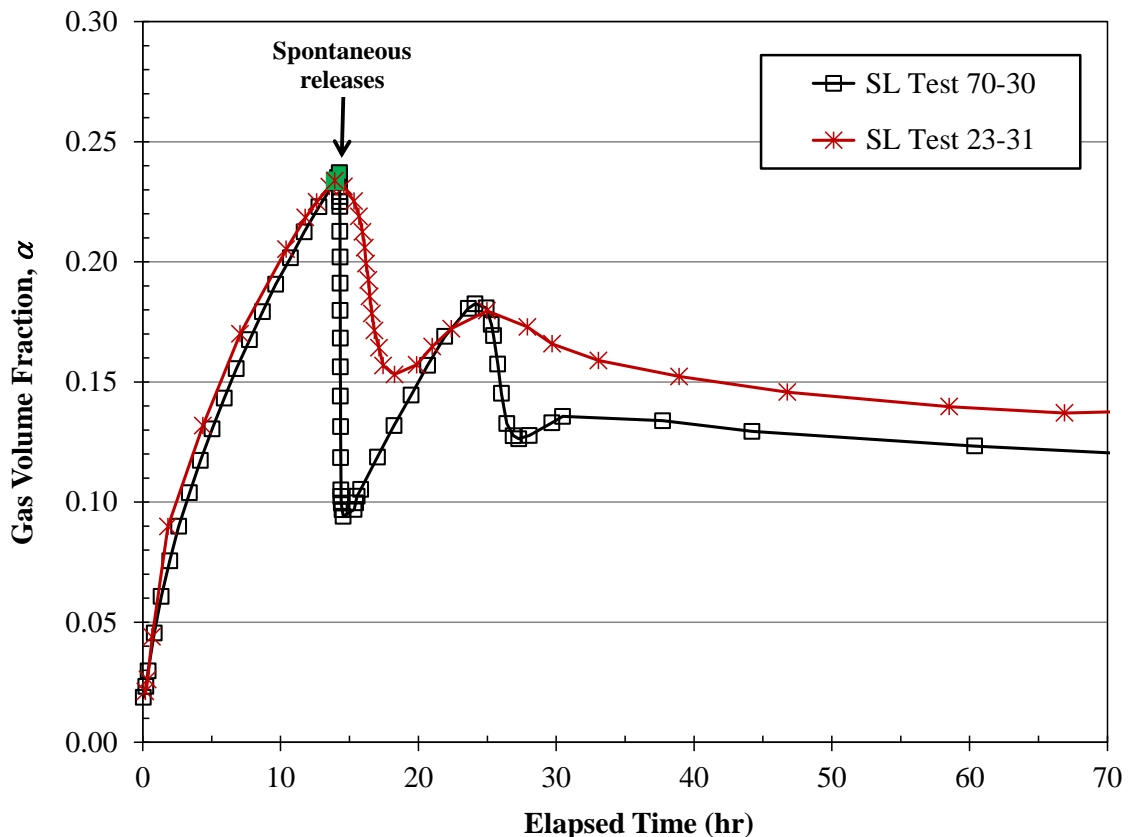


Figure 8.22. Effect of Vessel Size on Gas Release Characteristics in Single-Layer Tests Using the Same ~ 87 -Pa Estimated Shear Strength Slurry

8.5 Summary of RT Test Results

A summary of results and discussion of the implications of the RT tests completed in the 10-in., 23-in., and 70-in. vessels are provided in this section. Gas release quantities associated with the initial RT instabilities in the tests are first summarized. Secondly, modified energy ratios are calculated and briefly compared to a full-scale DST case. Finally, the RT stability criterion model, and the gravity yield parameter in particular, are discussed. SL test results are summarized in earlier Section 8.3.2.3 and, in general, are not discussed further here.

8.5.1 RT Instability Gas Releases

A summary of the magnitude of gas releases associated with initial RT instability events in the completed RT tests is provided in Table 8.5. The table also summarizes key test conditions and measured α_{RT} values. Gas releases are quantified in terms of the change in retained void fraction, $\Delta\alpha$, as a change in the specific volume of retained gas, $\Delta\phi$, and the fraction of the gas inventory released.¹ Figure 8.23 shows the fraction of the gas inventory released as a function of the ratio of α_{RT} to α_{NB} for all the completed RT tests.² The plot clearly shows that gas releases are relatively large when α_{RT} is greater than ~90% of the gas fraction for neutral buoyancy in the supernatant water. These include three of the first four RT tests in the 10-in. and 23-in. vessels and test 10-08. As discussed in Section 8.1.1 and Section 8.1.3.1, the results of these “non-classic” RT instability tests led to a shift away from testing in the 10-in. vessel and toward the use of lower-shear-strength simulants to obtain α_{RT} in the target range of 8 to 18.5 vol%.

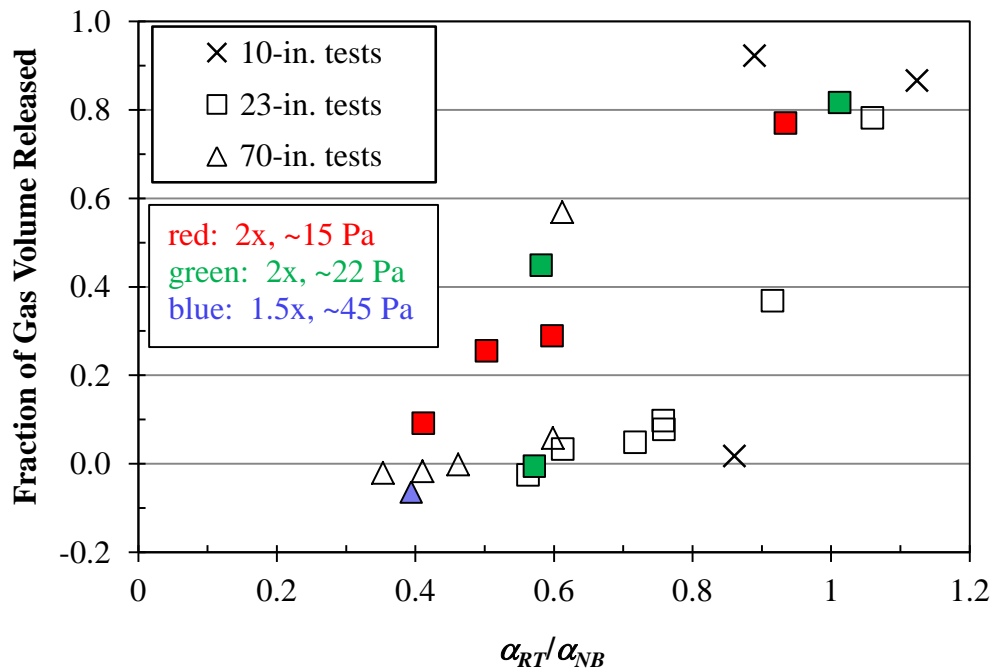


Figure 8.23. Fraction of Gas Released as a Function of the Ratio of α_{RT} to α_{NB} for Completed RT Tests

¹ As a reminder, the various gas quantities are defined as: a) the gas (void) fraction α is the volume of retained gas divided by the total volume of gaseous bottom-layer slurry; b) the specific gas volume fraction ϕ is the volume of gas per volume of gas-free bottom-layer slurry; and c) the fraction of the gas inventory released is simply the volume of gas released divided by the volume of gas retained just prior to the release. Also, $\phi = \alpha/(1-\alpha)$.

² Note that some slightly negative calculated gas releases are shown in Figure 8.23 and in Table 8.5. As discussed previously for the 70-in. vessel tests, an apparent negative release could be explained, for example, by expansion of gas as the lower slurry layer moves upward (e.g., resulting in a level increase). Within measurement uncertainty, the negative releases are effectively 0.

Table 8.5. Magnitude of RT Instability Gas Releases (ordered by vessel and sequence)

RT Test	Depth vs. Geo-Scaled	Lower: Upper Depth	Density kg/m ³	18-hr τ_S Pa	Est'd τ_S Pa	α_{RT}	α_{RT}/α_{NB}	Quantity of Gas Released from Lower Layer		
								Void Frac. $\Delta\alpha$	Specific $\Delta\phi$	Frac. of Inventory
10-02	2	1:1	1345	16	20	0.222	0.86	0.003	0.005	0.017
10-04	2	1:1	1353	15	20	0.295	1.12	0.242	0.37	0.87
10-08	4	1:1	1346	13	15	0.230	0.89	0.208	0.29	0.92
23-01	1	1:1	1422	39	51	0.273	0.92	0.081	0.14	0.37
23-03	1	1:1	1385	21	32	0.296	1.06	0.212	0.34	0.78
23-05	1	1:1	1348	14	15	0.146	0.56	-0.003	-0.004	-0.025
23-06	1	1:1	1390	22	25	0.214	0.76	0.013	0.022	0.078
23-07	2	1:1	1340	15	15	0.105	0.41	0.009	0.011	0.092
23-10	0.67	1:1	1340	15	16	0.183	0.72	0.007	0.011	0.049
23-12	1	1:1	1342	15	17	0.157	0.61	0.004	0.006	0.033
23-13	2	1:3	1342	15	16	0.153	0.60	0.039	0.055	0.29
23-15	2	1:5	1345	19	19	0.241	0.93	0.173	0.26	0.77
23-17	1	1:2	1343	15	16	0.195	0.76	0.016	0.024	0.098
23-19	2	3:1	1352	16	16	0.132	0.50	0.030	0.040	0.26
23-21	2	1:1	1379	25	24	0.161	0.58	0.065	0.090	0.45
23-23	2	3:1	1376	22	21	0.157	0.57	-0.001	-0.001	-0.006
23-24	2	1:3	1372	20	23	0.276	1.01	0.211	0.33	0.82
70-09	1	1:1	1440	51	45	0.126	0.41	-0.002	-0.003	-0.017
70-11	1	1:1	1464	67	63	0.147	0.46	0.000	0.000	-0.002
70-14	1	1:1	1410	28	26	0.103	0.35	-0.002	-0.003	-0.021
70-16	0.67	1:1	1446	45	50	0.185	0.60	0.009	0.014	0.058
70-20	1	1:1	1501	95	104	0.205	0.61	0.105	0.16	0.57
70-22	1.5	1:1	1439	42	41	0.121	0.39	-0.007	-0.010	-0.064

Figure 8.23 shows that the two 2× total slurry depth tests in the 23-in. vessel having $\alpha_{RT}/\alpha_{NB} > 0.9$ also released large fractions of the retained gas. These tests had relatively thin lower slurry layers and thick upper slurry layers (1:5 lower:upper in test 23-15 and 1:3 in test 23-24), which tended to result in higher α_{RT} and larger gas releases, as discussed in Section 8.2.2. The figure also indicates that gas releases in the majority of the 2× geometrically-scaled total slurry depth tests (filled squares), all in the 23-in. vessel, were, in general, larger than 0.67× and 1× depth tests run in either the 23-in. or the 70-in. vessel. It is also observed that the releases in the 2× tests become relatively larger compared to the lower-depth tests as α_{RT} and α_{RT}/α_{NB} increase.

The 70-in. vessel test (70-20) having α_{RT}/α_{NB} of 0.6 ($\alpha_{RT} \sim 20$ vol%, 57% of inventory released) is an exception to the rule that gas releases are relatively small in 1× total slurry depth tests. The gas release characteristics in this RT test were similar to the spontaneous gas release in the SL test (70-30) using the same simulant recipe. As noted in Section 8.3.2.2, the peak retained gas fraction around the RT event in test 70-20 was approximately 86% of the spontaneous release gas fraction α_{SR} found in SL test 70-30. It

was thereby postulated that proximity of α_{RT} to α_{SR} , specifically α_{RT}/α_{SR} less than ~ 0.85 , could be used to discriminate representative “classic” RT event releases from releases that are more characteristic of spontaneous, often bubble-cascade, events.

Excluding the $2\times$ total slurry depth tests and for α_{RT}/α_{NB} and α_{RT}/α_{SR} less than ~ 0.85 , Figure 8.23 shows that the gas releases are relatively small, i.e., $<10\%$ of the retained gas, in all cases and essentially none in several. This applies to all the later 23-in. and 70-in. vessel tests (including 23-05 and higher sequence tests except 10-08), which exhibited more classic in-sediment buoyancy RT instabilities. As shown in Table 8.5 for these cases, the fraction-of-inventory released metric does not always track with $\Delta\alpha$ and $\Delta\phi$, which are related in absolute terms by $\phi = \alpha/(1-\alpha)$. Compare, for example, the results for RT tests 23-06 ($\Delta\phi = 0.022$, 7.8% of inventory) and 23-07 ($\Delta\phi = 0.011$, 9.2% of inventory). In test 23-06, the specific release is twice as large, but because α_{RT} is also relatively high, 21.4 vol%, the fraction of the inventory released is 1.4% smaller than in test 23-07. Conversely, even though the fractional gas release is higher in test 23-07, the initial gas content is significantly less ($\alpha_{RT} = 10.5$ vol%), which equates to a lower specific release. As discussed in the earlier vessel-specific sections covering equal layer thickness tests (Section 8.1.3), one of the 23-in. tests (23-05) and four of the 70-in. tests (70-09, 70-11, 70-14, and 70-22) released negligible amounts of gas in the initial RT events (i.e., zero, indicated as negative amounts based on level change). These were all $1\times$ total depth tests except 70-22, which at $1.5\times$ -depth broke the trend of increasing release size with slurry depth observed in most of the $2\times$ -depth 23-in. vessel tests.

8.5.2 Modified Energy Ratio

As noted in Section 4.3.1, using the modified energy ratio is one approach considered for extrapolating gas releases in scaled RT tests to full-scale DSTs. The expression for the modified energy ratio, ER_S ,¹ given in Equation (4.4) and the associated definitions of the ratio of static pressures, γ_s , and the gas fraction ratio, k_s , are reproduced here for convenience.

$$ER_S = \frac{E_b}{E_y} = \frac{\alpha_{RT} \rho_{s1} g H_{s1}}{(1 - \alpha_{RT}) \varepsilon_y \tau_s} \left[\left(1 + \frac{1}{\gamma_s} \right) \ln(1 + \gamma_s) - k_s \right]$$

$$\gamma_s = \frac{\rho_{s1} g H_{s1}}{P_A + \rho_L g H_L} \quad k_s = \frac{\alpha_{NBS} (1 - \alpha_{RT})}{\alpha_{RT} (1 - \alpha_{NBS})}$$

The strain at failure, ε_y , is assumed to be 1 in calculations here. Because the densities of the slurries in the upper and gas-free lower layers in the completed RT tests are equal, the gas void fraction for neutral buoyancy between the two sediment layers, α_{NBS} , is zero, as is k_s .

Calculated values of ER_S for the completed 10-in., 23-in., and 70-in. vessel RT tests are presented in Table 8.6. The best-estimates of shear strength at the time of the initial RT instability were used in the calculations. For completeness, the table includes the RT tests that exceeded neutral buoyancy in water (23-03, 10-04, and 23-24). As noted in the previous section, these had large releases and did not exhibit

¹ The detailed derivation for this equation is provided in Appendix A.

classic RT behavior. Also shown in Table 8.6 are the results for the other tests that retained gas exceeding 85% of α_{NB} (in water) and generally had larger releases (tests 23-01, 10-02, 10-08, and 23-15).

Table 8.6. Modified Energy Ratios for Completed RT Tests (using best-estimate τ_S ; in sequence order and shaded by vessel size)

RT Test	Depth vs. Geo	Lower: Upper Depth	Meas. Density kg/m ³	Best-Est. τ_S Pa	Meas. α_{RT}	Bottom Slurry Thickness (cm)	Top Slurry Thickness (cm)	Supernate Thickness (cm)	Energy Ratio ER_S	Lower-Layer Specific Gas Release, $\Delta\phi$
23-01	1	1:1	1422	51.0	0.273	9.8	9.8	10.2	10.1	0.14
10-02	2	1:1	1345	19.9	0.222	8.7	9.0	7.3	17.1	0.005
23-03	1	1:1	1385	32.4	0.296	9.9	9.9	10.2	17.5	0.34
10-04	2	1:1	1353	19.5	0.295	8.7	8.7	7.4	24.7	0.37
23-05	1	1:1	1348	14.9	0.146	9.9	10.2	10.2	15.5	0
23-06	1	1:1	1390	25.0	0.214	9.8	9.9	10.2	14.7	0.022
23-07	2	1:1	1340	15.2	0.105	19.9	20.2	10.2	20.7	0.012
10-08	4	1:1	1346	14.7	0.230	17.4	17.4	6.8	47.2	0.29
70-09	1	1:1	1440	45.1	0.126	30.9	30.8	16.4	14.2	0
23-10	0.67	1:1	1340	16.2	0.183	6.6	6.6	10.2	12.1	0.011
70-11	1	1:1	1464	62.6	0.147	30.9	30.9	16.4	12.5	0
23-12	1	1:1	1342	17.1	0.157	10.0	10.0	10.2	14.3	0.006
23-13	2	1:3	1342	16	0.153	9.9	29.8	10.2	45.7	0.055
70-14	1	1:1	1410	26	0.103	30.8	30.9	16.4	19.1	0
23-15	2	1:5	1345	19	0.241	6.6	33.1	10.2	73.8	0.26
70-16	0.67	1:1	1446	50	0.185	20.5	20.5	16.5	13.4	0.014
23-17	1	1:2	1343	16	0.195	6.6	13.2	10.2	26.5	0.024
23-19	2	3:1	1352	16	0.132	29.6	10.0	10.2	12.8	0.040
70-20	1	1:1	1501	104	0.205	30.9	30.9	16.5	11.5	0.16
23-21	2	1:1	1379	24	0.161	19.9	19.9	10.2	21.3	0.090
70-22	1.5	1:1	1439	41	0.121	46.4	44.0	10.1	21.5	0
23-23	2	3:1	1376	21	0.157	29.9	10.0	10.2	12.1	0
23-24	2	1:3	1372	23	0.276	10.0	30.0	10.2	67.1	0.33
Full-1 ^(a)	1	1:1	1600	670	0.125 (est.)	394	394	211	16.0	-

(a) In the full-scale case shown, the estimated α_{RT} of 0.125 (12.5 vol%) is determined from Equation (4.2) for waste density and shear strength of 1600 kg/m³ and 670 Pa, respectively, and setting $Y_G = 0.03$. In the discussion of the full-scale tank ER_S in Section 4.3.2, and in the original TP test matrix (Table 3.5 of TP-DSGREP-001, Rev. 4.0 and all earlier versions, $Y_G = 0.09$ was used, which resulted in nearly the same α_{RT} at approximately three times the strength (2000 Pa). In turn, the calculated ER_S (~5) is about one-third of that shown in this table. The rationale for using a lower Y_G here is discussed in Section 8.5.3.

For all the equal slurry layer thickness tests (1:1) at $\leq 1.5 \times$ total slurry depth, the calculated modified energy ratios fall in the range of 10 to 22. A full-scale DST case shown in Table 8.6 has an ER_S in the middle of this range, 16.0, for an estimated α_{RT} of 12.5 vol% for waste of 670-Pa shear strength and 1600-kg/m³ density (assuming a nominal $Y_G = 0.03$, based on the discussion in Section 8.5.3 which follows). For $2 \times$ -depth tests (and $4 \times$ in test 10-08) of equal and varying relative slurry layer thicknesses,

the range of ER_S is much broader, ~ 12 to ~ 74 . This is not wholly unexpected considering the dependence of ER_S on the upper slurry layer depth H_{SI} . It was for this reason that a test matrix including different slurry layer depths was chosen, assuming, initially, that α_{RT} would be independent of sediment depth for a given simulant shear strength (recipe).¹ In this scenario, only ER_S and the magnitude of gas releases (potentially) would vary, and the relationship of the two could be directly evaluated. However, the complex dependence of α_{RT} and the quantity of gas released on slurry depth, as discussed in Sections 8.1.3.2 and 8.1.3.3 (Effect of Depth portions) and Section 8.2.2, muddled the picture.

Figure 8.24 shows the magnitude of gas releases, in terms of fraction of inventory, for the 23-in. and 70-in. vessel tests, excluding those with $\alpha_{RT}/\alpha_{NB} > 0.85$. With this subset of data, there are no clear trends in the relationship of the size of gas releases in (mostly) classic RT instabilities and ER_S . Even excluding RT test 70-20 ($ER_S \sim 12$, 57% of inventory released) based on the likelihood that it was influenced by spontaneous gas release characteristics ($\alpha_{RT}/\alpha_{NB} \sim 0.85$), the dependence of gas release and ER_S is not monotonic. The same conclusion is drawn if the trending is based on specific gas release $\Delta\phi$ instead of fraction of inventory. As noted above, the apparent ineffectiveness of ER_S as a screening tool for conditions potentially leading to large gas releases may be attributed to the complex relationship of α_{RT} with slurry layer depths (and other factors), as will be discussed further in the next section (8.5.3) in consideration of the RT stability (gravity yield) criterion.

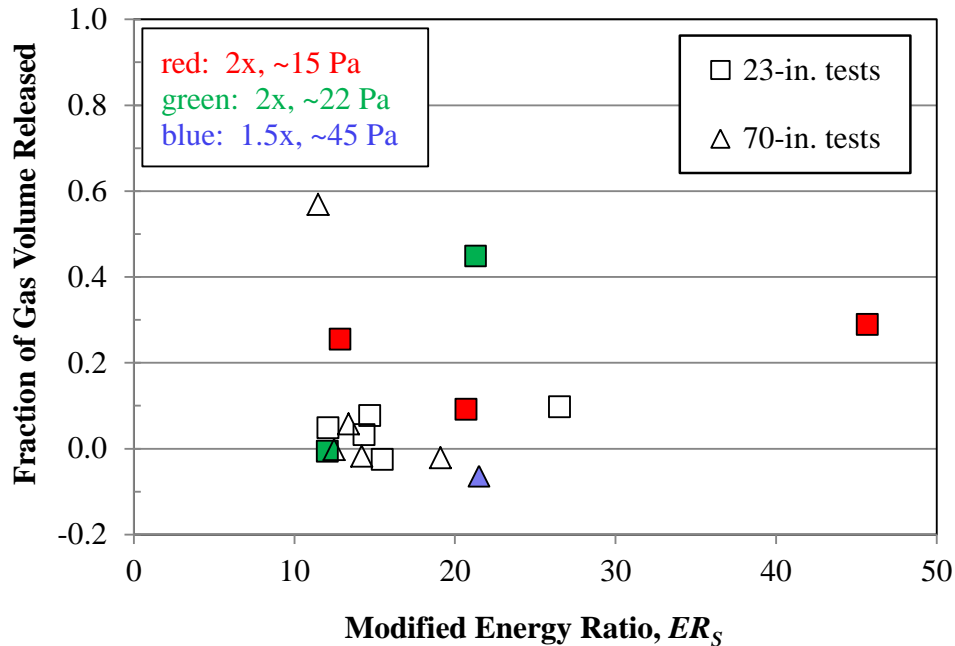


Figure 8.24. Fraction of Gas Released as a Function of the Modified Energy Ratio for Completed RT Tests ($\alpha_{RT}/\alpha_{NB} < 0.85$ cases)

¹ The original test matrix and planning assumptions are discussed in TP-DSGREP-001, Rev. 4.0 and all earlier versions (0.0, 1.0, 2.0, and 3.0).

8.5.3 RT Stability Criterion

The working model for defining the onset of RT instabilities is the RT stability criterion defined in Equation (4.1) of Section 4.1.1. The equation is repeated here, in final form, for convenience.

$$Y_G = \frac{2\tau_S}{\rho_S \alpha_{RT} gL}$$

In development of the original TP test matrix (Section 4.3.2), the gravity yield parameter was assumed to be constant (e.g., $Y_G = 0.09$) and the characteristic dimension L was assumed equal to the vessel diameter D . These assumptions led to the testable conclusion that α_{RT} would be directly proportional to $\tau_S/\rho_S gD$. Figure 8.8, a plot of the measured α_{RT} (filled points) for 23-in. and 70-in. tests in which the shear strength was the only variable, does not support the conclusion of simple linear proportionality versus τ_S/ρ_S . The linear-dependence trend lines (solid lines) show a dependence that appears linear in this range but has a significant non-zero y-intercept. Granted, the x-axis is τ_S rather than τ_S/ρ_S , but the variability in the density is not great enough in this range to explain the non-zero y-intercepts. This departure from the behavior implied by the RT stability criterion can also be seen in the Y_G values (non-filled points) in Figure 8.8. The gravity yield parameter is distinctly non-constant, ranging from ~0.02 to ~0.04 using D as the characteristic dimension.

A power-law type of proportionality was selected for further attempts to define an RT instability criterion. This form is almost certainly an over-simplification of the functionality of the instability behavior in a system of two finite layers. However, it serves as an approximation that does not over-define the correlating parameters, given that there are not many data points available for determining dependence on any given test parameter.

As a first step, a correlation of the form

$$\alpha_{RT} = c_1 \left(\frac{\tau_S}{\rho_S g} \right)^{c_2} D^{c_3} \quad (8.1)$$

was fitted¹ to the data from 23-in. and 70-in. vessel tests where the geometric scaling of the total solids layer depth was $1\times$ (as at full-scale) and the upper and lower layers were of equal thickness (1:1 layer thickness ratio).² The resulting correlation was

$$\alpha_{RT} = 4.55 \left(\frac{\tau_S}{\rho_S g} \right)^{0.554} D^{-0.661} \quad (8.2)$$

The dependence on the shear strength/density ($c_2 = 0.554$) is less strong than the dependence on the vessel diameter ($c_3 = -0.661$)¹, leading to the multiplying constant ($c_1 = 4.55$) having units of $m^{0.107}$. In

¹ Curve-fitting was carried out by using the Microsoft Excel® Solver function to minimize an error measure that was the sum of the squares of the relative standard errors in the predicted values for the selected set of tests.

² No $1\times$ depth tests were performed in the 10-in. vessel. Also, RT Tests 23-01, 10-02, and 23-03 were not considered in any step of the correlation development, because their lower peroxide concentration caused long delays before RT release occurred, and the shear strengths were not well defined at times so much longer than 18 hr.

this way, the correlation is “dimensional”. Figure 8.25 shows the relation between the α_{RT} predicted by this correlation and the measured α_{RT} . The data that were included in the correlation are shown by squares; the data that were excluded are shown by “x” symbols. The seven included measurements are closely matched by the correlation.

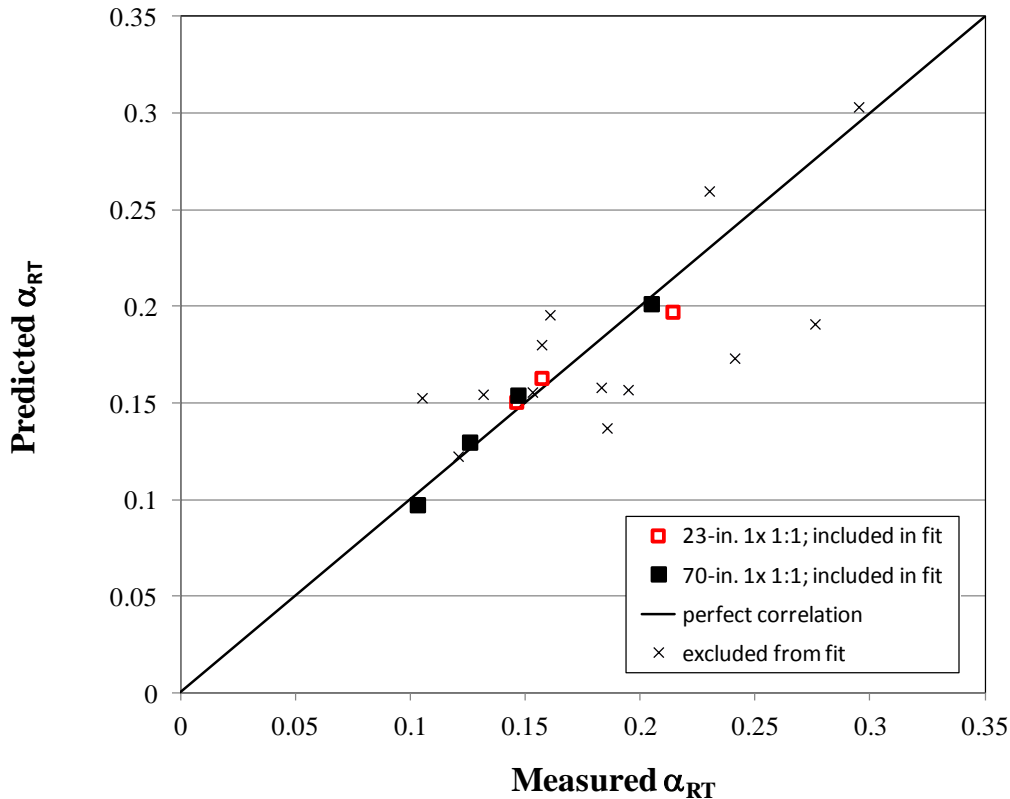


Figure 8.25. Comparison of Measured α_{RT} from RT Tests to Predicted Values Using a Dimensional Correlation Determined for a Limited Data Set (squares; 1× depth, 1:1 L:U in the 23-in. and 70-in. vessels)

In the second step, the dimensional correlation form was

$$\alpha_{RT} = c_1 \left(\frac{\tau_s}{\rho_s g} \right)^{c_2} D^{c_3} \left(\frac{H_{S2}}{D} \right)^{c_4} \tag{8.3}$$

adding in a dependence on the ratio of the lower-layer thickness to the vessel diameter. The correlation database was extended by adding the data for RT tests having $N \times$ geometric scaling of the total solids layer depth (with scale-factor N other than 1) and equal lower- and upper-layer depths (1:1). Exponents

¹ It is perhaps noteworthy that the coefficient on vessel diameter is approximately two-thirds ($\sim 1/D^{2/3}$). If the region (portion) of the sediment involved in the RT instability is a disk or cylinder of diameter aD , where a is a constant ≤ 1 , and arbitrary height h ($\leq H_s$), the relevant volume is $\pi a^2(D^2 h)/4$. The diameter of a sphere having the equivalent volume of the disk is $d_s = (3/2 a^2 h)^{1/3} D^{2/3}$. If d_s is the critical dimension of the RT instability, it has the aforementioned $D^{2/3}$ dependence. However, further development of the α_{RT} correlation below shows that the 2/3 coefficient on D does not appear to be universal.

c_2 and c_3 were held constant at the values of 0.554 and -0.661, as in Equation (8.2), and constants c_1 and c_4 were selected to minimize the curve-fit error measure, yielding the correlation

$$\alpha_{RT} = 2.98 \left(\frac{\tau_S}{\rho_S g} \right)^{0.554} D^{-0.661} \left(\frac{H_{S2}}{D} \right)^{-0.251} \quad (8.4)$$

The correlation indicates that, other factors being held constant, α_{RT} decreases (stability decreases) as the lower-layer thickness increases. Here, decreased stability implies that the RT instability occurs at a lower retained gas fraction differential between the two layers, not that gas releases are necessarily larger.

Finally, the remaining data for unequal layer thickness tests in the 23-in. vessel (where geometric scaling of the total slurry depth was 1× or 2× and the ratio of layer depths was p:q, not 1:1) were added into the correlation database, and a dimensional correlation of the form

$$\alpha_{RT} = c_1 \left(\frac{\tau_S}{\rho_S g} \right)^{c_2} D^{c_3} \left(\frac{H_{S2}}{D} \right)^{c_4} \left(\frac{H_{S1}}{H_{S2}} \right)^{c_5} \quad (8.5)$$

was fitted. The exponents c_2 through c_4 were held constant at the previously determined values, and the constants c_1 and c_5 were selected by error minimization to find a dependence on the ratio of upper to lower-layer thickness. The result was

$$\begin{aligned} \alpha_{RT} &= 3.06 \left(\frac{\tau_S}{\rho_S g} \right)^{0.554} D^{-0.661} \left(\frac{H_{S2}}{D} \right)^{-0.251} \left(\frac{H_{S1}}{H_{S2}} \right)^{0.042} \\ &= 3.06 \left(\frac{\tau_S}{\rho_S g} \right)^{0.554} D^{-0.410} H_{S2}^{-0.293} H_{S1}^{0.042} \end{aligned} \quad (8.6)$$

Like the predecessors in this step-wise correlation development (Equation (8.2) and Equation (8.4)), the multiplying constant ($c_1 = 3.06$) in this final dimensional form has units of $m^{0.107}$. Other factors being constant, α_{RT} increases (stability increases) as the upper-layer thickness H_{S1} increases. Increased stability refers to increased gas retention at the point of instability, not necessarily smaller gas releases.

Figure 8.26 (lower) shows the relation between α_{RT} predicted by this correlation (Equation (8.6)) and the measured α_{RT} . The gas fraction was predicted within +12%/-16% for most of the database. Both of the included 10-in tests showed under-prediction, perhaps because no 10-in. tests were included in the database for determining dependence on D . The two tests that lay outside the +12%/-16% band were test 23-07 (over-prediction by 28%) and test 23-24 (under-prediction by 24%). Both of these were 2× geo-scaled tests, with 23-07 having equal layers and the lowest tested shear strength and 23-24 having a lower:upper ratio of 1:3 and a moderate shear strength.

Prior to having developed the “best” and final dimensional α_{RT} correlation, Equation (8.6), an analogous step-wise fitting scheme was used to define a dimensionless α_{RT} correlation of the form

$$\alpha_{RT} = c_1 \left(\frac{\tau_S}{\rho_S g D} \right)^{c_2} \left(\frac{H_{S2}}{D} \right)^{c_3} \left(\frac{H_{S1}}{H_{S2}} \right)^{c_4} \quad (8.7)$$

In the first fitting step, the exponent c_2 of the primary dimensionless group $\tau_s/\rho_s g D$ from the gravity yield criterion was determined, independent of the length-scale ratio contributions. In subsequent error minimization fitting steps, the exponents of the lower-layer depth to vessel diameter and upper- to lower-layer depth ratios were established. The final dimensionless form is given by

$$\alpha_{RT} = 3.83 \left(\frac{\tau_s}{\rho_s g D} \right)^{0.567} \left(\frac{H_{S2}}{D} \right)^{-0.170} \left(\frac{H_{S1}}{H_{S2}} \right)^{0.096} = 3.83 \left(\frac{\tau_s}{\rho_s g} \right)^{0.567} D^{-0.397} H_{S2}^{-0.266} H_{S1}^{0.096} \quad (8.8)$$

where the multiplying constant c_1 (3.83) is dimensionless. Comparison of the exponents in the right-hand form of this correlation to Equation (8.6) shows that the dimensionless version has a somewhat stronger dependence on the upper-layer depth H_{S1} , a weaker dependence on the lower-layer depth H_{S2} , and relatively unchanged contributions from D and $\tau_s/\rho_s g$.

Figure 8.26 (upper) shows that the relationship between α_{RT} predicted by this dimensionless correlation (Equation (8.8)) and the measured α_{RT} is good, but it is slightly poorer than the dimensional version (lower plot in the figure). This is noted, for example, in the shift of the 1:1, 1× depth 70-in. vessel data series above the perfect dimensionless correlation line.

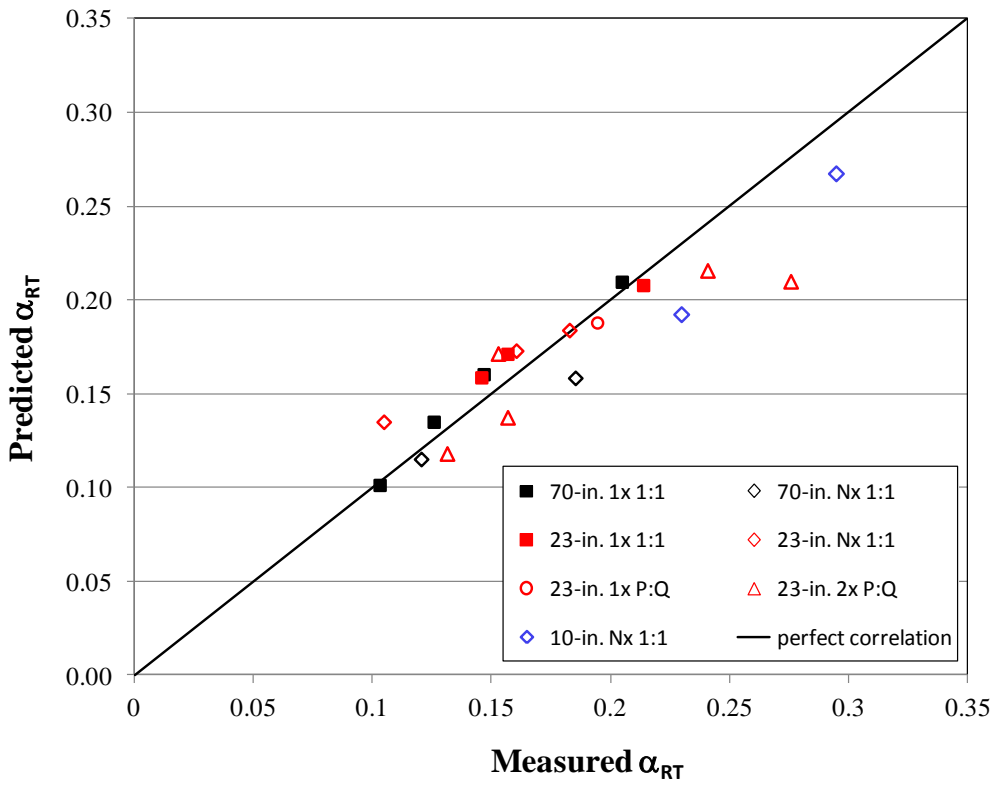
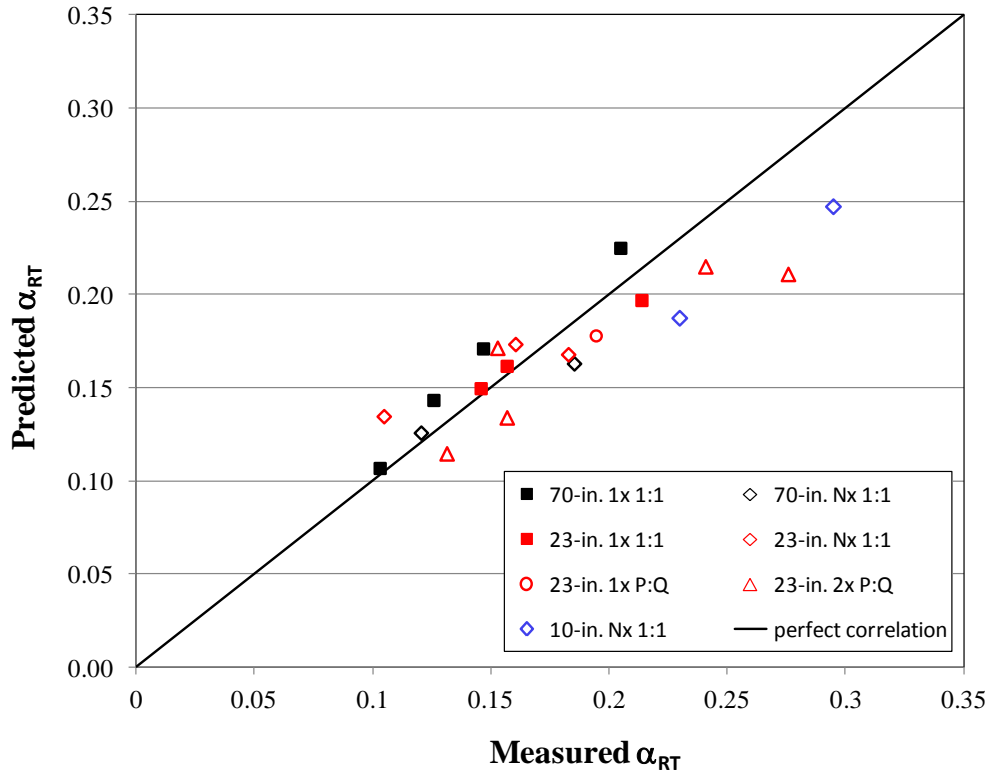


Figure 8.26. Comparison of Measured α_{RT} from RT Tests in Three Scale Vessels to Predicted Values Using a Dimensional Correlation (lower) and a Dimensionless Correlation (upper)

Combining the dimensional α_{RT} correlation (Equation (8.6)) with the definition of the gravity yield criterion (Equation (4.1)) gives a Y_G prediction of

$$Y_G = 0.654D^{-0.339} \left(\frac{\tau_S}{\rho_S g} \right)^{0.446} \left(\frac{H_{S2}}{D} \right)^{0.251} \left(\frac{H_{S1}}{H_{S2}} \right)^{-0.042} \quad (8.9)$$

Likewise, from the dimensionless form of the α_{RT} correlation (Equation (8.8)), Y_G can be predicted from

$$Y_G = 0.522 \left(\frac{\tau_S}{\rho_S g D} \right)^{0.433} \left(\frac{H_{S2}}{D} \right)^{0.170} \left(\frac{H_{S1}}{H_{S2}} \right)^{-0.096} \quad (8.10)$$

Either form can be used to “extrapolate” to full-scale tank conditions by entering tank dimensions and known waste properties, τ_S and ρ_S . Once Y_G is calculated, α_{RT} can be predicted from the Y_G definition (Equation (4.1)). Alternately, α_{RT} can be specified and the waste (or simulant) properties necessary to achieve it estimated as follows: a) substitute α_{RT} into the Y_G definition to give the group $\tau_S/\rho_S g D$ (or $\tau_S/\rho_S g$) in terms of Y_G ; b) substitute for the group $\tau_S/\rho_S g D$ (or $\tau_S/\rho_S g$) in terms of Y_G into Equation (8.10) (or Equation (8.9)); c) rearrange and solve for Y_G ; d) reenter the predicted Y_G and the specified α_{RT} into the gravity yield criterion and solve for τ_S/ρ_S ; and e) if either τ_S or ρ_S is known, solve for the other, or otherwise estimate τ_S and ρ_S to satisfy the calculated shear strength to density ratio. The latter is done with the RT test simulant, for example, by determining the solids content x_S that satisfies the ratio by simultaneously calculating the 18-hr τ_S from Equation (7.2) and the theoretical ρ_S from Equation (5.3). Once x_S is found, other pertinent physical properties such as the Bingham rheology model parameters τ_0 and μ_∞ can be estimated from their respective correlations (e.g., yield stress, Equation (7.7); and consistency, Equation (7.8)).

This approach was used to predict Y_G and simulant physical properties (to represent actual waste) for α_{RT} values of 8, 12.5, and 18.5 vol% in a full-scale DST (at 1× depth and 1:1 lower:upper layer ratio). The results using both the dimensional and dimensionless Y_G correlations are shown in Figure 8.27 and Table 8.7 along with the Y_G values calculated for the RT tests in the 10-in., 23-in., and 70-in. vessels. The plot of the dimensionless correlation-based results in Figure 8.27 (upper) shows that Y_G vs. $\tau_S/\rho_S g D$ for the full-scale vessel tends to fall within the band of the experimental results. The equivalent analysis using the dimensional correlation (lower plot in the figure) gives Y_G predictions at a given $\tau_S/\rho_S g D$ that are higher than all but one test result (RT Test 23-07). The dimensionless correlation results forecast lower shear strength at each α_{RT} value compared to the dimensional form. The dimensionless values are conservative from the perspective that gas releases would, presumably, be larger for weaker materials having the same fraction of retained gas.

This conservatism, the appeal of a dimensionless relationship, and the timing of its final development in comparison to the dimensional model led to the selection of Equation (8.10) for use in determining full-scale tank parameters for RT instability gas-release simulations (Section 9.0).

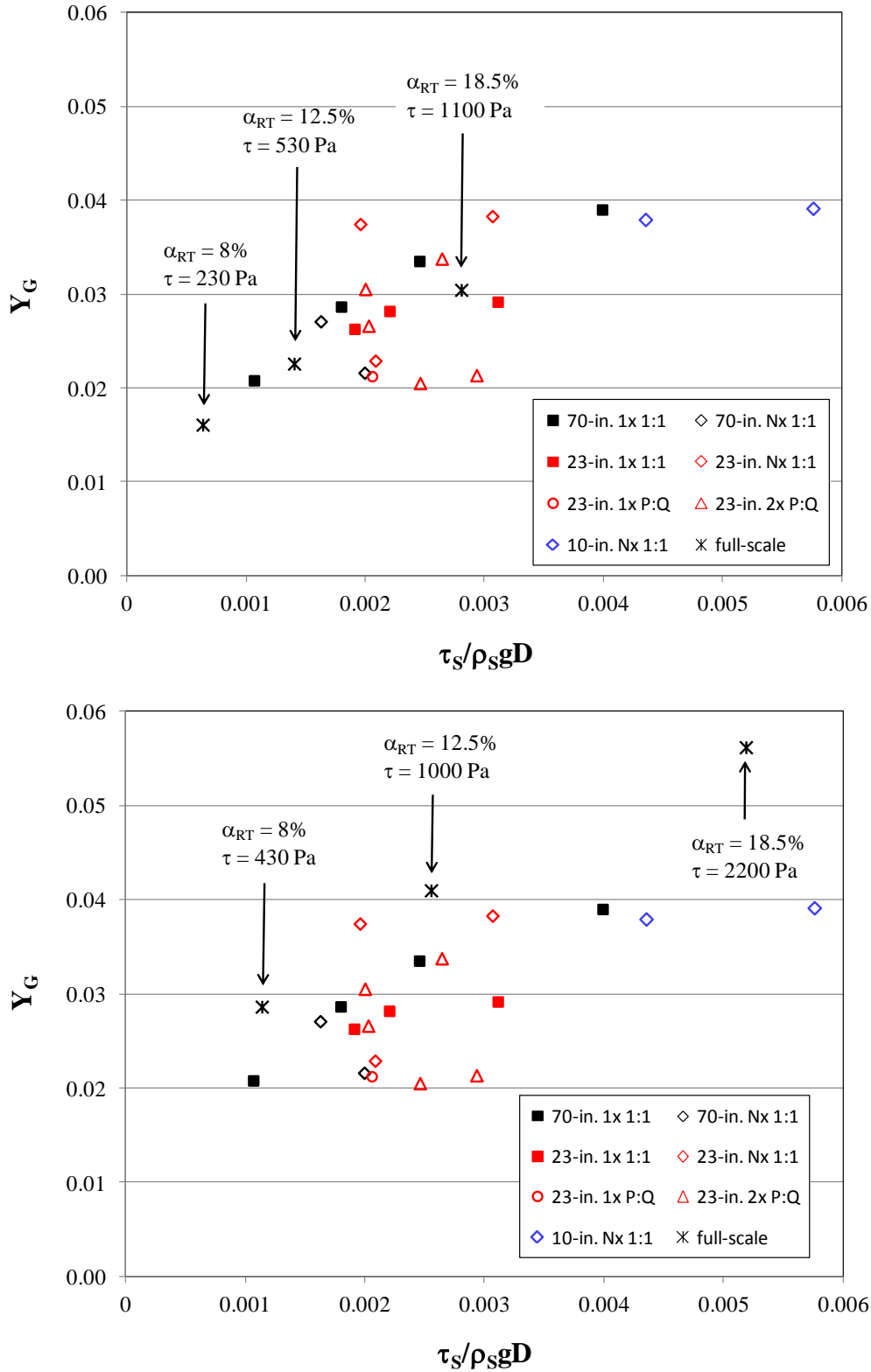


Figure 8.27. Comparison of Experimentally Determined Y_G Values to Predictions for a Full-Scale Vessel (1x Depth, 1:1) at Three Assumed α_{RT} Levels Using a Dimensional Correlation (lower) and a Dimensionless Correlation (upper)

Table 8.7. Gravity Yield Parameter Determined from RT Tests and Predicted for Full Scale (ordered by vessel and sequence)

RT Test or Case	Depth vs. Geo-Scaled	Lower: Upper Depth	Density kg/m ³	Est'd τ_s Pa	α_{RT}	Y_G
10-02	2	1:1	1345	20	0.222	0.053
10-04	2	1:1	1353	20	0.295	0.039
10-08	4	1:1	1346	15	0.230	0.038
23-01	1	1:1	1422	51	0.273	0.045
23-03	1	1:1	1385	32	0.296	0.027
23-05	1	1:1	1348	15	0.146	0.026
23-06	1	1:1	1390	25	0.214	0.029
23-07	2	1:1	1340	15	0.105	0.037
23-10	0.67	1:1	1340	16	0.183	0.023
23-12	1	1:1	1342	17	0.157	0.028
23-13	2	1:3	1342	16	0.153	0.027
23-15	2	1:5	1345	19	0.241	0.020
23-17	1	1:2	1343	16	0.195	0.021
23-19	2	3:1	1352	16	0.132	0.030
23-21	2	1:1	1379	24	0.161	0.038
23-23	2	3:1	1376	21	0.157	0.034
23-24	2	1:3	1372	23	0.276	0.021
70-09	1	1:1	1440	45	0.126	0.029
70-11	1	1:1	1464	63	0.147	0.033
70-14	1	1:1	1410	26	0.103	0.021
70-16	0.67	1:1	1446	50	0.185	0.022
70-20	1	1:1	1501	104	0.205	0.039
70-22	1.5	1:1	1439	41	0.121	0.027
Full Scale (Dimensional Correlation)	1	1:1	1662	426	0.08	0.029
	1	1:1	1762	1010	0.125	0.041
	1	1:1	1862	2166	0.185	0.056
Full Scale (Dimensionless Correlation)	1	1:1	1596	229	0.08	0.016
	1	1:1	1686	532	0.125	0.023
	1	1:1	1775	1118	0.185	0.030

9.0 Modeling of Rayleigh-Taylor Events

A series of computer simulations of the RT instability GREs was performed for each of the planned scaled tests and scaling up to full-scale. The objective was to understand the physical mechanisms during buoyant motion within a deep sludge settled layer and the resulting gas releases. The purpose of this activity is to determine the scaling behavior of gas releases from DSGREs. The results are FIO and are intended to be used only to provide insight when evaluating models and interpreting experimental results.

The methodology used in simulating the RT events is described in Section 9.1. The method used in selecting input parameters for simulations is described in Section 9.2. The simulation results for select equal slurry layer thickness tests are presented in Section 9.3. Results for varied slurry layer thickness ratios are presented in Section 9.4. The conclusions are presented in Section 9.5.

9.1 Modeling Approach

The computer simulations were performed using the ParaFlow computer program. The ParaFlow program solves the Navier-Stokes and transport equations based on the implicit lattice kinetics algorithm, developed at PNNL, which takes advantage of some of the strengths of the lattice-Boltzmann method, while improving stability for high-speed flows. The utility of the program was demonstrated for a number of related applications, including critical velocities in horizontal pipelines (Rector et al. 2009), both coarse- and fine-scale simulation of ultrafiltration associated with caustic leaching (Rector and Stewart 2010) and mixing of double-shell tanks (Wells 2011a).

The vessel walls and bottom are modeled using a no-slip boundary condition, and a movable slip boundary is placed at the liquid surface. As the gas expands, the surface moves upward, and the released gas is collected at the liquid surface to be inventoried at the end of the simulation.

The gas bubbles created in the sediment are expected to range in size. The size ratio between the smallest bubbles and the test vessel is sufficiently large to make it impractical to model individual bubbles. For this reason both the suspended solids and gas bubbles are modeled as continuum fields. The gas is represented using five continuum fields, each with a different bubble size. An assumption was made that the void fraction is divided equally among the different bubble sizes. The fluid drag, which controls the relative velocity with respect to fluid motion, is based on the local effective viscosity, which in turn depends on the local strain rate and solid and gas concentrations.

Since the slurry properties were based on measurements and the vessel geometry is fixed, the only adjustable parameter in the simulation is the bubble size distribution. The range of bubble sizes used in these simulations (0.1-, 0.25-, 0.4-, 0.55-, and 0.7-cm diameter) gave results that were consistent with the measured gas release data. This will be discussed in more detail in Section 9.3.1. It was assumed that the void fraction is divided equally among the different bubble sizes.

Sufficiently small gas bubbles are trapped in static sediment. The critical diameter for bubbles in a stagnant yield stress fluid is given by the following expression

$$d_{crit} = \frac{\tau_0}{gY\Delta\rho}$$

where Y is the critical yield number and is approximately 0.06 for a sphere (Chhabra 1992). For the sediments covered in the test matrix, the critical bubble size ranges from several centimeters to hundreds of centimeters. Bubbles with diameters smaller than the critical diameter will not be released from the sediment. Therefore, the bubbles will move relative to the sediment only when it is being sheared.

The slurry rheology is represented using the Bingham model described in Section 7.1.3. The apparent viscosity is a function of local strain rate, $\dot{\gamma}$, and weight percent solids, and is given by the expression

$$\mu_{app} = \frac{\tau_0 + \mu_{\infty} \dot{\gamma}}{\dot{\gamma}}$$

where τ_0 is the Bingham yield stress and μ_{∞} is the consistency. Examples are shown in Figure 9.1 for selected solids loadings using the correlation given in Section 7.1.3.

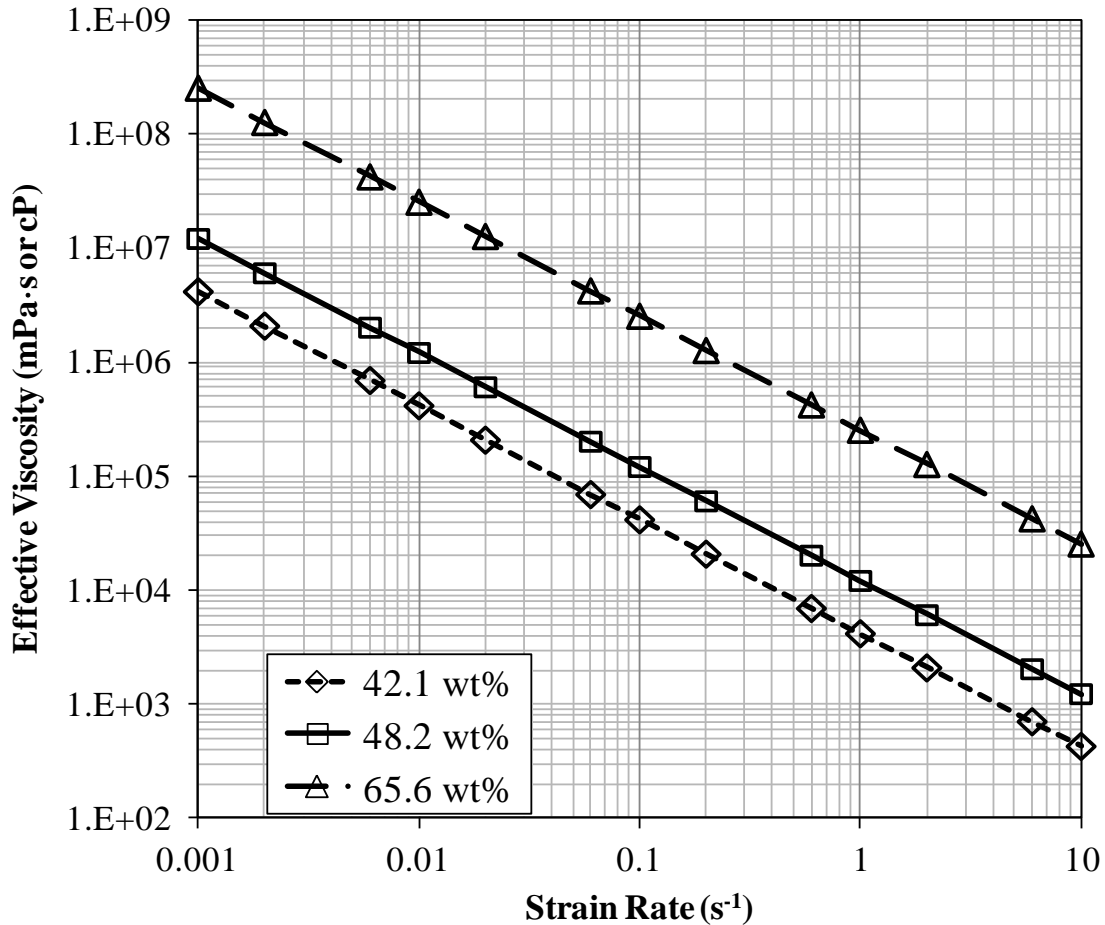


Figure 9.1. Apparent Viscosity as a Function of Local Strain Rate and Weight Percent Solids

Note that for the strain rates of interest ($<1 \text{ s}^{-1}$) the viscosity is dominated by the yield stress term and the effect of the consistency is negligible.

The rise velocity of the bubble field relative to the slurry is determined by the local apparent viscosity and the local drag coefficient, given by the expression

$$C_D = \frac{16}{\text{Re}_b} (1 + 0.15 \text{Re}_b^{0.687}) \quad \text{Re}_b = \frac{\rho U d_b}{\mu_{app}}$$

where d_b is the bubble diameter and U is the rise velocity.

The simulation is initialized with three layers (liquid, slurry, slurry with gas) with a small sinusoidal perturbation between the two slurry layers. The magnitude of the perturbation was selected to be large enough to exceed the stress required to start the RT motion. The transient was run until fluid motion ceased following the DSGRE.

9.2 Selecting Input Parameters for Simulations

The primary focus of the modeling activity is to support extrapolating the results from the scaled experiments to the full-scale tanks. A parameter of interest is the void fraction required to initiate an RT event, α_{RT} . A series of simulations can be used to predict the maximum gas release expected during an RT event. For this reason, a matrix of simulations was defined for a series of void fractions ($\alpha_{RT} = 8\%$, 12.5% , and 18.5%) at three different scales (vessel diameters of 23 in., 70 in., and 900 in.).

The solids weight percent associated with a particular void fraction and vessel size was determined using the dimensionless Y_G correlation, Equation (8.10), based on experimental data described in Section 8.5.3. This solids loading was then used to calculate the Bingham model parameters using the correlations presented in Section 7.1.3. Parameters obtained using this procedure are presented in Table 9.1.

A second set of ParaFlow simulations was performed corresponding to the experimental cases that had equal thicknesses for the top and bottom slurry layers (1:1) that scale geometrically to the full-scale tanks (1×). The parameters for the test cases that satisfy these conditions for the 23-in. vessel (Tests 23-01, 23-06, 23-12) and the 70-in. vessel (Tests 70-09, 70-11, 70-14, and 70-20) are presented in Table 9.2.

Table 9.1. Input Values for Parametric ParaFlow Simulations

Vessel Diameter	α_{RT} (vol%)	Y_G	x_S (wt%)	$\tau_S^{(a)}$ (Pa)	τ_0 (Pa)	μ_∞ (mPa•s)	Density (kg/m ³)
75 ft	8.0	0.0160	35.4	231	98	76	1596
75 ft	12.5	0.0225	40.7	529	251	130	1686
75 ft	18.5	0.0304	45.4	1121	575	208	1775
70 in.	8.0	0.0160	42.9	15.1	4.75	13.5	1361
70 in.	12.5	0.0225	48.2	34.7	12.0	23.0	1426
70 in.	18.5	0.0304	52.9	72.5	27.3	36.7	1488
23 in.	8.0	0.0160	60.3	4.69	1.28	6.4	1280
23 in.	12.5	0.0225	65.6	10.7	3.23	10.9	1336
23 in.	18.5	0.0304	70.4	22.4	7.31	17.3	1391

(a) Because of timing of activities, shear strength values shown in this table were determined from property-vs.- x_S correlations that were slightly different than the final versions shown in Section 7.1, which were used to calculate the equivalent full-scale (75 ft) values shown in Table 8.7 (Section 8.5.3). The differences are $\leq 1\%$ and would have a negligible effect on the results of the For Information Only simulations.

Table 9.2. Input Parameters for Test Case ParaFlow Simulations

Test Case	α_{RT} (vol%)	$\tau_S^{(a)}$ (Pa)	$\tau_0^{(a)}$ (Pa)	$\mu_\infty^{(a)}$ (mPa•s)	Density (kg/m ³)
23-01	27.3	32.5	11.1	21.9	1422
23-06	21.4	21.6	7.03	16.9	1390
23-12	15.7	11.3	3.41	11.2	1342
70-09	12.6	40.6	14.2	25.3	1440
70-11	14.7	54.0	19.5	30.3	1464
70-14	10.3	27.9	9.36	19.9	1410
70-20	20.5	82.5	31.4	39.7	1501

(a) Because of timing of activities, input parameters for the simulations were determined from property-vs.- x_S correlations that were slightly different than the final versions shown in Section 7.1. The differences, $\sim 10\%$ or less, are not expected to have an effect on interpretation of the results of the For Information Only simulations.

9.3 Simulation Results for Selected Equal Slurry Layer Thickness Tests

The mid-plane distributions for initial density and void fraction for the smallest bubbles for the 23-in. case with 18.5 vol% void fraction are shown in Figure 9.2. The green region in the density frame represents slurry with bubbles; the orange region, slurry without bubbles, and the blue region is the overlying liquid layer. A finite sinusoidal perturbation that was used to initiate the transient can be seen between the two slurry layers. The red region in the second frame indicates the void fraction of small bubbles at the initial (maximum) value.

The spatial distribution is the same for all bubble sizes. The fluid velocities were initialized to zero.

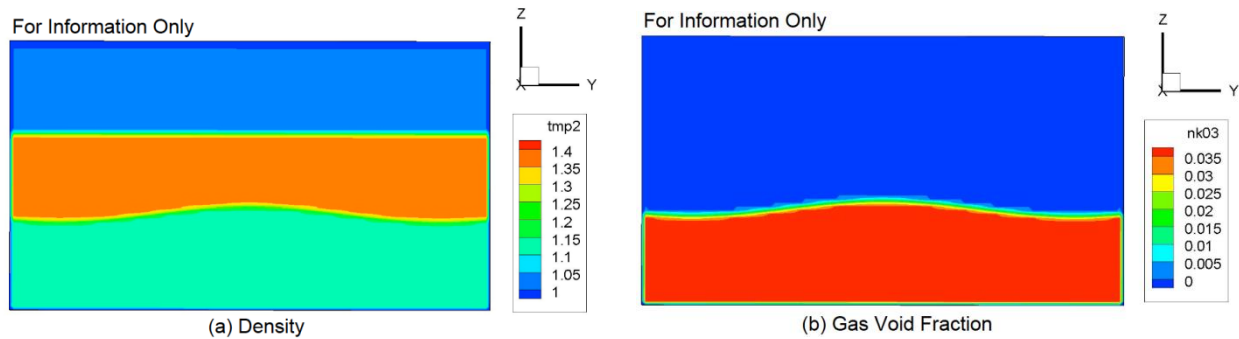


Figure 9.2. Density, g/mL (a), and Gas Void Fraction (b) for Smallest Bubbles at the 23-in. Mid-Plane at Time = 0 s. (Note: Graphics are provided For Information Only.)

The growth of the sinusoidal perturbation is shown in the density and void fraction distributions presented in Figure 9.3 (200 seconds into the transient). The z-direction velocity distribution shows the center region moving upward and the outer region moving downward. The y-direction velocities indicate a rotating vortex ring that is inducing the upward and downward motions.

The strain rate determines the local apparent viscosity and bubble rise velocity. The strain rates in the water region are not of interest and have been filtered out to make the peak slurry strain rates more evident. The peak regions are where the rotating vortex ring interacts with the vessel bottom and where the upward-moving slurry at the top surface is moving radially outward.

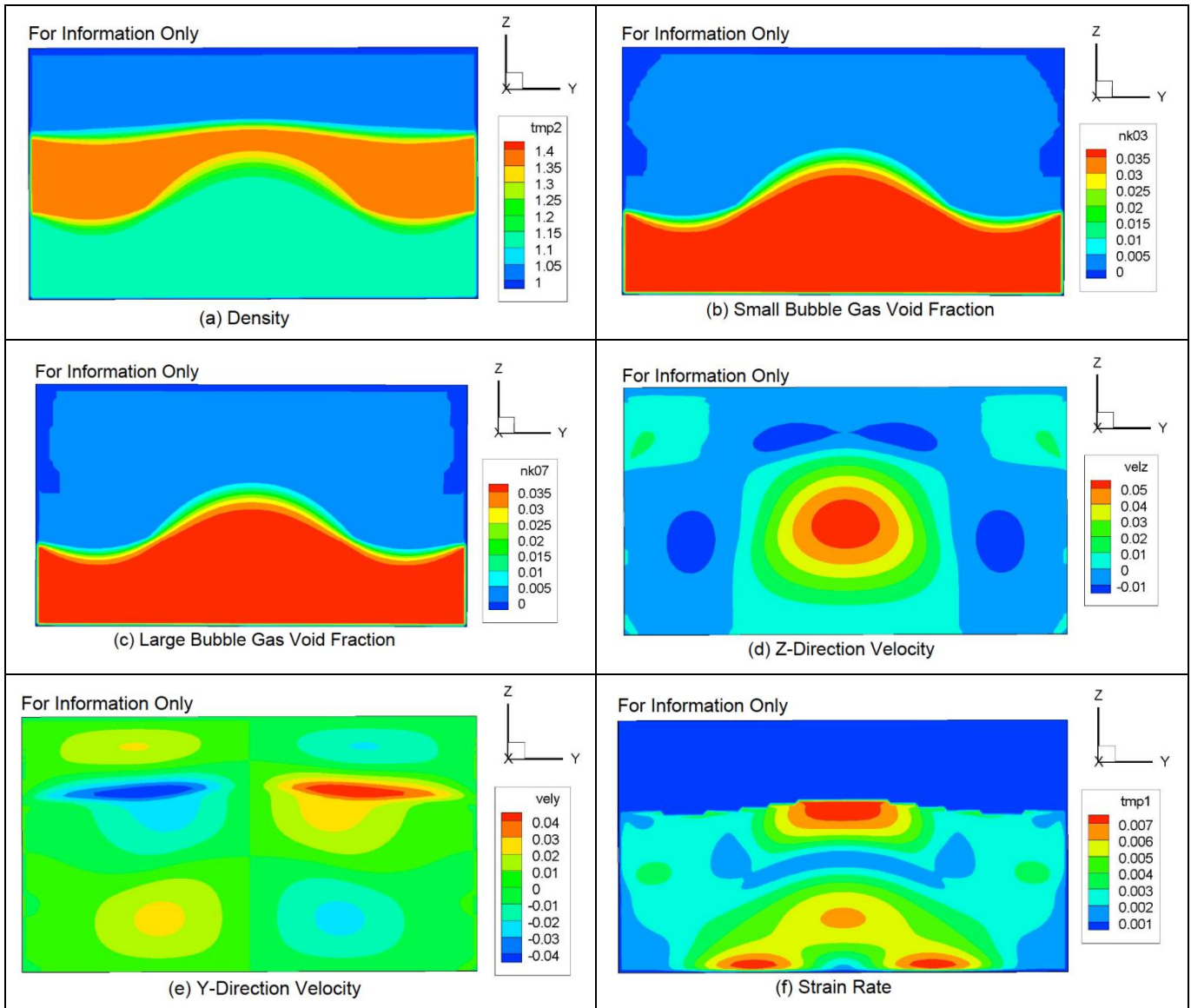


Figure 9.3. Density, g/mL (a), Gas Void Fraction for Smallest (b) and Largest Bubbles (c), z-Direction (d) and y-Direction (e) Velocities, cm/s, and Strain Rate, s^{-1} , at the 23-in. Mid-Plane (f) at Time = 200 s. (Note: Graphics are provided For Information Only.)

The density distribution shown in Figure 9.4 (at 350 seconds into the transient) shows the slurry with entrained gas bubbles penetrating to the slurry-liquid surface. The void fraction distributions for the smallest and largest bubbles show some very small differences since the large bubbles are migrating relative to the slurry motion. The strain rate is sufficiently large to reduce the viscosity and drag and to allow for large bubble motion relative to the slurry. The smallest bubbles continue to move with the slurry.

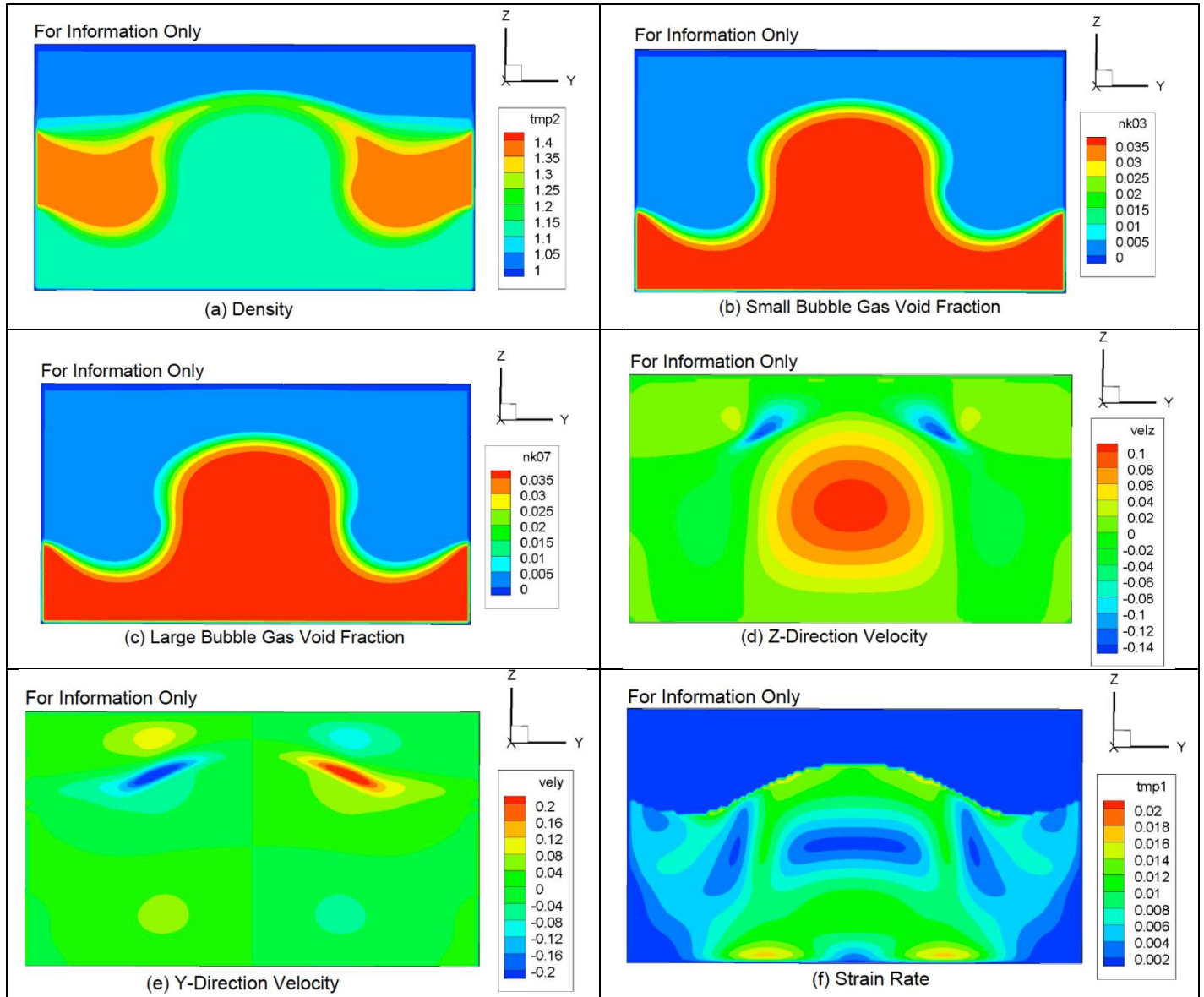


Figure 9.4. Density, g/mL (a), Gas Void Fraction for Smallest (b) and Largest Bubbles (c), z-Direction (d) and y-Direction (e) Velocities, cm/s, and Strain Rate, s^{-1} , at the 23-in. Mid-Plane (f) at Time = 350 s. (Note: Graphics are provided For Information Only.)

The void fraction and density distributions shown in Figure 9.5 (700 seconds into the transient) indicate that a portion of the lighter slurry has flowed up and over the denser slurry to form a cap. A noticeable amount of the large-bubble gas is being released and is accumulating at the top of the liquid layer. The velocities and strain rates are slowly decreasing.

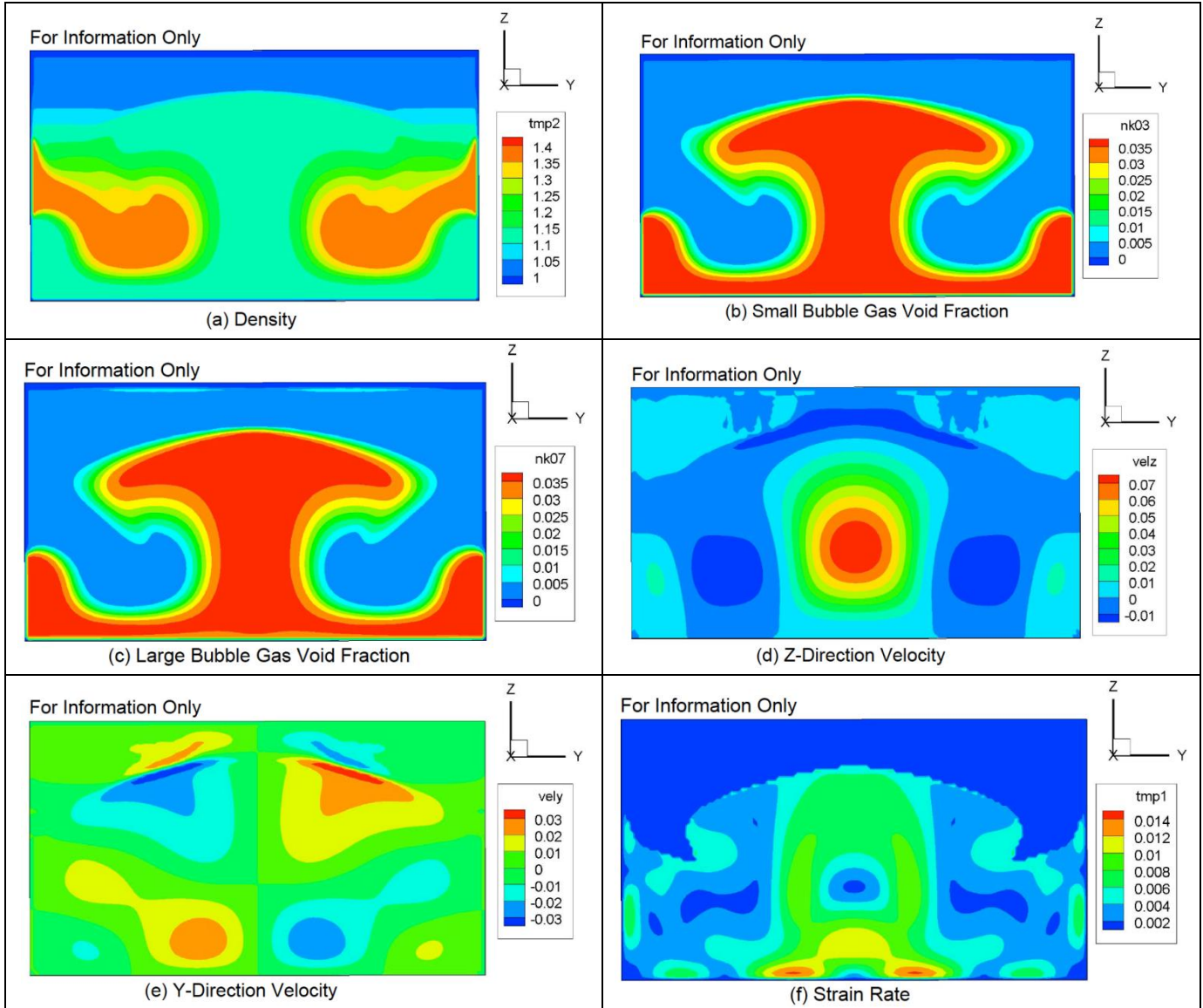


Figure 9.5. Density, g/mL (a), Gas Void Fraction for Smallest (b) and Largest Bubbles (c), z-Direction (d) and y-Direction (e) Velocities, cm/s, and Strain Rate, s⁻¹, at the 23-in. Mid-Plane (f) at Time = 700 s. (Note: Graphics are provided For Information Only.)

The final density and void fraction distributions are shown in Figure 9.6. Note that only a portion of the lighter slurry has moved over the denser slurry and the rest forms a tree-like structure with a significant heel left on the bottom. Very little of the small-bubble gas has been released but a significant portion of the large-bubble gas has been released. The quantities of released gas are presented in Table 9.3. The gas release is expressed in terms of volume at standard conditions and as a fraction of the initial gas for each size bubble and total gas. Note that the fraction of large-bubble gas is much higher than that for the smallest bubble size. For example, the fraction of 0.7-cm bubble gas released is 0.087 as compared to 0.027 for the 0.1-cm bubble gas.

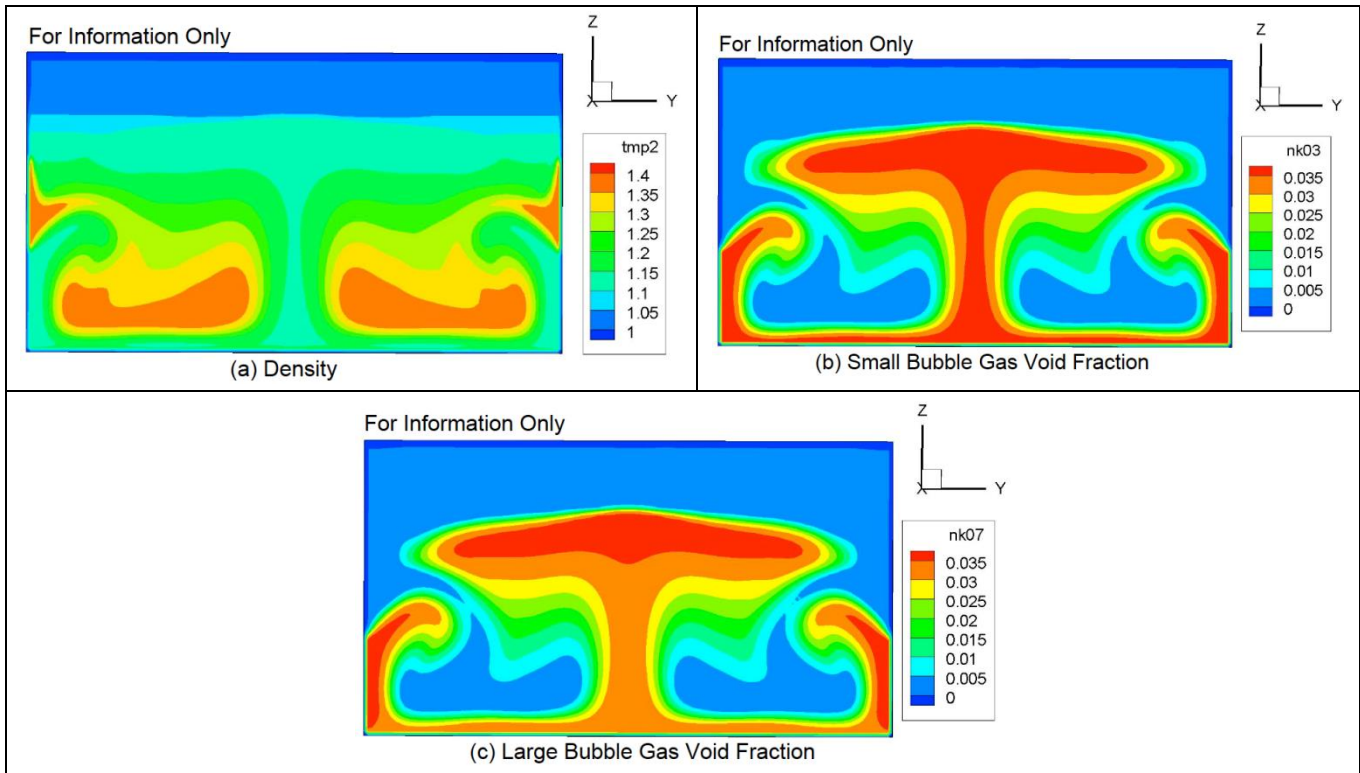


Figure 9.6. Final Distributions for the Density, g/mL (a), and Gas Void Fraction for the Smallest (b) and Largest Bubbles (c) at the 23-in. Mid-Plane. (Note: Graphics are provided For Information Only.)

Table 9.3. Gas Release as a Function of Vessel Size, Initial Void Fraction, and Bubble Size. (For Information Only)

Vessel Diameter	α_{RT} (vol%)	0.1 cm cm ³ (frac.)	0.25 cm cm ³ (frac.)	0.4 cm cm ³ (frac.)	0.55 cm cm ³ (frac.)	0.7 cm cm ³ (frac.)	Total cm ³ (frac.)	Total, $\Delta\phi$
23 in.	8.0	10.2(.025)	14.9(.037)	19.1(.048)	23.8(.060)	28.7(.072)	96.7(.048)	0.00417
23 in.	12.5	16.7(.026)	27.8(.042)	36.4(.056)	45.0(.069)	53.1(.081)	179.0(.055)	0.00786
23 in.	18.5	28.9(.027)	54.2(.051)	68.2(.064)	80.8(.076)	92.0(.087)	324.1(.061)	0.01385
70 in.	8.0	198(.016)	343(.028)	445(.036)	534(.043)	621(.050)	2141(.034)	0.00296
70 in.	12.5	326(.016)	611(.030)	753(.037)	871(.043)	991(.049)	3551(.035)	0.00500
70 in.	18.5	496(.015)	996(.031)	1280(.039)	1509(.046)	1737(.053)	6017(.037)	0.00840
900 in.	8.0	6.34e4(.002)	2.91e5(.011)	3.61e5(.014)	4.19e5(.016)	4.70e5(.018)	1.60e6(.012)	0.00104
900 in.	12.5	6.04e4(.001)	4.83e5(.011)	6.55e5(.015)	7.74e5(.018)	8.59e5(.020)	2.83e6(.013)	0.00186
900 in.	18.5	1.59e5(.002)	7.81e5(.011)	1.16e6(.017)	1.42e6(.020)	1.60e6(.023)	5.12e6(.015)	0.00340

The final distributions for the 70-in. and full-scale cases at initial void fraction of 18.5% are presented in Figure 9.7 and Figure 9.8 for comparison. The general features are similar. For example, the shape of the buoyant plume is similar at all scales. A major difference is that the bubble void fraction for the larger vessels increases as the gas rises in the vessel, resulting in a larger void fraction in the upper region. This is discussed in more detail in Section 9.3.1.

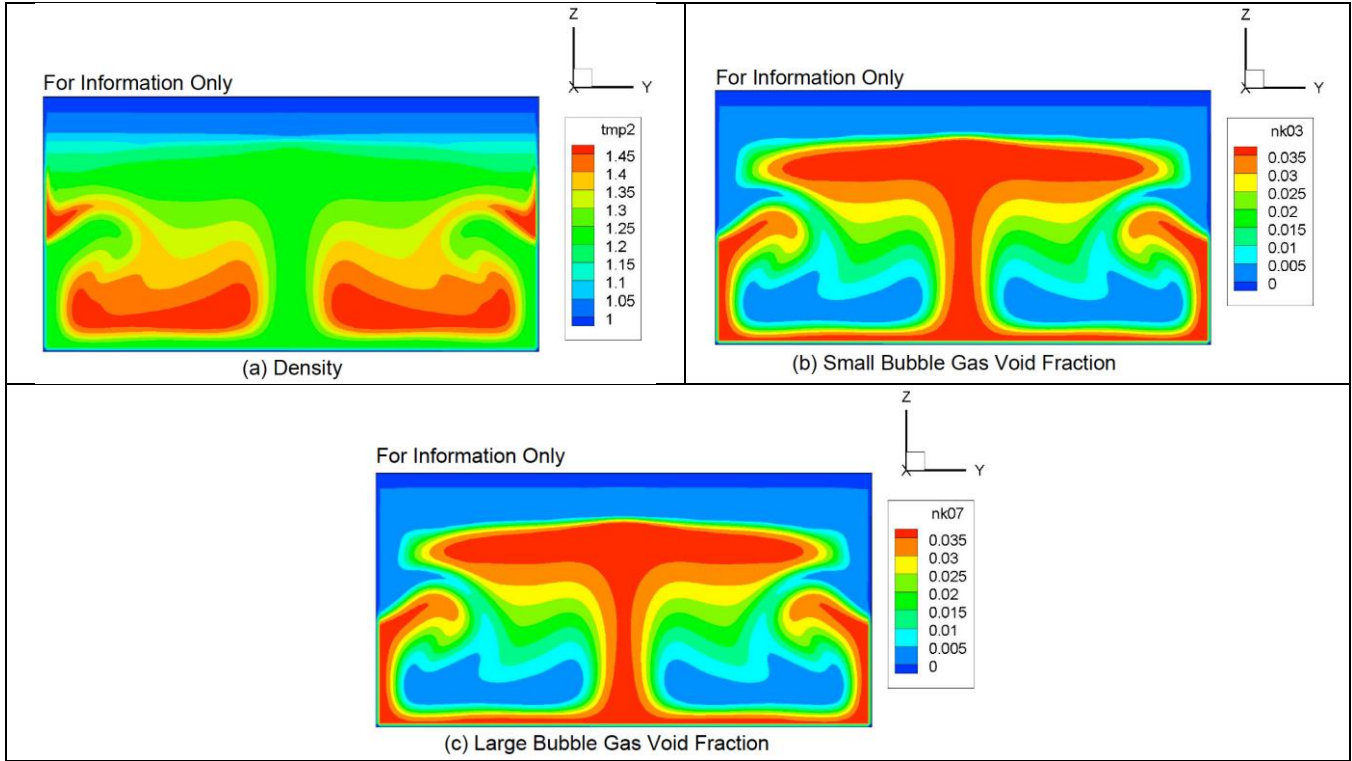


Figure 9.7. Final Distributions for the Density, g/mL (a), and Gas Void Fraction for the Smallest (b) and Largest Bubbles (c) at the 70-in. Mid-Plane. (Graphics are provided For Information Only.)

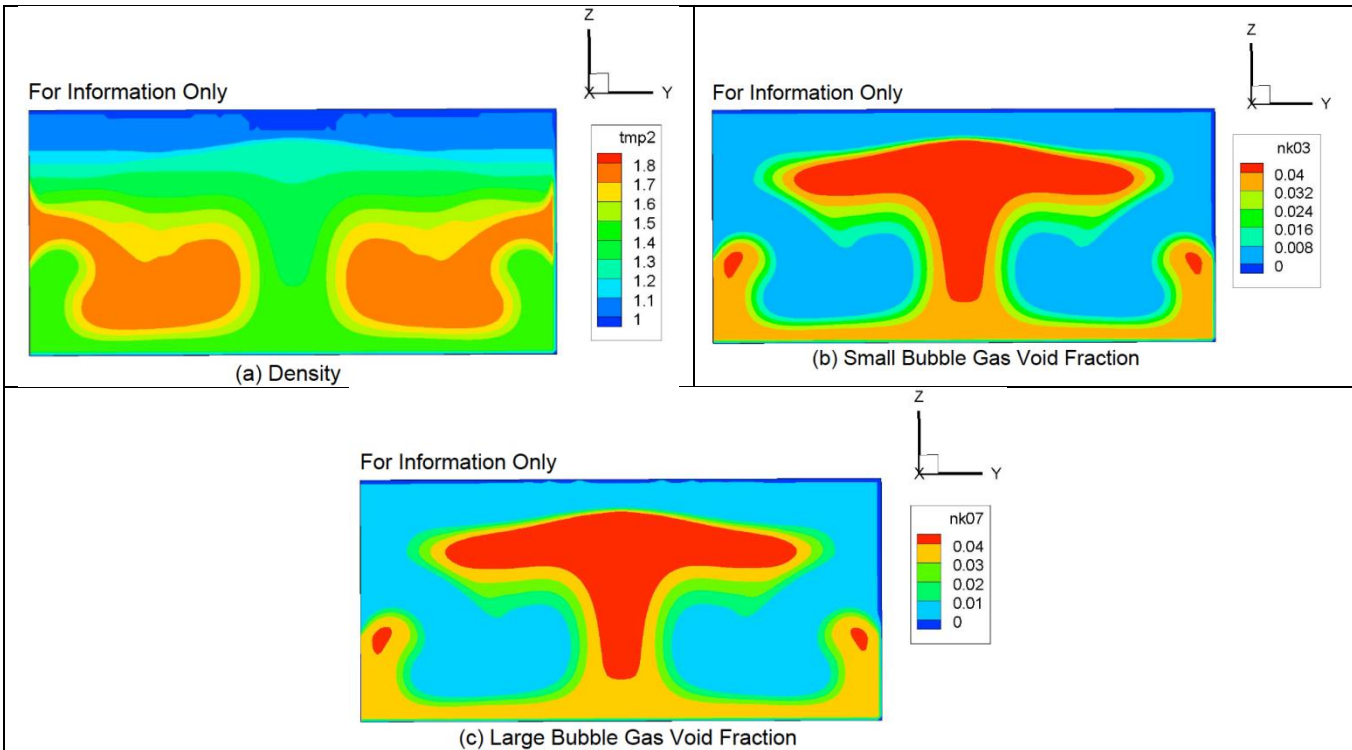


Figure 9.8. Final Distributions for the Density, g/mL (a), and Gas Void Fraction for the Smallest (b) and Largest Bubbles (c) at Full Scale. (Graphics are provided For Information Only.)

The features exhibited in these simulations look similar to those observed during the RT tests. However, the times associated with this transient appear to be significantly longer than those experienced during the test. The following are some observations on the differences between the simulations and tests:

- In the experiments, the movement of the lower slurry is not visible before the lower layer reaches the slurry surface. The observed experimental transient begins when the lower slurry begins to flow over the upper slurry, which is well into the simulated transient.
- The simulation is based on a Bingham model for viscosity from a fit of rheological data taken at relatively high strain rates with only a single data point below 3 s^{-1} . The apparent viscosity is dominated by the Bingham yield stress. If the rheological behavior is better described by a Herschel-Bulkley or similar model, the apparent viscosity at low strain rates could be significantly lower, reducing the transient time in the model prediction.
- The difference in apparent viscosity between the lower and upper slurry layers is due to the difference in void fraction (on the order of 10-20%). The observed behavior during the test is that the lower slurry penetrates the upper slurry and flows out over a relatively stationary surface. The simulation predicts that both the upper and lower slurries move so that there is little relative motion at the interface. This implies that the slurry surface had significantly more strength in the actual test than in the simulation, so that the lower slurry spilled out and stopped after a short period of time.

9.3.1 Results for Gas Release

The generated gas is represented using five continuum fields, one for each bubble size (0.1-, 0.25-, 0.4-, 0.55-, 0.7-cm diameter bubbles). It was assumed that the void fraction is divided equally among the different bubble sizes. As the gas is released from the slurry during the transient, it is collected at the top of the simulation domain. The captured gas for all five bubble fields is summed to yield the total gas released, which can be expressed in terms of fraction of the original gas inventory.

The predicted total gas release results are presented in Figure 9.9 for the matrix of simulations for three void fractions ($\alpha_{RT} = 8\%$, 12.5% , and 18.5%) at three different scales (vessel diameters of 23 in., 70 in., and 900 in.). In addition, the predicted total gas releases for five of the experimental cases (23-06, 23-12, 70-09, 70-11, and 70-14) are compared with measured values.

The simulation results show that predicted total gas release decreases with increasing vessel diameter and decreasing initial void fraction. These trends are consistent with the experimental results shown for the selected cases. The predicted total gas release in all of these cases exceeds the experimental values, indicating that the selected bubble size distribution results in conservative predictions. The disparity between the 70-in. predictions and measured values is addressed later in this section.

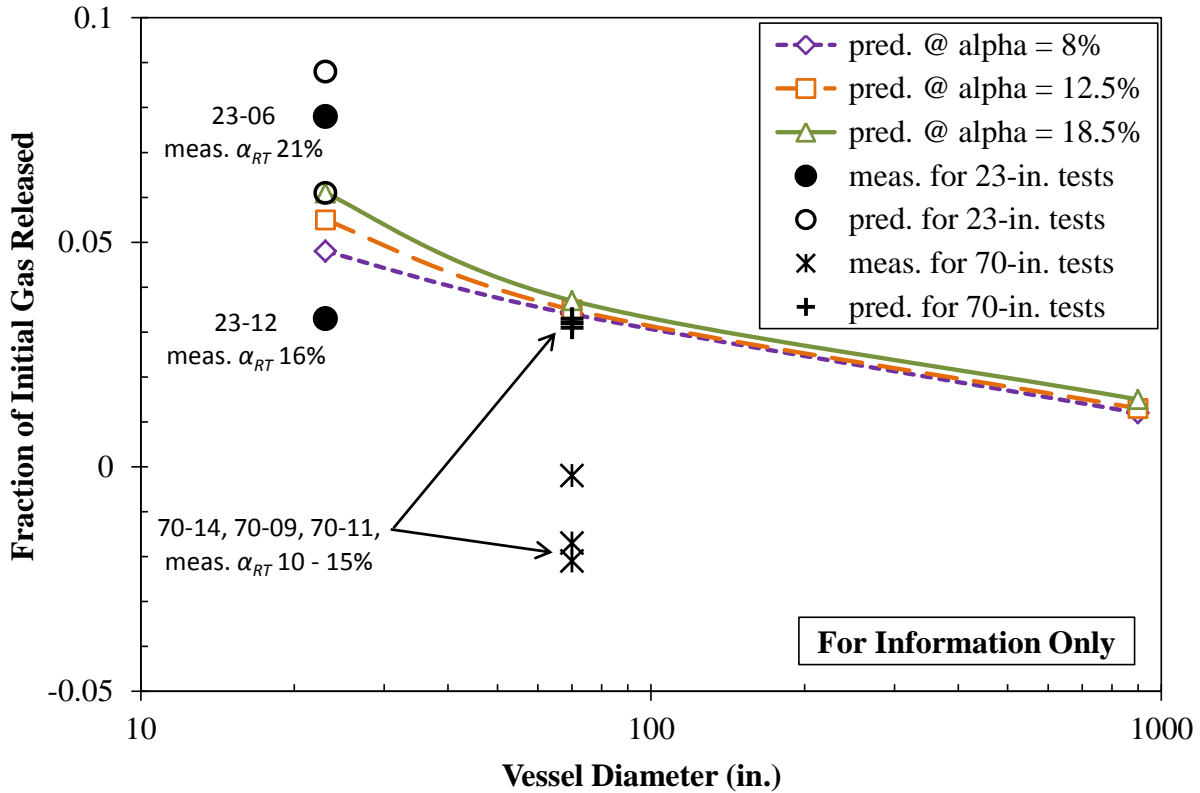


Figure 9.9. Total Gas Release as a Function of Vessel Size and Initial Void Fraction. (Graphic provided For Information Only)

Figure 9.10 shows the same results with the addition of the high-initial-void-fraction experimental cases 23-01 and 70-20. The predicted values for these two cases are substantially lower than those measured. The primary release mechanism being modeled in ParaFlow is the movement of isolated gas bubbles due to convection and rise through the sheared slurry. The model does not address the effects of bubble coalescence or bubble cascade. For this reason, the recommendation is that the use of simulation results should be restricted to cases having low (e.g., <20%) initial gas volume fraction. If it can be established that the void fraction does not exceed a specified value (such as 10 vol%) the results from these RT simulations should be applicable.

The bubble rise velocity is a function of bubble diameter. The larger bubbles are more likely to rise to the slurry surface while the smaller bubbles tend to be convected along with the slurry like a tracer. The gas release as a function of bubble size is presented in Table 9.3 for the parametric cases. The input parameters used for these simulations were presented in Table 9.1. The amount of gas released for each bubble field is expressed in both volume at standard conditions and as a fraction of the initial inventory. Note that the total gas released is dominated by the largest bubble sizes, especially as the vessel diameter increases.

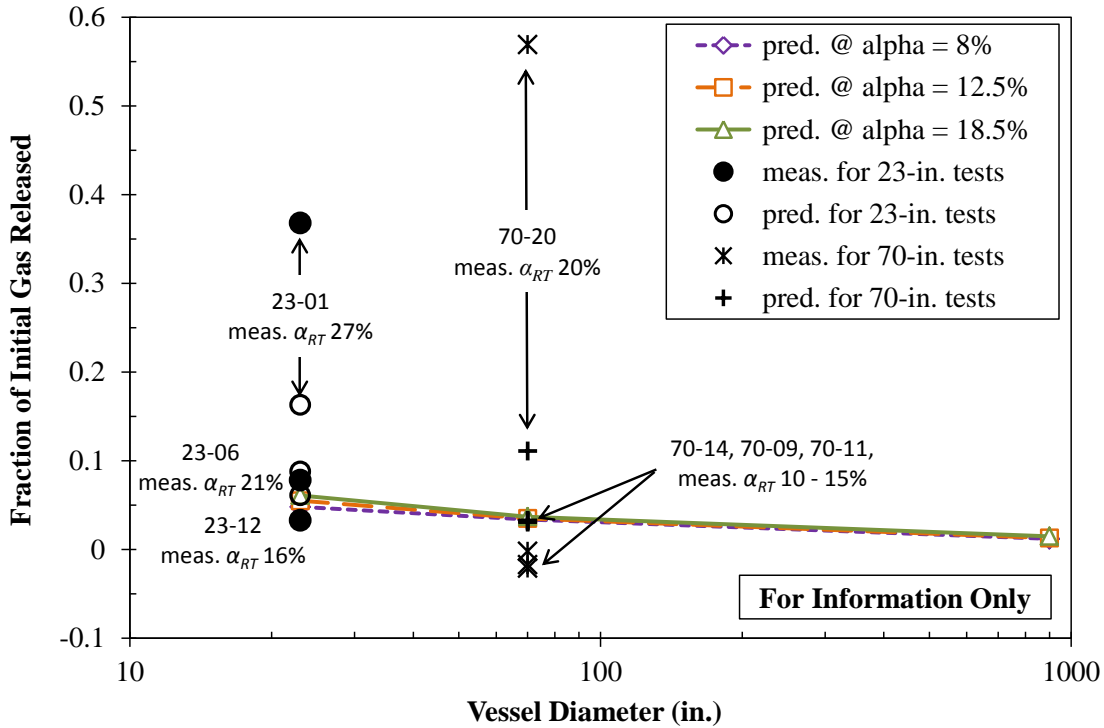


Figure 9.10. Total Gas Release as a Function of Vessel Size and Initial Void Fraction. (Graphic provided For Information Only)

The gas release simulation results for selected test cases are compared with measured values in Table 9.4. Note that the measured gas release values for cases 70-09, 70-11, and 70-14 are negative numbers. The gas release is determined by the change in fluid level. However, the level is also affected by the movement of higher-pressure gas from the lower region of the vessel and expanding into the upper region. The effects of both gas expansion and gas release are accounted for in the simulations. The adjusted gas release values are based on the predicted level change and are comparable with the measured values for initial void fractions below 20% (excluding tests 23-01 and 70-20).

Table 9.4. Comparison of Simulation Results and Measured Gas Release. (For Information Only)

Test Case	Vessel Diameter (in.)	α_{RT} (vol%)	Density (kg/m ³)	$\tau_0^{(a)}$ (Pa)	$\mu_\infty^{(a)}$ (mPa·s)	Predicted Gas Release (fraction)	Adjusted Gas Release (fraction)	Measured Gas Release (fraction)
23-01	23	27.3	1422	11.1	21.9	0.163	0.150	0.368
23-06	23	21.4	1390	7.03	16.9	0.088	0.079	0.078
23-12	23	15.7	1342	3.41	11.2	0.061	0.049	0.033
70-09	70	12.6	1440	14.2	25.3	0.031	-0.011	-0.017
70-11	70	14.7	1464	19.5	30.3	0.033	-0.004	-0.002
70-14	70	10.3	1410	9.36	19.9	0.032	-0.010	-0.021
70-20	70	20.5	1501	31.4	39.7	0.111	0.083	0.569

(a) Because of timing of activities, input parameters for the simulations were determined from property-vs.- x_S correlations that were slightly different than the final versions shown in Section 7.1. The differences, ~10% or less, are not expected to have an effect on interpretation of the results of the FIO simulations.

9.3.2 Results for Strain Rate and Gas Release Rate vs. Time

The amount of gas released during the transient depends to a large degree on the bubble rise velocity, as demonstrated by the gas release fractions for the different bubble sizes. The rise velocity depends on the apparent viscosity, which is a function of the local strain rate. Therefore, the transient behavior of the strain rate distribution will help us understand the gas release as a function of time and the difference in gas release at different vessel scales.

Figure 9.11 through Figure 9.13 provide information on transient strain rate behavior. Figure 9.11 is the maximum strain rate within the slurry region as a function of time for the three parametric simulations with the initial void fraction of 18.5 vol%. The values for the 23-in. vessel correspond to the cross-section pictures presented in Figure 9.2 through Figure 9.6. The point of maximum strain rate is not always the same. During certain periods it is near the bottom of the vessel where the rotating vortex interacts with the vessel floor. At other times the maximum strain rate is in the upper slurry region. This change in location can be seen in the transition from the rapidly decreasing strain rate to a slower decrease.

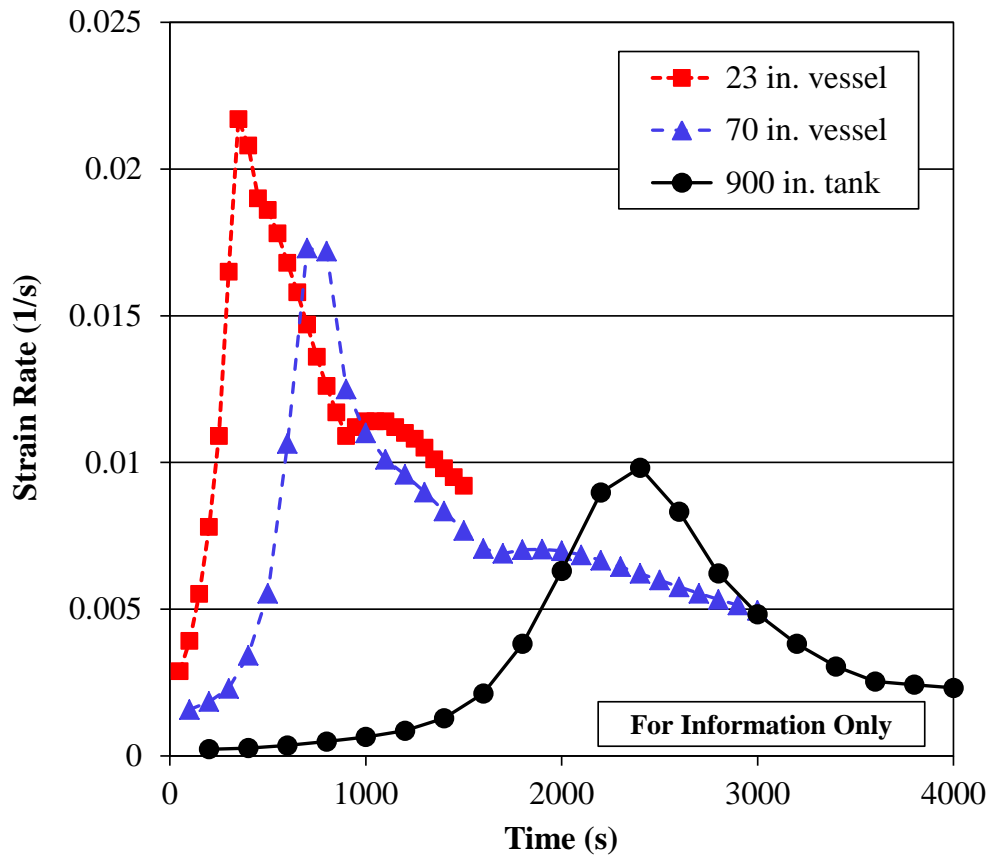


Figure 9.11. Maximum Slurry Strain Rate as a Function of Time for $\alpha_{RT} = 18.5\%$. (Graphic provided For Information Only)

The maximum strain rate decreases with vessel diameter while the duration of the transient increases. The peak strain rate occurs just after the lower slurry penetrates to the upper surface (at approximately 450 s). The velocities and strain rate then decrease rapidly for a couple of minutes, after which the

transient enters a phase of slow deceleration. The simulation transient time is significantly longer than the observed transient, as discussed earlier in Section 9.3.

The maximum strain rate during the transient is presented in Figure 9.12 as a function of vessel diameter and initial void fraction. The strain rates do not differ significantly with void fraction, but there is a noticeable trend toward decreasing maximum strain rate with increasing vessel diameter. This is one explanation for the reduced gas release at larger vessel diameters. The lower strain rate increases the apparent viscosity and reduces the bubble rise velocity.

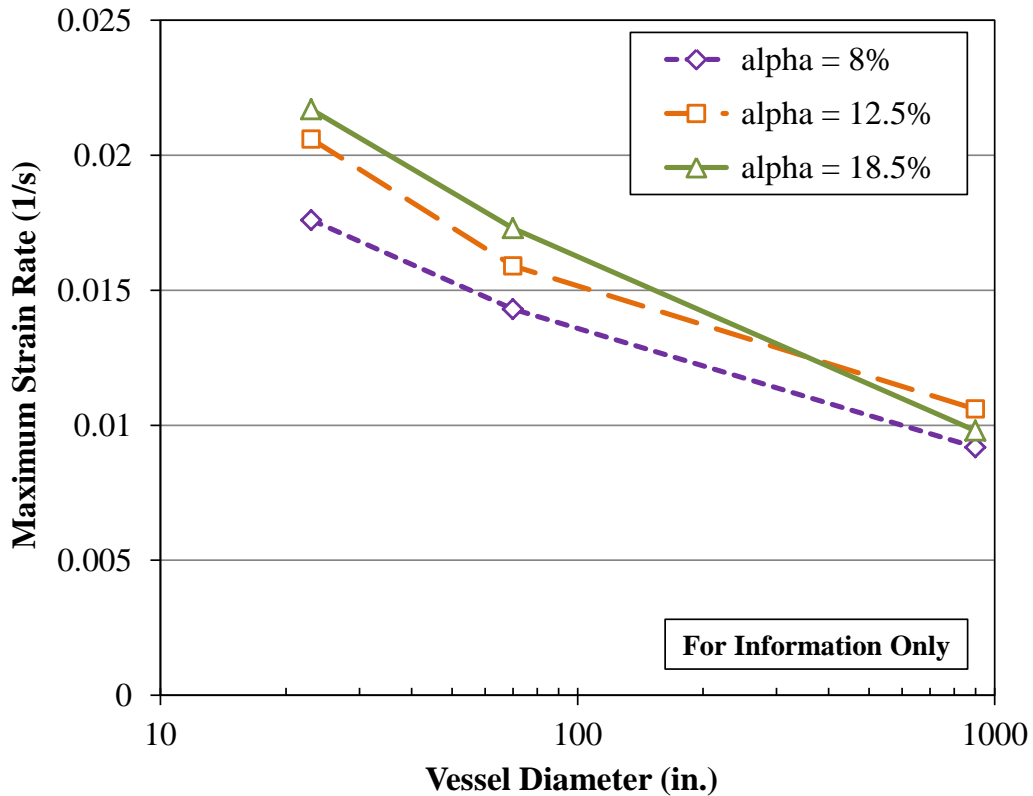


Figure 9.12. Maximum Strain Rate as a Function of Vessel Diameter and Initial Void Fraction. (Graphic provided For Information Only)

The importance of the effect of strain rate on gas release may depend on the location. The strain rate at a point near the slurry surface may have more impact than at other locations. Figure 9.13 shows the strain rate as a function of time at a point near the slurry surface and displaced from the vessel center by approximately one-twentieth the tank radius. The peak strain rate is less than a third of that shown in Figure 9.11, but the curves share many of the same features and time frame. There is no apparent transition to a different deceleration rate as seen in Figure 9.11.

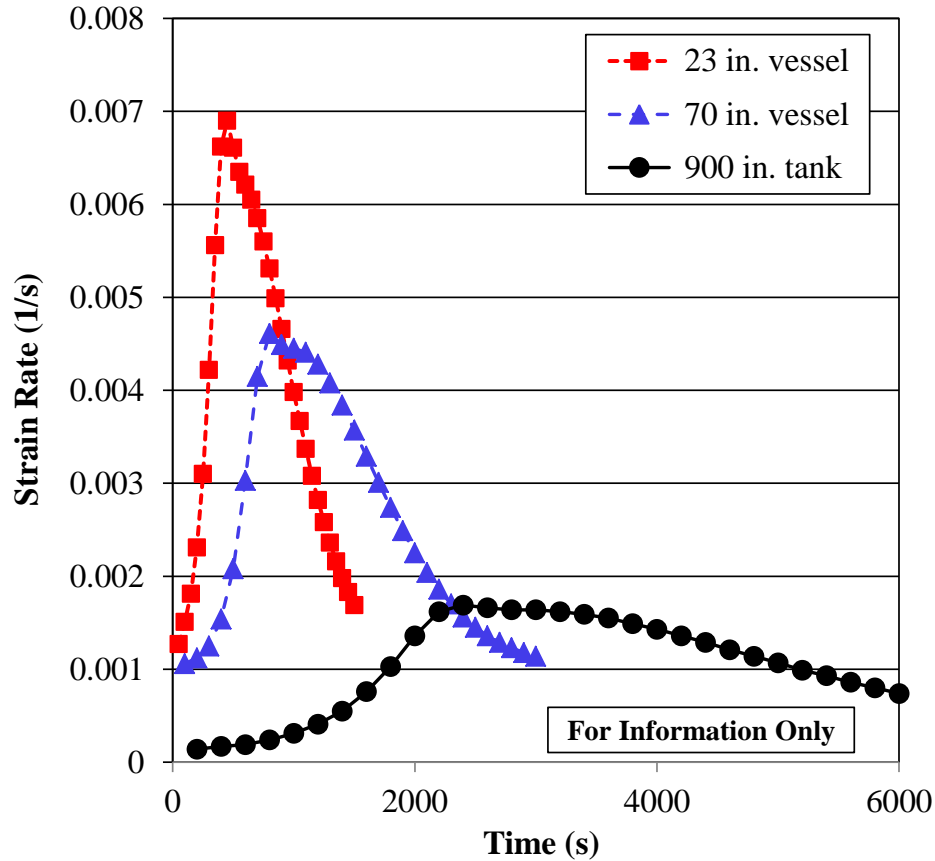


Figure 9.13. Strain Rate at Location Near Slurry Surface as a Function of Time for $\alpha_{RT} = 18.5\%$.
(Graphic provided For Information Only)

The gas release rate as a function of time is shown in Figure 9.14 for the three parametric simulations with the initial void fraction of 18.5 vol%. The release rate is expressed in terms of fraction of initial gas inventory to allow comparison of tests with different vessel sizes. The integral under the curve corresponds to the total gas released reported in Table 9.2. The time of peak gas release is close to that for peak strain rate and is near the time that the lower slurry penetrates to the upper surface. The peak release rate decreases with increasing vessel diameter, more dramatically than strain rate.

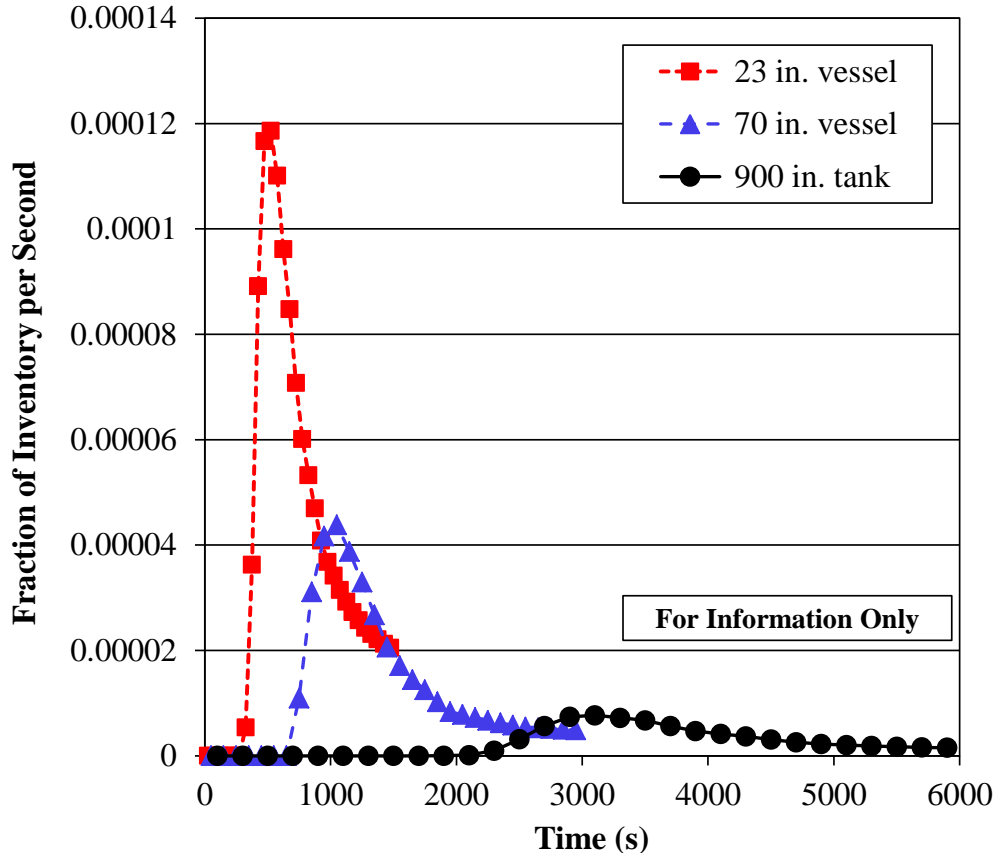


Figure 9.14. Rate of Gas Release as a Function of Time for $\alpha_{RT} = 18.5\%$. (Graphic provided For Information Only)

9.4 Results for Varied Slurry Layer Thickness Ratios

Simulations were performed for slurry thickness ratios of 1:3 and 1:5 (lower-layer:upper-layer ratio). Two simulations were performed for the 1:5 thickness ratio; the simulations were initialized with a sinusoidal perturbation between the two slurry layers with the same magnitude but different wavelengths. The wavelengths were 0.8 and 0.57 times the vessel diameter, respectively. Figure 9.15 shows the small-bubble void fraction distribution for the two cases after 10 s.

Note that the shorter wavelength resulted in a more unstable RT behavior. The reason for this is that the RT convection is due to a vortex ring that induces upward motion in the center and downward motion around the periphery. A cross-section of this ring shows that the rotating region is nearly circular, where the inward and outward flow regions are separated by the same distance as the upward and downward flow regions, not elliptical. This implies that when the bottom-layer thickness is larger than the vessel radius, the controlling dimension is the vessel diameter. However, when the bottom-layer thickness is less than the vessel radius, the layer thickness becomes the limiting dimension in the size of the vortex ring. This has an impact on the RT stability criterion, as discussed in Section 8.5.3.

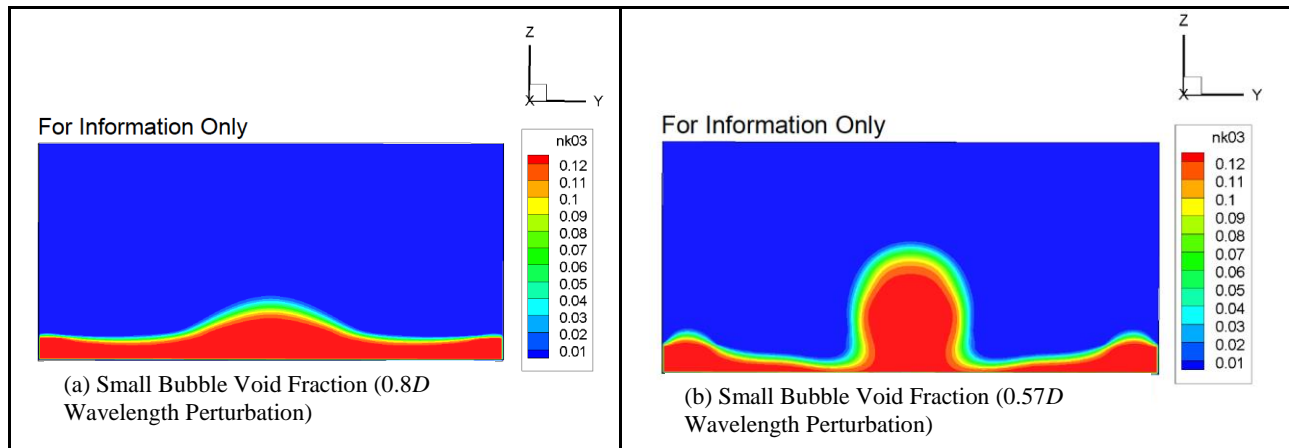


Figure 9.15. Comparison of Small-Bubble Void Fraction at $t = 10$ s After Initialization with Different Wavelength Perturbations, 0.8 (a) and 0.57 (b) times the Vessel Diameter (Note: Graphics are provided For Information Only.)

9.5 Conclusions

Conclusions resulting from the modeling work include:

- Buoyant motion within a sediment layer has been simulated for a series of void fractions ($\alpha_{RT} = 8\%$, 12.5%, and 18.5%) at three different scales (vessel diameters of 23 in., 70 in., and 900 in.). The results show that total gas release decreases with decreasing initial void fraction and increasing vessel diameter. This suggests that tests at 70-in. have more relative gas release than would occur at full scale.
- Simulations were performed corresponding to the experimental cases that had equal thicknesses for the top and bottom slurry layers that scale geometrically to the full-scale tanks. Comparisons of simulation results to measured gas release values indicate that for low initial void cases (<20%) the simulations give conservative results.
- The strain rate distribution was also evaluated. The strain rates do not differ significantly with void fraction, but there is a noticeable trend toward decreasing maximum strain rate with increasing vessel diameter. This is one explanation for the reduced gas release at larger vessel diameters. The lower strain rate increases the apparent viscosity and reduces the bubble rise velocity.
- The controlling length for stability for a thin layer on the vessel bottom appears to be the sediment thickness, not the vessel diameter.
- Thin layers on the vessel bottom are more stable than thicker layers. This is opposite to the behavior of clay layers (of different thickness) being supported by a gas layer.

10.0 Extrapolation of Results

Section 10.1 discusses considerations for and efforts to extrapolate gas release results from RT tests in the 23-in. and 70-in. vessels to a full-scale DST. Section 10.2 recaps the comparison of experimental results to numeric simulations and the use of simulations to predict gas release at full scale.

10.1 Extrapolation from Experimental Results

The ultimate goal of modeling and testing, under the RT instability gas release tasks, was to estimate, or set a bounding value for, the gas release from a full-scale RT instability in a Hanford waste tank. The conditions preceding the event are expected to be limited to retained gas fractions that are less than ~ 0.20 , based on: 1) past operational experience with sludge layers that are somewhat less deep than the ones expected in the future; and 2) the expectation that strong sludges of depth similar to that planned for Hanford tanks in the future will tend to form channels that allow gas to be continuously released from all the waste. This expected upper limit on gas volume fraction, which was studied in DSGREP intermediate- and tall-column tests (Powell et al. 2014; Schonewill et al. 2014), is taken into account in interpreting the RT test results.

Considerations in extrapolating small-scale test results to the full-scale tank include the following.

- The diameter of a vessel provides a meaningful length scale for estimating the gas fraction, α_{RT} , at which RT instabilities occur, and this gas retention limit has a bearing on the size of the gas release.
- Cases in which α_{RT} exceeds 85-90% of the neutral-buoyancy gas fraction in the supernatant liquid, α_{NB} , produce releases whose mechanism is not solely that of RT instability, and in addition, depend on the presence of retained gas fractions greater than ~ 0.20 .
- Similarly, cases in which α_{RT} approaches the gas fraction for spontaneous release (α_{SR}) determined for the sludge (slurry) in the absence of an upper slurry layer (e.g., SL tests) produce releases whose mechanism is not solely that of RT instability (e.g., if $\alpha_{RT} > \sim 0.85 \alpha_{SR}$). Again, these typically depend on the presence of retained gas fractions greater than ~ 0.20 .
- Geometric scaling of sludge depth ($1\times$) is based on tank 241-AN-106 being filled to the proposed maximum post-retrieval level (Section 4.2.1). Experimental studies at greater than $1\times$ total slurry depth provide insight into understanding scale-dependence of α_{RT} and gas releases from RT instabilities, but they do not provide a direct means to extrapolate to full scale.
- The fraction of gas inventory released in RT tests did not show a clear dependence either on α_{RT} or on modified energy ratios in the tested range of ER_S : $\sim 10 - 22$ for equal slurry layer thicknesses and $\leq 1.5\times$ total slurry depth; and $\sim 12 - 74$ for $2\times$ depth and varying relative slurry layer thicknesses (Section 8.5.2).

Applying these considerations to completed RT tests further limits the available options for direct extrapolation of results to full scale. For the following discussion, Table 8.5 in the summary RT Instability Gas Releases section (8.5.1) provides a useful summary of α_{RT} and the magnitude of gas releases associated with the RT instability event, both in terms of the fraction of the gas inventory present at the start of the event that was released and the specific gas release $\Delta\phi$ (volume of gas released/unit

volume of gas-free lower-layer slurry). Using the global criterion that $\alpha_{RT} < 0.20$, in conjunction with other discriminators, removes the following test data from further evaluation:

- All 10-in. vessel test data – The three completed 10-in. tests had $\alpha_{RT}/\alpha_{NB} > 0.85$ ($\alpha_{RT} \geq 22$ vol%). Additionally, two of these had 2× total slurry depth (tests 10-02 and 10-04), and the other was 4×-depth (test 10-08).
- Additional $\alpha_{RT}/\alpha_{NB} > 0.85$ cases – Four 23-in. vessel tests fall in this category. Two of these are initial 1×-depth tests (23-01 and 23-03) that were a basis for adjustments in the test matrix (to use lower τ_5) and in the concentration of H_2O_2 used in future 23-in. vessel tests (Section 8.1.3.1). The other two tests (23-15 and 23-24) also had 2× total slurry depth.
- Spontaneous gas release characteristics – Several of the tests having $\alpha_{RT}/\alpha_{NB} > 0.85$ would have also failed a screening based on $\alpha_{RT}/\alpha_{SR} > 0.85$, where α_{SR} is derived from SL tests using the same simulant formulation in the same vessel. RT test 70-20 had a peak retained gas fraction of 20.5 vol% prior to the defined RT event (19.6 vol%), $\alpha_{RT}/\alpha_{SR} \sim 0.85$, and exhibited spontaneous gas release characteristics both before and during the RT instability (Sections 8.1.3.3 and 8.3.2.2).

One other RT test (23-06, $\alpha_{RT} = 21.4$ vol%, 1×-depth) did not meet the $\alpha_{RT} < 0.20$ requirement, but there are no secondary considerations from the list above to dismiss it. Including results from this test and all others having $\alpha_{RT} < 0.20$, Figure 10.1 shows the volume fraction of the retained gas inventory at the time of the RT event that was released as a function of α_{RT} . This figure is similar to Figure 8.23 (Section 8.5.1) except that data are removed using the first-cut screening criteria described above, and the independent parameter here is α_{RT} instead of α_{RT}/α_{NB} . Figure 10.1 includes 2× total slurry depth tests in the 23-in. vessel (green and red filled squares) that as a group tend to have significantly higher gas releases. Considering that geometric scaling of sludge depth is already defined in terms of the maximum fill level in the DST, these data may also be excluded (along with the 1.5× depth test in the 70-in. vessel, a blue-filled triangle in the figure). After doing so, the maximum gas release fraction shown in Figure 10.1 is 0.098 (9.8%; $\Delta\phi = 0.024$) at α_{RT} of 19.5 vol%, which is for test 23-17, a 1×-depth, 1:2 lower:upper slurry layer thickness test. From this “peak”, gas releases in both 23-in. and 70-in. vessel tests decrease in size with decreasing α_{RT} , reaching a point of no measurable gas release at $\alpha_{RT} \sim 0.15$ (~15 vol%).

Neglecting the 2×-depth result at $\alpha_{RT} = 0.157$ (test 23-23, and no gas release) shown in Figure 10.1, there are three tests for which the total slurry depth is 1× and α_{RT} is in the range of 0.14 to 0.16. These are replicate RT tests 23-05 ($\alpha_{RT} = 0.146$; -0.025 fraction released, $\Delta\phi = -0.004$) and 23-12 ($\alpha_{RT} = 0.157$; 0.033 fraction released, $\Delta\phi = 0.006$), and 70-11 ($\alpha_{RT} = 0.147$; -0.002 fraction released, $\Delta\phi = 0.000$); see Section 8.1). This set of tests is the only group for which data are available in the same α_{RT} range for multiple vessels and other screening criteria are met. Extrapolation of these limited data along a line of constant α_{RT} to a full-scale tank suggests that gas release at full scale would also be small, as follows. The average of the gas releases for the replicate 23-in. vessel tests is a release fraction of 0.004 (0.4%; average $\Delta\phi = 0.001$). This is smaller than the uncertainty of the gas releases using error-propagation of the resolution of measurements (~ 0.03 as a fraction of inventory released, $\Delta\phi \sim 0.007$). Extrapolating through the midpoints of the average 23-in. and 70-in. vessel gas releases gives near zero gas release at full-scale. A more conservative approach is to assume a release at full scale equal to that in the 23-in.

gas release quantities directly and are not dependent on the equivalent of an experimental level measurement, which is subject to competing effects due to expansion as gaseous lower-layer simulant rises during an in-sediment buoyant-displacement event. When the simulation results are put in terms of an equivalent level measurement, Table 9.4 shows that simulation and experimental results are nearly equal (“Adjusted” vs. “Measured” Gas Release, excluding $\alpha_{RT} > \sim 0.2$ cases).

Numerical simulation results for 23-in., 70-in., and 900-in. (full-scale) diameter vessels are shown in Figure 10.2 using α_{RT} values of 8, 12.5, and 18.5 vol%. This figure shows the same data as Figure 9.9 (Section 9.3.1), but without the predicted vs. measured gas release results for specific RT test cases. Input parameters for the simulations shown in Figure 10.2 are summarized in Table 9.1 (Section 9.2). The parameters are derived from the gravity yield criterion (e.g., Equation (4.2)) and a dimensionless correlation for the gravity yield parameter Y_G , which is a function of vessel diameter, sludge layer depths, and simulated-waste (simulant) physical properties. The Y_G correlation is based on a nearly complete set of the RT test data (Section 8.5.3), and thus its use for full-scale simulation inputs is also an extrapolation. Based on RT simulant-like waste properties, the estimated shear strengths for α_{RT} of 8, 12.5, and 18.5 vol% are 230, 530, and 1100 Pa, respectively. These relatively low shear strengths for tank waste sludge are conservative from the perspective that gas releases would, presumably, be larger for weaker materials having the same fraction of retained gas.

Figure 10.2 shows that sizes of gas releases decrease with decreasing α_{RT} , which is consistent with the experimental results shown in Figure 10.1 in the previous section. Importantly, Figure 10.2 also shows that gas releases become smaller as vessel diameter increases. Predicted releases at full scale range from ~1.2 to 1.5% of the retained gas inventory. This is consistent with the approximate range of 0 to 3% estimated by extrapolating experimental data at $\alpha_{RT} \sim 15$ vol%, as discussed in Section 10.1.

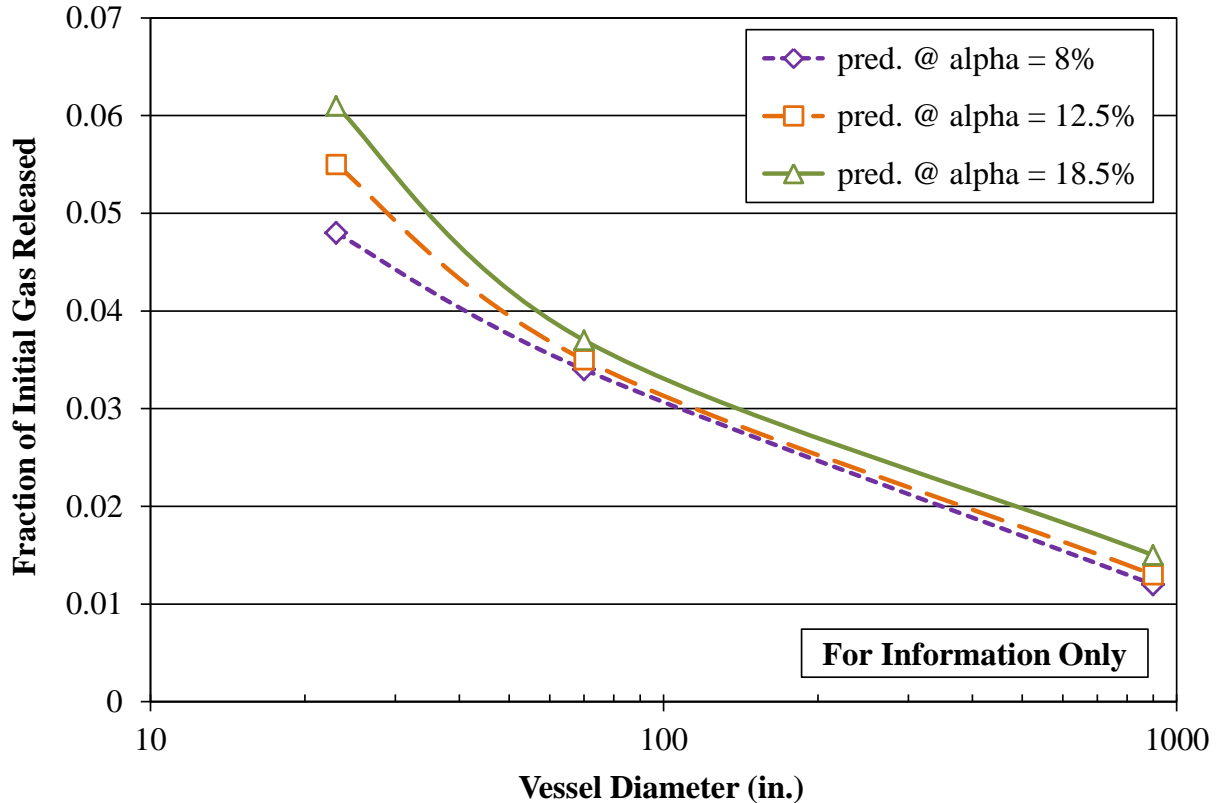


Figure 10.2. Total Gas Release as a Function Initial Void Fraction α_{RT} Extrapolated to Full Scale with Comparison to Experiments (Note: Numerical Simulation – For Information Only)

10.3 Overall Estimate of Gas Release in Full-Scale DSTs

Because the numerical results are FIO, the overall conclusion for the estimated gas release fraction in a full-scale DST will be based on the experimental results, which gave the approximate range of 0 to 3% for the fraction of retained gas that is released based on the extrapolation of experimental data at $\alpha_{RT} \sim 15$ vol%, as discussed in Section 10.1. The key limitations on the experimental results showing relatively low gas release are that releases at higher α_{RT} (e.g., >20 vol%) appear to be influenced by either spontaneous bubble cascades or by being near or above α_{NB} in the supernatant water layer.

For the bubble-cascade limitation, the waste strength in full-scale DSTs is expected to exceed the range where bubble-cascade gas releases have been observed, e.g., in simulants weaker than 200 Pa (see, for example, Stewart et al. 1996 and Gauglitz et al. 1996). Specifically, the current study is directed primarily at the sludge layer configurations that would result from planned transfers to DSTs AN-101 and AN-106. The waste in these DSTs is sufficiently strong (on the order of 1000-Pa shear strength, and certainly greater than 200 Pa; see Follett 2014) that bubble cascades should not occur. Regarding the limitation of being near α_{NB} , the actual retained gas fraction in AN-106 is relatively low (about 8 vol%; see Meacham 2010) and it is expected to be similarly low in AN-101 based on this tank also containing strong sludge waste from C-Farm (Follett 2014) that should have similar gas retention behavior (Meacham 2010), while α_{NB} in the tank waste supernatant liquid is relatively high (about 30 vol%; see Meacham and Kirch 2013). Therefore, any RT motion for waste having ~ 8 vol% retained gas, for

example, an RT instability occurring between a freshly transferred gas-free waste layer and an existing lower sludge layer at typical steady-state conditions, would be well below α_{NB} and in an α_{RT} range where the experimental results show small releases. Accordingly, the estimated low gas release fractions for a full-scale DST, should an RT instability even occur, are for conditions that are reasonably represented by the experimental results, e.g., well below α_{NB} and not influenced by a bubble-cascade release.

Finally, using the experiment-based gravity yield parameter correlations for the onset of RT instability at an α_{RT} of 8 vol%, which is the estimated void fraction in AN-101 and AN-106 (Meacham 2010), RT motion will not occur unless the waste (simulant) shear strength is less than 430 Pa (dimensional Y_G correlation) or 230 Pa (dimensionless Y_G correlation) (see Figure 8.27 and Table 8.7 in Section 8.5.3). This indicates that for the strengths measured in AN-101 and AN-106 (again, on the order of 1000 Pa; Follett 2014), an 8% void fraction (difference between layers) is not high enough to initiate RT motion.

11.0 Summary and Conclusions

This section provides brief conclusions to the RT instability experimental and modeling studies presented in this report. For experimental results and analytical modeling efforts, it draws from the Rayleigh-Taylor Instability Test Results in Section 8.0, which are assessed as a whole in the Summary of RT Test Results (Section 8.5). FIO numerical Modeling of Rayleigh-Taylor Events is covered in Section 9.0. It includes validation of the numerical modeling approach by comparison to experimental results, and simulation of RT instability gas releases in a full-scale tank. Conclusions from the numerical modeling investigation are presented in Section 9.5. Extrapolation of Results to full-scale DSTs in Section 10.0 further summarizes important expected outcomes based on the experimental and modeling studies and operating conditions in tanks AN-101 and AN-106. Significant conclusions from this work are described below:

1. An RT instability and resulting in-sediment buoyant motion are driven by a density inversion. This configuration can be established, for example, as it was experimentally, by layering gas-free sludge on top of a lower layer in which gas is generated and retained. Test results show that the retained gas fraction at the onset of an RT instability, α_{RT} , increases with increasing simulant shear strength for a given vessel size and, that as vessel diameter increases, a given value of α_{RT} is obtained with higher shear strength simulants. These are expected outcomes based on the governing gravity yield criterion model (Equation (4.1) in Section 4.1.1).
2. Experimental results show that the gravity yield parameter Y_G in the gravity yield criterion model has a value closer to 0.03 (~0.02 to 0.04, Section 8.5.3) than to the “constant” value of 0.09 originally assumed for planning tests. Important outcomes of this are that simulants had to be two- to three-times weaker for α_{RT} to be in the 8 to 18.5 vol% target range, and it became experimentally impractical to use simulants weak enough to obtain meaningful results from testing in the smallest (10-in.) vessel. As a result, testing in the 10-in. vessel was discontinued, and the preferred option of extrapolating results to full-scale using three geometrically-scaled systems was eliminated.
3. Experimental studies of RT instability using sediment beds composed of two slurry layers of equal thickness in both the 23-in. and 70-in. vessels (Section 8.1.3) or two slurry layers of varying relative thickness (ranging from 1:5 to 3:1 lower:upper) in the 23-in. vessel (Section 8.2.2) showed that α_{RT} is a function of simulant depth. The geometrically-scaled total slurry depth (1× in DST AN-101 when full, Section 4.2.1) in RT tests ranged from 0.67× to 1.5× in the 70-in. vessel and 0.67× to 2× in the 23-in. vessel. In general, equal layer thickness (1:1) test results indicate a trend of increasing α_{RT} with decreasing total (H_S) and lower slurry layer (H_{S2}) depths for simulant of a given strength. Additionally, at a given H_{S2} , deeper upper slurry layers (in varying relative layer thickness tests) appear to stabilize against RT instability, requiring larger α_{RT} .
4. Overall, it was found that α_{RT} is a complex function of simulant physical properties (shear strength and density), vessel diameter, and sediment layer depths, and consistent with this, the gravity yield parameter Y_G is not constant. Power-law correlations were obtained for Y_G in terms of the relevant parameters in both dimensional and dimensionless forms. These allowed extrapolation of Y_G to full scale for the purpose of estimating waste physical properties in the DST at given α_{RT} values (e.g., the target values for experiments, 8, 12.5, and 18.5 vol%) for use as inputs in numerical simulation inputs, for example.

5. Test results demonstrate that the quantity of gas released in RT instabilities generally increases with increasing α_{RT} . For $\alpha_{RT} > 0.2$, larger gas releases often were observed. Typically, these larger releases occurred in cases where α_{RT} approached or exceeded the gas fraction necessary for the slurry to be neutrally buoyant in the supernatant water, α_{NB} (e.g., in cases where $\alpha_{RT}/\alpha_{NB} > \sim 0.85$).
6. A large release was also observed in a case where α_{RT} was ~ 0.20 and $\sim 86\%$ of the gas fraction α_{SR} at which spontaneous gas release occurred in the absence of RT motion for the same simulant recipe (solids content). Spontaneous gas releases were investigated in single-slurry-layer (SL) tests in which no upper (gas-free) slurry layer was present. These tests showed that α_{SR} peaked at ~ 30 -Pa estimated shear strength and decreased with increasing strength. The sizes of spontaneous gas releases also decreased with increasing shear strength, but were still substantial in the strongest simulant used (e.g., $\sim 67\%$ of retained inventory at ~ 90 -Pa estimated shear strength in the 70-in. vessel). Gas was released by a bubble cascade mechanism in these tests and was especially apparent in slurries with estimated shear strength of 50 Pa or less. The data suggest that, when α_{RT} approaches α_{SR} , an RT instability gas release will take on the characteristics of a spontaneous release, consistent with the gas retention and release behavior of the simulant.
7. In 23-in. vessel tests at $2\times$ total slurry depth, gas releases tended to be larger than in $1\times$ -depth tests having the same α_{RT} , even for $\alpha_{RT} < 0.20$. Greater upper slurry layer depth in (most) $2\times$ -depth tests increased the potential for gas expansion when the lower layer rose as a result of RT motion and may have led to the larger releases.
8. Varying relative layer thickness and increased total depth tests were conducted in part to assess the relationship of gas releases and a modified energy ratio ER_S . The modified energy ratio, an analytical model developed in this work, expresses the ratio of the energy associated with in-sediment buoyant motion of gaseous slurry resulting from an RT instability to the energy required to yield the sediment and initiate flow. However, the experimental results show no clear trends in the relationship between the size of gas releases in classic RT instabilities and ER_S . Therefore, the ER_S model as currently formulated is not a useful screening tool for assessing conditions that would potentially lead to large gas releases in RT events in full-scale tanks, if they should occur at all.
9. Because geometric scaling of sludge depth ($1\times$) is based on a conservative assumption of tank AN-106 being filled to the proposed maximum post-retrieval level, only results from RT tests at $\leq 1\times$ total sediment depth are considered in extrapolation to full scale. Additionally, for the reasons identified above, consideration was also restricted to $\alpha_{RT} < 0.20$.
10. Considering $\leq 1\times$ total slurry depth cases, experimentally observed gas releases were as high as $\sim 10\%$ of the retained inventory for $\alpha_{RT} \sim 0.20$ (e.g., 9.8% of the retained gas at $\alpha_{RT} = 0.195$), decreased to 0 to $\sim 3\%$ of inventory released at α_{RT} of ~ 0.15 (e.g., at most, 3.3% of the retained gas at $\alpha_{RT} = 0.157$), and were still smaller (effectively zero) for $\alpha_{RT} < 0.15$.
11. Two replicate 23-in. vessel tests (15- to 17-Pa estimated shear strength) and a 70-in. vessel test (~ 63 -Pa estimated shear strength), all at $1\times$ total slurry depth, had α_{RT} values in the range of 0.14 to 0.16. The average of the gas releases for the replicate 23-in. vessel tests was a release fraction of 0.004 (0.4% of inventory), and it was essentially zero (slightly negative) in the 70-in. vessel test. Extrapolation of these data along a line of constant α_{RT} to a full-scale tank suggests

that gas release in a DST would also be near zero for α_{RT} of ~ 0.15 . A more conservative approach is to assume a release at full scale equal to the average value in the 23-in. vessel plus the measurement uncertainty, about 3% of the retained gas inventory, which is comparable to the fraction of the gas released in the larger of the replicate tests (3.3%).

12. FIO numerical simulation of RT instability gas releases were qualitatively and quantitatively consistent with the RT test results in those cases where α_{RT} is less than ~ 0.2 . Quantitatively, the simulations for specific test cases conservatively predicted gas releases as large as, or larger than, those observed experimentally. Like the experiments, the simulations show that sizes of gas releases decrease with decreasing α_{RT} . Simulations also show that gas releases become smaller as vessel diameter increases. Predicted releases in a full-scale tank range from ~ 1.2 to 1.5% of the retained gas inventory for α_{RT} in the range of 8 to 18.5 vol%. This is consistent with the approximate range of 0 to 3% estimated by extrapolating experimental data at $\alpha_{RT} \sim 15$ vol%.
13. Based on the dimensionless form Y_G correlation derived from the RT tests and RT simulant-like waste properties, the estimated shear strengths for α_{RT} of 8 and 18.5 vol% are 230 and 1100 Pa, respectively. Using these relatively low shear strengths for tank waste sludge in the simulations is conservative from the perspective that gas releases would, presumably, be larger for weaker materials having the same fraction of retained gas. Shear strengths of 430 Pa and 2200 Pa are estimated for α_{RT} of 8 and 18.5 vol% if the dimensional form Y_G correlation is used instead. Therefore, correlation-based estimates suggest that α_{RT} would need to be considerably greater than ~ 0.08 for waste of ~ 1000 -Pa shear strength, which is on the order of the strength measured in tanks AN-101 and AN-106 (Follett 2014), for an RT instability to occur.
14. Considering full-scale tank operations from another point of view, waste “layers” that have the same gas-free density and strength would need to have differences in retained gas fraction on the order of α_{RT} to be RT unstable. For typical and expected retained gas fractions of about 8 vol% in AN-101 and AN-106 (Meacham 2010), retaining sufficient gas to create RT instability and a resulting large gas release is not expected. Using α_{RT} of 0.08 (8 vol%) as a conservative benchmark for small gas releases, for example, a lower sludge layer in the DST would need a retained gas fraction of 0.16 (16 vol%) to become unstable if the layer above it has a “typical” 8 vol% steady-state retained gas fraction. Note that the lower region of AN-106 has a measured void fraction of 0.08 and reaching a retained gas fraction of 0.16 would be a significant departure from the current behavior.

12.0 References

ASTM C1750-11. 2011. *Standard Guide for Development, Verification, Validation, and Documentation of Simulated High-Level Tank Waste*. ASTM International, West Conshohocken, Pennsylvania.

Chhabra RP. 1992. *Bubbles, Drops, and Particles in Non-Newtonian Fluids*. CRC Press, Inc. Boca Raton, Florida.

Daniel RC, CA Burns, AD Crawford, LR Hylden, SA Bryan, PJ MacFarlan, and PA Gauglitz. 2014. *Morphology of Gas Release in Physical Simulants*. PNNL-23179 (DSGREP-RPT-004, Rev. 0), Pacific Northwest National Laboratory, Richland, Washington.

Epstein M and PA Gauglitz. 2010. *An Experimental Study of the Stability of Vessel-Spanning Bubbles in Cylindrical, Annular, Oblong, and Conical Containers*. FAI/09-272, Rev. 2, Fauske and Associates, LLC, Burr Ridge, Illinois.

Follett JR. 2014. Cone Penetrometer Shear Strength Measurements of Sludge Waste in Tanks 241-AN-101 and 241-AN-106. RPP-RPT-56585, Rev. 0, Washington River Protection Solutions, Richland, Washington.

Gauglitz PA, SD Rassat, PR Bredt, JH Konynenbelt, SM Tingey, and DP Mendoza. 1996. *Mechanisms of Gas Bubble Retention and Release: Results for Hanford Waste Tanks 241-S-102 and 241-SY-103 and Single-Shell Tank Simulants*. PNNL-11298, Pacific Northwest National Laboratory, Richland, Washington.

Gauglitz PA, BE Wells, JA Fort, and PA Meyer. 2009. *An Approach to Understanding Cohesive Slurry Settling, Mobilization, and Hydrogen Gas Retention in Pulsed Jet Mixed Vessels*. PNNL-17707 (WTP-RPT-177), Rev. 0, Pacific Northwest National Laboratory, Richland, Washington.

Gauglitz PA, WC Buchmiller, JJ Jenks, J Chun, RL Russell, AJ Schmidt, and MM Mastor, Jr. 2010. *The Disruption of Vessel-Spanning Bubbles with Sloped Fins in Flat-Bottom and 2:1 Elliptical-Bottom Vessels*. PNNL-19345, Rev. 0, Pacific Northwest National Laboratory, Richland, Washington.

Gauglitz PA, WC Buchmiller, SG Probert, AT Owen, and FJ Brockman. 2012a. *Strong-Sludge Gas Retention and Release Mechanisms in Clay Simulants*. PNNL-21167, Rev. 0, Pacific Northwest National Laboratory, Richland, Washington.

Gauglitz PA, DN Tran, and WC Buchmiller. 2012b. *Simulant Development for Hanford Double-Shell Tank Mixing and Waste Feed Delivery Testing*. PNNL-21791, Rev. 0, Pacific Northwest National Laboratory, Richland, Washington.

Gauglitz PA, BE Wells, WC Buchmiller, and SD Rassat. 2013. *Rayleigh-Taylor Instability within Sediment Layers due to Gas Retention: Preliminary Theory and Experiments*. PNNL-22339, Rev. 0, Pacific Northwest National Laboratory, Richland, Washington.

Meacham JE. 2010. *Gas Retention and Release from Hanford Site High Shear Strength Waste*. RPP-RPT-26836, Rev. 0, Washington River Protection Solutions, Richland, Washington.

Meacham JE and NW Kirch. 2013. *Initial Assessment for Potential Gas Release Events in Hanford Site Deep Sludge Double-Shell Tank Waste*. RPP-RPT-54305, Rev. 0, Washington River Protection Solutions LLC, Richland, Washington.

Meyer PA, ME Brewster, SA Bryan, G Chen, LR Pederson, CW Stewart, and G Terrones. 1997. *Gas Retention and Release Behavior in Hanford Double-Shell Waste Tanks*. PNNL-11536, Rev. 1, Pacific Northwest National Laboratory, Richland, Washington.

Meyer PA and CW Stewart. 2001. *Preventing Buoyant Displacement Gas Release Events in Hanford Double-Shell Waste Tanks*. PNNL-13337, Pacific Northwest National Laboratory, Richland, Washington.

Powell MR, PA Gauglitz, KM Denslow, CM Fischer, DJ Heldebrant, MS Prowant, SA Sande, JM Davis, and MR Telander. 2014. *Evaluation of Gas Retention in Waste Simulants: Intermediate-Scale Column and Open-Channel-Depth Tests*. PNNL-23136 (DSGREP-RPT-003, Rev. 0), Pacific Northwest National Laboratory, Richland, Washington.

Rector DR, ML Stewart, and AP Poloski. 2009. "Modeling of Sediment Bed Behavior for Critical Velocity in Horizontal Piping." Presented at the 2009 Waste Management Conference, March 1–5, 2009, Phoenix, Arizona.

Rector DR and ML Stewart. 2010. "Modeling of Leaching Filter Pressure Drop and Fouling Behavior." Presented at the 2010 Waste Management Conference, March 7–11, 2010, Phoenix, Arizona.

Schonewill PP, PA Gauglitz, RW Shimskey, KM Denslow, MR Powell, JR Bontha, GK Boeringa, DN Tran, NK Karri, DJ Heldebrant, JE Meacham, DB Smet, WE Bryan, and RB Calmus. 2014. *Evaluation of Gas Retention in Waste Simulants: Tall Column Experiments*. PNNL-23xxx (DSGREP-RPT-005, Rev. 0) (to appear), Pacific Northwest National Laboratory, Richland, Washington.

Stewart CW, ME Brewster, PA Gauglitz, LA Mahoney, PA Meyer, KP Recknagle, and HC Reed. 1996. *Gas Retention and Release Behavior in Hanford Single-Shell Tanks*. PNNL-11391, Pacific Northwest National Laboratory, Richland, Washington.

Stewart CW, SA Hartley, PA Meyer, and BE Wells. 2005. *Predicting Peak Hydrogen Concentrations from Spontaneous Gas Releases in Hanford Waste Tanks*. PNNL-15238, Pacific Northwest National Laboratory, Richland, Washington.

Uytioco EM. 2010. *BDGRE and Supernatant Limit Assessment for Enhanced Use of AN Farm for C Farm Single Shell Tank Retrieval*. RPP-RPT-44254, Rev. 1, Washington River Protection Solutions, Richland, Washington.

Van Kessel T. 1999. *Evaluation Report of Depot Modelling*. Technical Report Z2517/DM24, Delft Hydraulics, the Netherlands.

Van Kessel T and WGM van Kesteren. 2002. "Gas Production and Transport in Artificial Sludge Depots." *Waste Management* 22(1):19–28.

Weber RA. 2009. *Methodology and Calculations for the Assignment of Waste Groups for the Large Underground Storage Tanks at the Hanford Site*. RPP-10006, Rev. 8, Washington River Protection Solutions, Richland, Washington.

Wells BE, RL Russell, LA Mahoney, GN Brown, DE Rinehart, WC Buchmiller, EC Golovich, and JV Crum. 2010. *Hanford Sludge Simulant Selection for Soil Mechanics Property Measurement*. PNNL-19250, Pacific Northwest National Laboratory, Richland, Washington.

Wells BE, PA Gauglitz, and DR Rector. 2011a. *Comparison of Waste Feed Delivery Small Scale Mixing Demonstration Simulant to Hanford Waste*. PNNL-20637, Pacific Northwest National Laboratory, Richland, Washington.

Wells BE, DE Kurath, LA Mahoney, Y Onishi, JL Huckaby, SK Cooley, CA Burns, EC Buck, JM Tingey, RC Daniel, and KK Anderson. 2011b. *Hanford Waste Physical and Rheological Properties: Data and Gaps*. PNNL-20646 (EMSP-RPT-006), Pacific Northwest National Laboratory, Richland, Washington.

Wells BE, SK Cooley, and JE Meacham. 2013. *Prediction of Peak Hydrogen Concentrations for Deep Sludge Retrieval in Tanks AN-101 and AN-106 from Historical Data of Spontaneous Gas Release Events*. PNNL-22866 (DSGREP-RPT-001), Pacific Northwest National Laboratory, Richland, Washington.

Appendix A

Modified Energy Ratio Derivation

Appendix A

Modified Energy Ratio Derivation

This appendix contains the detailed derivation for the modified energy ratio (ER_s) for transport through a sediment layer.

A.1 Energy Ratio for Transport through Sediment Layer

Assign subscripts $s1$ to the upper sediment layer and $s2$ to the lower sediment layer. The stored buoyant energy can be calculated from the work done in raising the gob a distance H_{s1} , given by

$$E_b = \int_0^{H_{s1}} F(z) dz$$

The gob moving up through the upper sediment layer will experience a buoyancy force

$$F(z) = g[\rho_{s1}V(z) - \rho_{s2}V_{s2}]$$

The first term is the weight of the upper sediment layer that has been displaced by the expanding gob. The variable V_{s2} refers to the volume of sediment within the gob. Therefore,

$$V_0 = V_{s2} + V_{g0}$$

$$V(z) = V_{s2} + V_g(z)$$

$$V_g(z) = V_{g0}P_0 / P(z)$$

$$P_0 = P_A + \rho_L gh + \rho_{s1}gH_{s1}$$

$$P(z) = P_A + \rho_L gh + \rho_{s1}gz$$

$$F(z) = g \left[\rho_{s1} \left(V_{g0} \frac{P_A + \rho_L gh + \rho_{s1}gH_{s1}}{P_A + \rho_L gh + \rho_{s1}gz} + V_{s2} \right) - \rho_{s2}V_{s2} \right]$$

$$F(z) = g[\rho_{s1}(V_{g0}F_P(z) + V_{s2}) - \rho_{s2}V_{s2}]$$

where

$$F_P(z) = \frac{P_A + \rho_L gh + \rho_{s1}gH_{s1}}{P_A + \rho_L gh + \rho_{s1}gz}$$

The second term refers to the weight of the constant volume of sediment within the gob, which is established at the time of release. The initial void fraction for release into a liquid layer was determined using neutral buoyancy plus a correction term to account for the strength of the sediment. In this case, the neutral buoyancy is defined relative to the overlaying sediment layer. The initial void fraction for this case is based on the RT stability criterion (Gauglitz et al. 2013) expressed as

$$\frac{(\tau_1 + \tau_2)}{(\rho_1 - \rho_2)gD} = \frac{(\tau_1 + \tau_2)}{[\rho_{s1} - (1 - \alpha_{RT})\rho_{s2}]gD} = 0.09$$

$$\alpha_{RT} = \frac{(\tau_1 + \tau_2)}{0.09gD\rho_{s2}} + \left(1 - \frac{\rho_{s1}}{\rho_{s2}}\right) = \frac{(\tau_1 + \tau_2)}{0.09gD\rho_{s2}} + \alpha_{NBS}$$

where

$$\alpha_{NBS} = 1 - \frac{\rho_{s1}}{\rho_{s2}}$$

Therefore,

$$V_{s2} = (1 - \alpha_{RT})V_0 \quad \rho_{s2} = \frac{\rho_{s1}}{(1 - \alpha_{NBS})}$$

$$F(z) = g \left[\rho_{s1}\alpha_{RT}V_0F_P(z) + \rho_{s1}(1 - \alpha_{RT})V_0 - \frac{\rho_{s1}(1 - \alpha_{RT})}{(1 - \alpha_{NBS})}V_0 \right]$$

$$F(z) = \rho_{s1}V_0g \left[\alpha_{RT}F_P(z) + (1 - \alpha_{RT}) - \frac{(1 - \alpha_{RT})}{(1 - \alpha_{NBS})} \right]$$

$$\left[\frac{(1 - \alpha_{RT})}{\alpha_{RT}} - \frac{(1 - \alpha_{RT})}{\alpha_{RT}(1 - \alpha_{NBS})} \right] = \frac{(1 - \alpha_{RT})}{\alpha_{RT}} \left[1 - \frac{1}{(1 - \alpha_{NBS})} \right] = \frac{(1 - \alpha_{RT})}{\alpha_{RT}} \left[-\frac{\alpha_{NBS}}{(1 - \alpha_{NBS})} \right]$$

$$F(z) = \alpha_{RT}\rho_{s1}V_0g \left[F_P(z) - \frac{\alpha_{NBS}(1 - \alpha_{RT})}{\alpha_{RT}(1 - \alpha_{NBS})} \right]$$

$$F(z) = \alpha_{RT}\rho_{s1}V_0g \left[\frac{1 + \gamma_s}{1 + \gamma_s z / H_{s1}} - k_s \right]$$

where

$$\gamma_s = \frac{\rho_{s1} g H_{s1}}{P_A + \rho_L g h} \quad k_s = \frac{\alpha_{NBS} (1 - \alpha_{RT})}{\alpha_{RT} (1 - \alpha_{NBS})}$$

The integral equation can then be evaluated to give the buoyant potential energy available during a buoyant displacement through the upper sediment layer

$$E_b = \alpha_{RT} \rho_{s1} V_0 g H_{s1} \left[\left(1 + \frac{1}{\gamma_s} \right) \ln(1 + \gamma_s) - k_s \right]$$

The energy required to release gas from a plastic solids layer is given by the expression

$$E_y = V_0 \varepsilon_y \tau_y (1 - \alpha_{RT})$$

For comparison, see the energy ratio expression for E_y in Equation (4.6.14) of Meyer et al. (1997). The strain at failure, ε_y , is the 100% strain present at the point where failure is assumed to occur – see *op. cit.*

The modified energy ratio then becomes

$$ER_S = \frac{E_b}{E_y} = \frac{\alpha_{RT} \rho_{s1} g H_{s1}}{(1 - \alpha_{RT}) \varepsilon_y \tau_y} \left[\left(1 + \frac{1}{\gamma_s} \right) \ln(1 + \gamma_s) - k_s \right]$$

A.2 References

Gauglitz PA, BE Wells, WC Buchmiller, and SD Rassat. 2013. *Rayleigh-Taylor Instability within Sediment Layers due to Gas Retention: Preliminary Theory and Experiments*. PNNL-22339, Rev. 0, Pacific Northwest National Laboratory, Richland, Washington.

Meyer PA, ME Brewster, SA Bryan, G Chen, LR Pederson, CW Stewart, and G Terrones. 1997. *Gas Retention and Release Behavior in Hanford Double-Shell Waste Tanks*. PNNL-11536, Rev. 1, Pacific Northwest National Laboratory, Richland, Washington.

Appendix B
Slurry Simulant Properties

Appendix B

Slurry Simulant Properties

This appendix provides a summary of slurry simulant properties for samples taken from each of the completed RT tests (see Section 8.1.1 and Section 8.2.1) and single-slurry-layer (SL) tests (see Section 8.3.1). Measured simulant density, shear strength, and rheological properties are compiled in Section B.1 on a test-by-test basis for the RT tests using two slurry layers. Simulant physical properties for SL tests, including water-diluted samples, are tabulated in Section B.2. Section B.3 summarizes graphically the density, shear strength, and rheology measurements for all test batches.

B.1 Measured Density and Rheology – RT Tests

Measured slurry simulant density and rheological properties for samples taken in each of the completed RT tests using two slurry layers are provided in Table B.1 (see Section B.2 for SL test sample properties). See Table 8.1 (Section 8.1.1) and Table 8.2 (Section 8.2.1) in the discussion of the RT test matrices for summaries of purpose and conditions in each test. Entries in Table B.1 are sequence-ordered by RT Test number.¹ Simulant characterization methods and instrumentation are described in Section 6.3.

At least two samples were taken in each RT test, one from a batch of the upper-layer slurry at the final solids content, and one from a batch of the lower-layer slurry at the solids content before addition of H₂O₂. Sample numbers include test number, slurry layer, and batch information. For example, sample 70-09-UA is for batch (or blend) “A” of the upper-layer “U” slurry in RT Test 70-09, and sample 70-09-LB is for the “B” batch of the lower-layer “L” slurry in the same test. Table B.1 summarizes the following batch properties: solids mass fraction, x_s ; measured slurry density, ρ_s ; measured shear strength, τ_s , after standing undisturbed (post-mixing) for ~1 hr and ~18 hr; and Bingham plastic model yield stress, τ_0 , and consistency, μ_∞ , obtained from curve fits of rheograms (down-curves). Note that the estimated shear strength at the time of RT instability is summarized, for example, in Table 8.5 of Section 8.5.1 and is not repeated in Table B.1.

Representative rheograms, typical of those from which the Bingham plastic model parameters of Table B.1 were obtained, are also shown below. The 13 example rheograms are from samples of upper-layer slurry and lower-layer slurry prior to H₂O₂ addition (i.e., higher solids content than the upper-layer slurry in the same RT test). Results for these samples, along with others, were included in development of shear strength and Bingham model parameter vs. solids content correlations described in Section 7.1 that were subsequently used to provide inputs for numerical simulations (Section 9.0). The solids content of the representative subset of samples for which rheograms are shown spans the range used in all the two slurry layer RT tests: 42.1 wt%, Figure B.1; 44.8 wt%, Figure B.2; 45.2 wt%, Figure B.3; 47.1 wt%, Figure B.4; 48.1 wt%, Figure B.5; 48.6 wt%, Figure B.6; 49.7 wt%, Figure B.7; 51.3 wt%, Figure B.8; 51.5 wt%, Figure B.9; 52.9 wt%, Figure B.10; 54.0 wt%, Figure B.11; 54.1 wt%, Figure B.12; and

¹ The RT Test numbers include the nominal vessel diameter in inches (10-, 23-, or 70-) followed by the two-digit sequence number, which identifies the order that the test was run. For example, RT Test 70-09 was the ninth test in the series, and it was conducted in the 70-in. diameter vessel.

55.8 wt%, Figure B.13. The specific samples from which these rheograms were taken are summarized in Table B.1.

Table B.1. Simulant Properties for Samples Taken in Completed RT Tests (in sequence order and shaded by vessel size)

RT Test No.	Sample I.D.	x_s (wt%)	Meas. ρ_s (g/mL)	Measured Shear Strength, τ_s (Pa)		Bingham Plastic Model Parameters		Rheogram Figure
				~1-hr	~18-hr	Yield Stress, τ_0 (Pa)	Consistency (cP)	
23-01	23-01-UA	47.9	1.422	26.0	38.6	10.4	20.5	--
	23-01-LA	49.4	1.429	33.3	50.0	12.1	22.8	--
10-02	10-02-UA	42.1	1.345	10.0	16.0	4.07	14.9	--
	10-02-LA	43.4	1.362	12.0	17.3	4.61	15.4	--
23-03	23-03-UA	45.2	1.385	16.6	21.3	7.42	17.6	--
	23-03-LA	46.6	1.400	17.3	23.3	7.84	18.6	--
10-04	10-04-UA	42.1	1.353	11.3	14.6	5.08	15.5	--
	10-04-LA	44.9	1.385	13.3	18.0	6.12	17.0	--
23-05	23-05-UA	42.1	1.348	10.0	14.0	4.29	14.9	--
	23-05-LA	44.9	1.383	12.0	18.0	5.78	16.4	--
23-06	23-06-UA	45.2	1.39	16.0	22.0	7.59	17.3	B.3
	23-06-LA	48.1	1.43	22.0	31.3	10.4	19.8	--
23-07	23-07-UA	42.1	1.34	11.3	15.3	4.75	14.7	--
	23-07-LA	44.9	1.38	14.6	20.0	6.42	16.5	--
10-08	10-08-UA	42.1	1.346	8.7	13.3	4.38	14.5	--
	10-08-LA	44.9	1.372	12.7	18.6	5.77	15.9	--
70-09	70-09-UA	49.7	1.44	36.0	60.0	16.5	24.6	--
	70-09-UA rep	49.7	n/m	n/m	51.3	n/m	n/m	--
	70-09-UB	49.7	1.437	29.3	42.0	15.7	24.3	--
	70-09-LA	52.9	1.49	55.3	86.6	25.2	35.0	--
	70-09-LA rep.	52.9	n/m	n/m	74.6	n/m	n/m	--
	70-09-LB	52.9	1.472	54.0	73.3	24.8	34.5	B.10
23-10	23-10-UA	42.1	1.340	10.0	15.3	4.51	15.0	--
	23-10-UA rep.	42.1	n/m	9.3	14.0	n/m	n/m	--
	23-10-LA	44.8	1.382	11.3	20.0	5.66	16.3	B.2
	23-10-LA rep.	44.8	n/m	10.7	16.6	n/m	n/m	--
70-11	70-11-UA	51.5	1.464	42.6	65.9	24.0	32.0	B.9
	70-11-UA rep.	51.5	n/m	n/m	68.6	n/m	n/m	--
	70-11-UB	51.5	n/m	45.3	61.3	n/m	n/m	--
	70-11-LA	54.0	1.499	58.6	88.6	34.2	44.4	B.11
	70-11-LB	54.0	n/m	61.3	83.3	n/m	n/m	--
23-12	23-12-UA	42.1	1.342	12.0	15.3	4.41	14.8	B.1
	23-12-LA	44.9	1.382	16.6	19.3	5.64	16.4	--

Table B.1. (cont.)

RT Test No.	Sample I.D.	x_s (wt%)	Meas. ρ_s (g/mL)	Measured Shear Strength, τ_s (Pa)		Bingham Plastic Model Parameters		Rheogram Figure
				~1-hr	~18-hr	Yield Stress, τ_0 (Pa)	Consistency (cP)	
23-13	23-13-UA	42.1	1.342	10.0	14.6	4.48	14.7	--
	23-13-LA	44.8	1.381	14.0	20.6	5.99	15.9	--
70-14	70-14-UA	47.1	1.410	17.3	28.6	11.0	19.7	B.4
	70-14-UB	47.1	n/m	16.6	27.3	n/m	n/m	--
	70-14-LA	48.6	1.431	18.0	29.3	12.2	21.6	B.6
	70-14-LB	48.6	n/m	20.0	32.6	n/m	n/m	--
23-15	23-15-UA	42.1	1.345	10.0	18.6	4.49	15.0	--
	23-15-LA	44.9	1.383	14.0	26.6	5.75	16.6	--
70-16	70-16-UA	49.7	1.446	26.6	45.3	16.8	26.4	B.7
	70-16-UB	49.7	n/m	29.3	44.6	n/m	n/m	--
	70-16-LA	51.3	1.464	31.3	54.0	18.9	29.0	--
	70-16-LB	51.3	n/m	35.3	48.6	n/m	n/m	--
23-17	23-17-UA	42.1	1.343	9.3	15.3	5.07	15.6	--
	23-17-LA	44.8	1.378	12.0	20.0	6.37	16.7	--
23-19	23-19-UA	42.1	1.352	10.7	16.0	4.40	15.0	--
	23-19-LA	44.8	1.379	16.0	22.0	5.92	16.5	--
70-20	70-20-UA	54.1	1.499	64.0	94.6	35.6	44.1	B.12
	70-20-UB	54.1	1.503	62.6	94.6	n/m	n/m	--
	70-20-LA	55.8	1.520	79.3	115	44.6	54.2	B.13
	70-20-LB	55.8	1.518	73.3	111	n/m	n/m	--
23-21	23-21-UA	45.2	1.379	16.0	24.6	7.92	17.6	--
	23-21-LA	48.1	1.412	20.6	33.3	9.95	19.9	B.5
70-22	70-22-UA	49.7	1.439	28.0	44.0	17.1	24.8	--
	70-22-UB	49.7	n/m	25.3	41.3	n/m	n/m	--
	70-22-UC	49.7	n/m	26.0	42.0	n/m	n/m	--
	70-22-LA	51.3	1.463	29.3	48.0	19.2	27.7	B.8
	70-22-LB	51.3	n/m	28.6	49.3	n/m	n/m	--
	70-22-LC	51.3	n/m	28.0	47.3	n/m	n/m	--
23-23	23-23-UA	45.2	1.376	14.0	22.0	6.92	17.2	--
	23-23-LA	48.1	1.413	20.0	34.0	10.0	19.5	--
23-24	23-24-UA	45.2	1.372	13.3	20.0	6.22	16.6	--
	23-24-LA	48.1	1.409	20.0	33.3	8.94	19.2	--

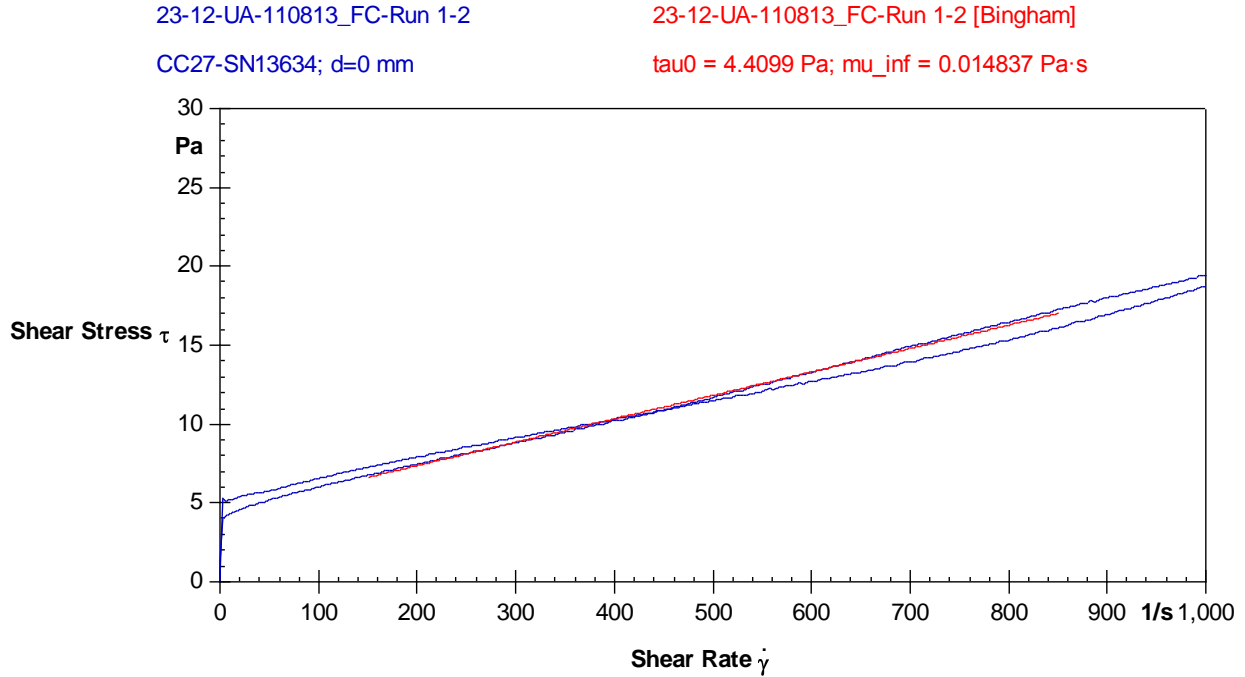


Figure B.1. Rheogram (Flow Curve) for 42.1-wt% Solids 90:10 M30:B Simulant, Upper Layer of Test 23-12 (Sample ID: 23-12-UA-110813; Shear Stress, τ (Pa) vs. Shear Rate, $\dot{\gamma}$ (s^{-1}); second down-curve Bingham model fit)

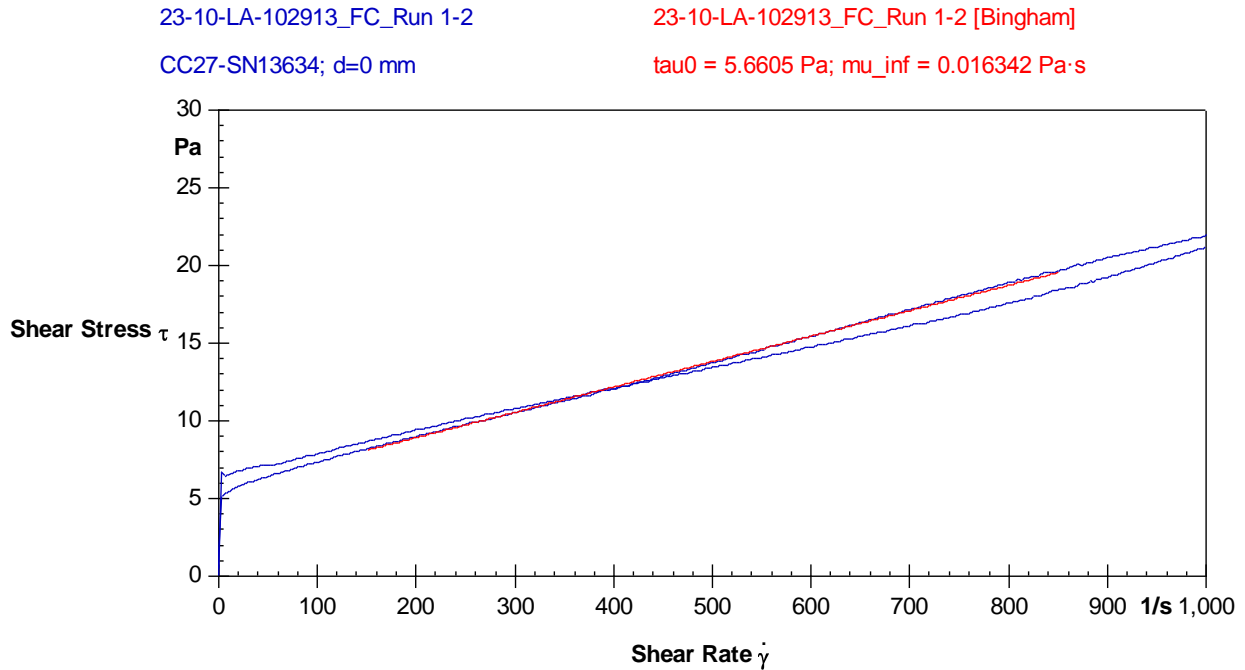


Figure B.2. Rheogram (Flow Curve) for 44.8-wt% Solids 90:10 M30:B Simulant, Lower Layer of Test 23-10 (pre- H_2O_2 ; Sample ID: 23-10-LA-102913; Shear Stress, τ (Pa) vs. Shear Rate, $\dot{\gamma}$ (s^{-1}); second down-curve Bingham model fit)

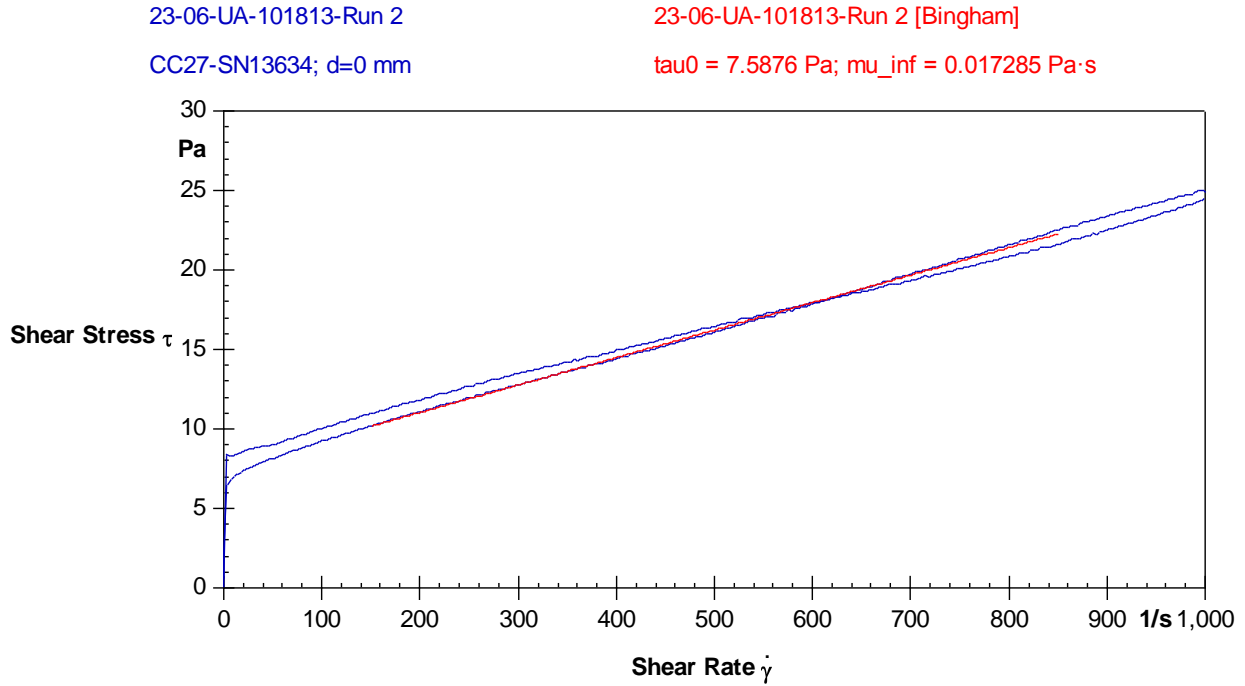


Figure B.3. Rheogram (Flow Curve) for 45.2-wt% Solids 90:10 M30:B Simulant, Upper Layer of Test 23-06 (Sample ID: 23-06-UA-101813; Shear Stress, τ (Pa) vs. Shear Rate, $\dot{\gamma}$ (s^{-1}); second down-curve Bingham model fit)

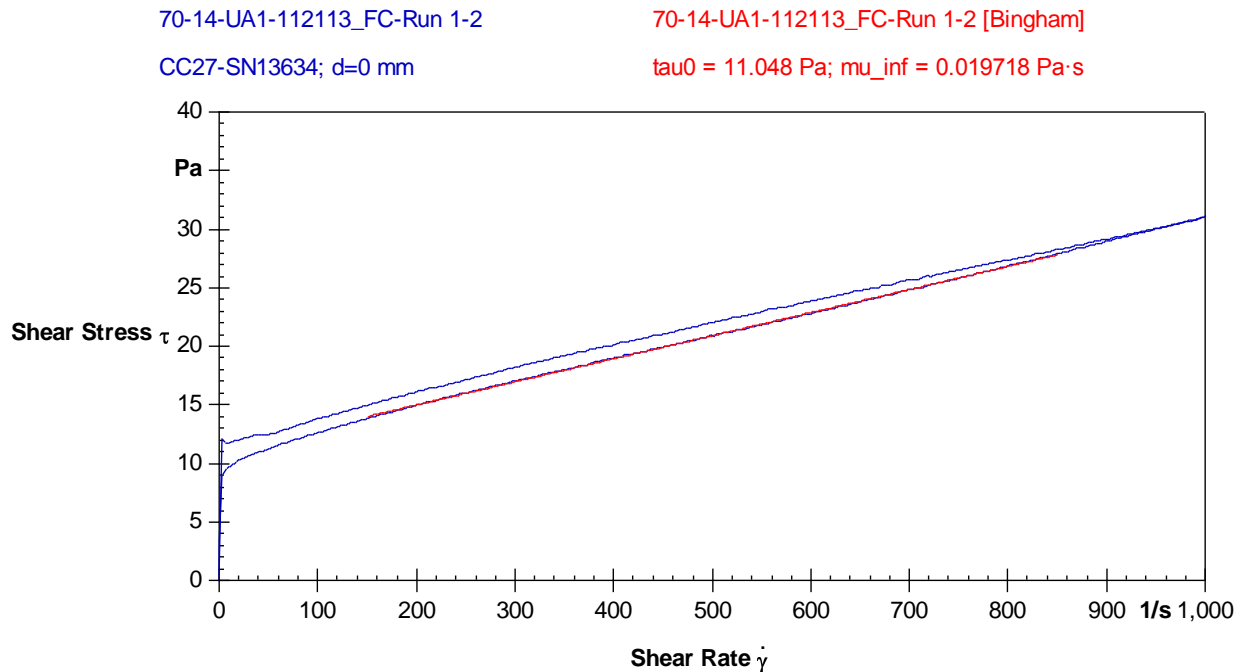


Figure B.4. Rheogram (Flow Curve) for 47.1-wt% Solids 90:10 M30:B Simulant, Upper Layer of Test 70-14 (Sample ID: 70-14-UA1-112113; Shear Stress, τ (Pa) vs. Shear Rate, $\dot{\gamma}$ (s^{-1}); second down-curve Bingham model fit)

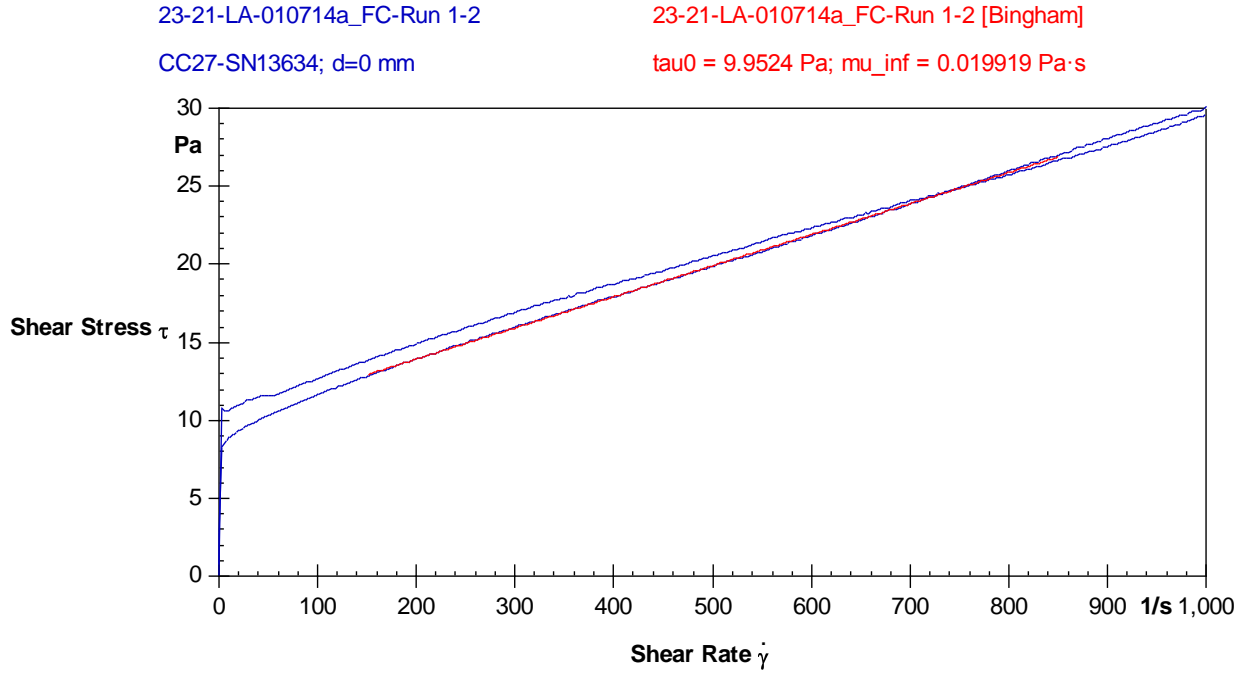


Figure B.5. Rheogram (Flow Curve) for 48.1-wt% Solids 90:10 M30:B Simulant, Lower Layer of Test 23-21 (pre-H₂O₂; Sample ID: 23-21-LA-010714a; Shear Stress, τ (Pa) vs. Shear Rate, $\dot{\gamma}$ (s⁻¹); second down-curve Bingham model fit)

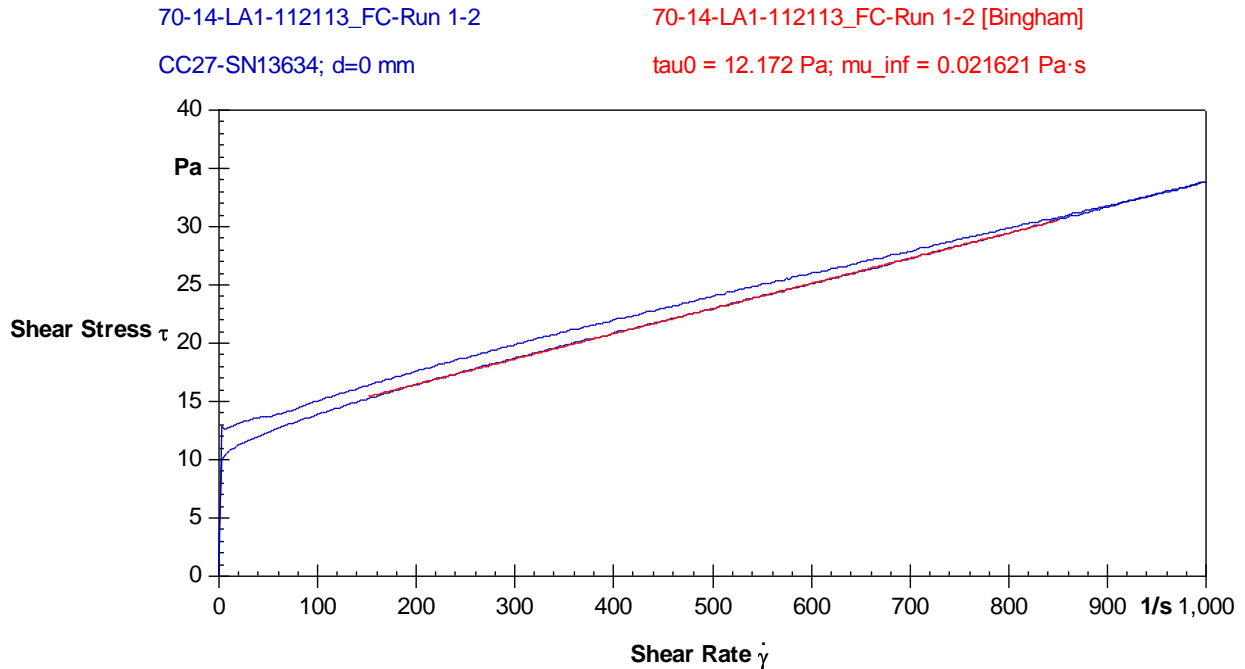


Figure B.6. Rheogram (Flow Curve) for 48.6-wt% Solids 90:10 M30:B Simulant, Lower Layer of Test 70-14 (pre-H₂O₂; Sample ID: 70-14-LA1-112113; Shear Stress, τ (Pa) vs. Shear Rate, $\dot{\gamma}$ (s⁻¹); second down-curve Bingham model fit)

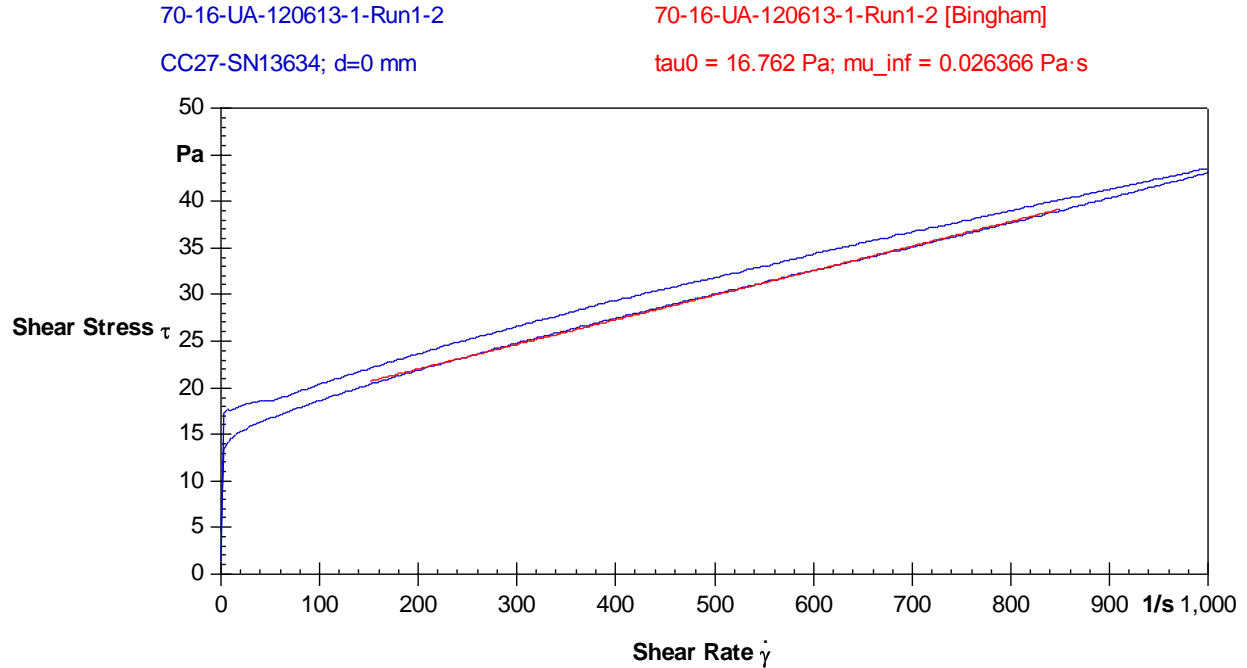


Figure B.7. Rheogram (Flow Curve) for 49.7-wt% Solids 90:10 M30:B Simulant, Upper Layer of Test 70-16 (Sample ID: 70-16-UA-120613; Shear Stress, τ (Pa) vs. Shear Rate, $\dot{\gamma}$ (s^{-1}); second down-curve Bingham model fit)

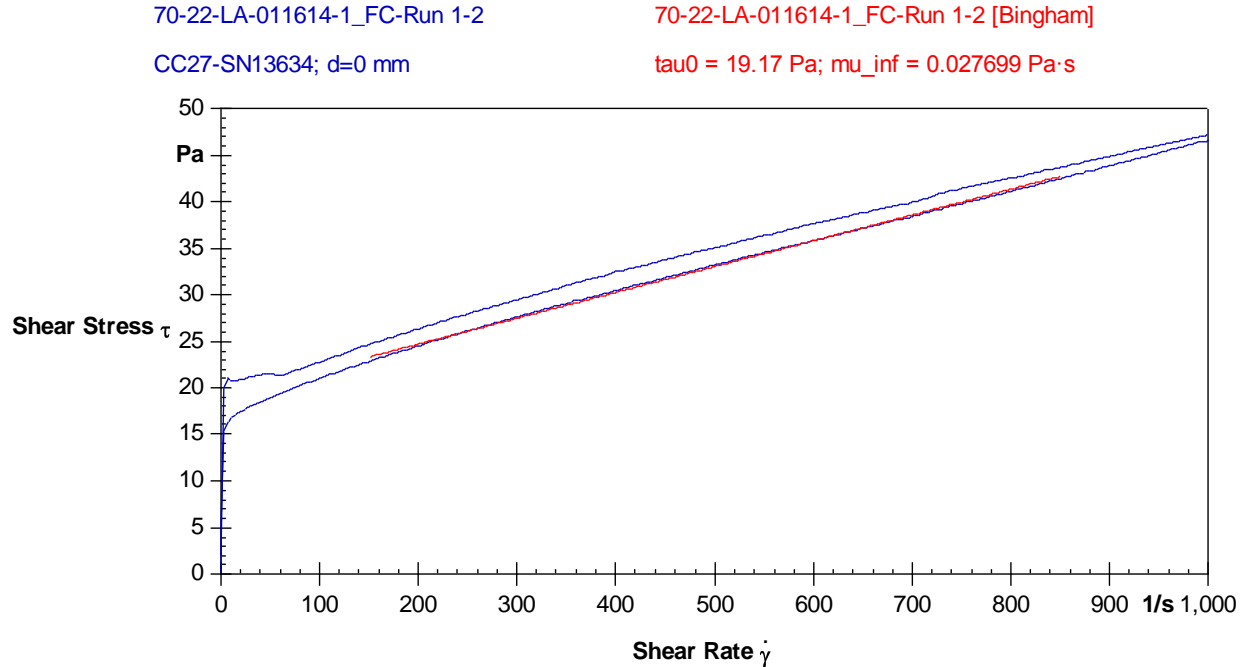


Figure B.8. Rheogram (Flow Curve) for 51.3-wt% Solids 90:10 M30:B Simulant, Lower Layer of Test 70-22 (pre- H_2O_2 ; Sample ID: 70-22-LA-011614-1; Shear Stress, τ (Pa) vs. Shear Rate, $\dot{\gamma}$ (s^{-1}); second down-curve Bingham model fit)

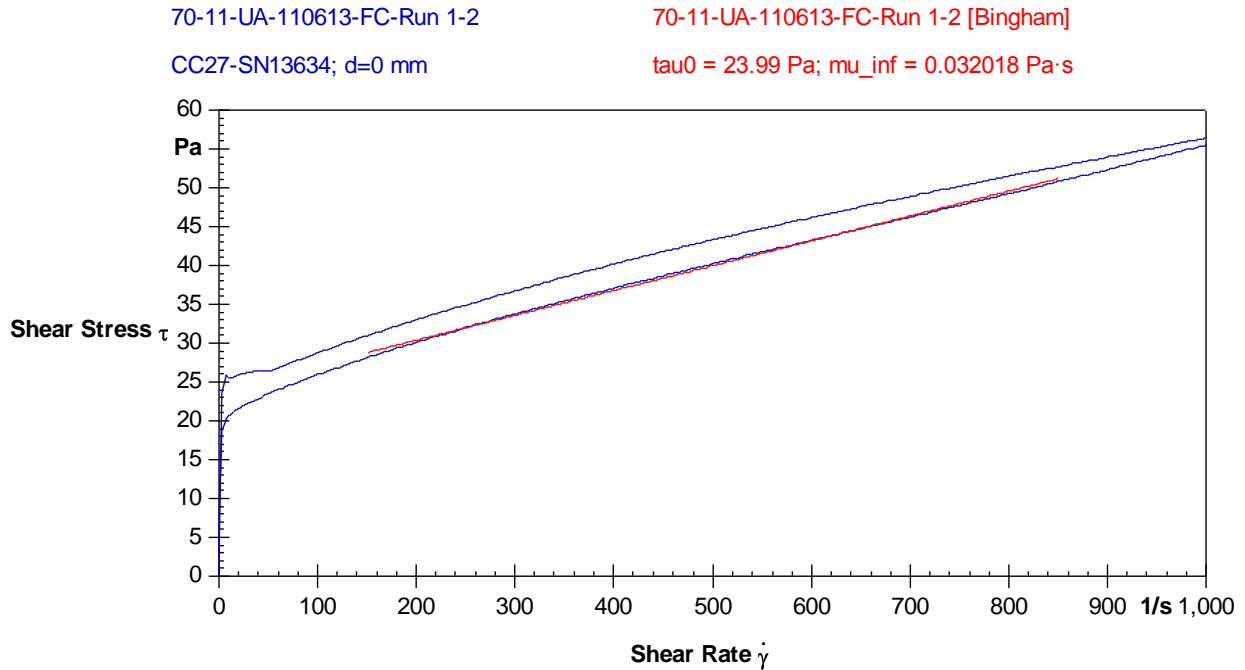


Figure B.9. Rheogram (Flow Curve) for 51.5-wt% Solids 90:10 M30:B Simulant, Upper Layer of Test 70-11 (Sample ID: 70-11-UA-110613; Shear Stress, τ (Pa) vs. Shear Rate, $\dot{\gamma}$ (s^{-1}); second down-curve Bingham model fit)

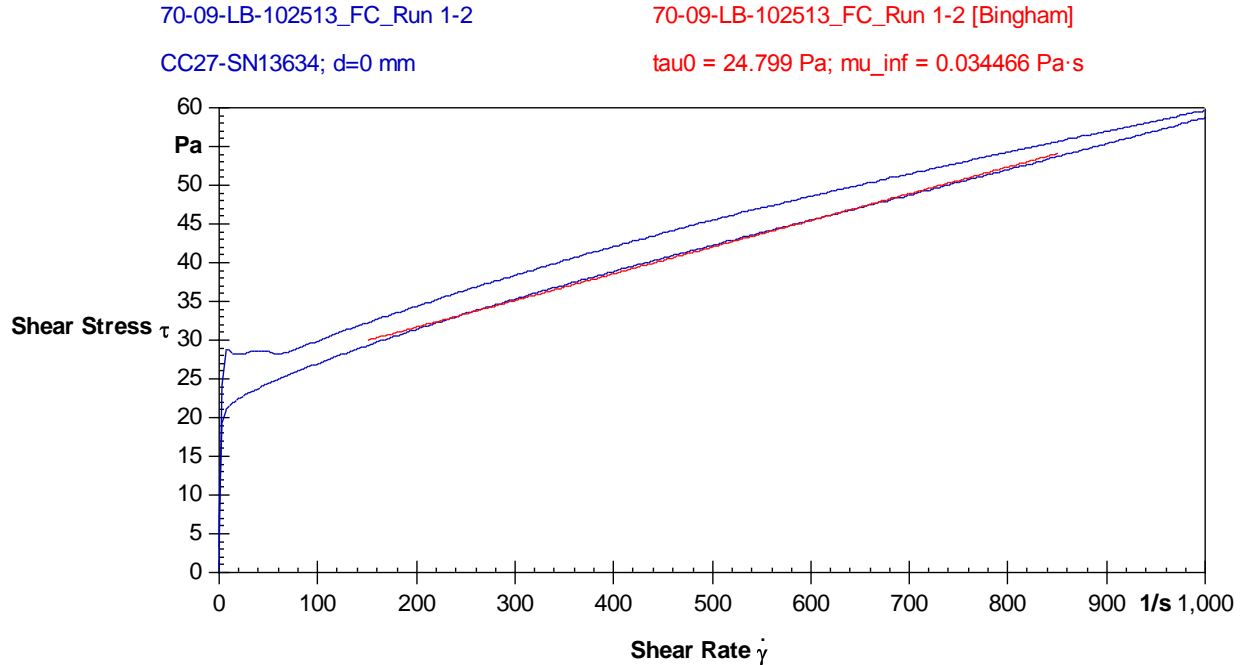


Figure B.10. Rheogram (Flow Curve) for 52.9-wt% Solids 90:10 M30:B Simulant, Lower Layer of Test 70-09 (pre- H_2O_2 ; Sample ID: 70-09-LB-102513; Shear Stress, τ (Pa) vs. Shear Rate, $\dot{\gamma}$ (s^{-1}); second down-curve Bingham model fit)

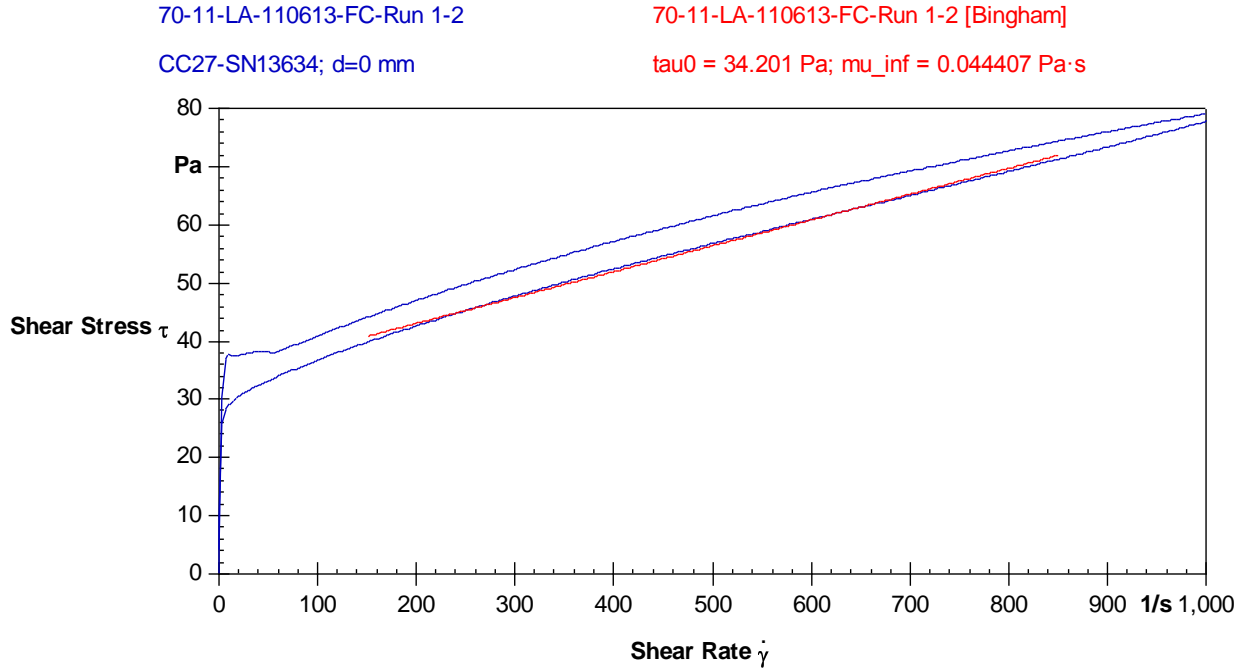


Figure B.11. Rheogram (Flow Curve) for 54.0-wt% Solids 90:10 M30:B Simulant, Lower Layer of Test 70-11 (pre- H_2O_2 ; Sample ID: 70-11-LA-110613; Shear Stress, τ (Pa) vs. Shear Rate, $\dot{\gamma}$ (s^{-1}); second down-curve Bingham model fit)

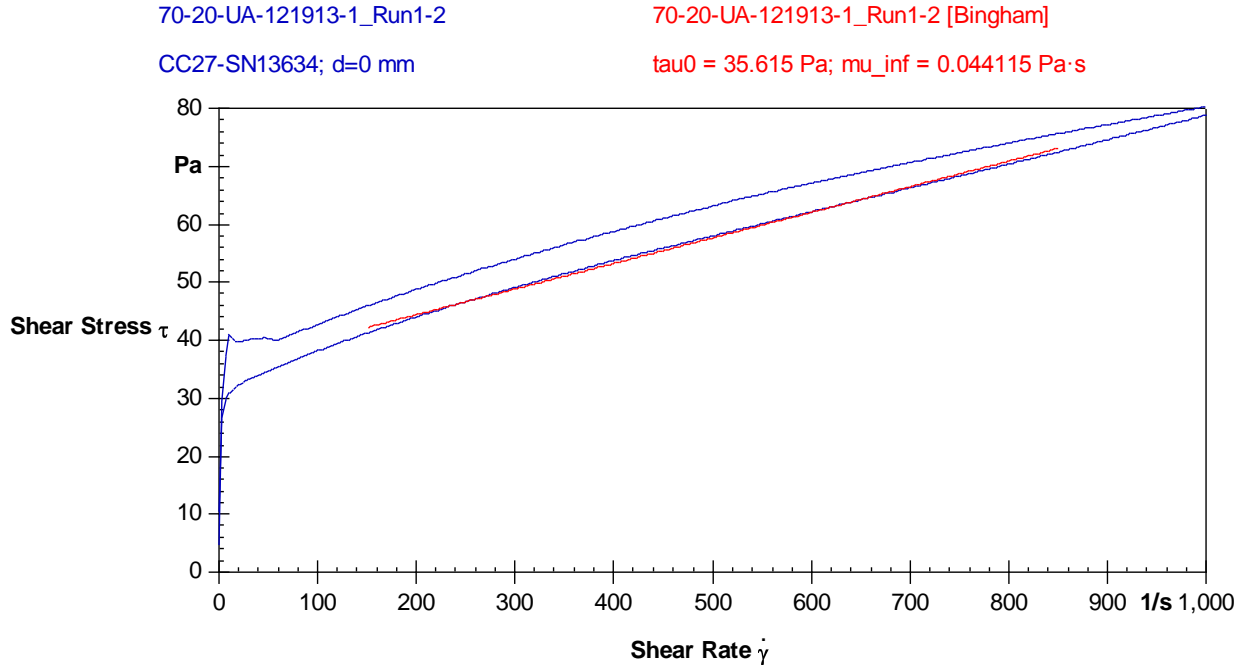


Figure B.12. Rheogram (Flow Curve) for 54.1-wt% Solids 90:10 M30:B Simulant, Upper Layer of Test 70-20 (Sample ID: 70-20-UA-121913; Shear Stress, τ (Pa) vs. Shear Rate, $\dot{\gamma}$ (s^{-1}); second down-curve Bingham model fit)

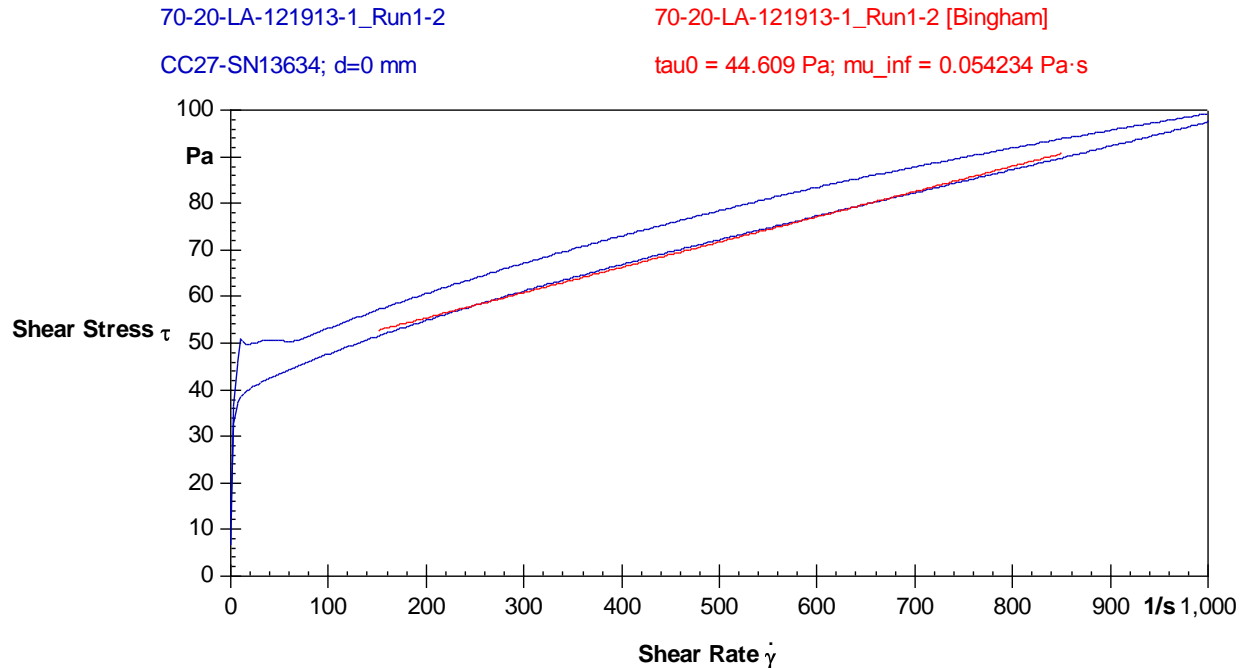


Figure B.13. Rheogram (Flow Curve) for 55.8-wt% Solids 90:10 M30:B Simulant, Lower Layer of Test 70-20 (pre-H₂O₂; Sample ID: 70-20-LA-121913-1; Shear Stress, τ (Pa) vs. Shear Rate, $\dot{\gamma}$ (s⁻¹); second down-curve Bingham model fit)

B.2 Measured Density and Rheology – Single-Slurry-Layer Tests

Measured slurry simulant density and rheological properties for samples taken in each of the completed tests using a single slurry layer are provided in Table B.2 (see Section B.1 for properties of samples in two-slurry-layer RT tests). See Table 8.3 in the discussion of the SL Test Matrix (Section 8.3.1) for a summary of purpose and conditions in each test. Entries in Table B.2 are sequence-ordered by test number.¹ Simulant characterization methods and instrumentation are described in Section 6.3.

At least one sample was taken in each single slurry layer test for the purposes of determining acceptability of batch properties (see Section 6.4.1). These acceptance samples were taken before addition of H₂O₂, which is consistent with testing of lower-layer samples in RT tests using two slurry layers. Because the slurry simulant in SL tests is analogous to lower-layer slurry in RT tests, the slurry batch and sample numbers in the SL tests use the lower-layer “L” designation. Sample numbers include test number, slurry layer, and batch information. For example, sample 70-26-LA is for batch (or blend) “A” of the “lower-layer” slurry in Test 70-26, and sample 70-26-LB is for the “B” batch of the slurry in the same test. In these SL tests, additional samples were taken and diluted with water equivalent to the amount of H₂O₂ solution that was subsequently added. These samples are identified by the “-W” extension. The post-H₂O₂ addition slurry batches and the -W samples had the same solids concentration

¹ In many of the SL tests, a portion of a large slurry batch (one of two) prepared for a 70-in. vessel test was used in parallel in a 23-in. vessel test. For example, Tests 70-26 and 23-27 are the 26th and 27th tests, sequential with the two slurry layer RT tests, and both SL tests use slurry from one of the Test 70-26 batches. In these paired tests, samples are identified by the 70-in. vessel Test Number.

as an upper-layer slurry used in at least one RT test (see Table B.1, for example). Table B.2 summarizes the following sample properties: solids mass fraction, x_S ; measured slurry density, ρ_S ; measured shear strength, τ_S , after standing undisturbed (post-mixing) for ~1 hr and ~18 hr; and Bingham plastic model yield stress, τ_y , and consistency, μ_{cs} , obtained from curve fits of rheograms (second down-curves).

Table B.2. Simulant Properties for Samples Taken in Completed Single-Slurry-Layer Tests (in sequence order and shaded by primary vessel size)

Test No.	Sample I.D.	x_S (wt%)	Meas. ρ_S (g/mL)	Measured Shear Strength, τ_S (Pa)		Bingham Plastic Model Parameters	
				~1-hr	~18-hr	Yield Stress, τ_y (Pa)	Consistency (cP, mPa•s)
23-25	23-25-LA	44.8	1.369	12.7	18.7	5.4	15.6
	23-25-LA-W	42.1	1.339	7.3	12.7	3.6	14.8
70-26 (& 23-27)	70-26-LA	52.9	1.483	37.3	62.0	23.7	32.8
	70-26-LB	52.9	1.484	38.6	63.3	24.2	33.3
	70-26-LA-W	49.7	1.437	20.7	32.6	13.9	22.6
70-28 (& 23-29)	70-28-LA	50.1	1.442	20.7	38.6	14.0	22.8
	70-28-LB	50.1	1.442	22.7	38.6	14.2	22.8
	70-28-LB-W	47.1	1.395	13.3	20.7	9.0	18.7
70-30 (& 23-31)	70-30-LA	57.6	1.546	114	161	54.6	69.2
	70-30-LB	57.6	1.543	115	155	54.3	65.9
	70-30-LA-W	54.1	1.494	52.0	80.6	31.5	41.1
23-32	23-32-LA	48.1	1.415	17.3	30.0	9.4	18.8
	23-32-LA-W	45.2	1.374	10.0	18.7	6.1	16.3

B.3 Summary of Test Batch Physical Properties

The measured RT test simulant density, shear strength, and rheology measurements for samples taken in all RT and SL tests, except water-dilution samples, are summarized graphically in this section. See Table B.1 in Section B.1 for a tabulation of the measured physical properties of representative upper- and lower-layer slurry batches used in RT tests and Table B.2 in Section B.2 for the properties of slurry batches used in SL tests.

B.3.1 Slurry Density

Figure B.14 compares the measured densities to theoretical values for batch samples from all the completed RT and SL tests. As discussed in Section 5.2, the theoretical density of RT test simulant having a 90 wt% to 10 wt% ratio of Min-U-Sil30 and bentonite clay solids (90:10 M30:B) and a total solids weight fraction x_S (not weight percent) is

$$\rho_S = \left(\frac{0.9x_S}{\rho_{M30}} + \frac{0.1x_S}{\rho_B} + \frac{1-x_S}{\rho_w} \right)^{-1} \quad (\text{B.1})$$

The weight fraction of water in the slurry is $1-x_s$, as shown in the rightmost term. The densities of individual components used in calculation of the theoretical slurry density were: water, $\rho_w = 0.998 \text{ g/mL}$ (998 kg/m^3); M30, $\rho_{M30} = 2.65 \text{ g/mL}$ (2650 kg/m^3); and B, $\rho_B = 2.55 \text{ g/mL}$ (2550 kg/m^3).

Figure B.14 shows that the measured densities for all the sampled test batches tended to be slightly lower than the theoretical values, and the trend is consistent across the range of solids content used in all the RT and SL tests. In the worst case, the measured density was 1.2% lower than theoretical, and only four samples had densities that were $\geq 1.0\%$ low. Although not included in Figure B.14, the densities of water-diluted samples (Table B.2) were comparably low. The most likely explanations for low slurry densities are: 1) residual moisture on the solid components, which would reduce the individual component and theoretical slurry densities; and 2) retention of small gas bubbles in samples, despite efforts to remove them by stirring before loading the graduated cylinder for the density measurement. A residual gas content of $\sim 1 \text{ vol}\%$ due to entrainment during batch preparation, for example, is quite plausible and would fully account for a low slurry density of magnitude comparable to the retained gas fraction. Note, however, that density samples did not contain H_2O_2 , and, therefore, gas was not being generated during measurements. Results for multiple samples at a given solids content in Figure B.14 also show density variation of up to $\sim 1\%$. This may be attributed to a combination of variability in batch preparation, batch in-homogeneity during sampling, and measurement uncertainty, including possible differences in residual retained gas content.

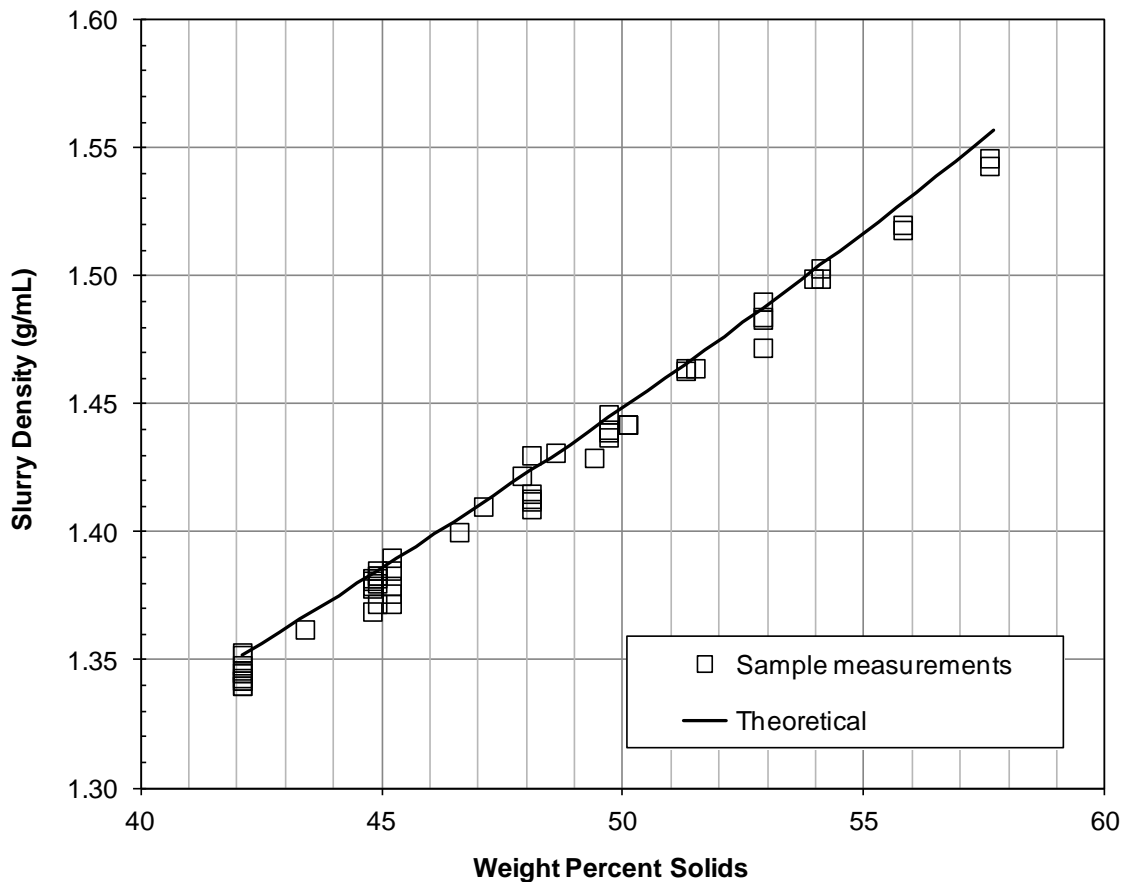


Figure B.14. Comparison of Measured 90:10 M30:B Simulant Batch Sample Densities to Theoretical Values as a Function of Solids Content (for undiluted samples from all RT and SL tests)

B.3.2 Slurry Shear Strength and Rheology

The shear strengths of individual slurry samples from all completed RT and SL tests, measured ~1 hr and ~18 hr after mixing (and standing undisturbed), are shown in Figure B.15 as a function of batch solids content. The shear strength correlations (lines) that were developed from 13 multi-sample averages using select RT test batch samples (no SL test samples) are also shown in the figure. These 1-hr and 18-hr τ_S vs. x_S correlations are described in Section 7.1.2.1 and originally presented in Figure 7.1.

Similarly, Figure B.16 shows the Bingham plastic rheology model parameters, yield stress (τ_y , Pa) and consistency (μ_{∞} , 1 mPa•s = 1 cP), for individual slurry samples in comparison to correlations developed from 13 multi-sample averages. The τ_y and μ_{∞} vs. x_S correlations are described in Section 7.1.3 and originally shown in Figure 7.5. Like Figure 7.5, Figure B.16 also includes the 1-hr and 18-hr τ_S correlations to more readily compare the magnitudes of the Bingham yield stress and the slurry shear strength.

In general, the shear strength and Bingham parameters of all individual samples are reasonably represented by and scattered around the corresponding correlations over the entire range of slurry solids content. The agreement is not unexpected given that the correlations were developed from a more limited, but still extensive, subset of the data. Results for multiple batch samples at a given solids content in Figure B.15 and Figure B.16 also show variation. Scatter in the data may be attributed to a combination of variability in batch preparation, batch in-homogeneity during sampling, and measurement reproducibility/uncertainty. Shear strengths are also impacted by differences in the timing of measurements after mixing the sample, because of the transient development of strength with the M30:B RT test simulant (see Section 7.1.2). The nominal 1-hr shear strength was typically measured between 60 and 75 min. after mixing, standing undisturbed, and the 18-hr measurements were generally made 17 to 19 hr post-mixing.

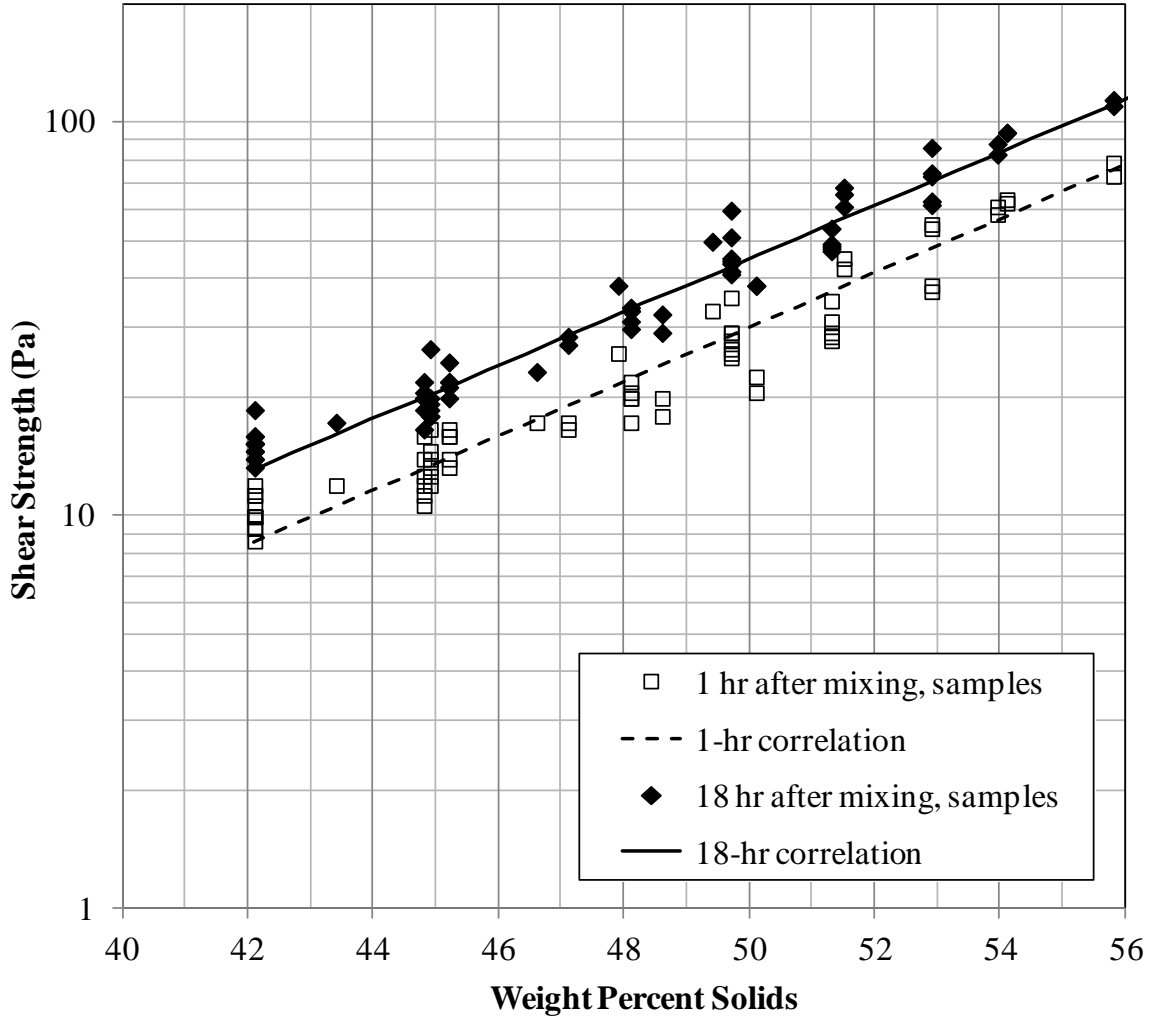


Figure B.15. Comparison of Measured 1-hr and 18-hr Slurry Shear Strengths for Individual Batch Samples to Correlations Developed from 13 Multi-Sample Averages as a Function of Solids Content (for undiluted samples from all RT and SL tests)

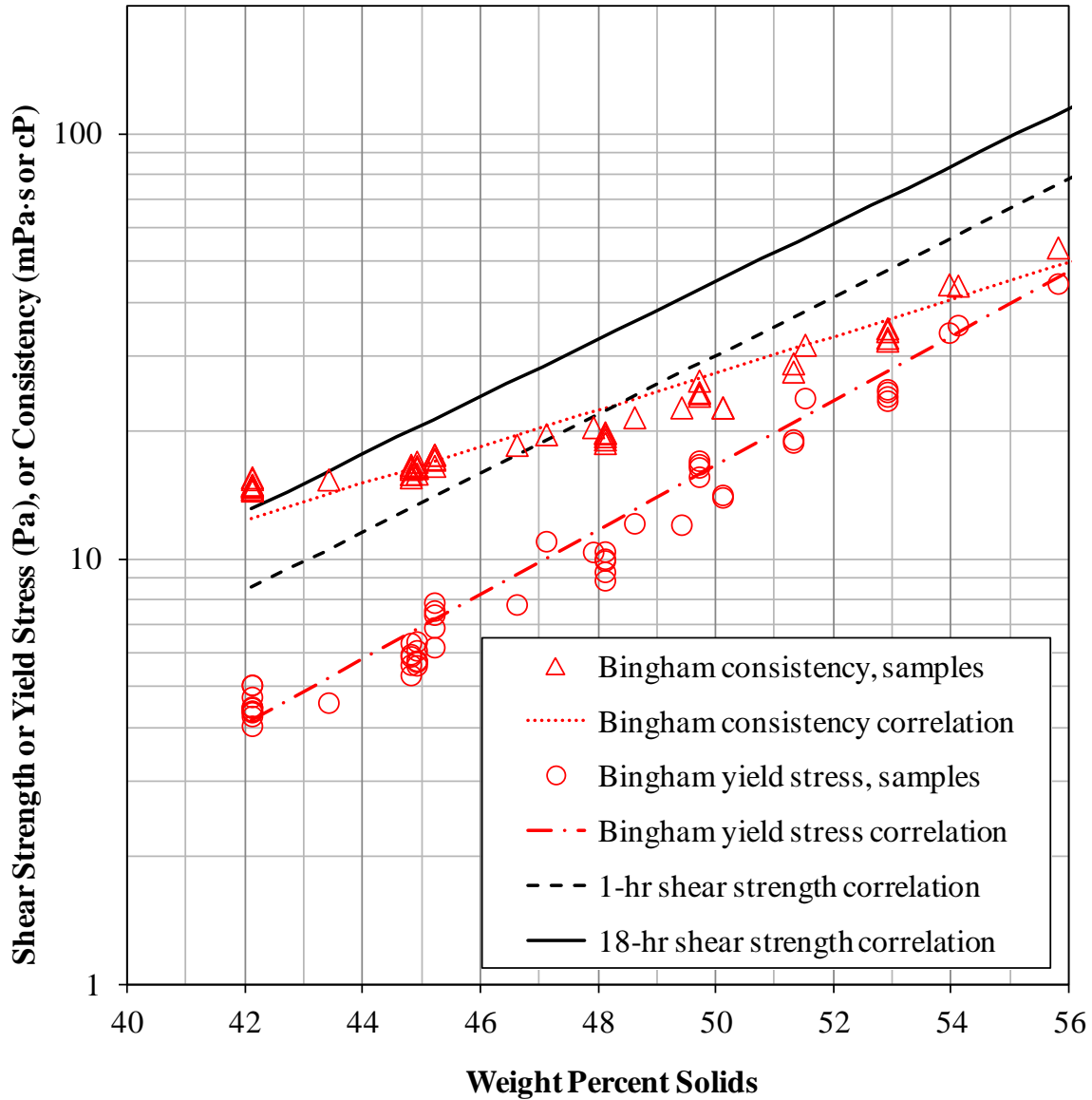


Figure B.16. Comparison of Bingham Yield Stress (Pa) and Consistency (mPa•s) for Individual Batch Samples to Bingham Parameter and Shear Strength (Pa) Correlations Developed from 13 Multi-Sample Averages as a Function of Solids Content (for undiluted samples from all RT and SL tests)

Appendix C

Detailed Test Results

Appendix C

Detailed Test Results

This appendix provides additional test results for all completed Rayleigh-Taylor (RT) tests and single-layer (SL) slurry tests. For example, Section C.1 includes additional details of gas retention as a function of time.

C.1 Gas Retention with Time

A listing of all completed RT instability gas release tests is provided in Table C.1, and a listing of all completed SL tests investigating spontaneous gas releases is provided in Table C.2.

Table C.1 replicates much of the information given in Table 8.1 in the discussion of the RT Test Matrix for equal slurry layer thickness tests in all three reduced-scale vessels (Section 8.1.1) and, similarly, information from Table 8.2 for RT tests of varying relative slurry layer thicknesses in the 23-in. vessel (Section 8.2.1). The table provides: a mapping of sequence-ordered RT Test numbers¹ to TP test numbers; test conditions, including the total slurry fill depth in the test vessel (\times geometrically scaled), the ratio of lower-to-upper slurry layer thicknesses, and H_2O_2 concentration in the lower (or single) slurry layer, which affects the gas generation rate; simulant properties, including specified solids content (wt% total of a 90:10 Min-U-Sil30:Bentonite blend), measured shear strength, and measured density; the retained gas volume fraction for the slurry to become neutrally buoyant in the supernatant water; and the retained gas fraction at the point of the observed initial RT instability, α_{RT} . The table also shows the elapsed time from completion of filling the lower slurry layer in the test vessel to the RT event. From this and the model of shear strength as a function of time undisturbed (Section 7.1.2.3), a best-estimate of slurry shear strength at the RT event time was calculated, and the results are shown in Table C.1 along with the value measured on a sample left undisturbed after mixing for ~ 18 hr.

Table C.2 provides information comparable to Table C.1, but for SL tests. Differences include tabulation of the retained gas fraction at the point of the initial spontaneous gas release, α_{SR} , and the elapsed time after filling the single slurry layer to the spontaneous release (SR) event. For RT tests, shear strengths presented in Table C.1 are for or based on measurements for upper-layer slurry, which has the same final solids content of the lower-layer slurry used in the test. In SL tests, there is no upper layer from which to take a sample at the final solids content, but water-dilution samples were prepared to that solids concentration and analyzed. The best-estimate of shear strengths at the time of the SR event based on the 1-hr and 18-hr water-dilution sample measurements are shown in Table C.2 along with the best-estimate τ_5 derived from the multi-sample shear strength vs. solids correlations (Section 7.1.2.1). These τ_5 estimates are reproduced from Table 8.4 and are discussed further there (Section 8.3.2.3).

Retained gas volume fraction vs. time plots are shown below for each completed RT and SL test, where elapsed time is measured from completion of addition of the gas-generating lower-layer (or

¹ The RT Test numbers include the nominal vessel diameter in inches (10-, 23-, or 70-) followed by the two-digit sequence number, which identifies the order that the test was run. For example, RT Test 70-09 was the ninth test in the series, and it was conducted in the 70-in. diameter vessel.

single-layer) slurry to the vessel.¹ The figure numbers are tabulated by test in Table C.1 and Table C.2. Each plot includes data to and extending beyond the point of the initial RT instability or SR event, which was the focus of the discussion of results in Section 8.1 (equal slurry layer thickness RT tests), Section 8.2 (varying relative slurry layer thickness RT tests), and Section 8.3 (SL tests). For reference, the retained void fraction at which the slurry would be neutrally buoyant in the supernatant water is also shown. The time of observed initial in-sediment buoyant motion, i.e., the defined RT event, or the time of the initial spontaneous release event in SL tests is marked on the plots by red symbols and arrows. Quantitative information on gas releases associated with SR events is given in Section 8.3.2.3, and the gas release data for RT instabilities is summarized in Section 8.5.1.

In general, gas retention continued after the initial RT event and subsequent gas releases from higher retained gas fractions were often larger than the initial releases. As discussed in Section 8.4, these secondary releases in RT tests have much in common with the spontaneous releases in the SL tests, and similar gas retention-release cycles (e.g., saw-tooth patterns) were observed in previous experimental studies by Gauglitz et al. (1996) using bentonite clay simulants (single slurry layer and no supernatant). It was noted that the maximum gas retention at the point of release and the periodicity were a function of slurry shear strength. For strong materials (e.g., >200 Pa), the retained gas fraction increased to a fixed constant value, beyond which further generated gas was released through established pathways. A similar network of connected channels is expected in relatively strong Hanford sludge.

¹ Gas volume (V_g) fractions are defined with respect to the gas-free bottom slurry layer volume (V_{S2}),
 $\alpha = V_g / (V_g + V_{S2})$

Table C.1. Listing of Completed RT Tests (in sequence order and shaded by vessel size)

RT Test No.	TP Test No.	Figure	Slurry Layer Depth		H ₂ O ₂ (wt%)	x _s (wt%)	τ _S (Pa)		Meas. ρ _S (g/mL)	α _{NB} (vol%)	Meas. α _{RT} (vol%)	Time to RT (hr)
			Total, H _S	Lower: Upper, H _{S2} :H _{S1}			Meas. 18-hr	Best-Est.				
			23-01	23-2			C.1	1				
10-02	10-2	C.2	2	1:1	0.1	42.1	16.0	19.9	1.345	25.8	22.2	52
23-03	23-6	C.3	1	1:1	0.1	45.2	21.3	32.4	1.385	27.9	29.6	82
10-04	10-2	C.4	2	1:1	0.2	42.1	14.6	19.5	1.353	26.2	29.5	41
23-05	23-B (N/A)	C.5	1	1:1	0.2	42.1	14.0	14.9	1.348	26.0	14.6	15
23-06	23-A (23-6)	C.6	1	1:1	0.2	45.2	22.0	25.0	1.39	28.2	21.4	21
23-07	23-C (N/A)	C.7	2	1:1	0.2	42.1	15.3	15.2	1.34	25.5	10.5	9.2
10-08	10-5 (alt. τ _S)	C.8	4	1:1	0.2	42.1	13.3	14.7	1.346	25.9	23.0	24
70-09	70-A (~70-7)	C.9	1	1:1	0.2	49.7	51.1	45.1	1.44	30.7	12.6	7.4
23-10	23-D (N/A)	C.10	0.67	1:1	0.2	42.1	15.3	16.2	1.34	25.5	18.3	19
70-11	70-C (~70-2)	C.11	1	1:1	0.15	51.5	67.3	62.6	1.464	31.8	14.7	10
23-12	23-E (N/A)	C.12	1	1:1	0.2	42.1	15.3	17.1	1.342	25.6	15.7	15
23-13	23-I	C.13	2	1:3	0.2	42.1	14.7	15.8	1.342	25.6	15.3	18
70-14	70-B	C.14	1	1:1	0.1	47.1	28.0	26.3	1.410	29.2	10.3	12
23-15	23-H	C.15	2	1:5	0.2	42.1	18.7	19.2	1.345	25.8	24.1	28
70-16	70-D	C.16	0.67	1:1	0.1	49.7	45.0	50.3	1.446	31.0	18.5	29
23-17	23-F	C.17	1	1:2	0.2	42.1	15.3	16.0	1.343	25.7	19.5	22
23-19	23-J	C.18	2	3:1	0.2	42.1	16.0	15.7	1.352	26.2	13.2	12
70-20	n/a	C.19	1	1:1	0.1	54.1	94.6	104	1.501	33.5	20.5	22
23-21	23-K	C.20	2	1:1	0.2	45.2	24.7	24.5	1.379	27.6	16.1	14
70-22	70-E	C.21	1.5	1:1	0.1	49.7	42.4	40.8	1.439	30.6	12.1	13
23-23	23-M	C.22	2	3:1	0.2	45.2	22.0	21.1	1.376	27.5	15.7	12
23-24	23-L	C.23	2	1:3	0.2	45.2	20.0	23.3	1.372	27.3	27.6	31
Key:			× Geo-Scaled	Relative Depth		Total Solids	Shear Strength		Density	NB Gas Frac	RT Gas Fraction	Initial Event

Table C.2. Listing of Completed SL Tests (in sequence order and shaded by vessel size)

SL Test No.	TP Test No.	Figure	Slurry Layer Depth		H ₂ O ₂ (wt%)	x _s (wt%)	Best-Estimate τ_s (Pa)		Meas. ρ_s (g/mL)	α_{NB} (vol%)	Meas. α_{SR} (vol%)	Time to SR (hr)
			Total, H _S	Lower: Upper, H _{S2} :H _{S1}			Dil'n Sample	Correl-ation				
23-25	23-P	C.24	0.5	1:0	0.2	42.1	14	16	1.339	25.5	30.1	36
70-26	70-I	C.25	0.5	1:0	0.2	49.7	36	49	1.437	30.5	27.1	27
23-27	23-S	C.26	0.5	1:0	0.2	49.7	37	50	1.437	30.5	29.0	30
70-28	70-H	C.27	0.5	1:0	0.2	47.1	24	33	1.395	28.5	28.1	30
23-29	23-R	C.28	0.5	1:0	0.2	47.1	24	34	1.395	28.5	31.1	36
70-30	70-J	C.29	0.5	1:0	0.2	54.1	81	87	1.494	33.2	23.7	14
23-31	23-S	C.30	0.5	1:0	0.2	54.1	80	87	1.494	33.2	23.4	14
23-32	23-Q	C.31	0.5	1:0	0.2	45.2	20	26	1.374	27.4	28.8	38
Key:			× Geo-Scaled	Relative Depth		Total Solids	Shear Strength		Density	NB Gas Frac	SR Gas Fraction	Initial Event

Test 23-01

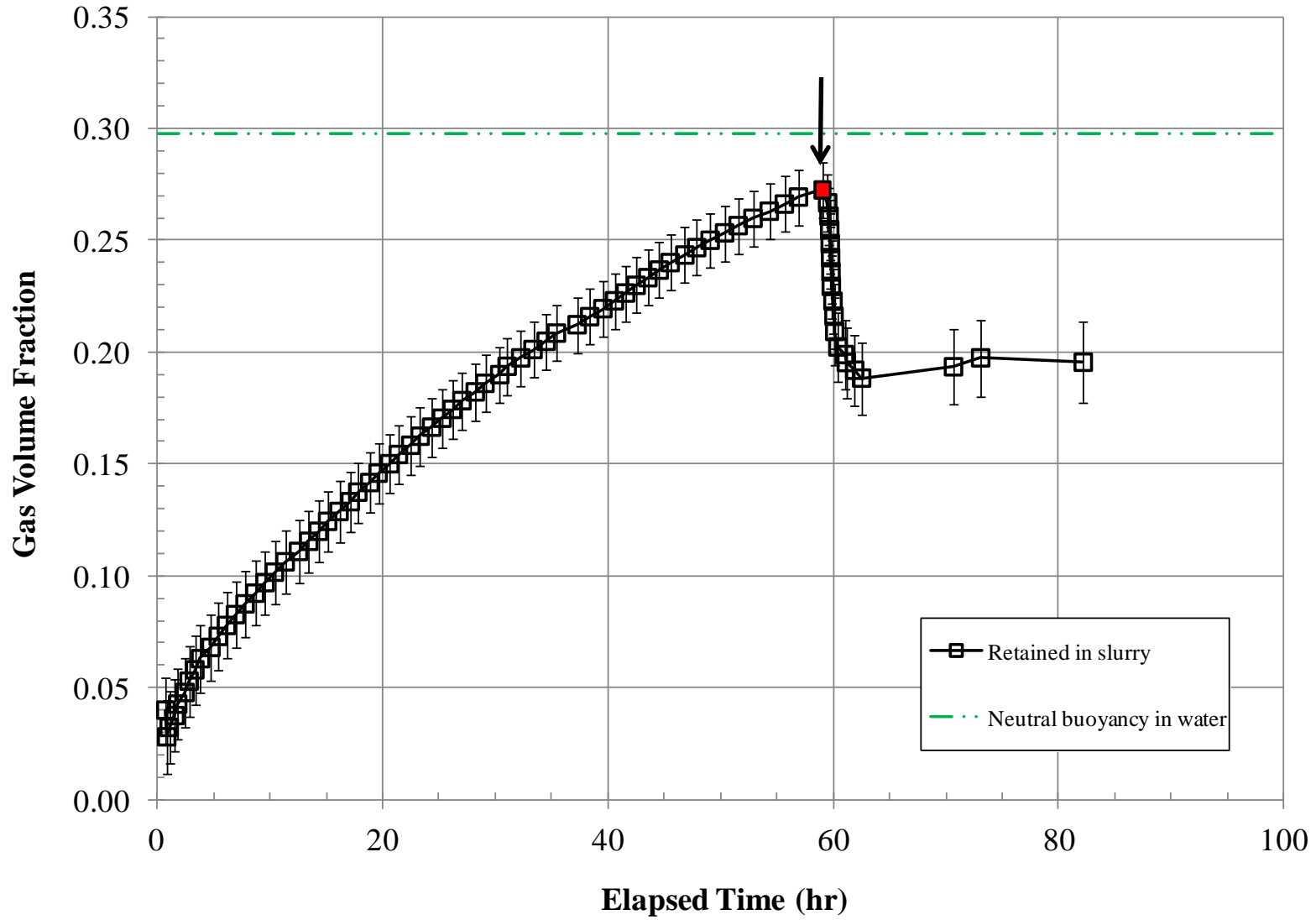
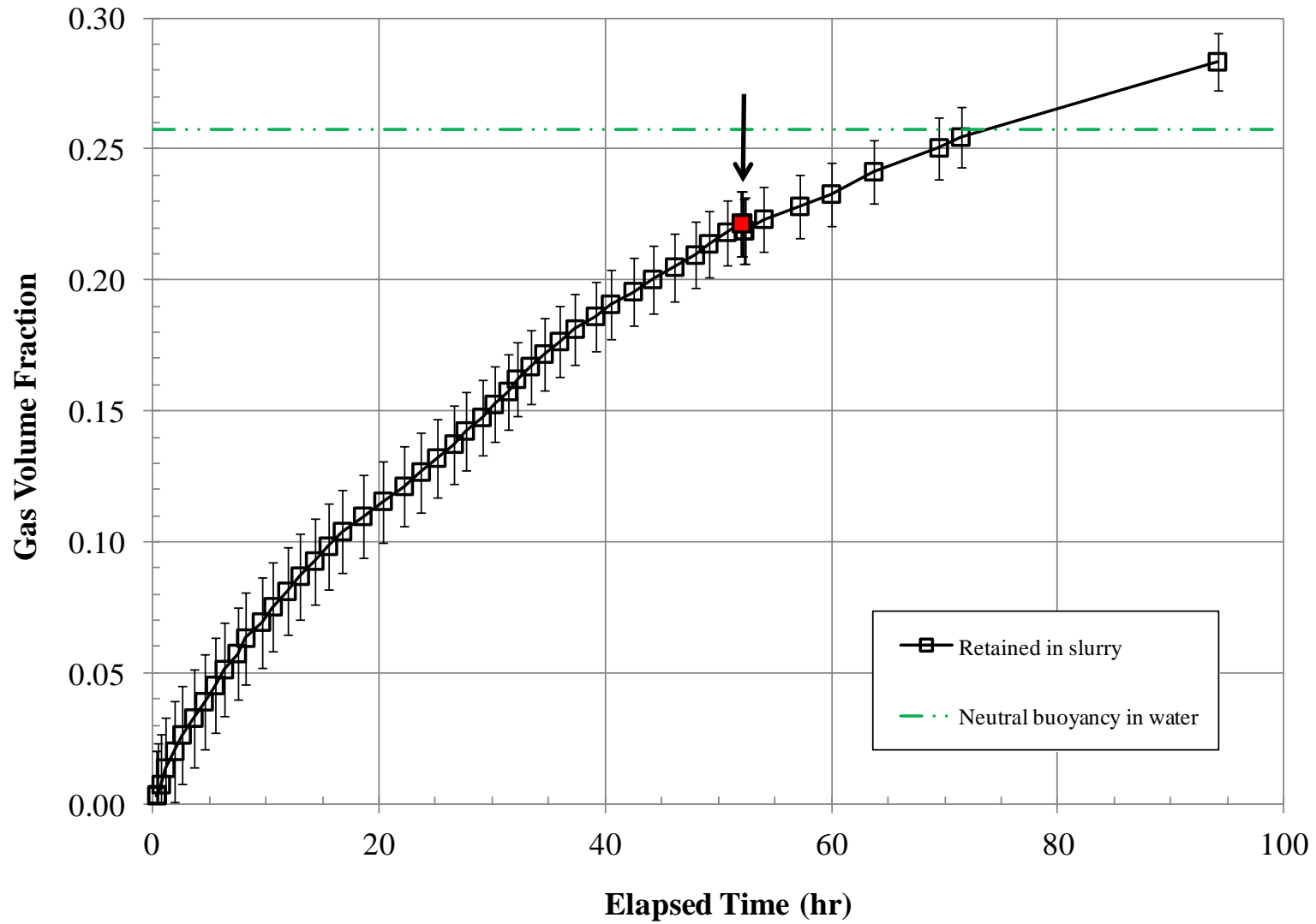


Figure C.1. Time Dependence of Retained Gas Fraction α from Level Measurements for RT Test 23-01 (assumes all gas retained in lower layer)

C.5

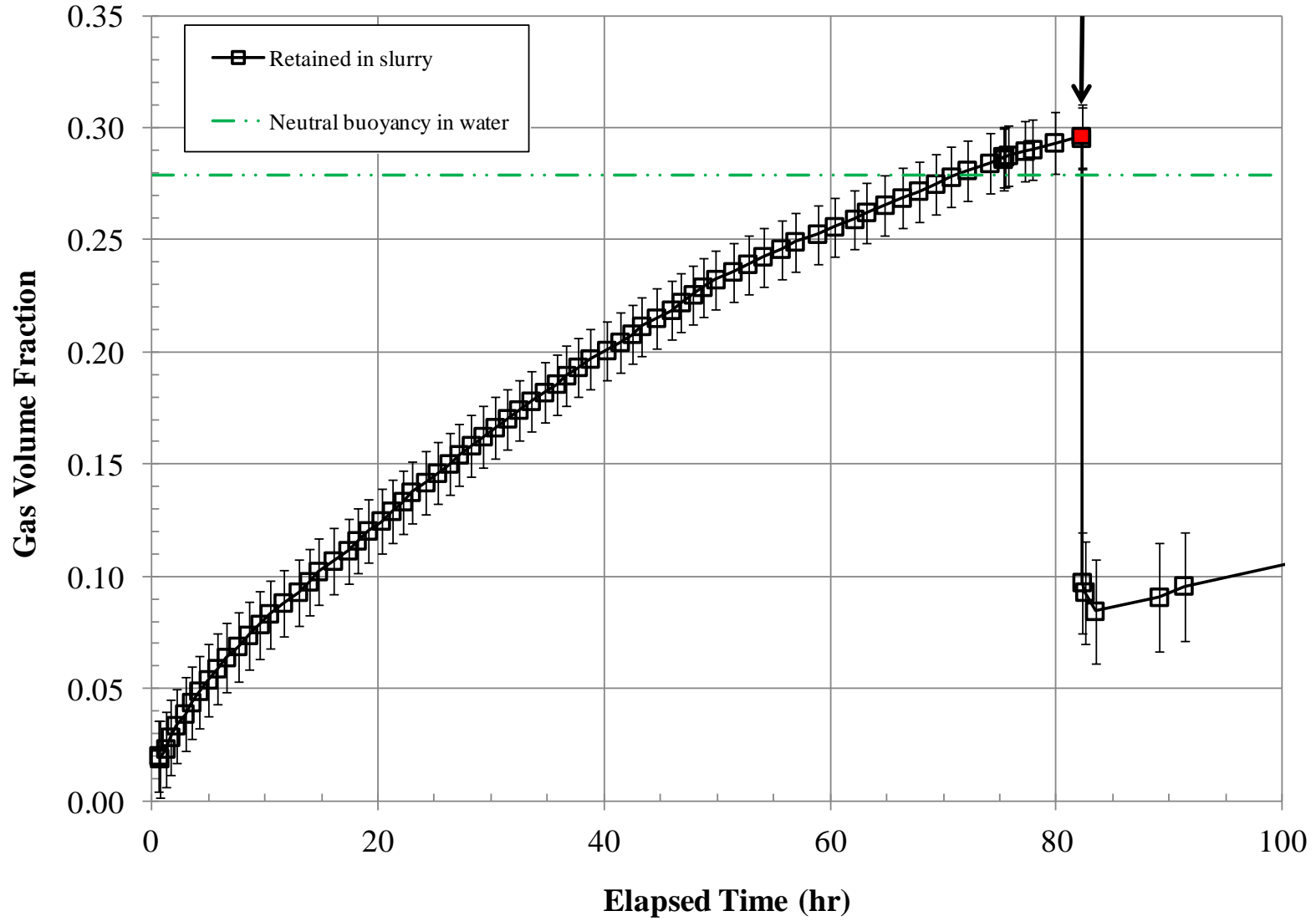
Test 10-02



C.6

Figure C.2. Time Dependence of Retained Gas Fraction α from Level Measurements for RT Test 10-02 (assumes all gas retained in lower layer)

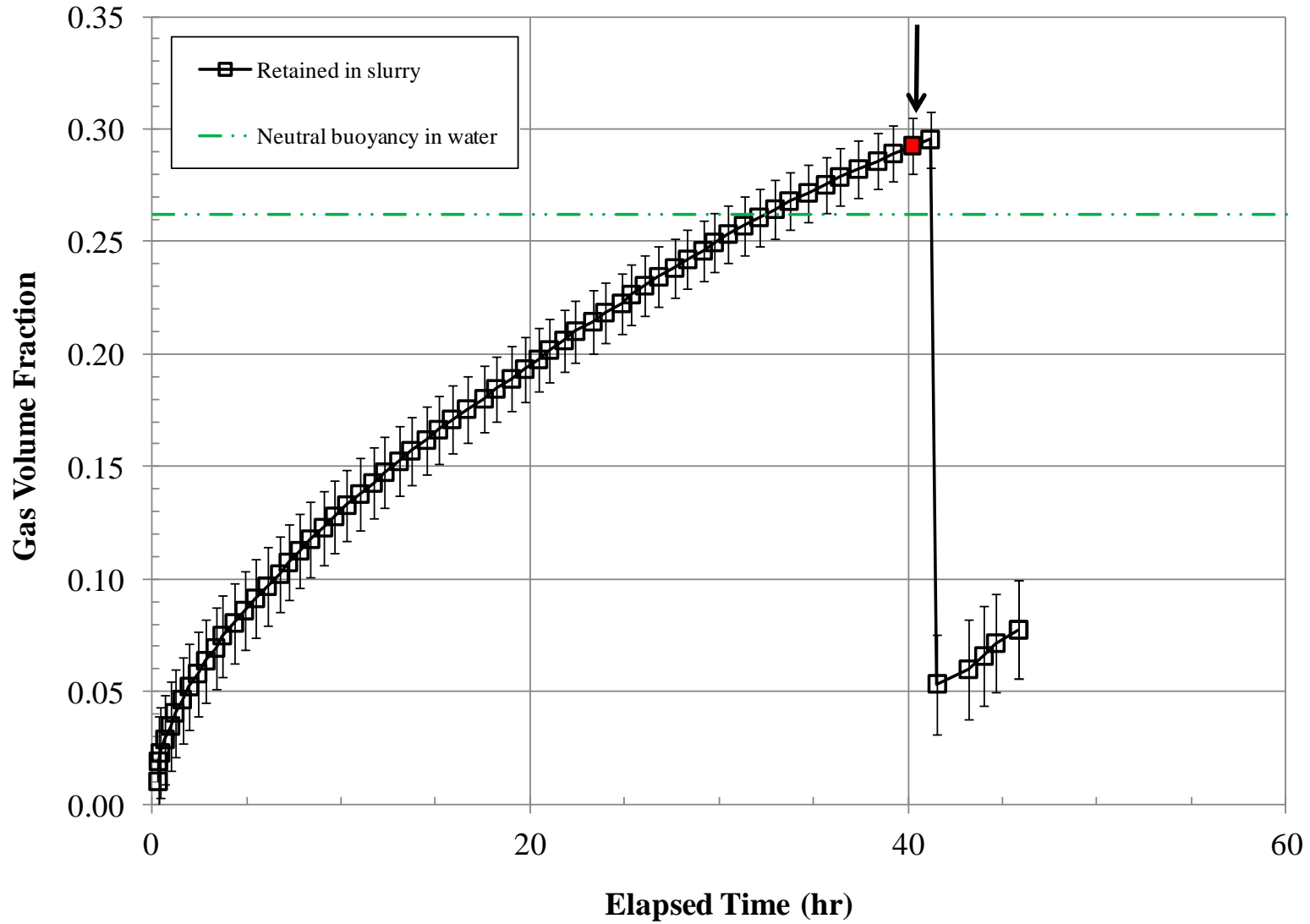
Test 23-03



C.7

Figure C.3. Time Dependence of Retained Gas Fraction α from Level Measurements for RT Test 23-03 (assumes all gas retained in lower layer)

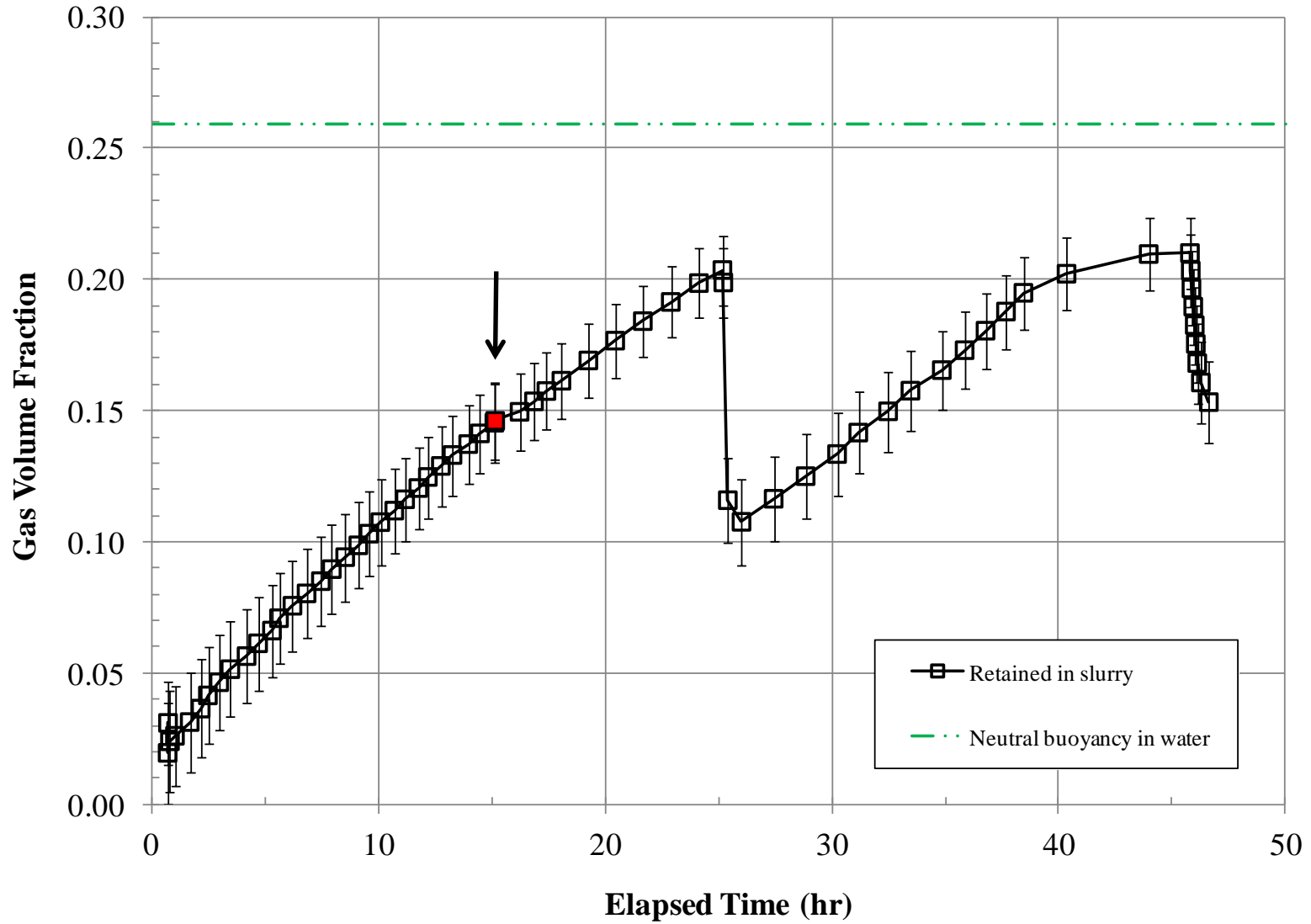
Test 10-04



C.8

Figure C.4. Time Dependence of Retained Gas Fraction α from Level Measurements for RT Test 10-04 (assumes all gas retained in lower layer)

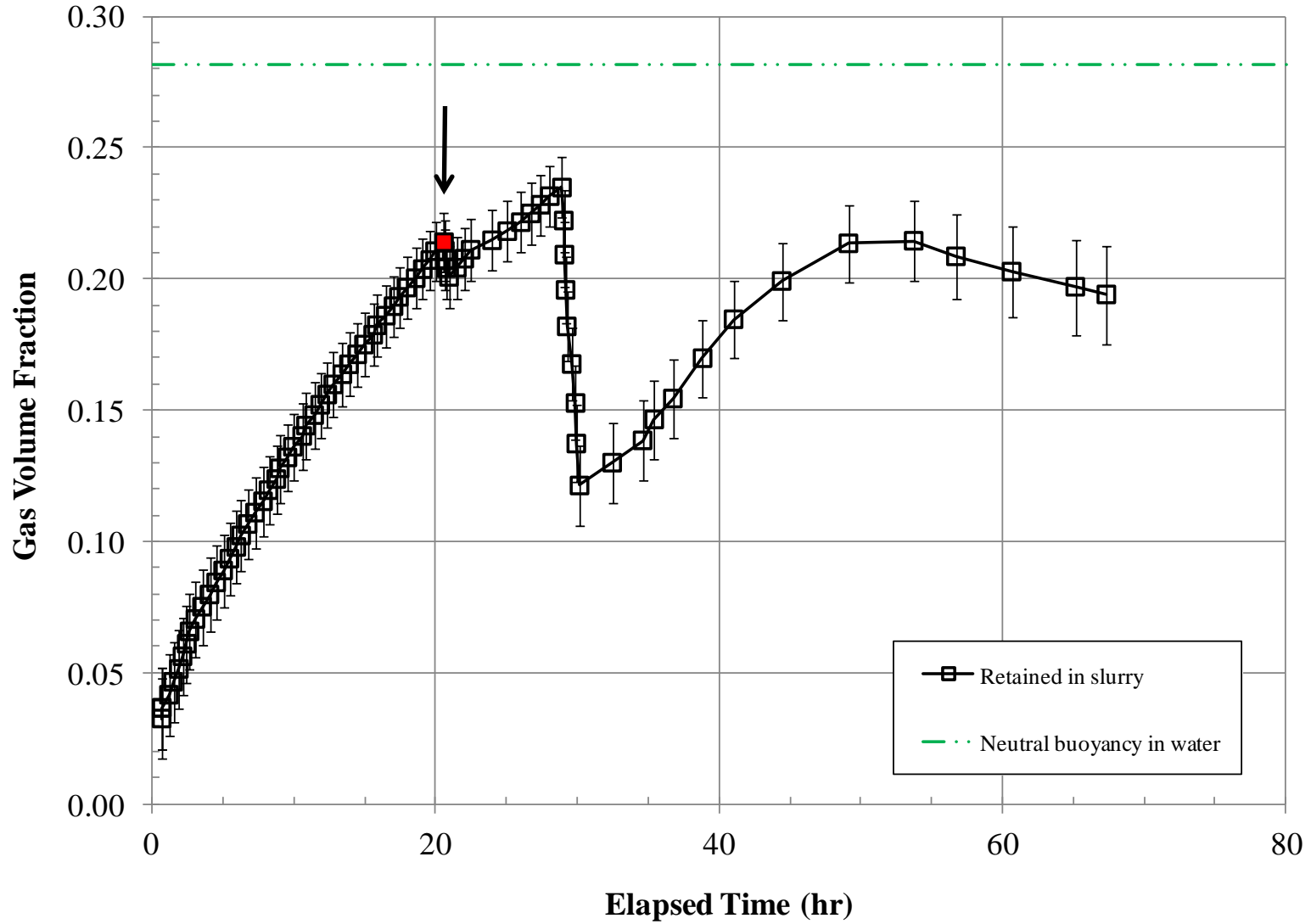
Test 23-05



C.9

Figure C.5. Time Dependence of Retained Gas Fraction α from Level Measurements for RT Test 23-05 (assumes all gas retained in lower layer)

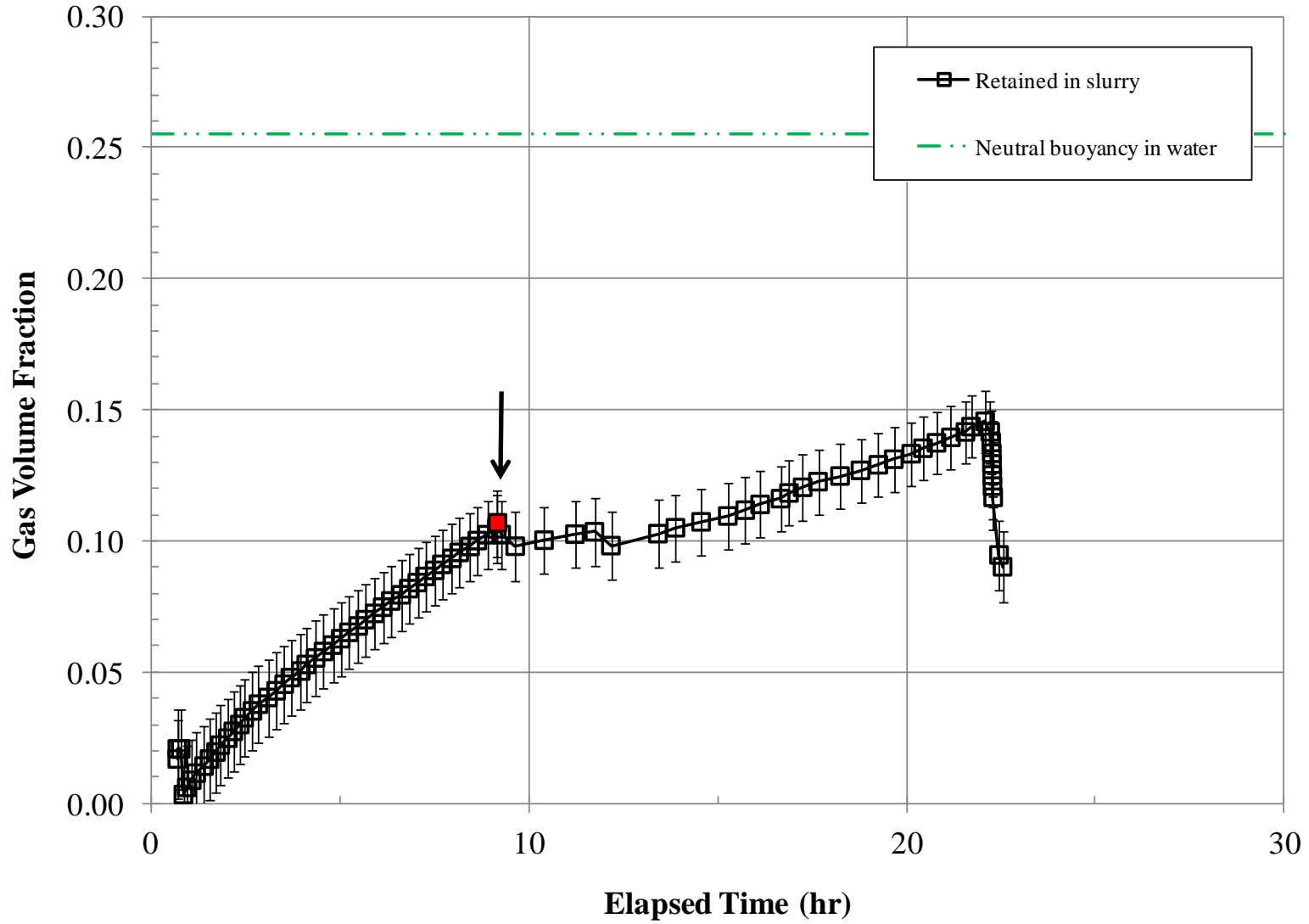
Test 23-06



C.10

Figure C.6. Time Dependence of Retained Gas Fraction α from Level Measurements for RT Test 23-06 (assumes all gas retained in lower layer)

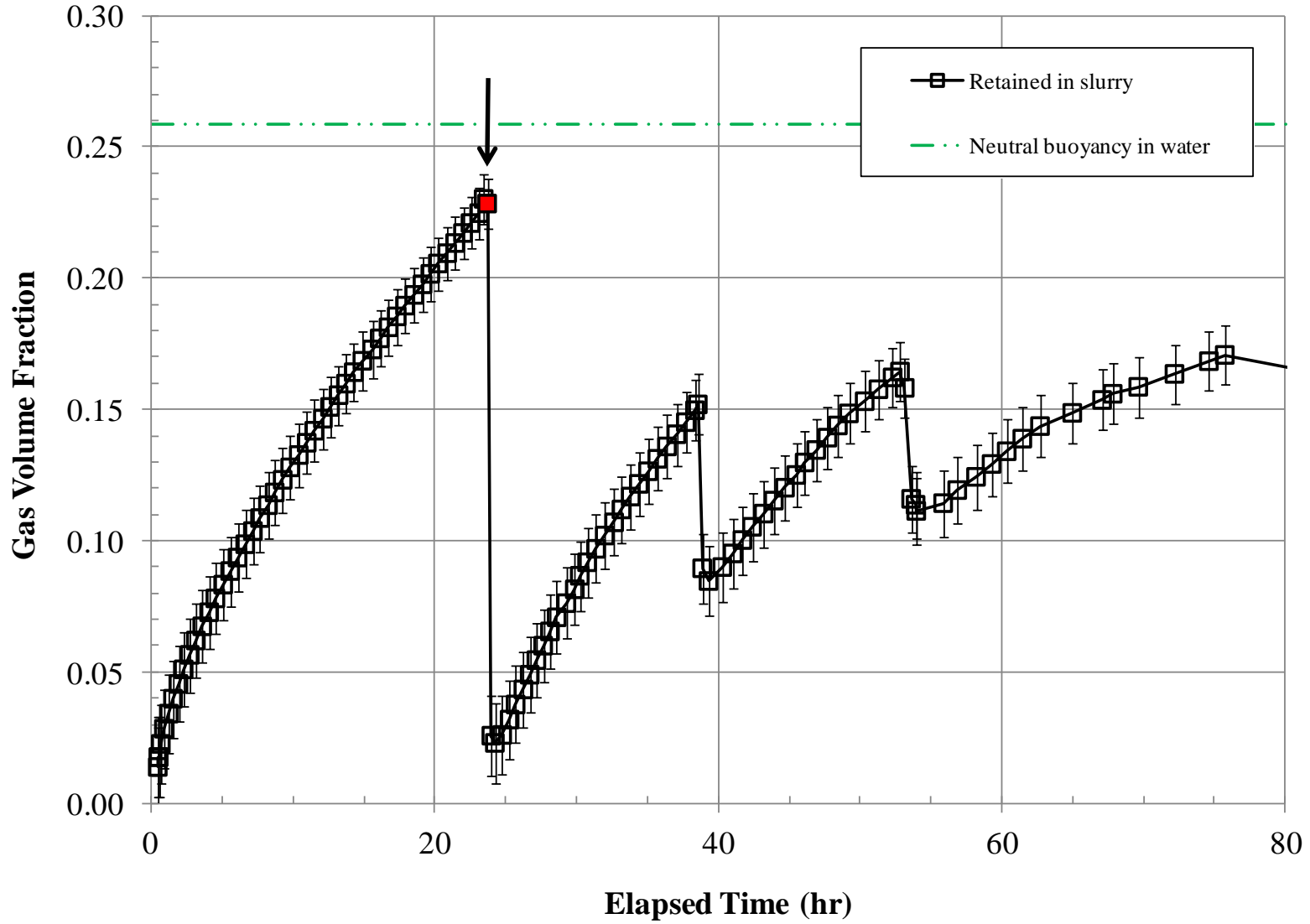
Test 23-07



C.11

Figure C.7. Time Dependence of Retained Gas Fraction α from Level Measurements for RT Test 23-07 (assumes all gas retained in lower layer)

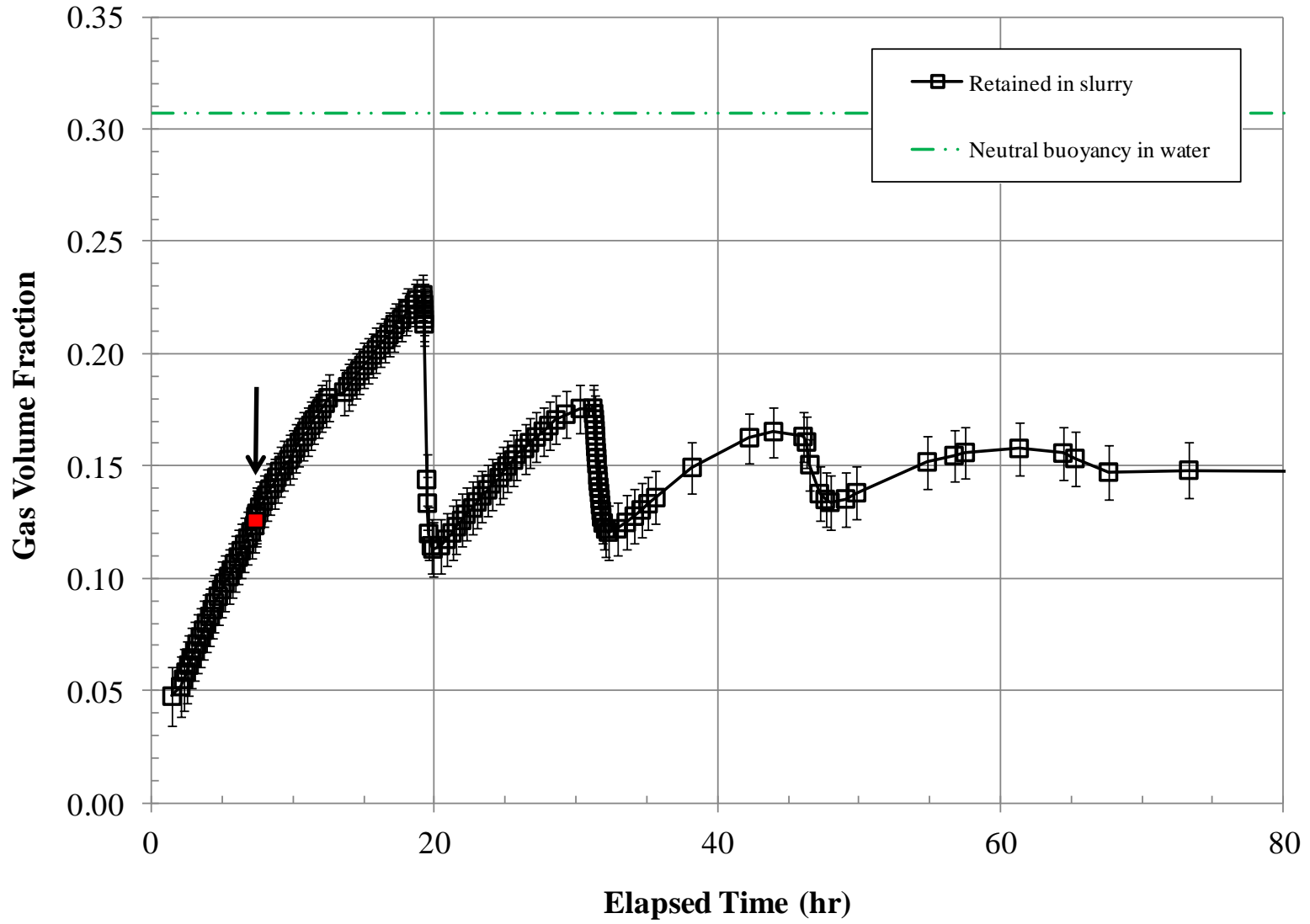
Test 10-08



C.12

Figure C.8. Time Dependence of Retained Gas Fraction α from Level Measurements for RT Test 10-08 (assumes all gas retained in lower layer)

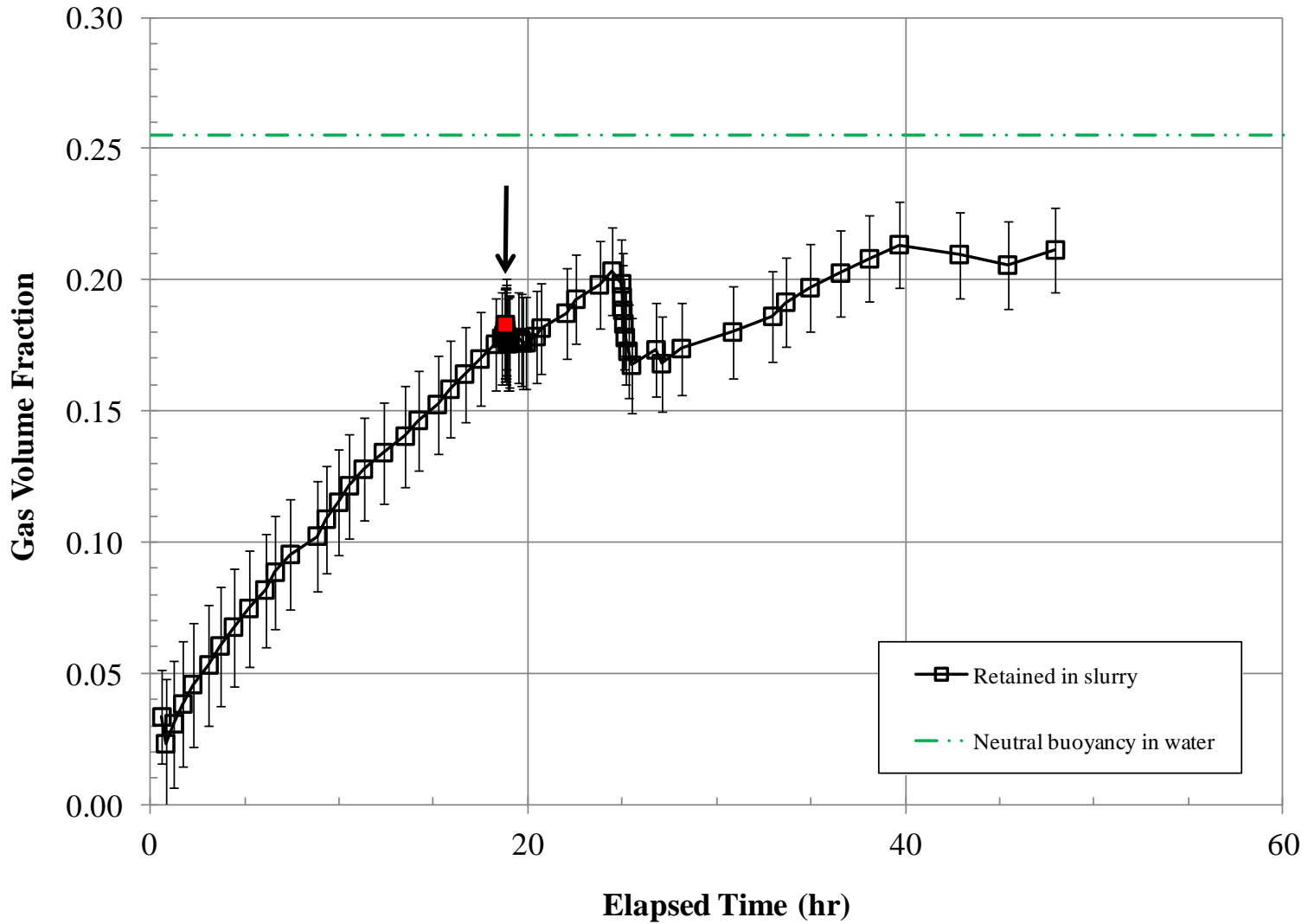
Test 70-09



C.13

Figure C.9. Time Dependence of Retained Gas Fraction α from Level Measurements for RT Test 70-09 (assumes all gas retained in lower layer)

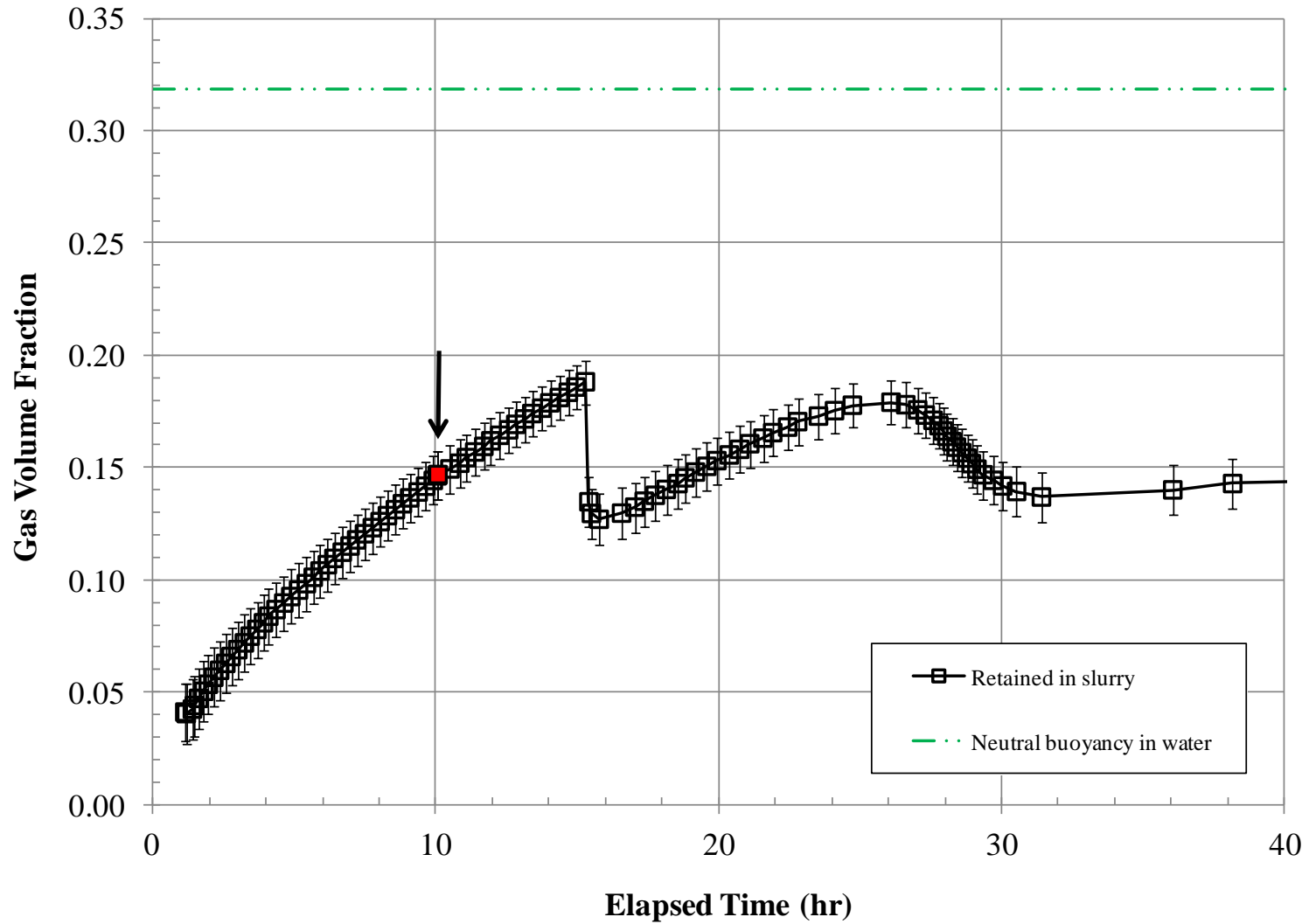
Test 23-10



C.14

Figure C.10. Time Dependence of Retained Gas Fraction α from Level Measurements for RT Test 23-10 (assumes all gas retained in lower layer)

Test 70-11



C.15

Figure C.11. Time Dependence of Retained Gas Fraction α from Level Measurements for RT Test 70-11 (assumes all gas retained in lower layer)

Test 23-12

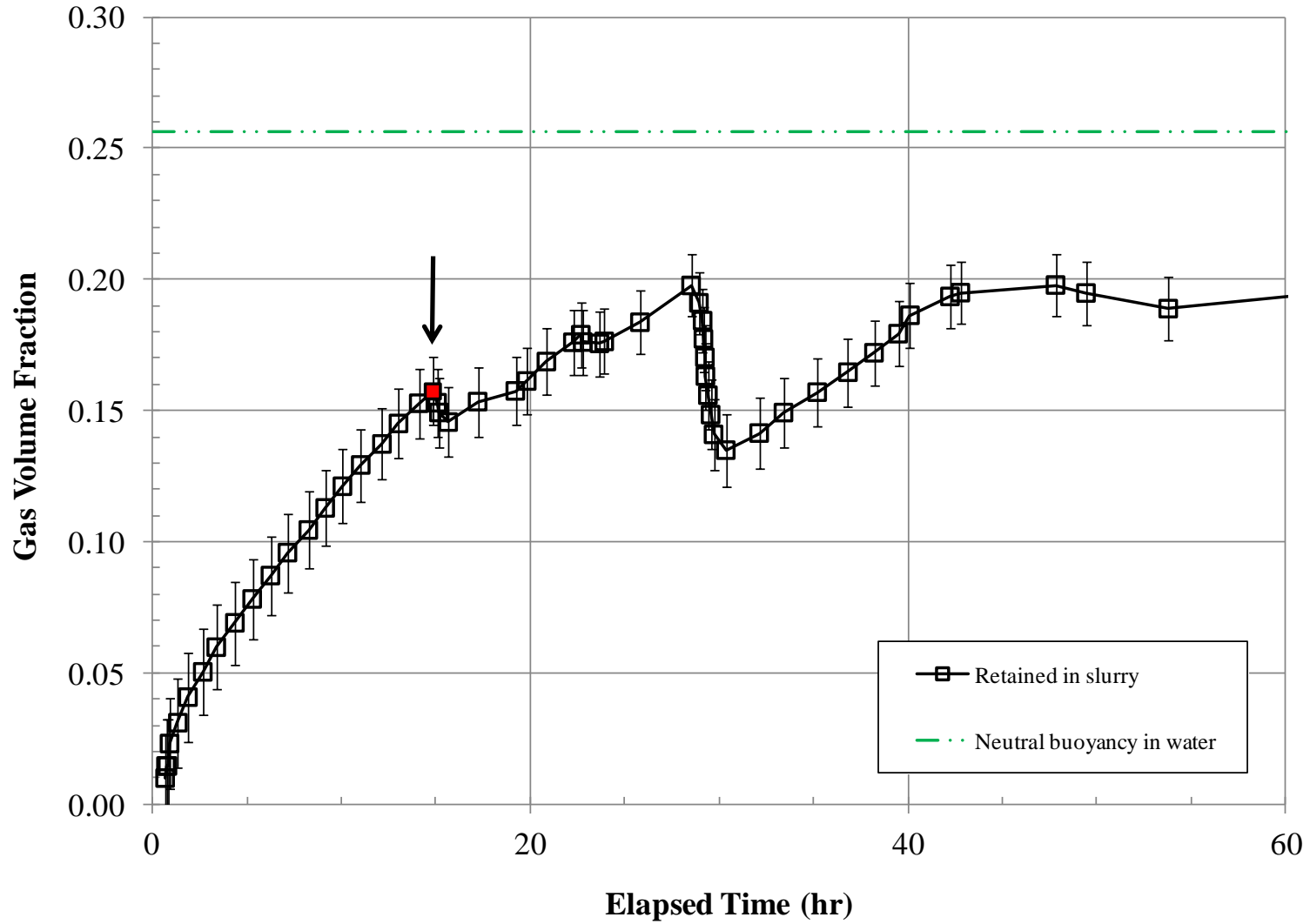
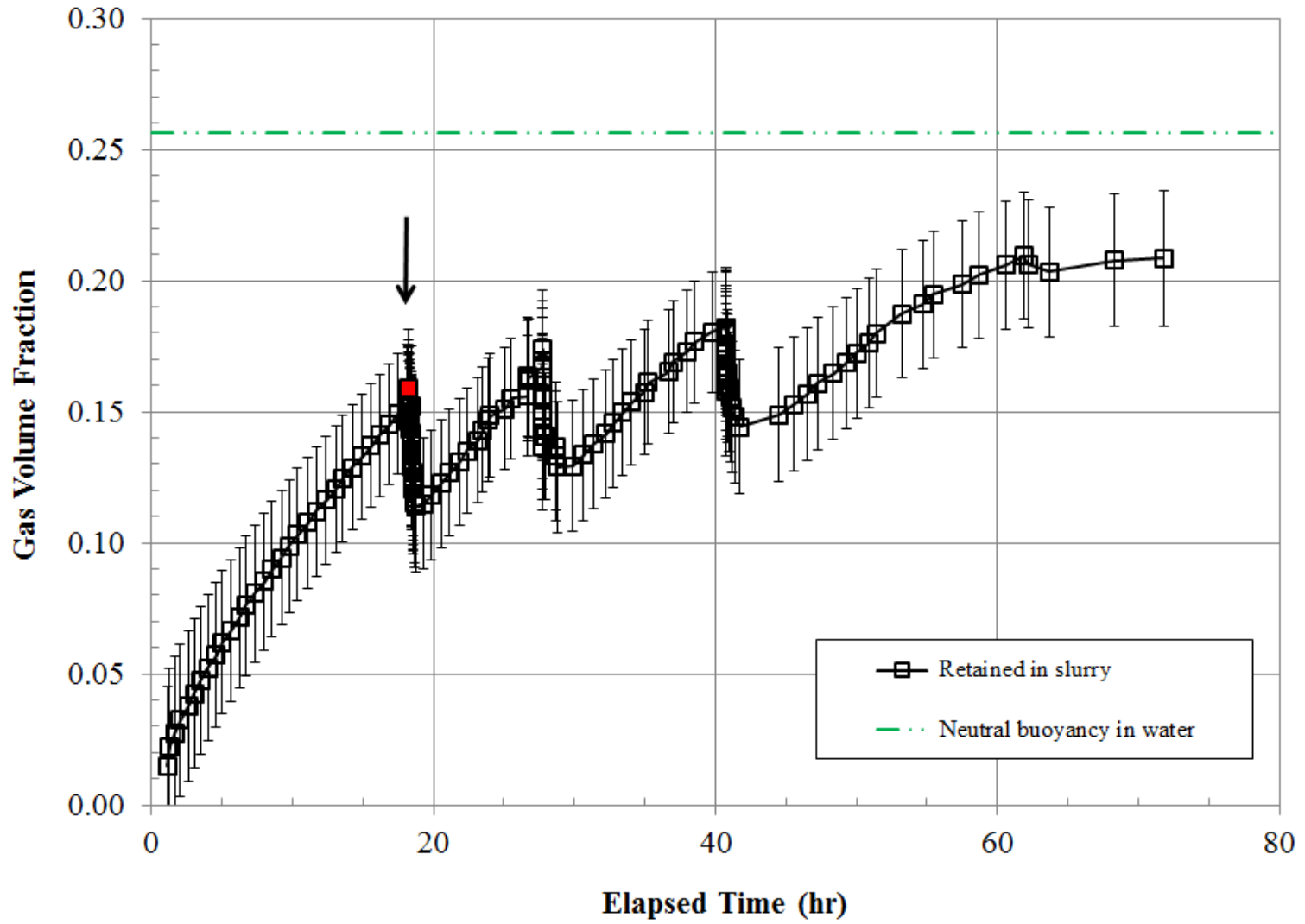


Figure C.12. Time Dependence of Retained Gas Fraction α from Level Measurements for RT Test 23-12 (assumes all gas retained in lower layer)

Test 23-13



C.17

Figure C.13. Time Dependence of Retained Gas Fraction α from Level Measurements for RT Test 23-13 (assumes all gas retained in lower layer)

Test 70-14

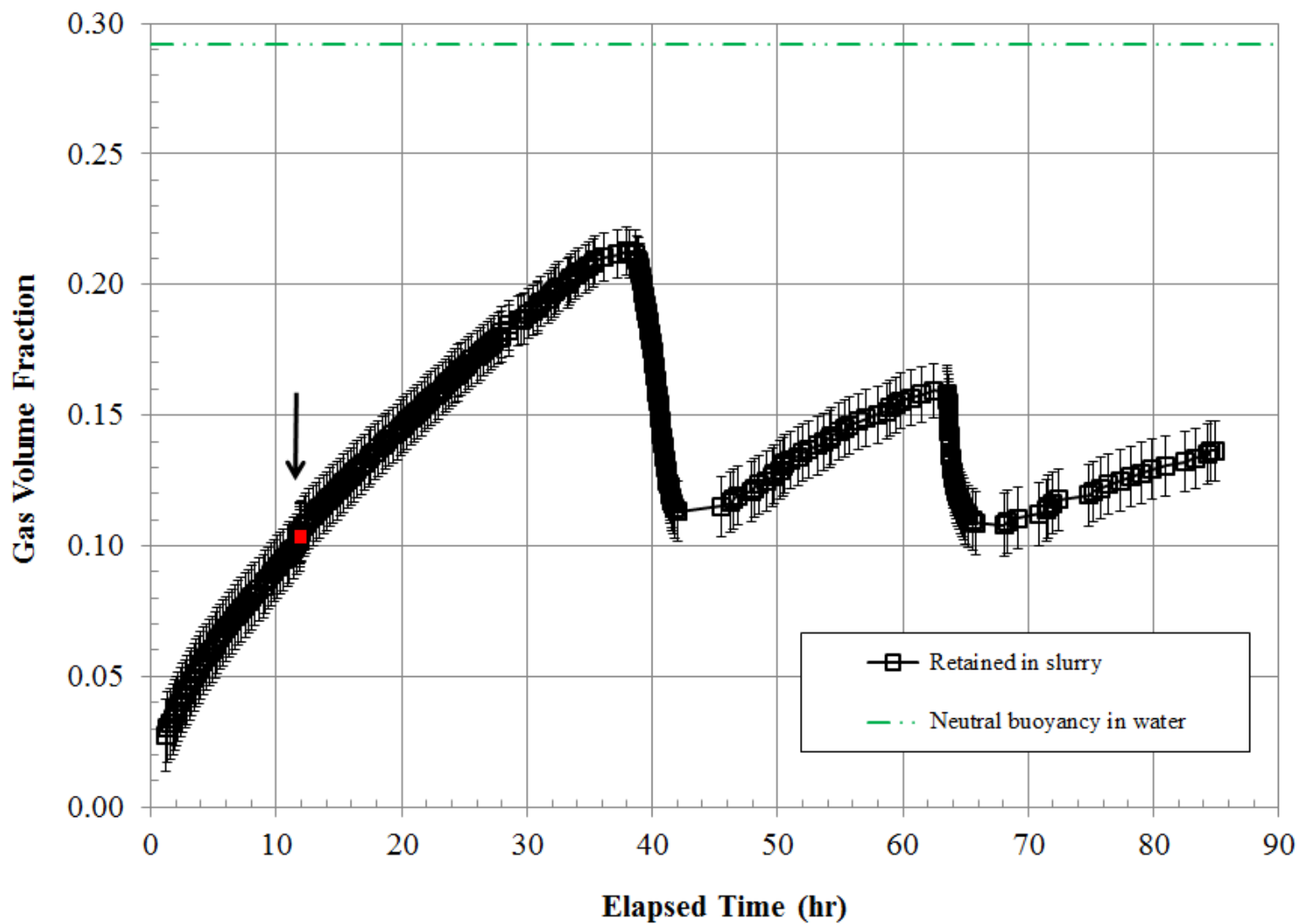
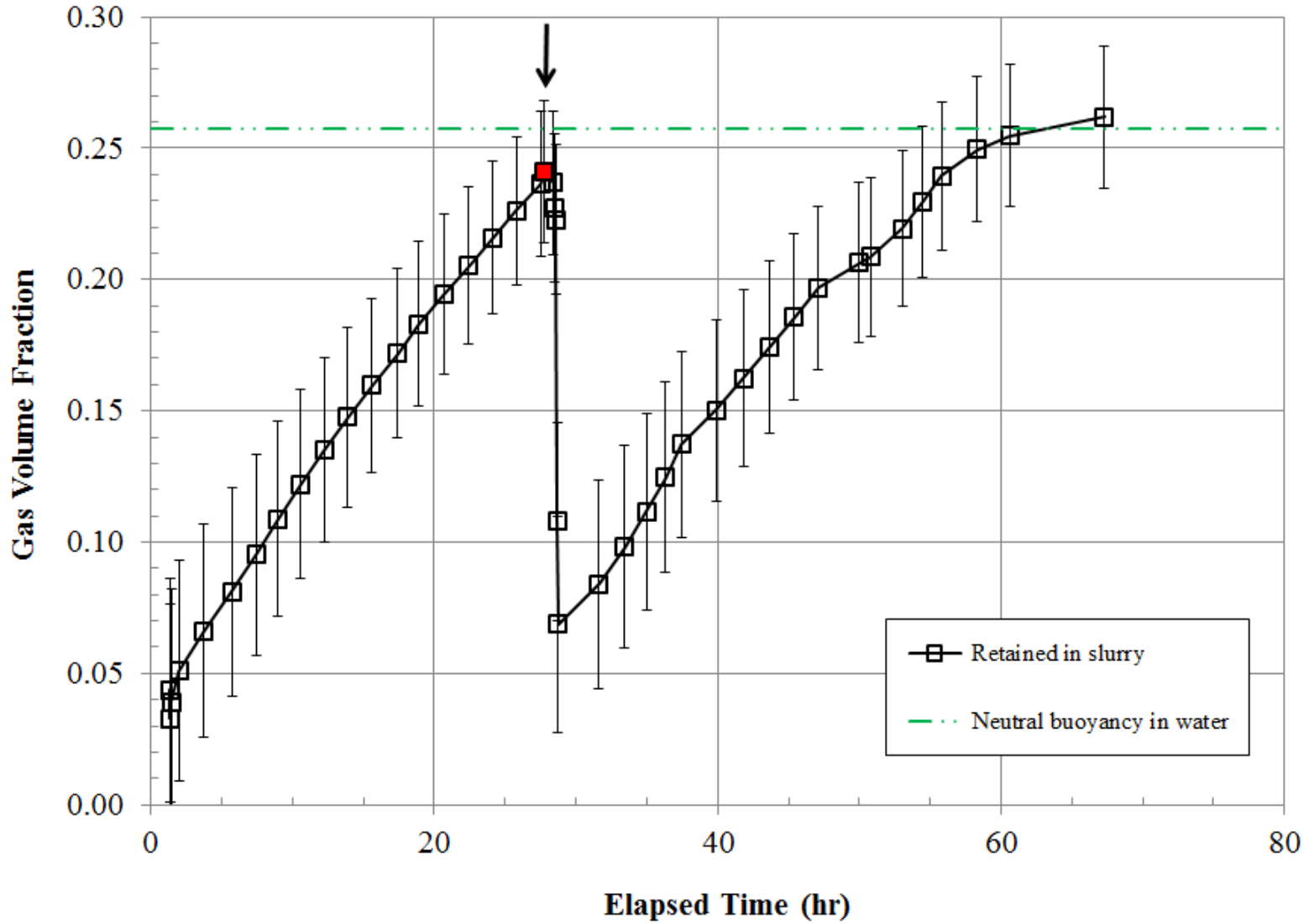


Figure C.14. Time Dependence of Retained Gas Fraction α from Level Measurements for RT Test 70-14 (assumes all gas retained in lower layer)

Test 23-15



C.19

Figure C.15. Time Dependence of Retained Gas Fraction α from Level Measurements for RT Test 23-15 (assumes all gas retained in lower layer)

Test 70-16

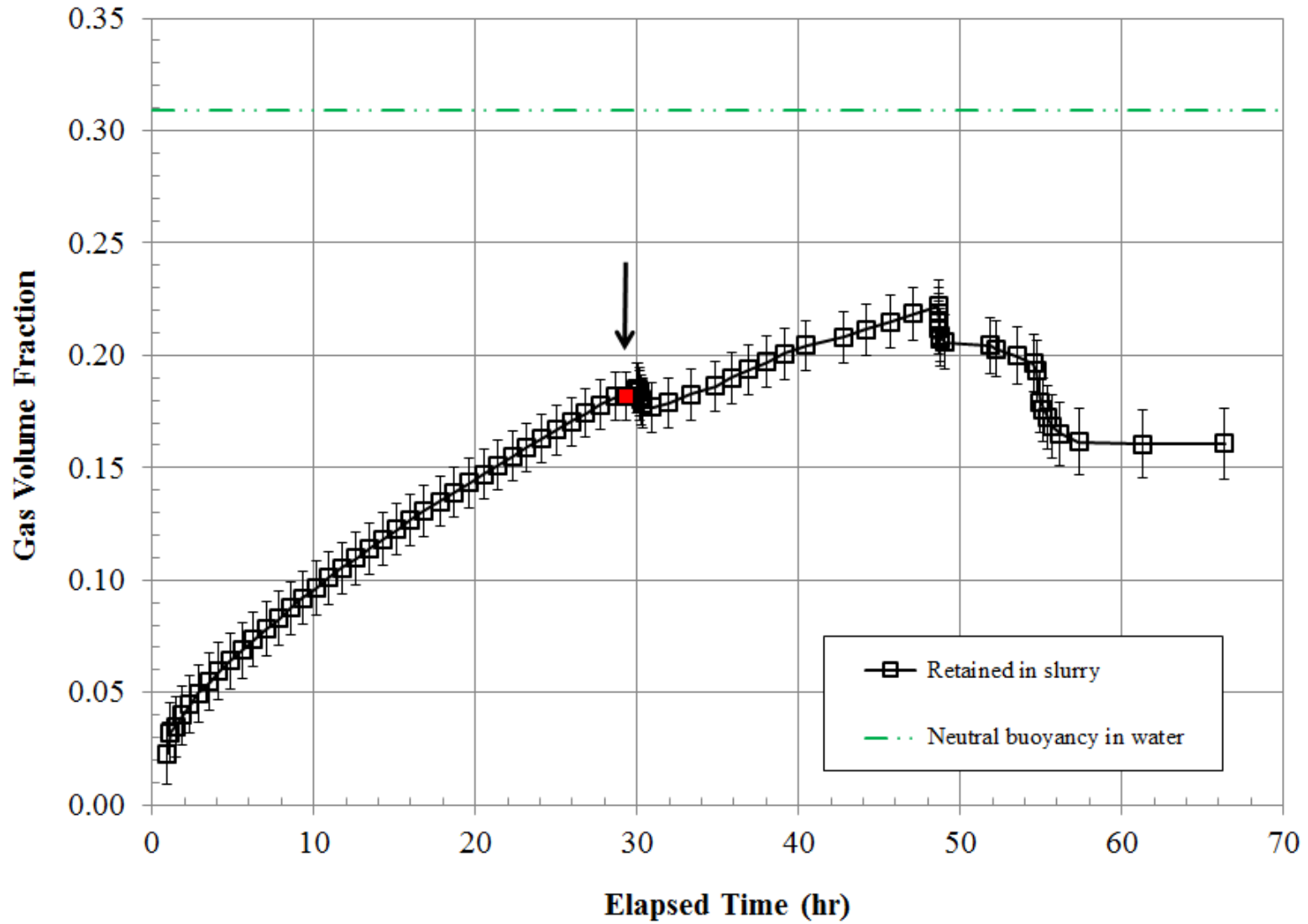


Figure C.16. Time Dependence of Retained Gas Fraction α from Level Measurements for RT Test 70-16 (assumes all gas retained in lower layer)

Test 23-17

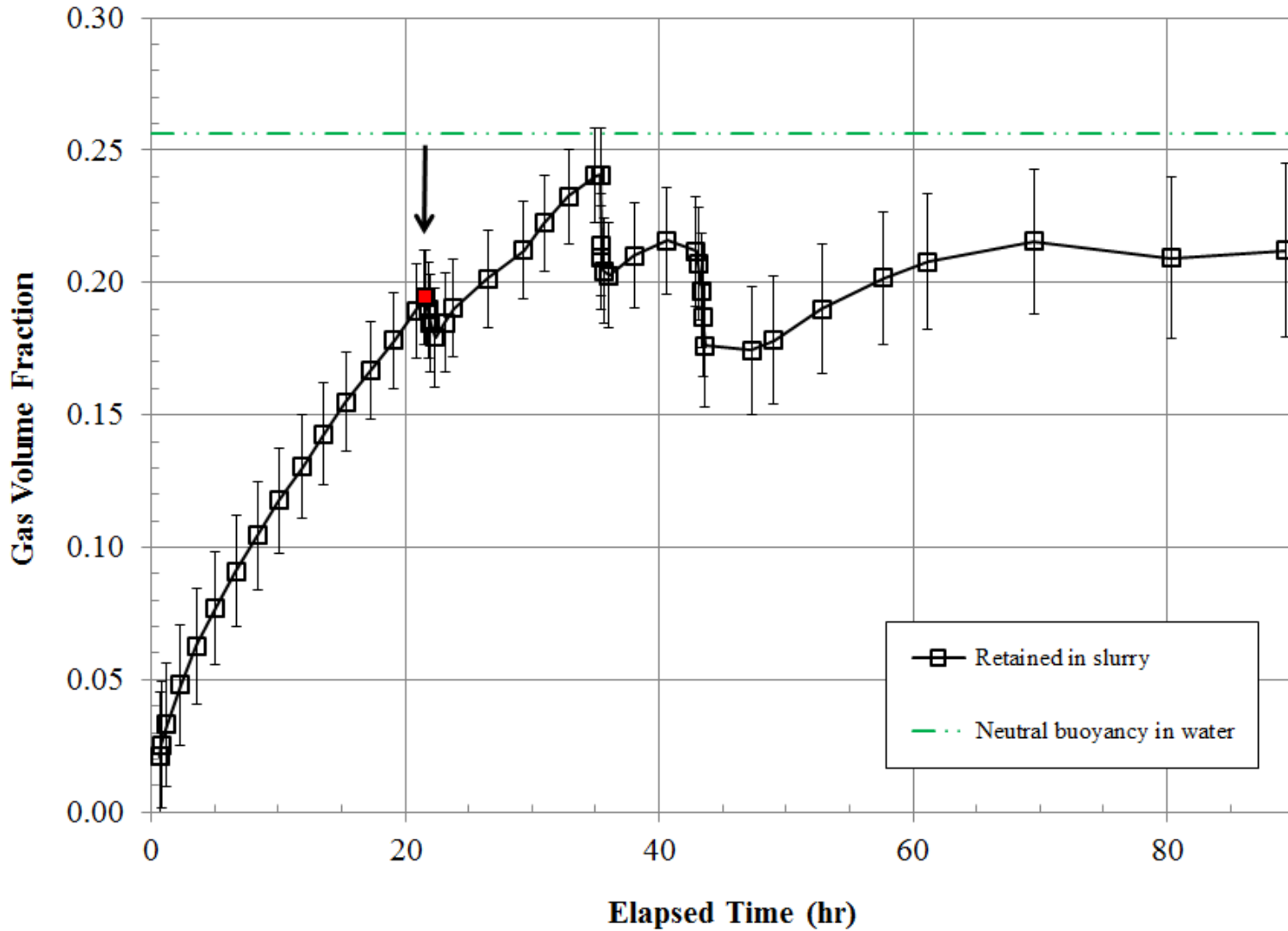


Figure C.17. Time Dependence of Retained Gas Fraction α from Level Measurements for RT Test 23-17 (assumes all gas retained in lower layer)

Test 23-19

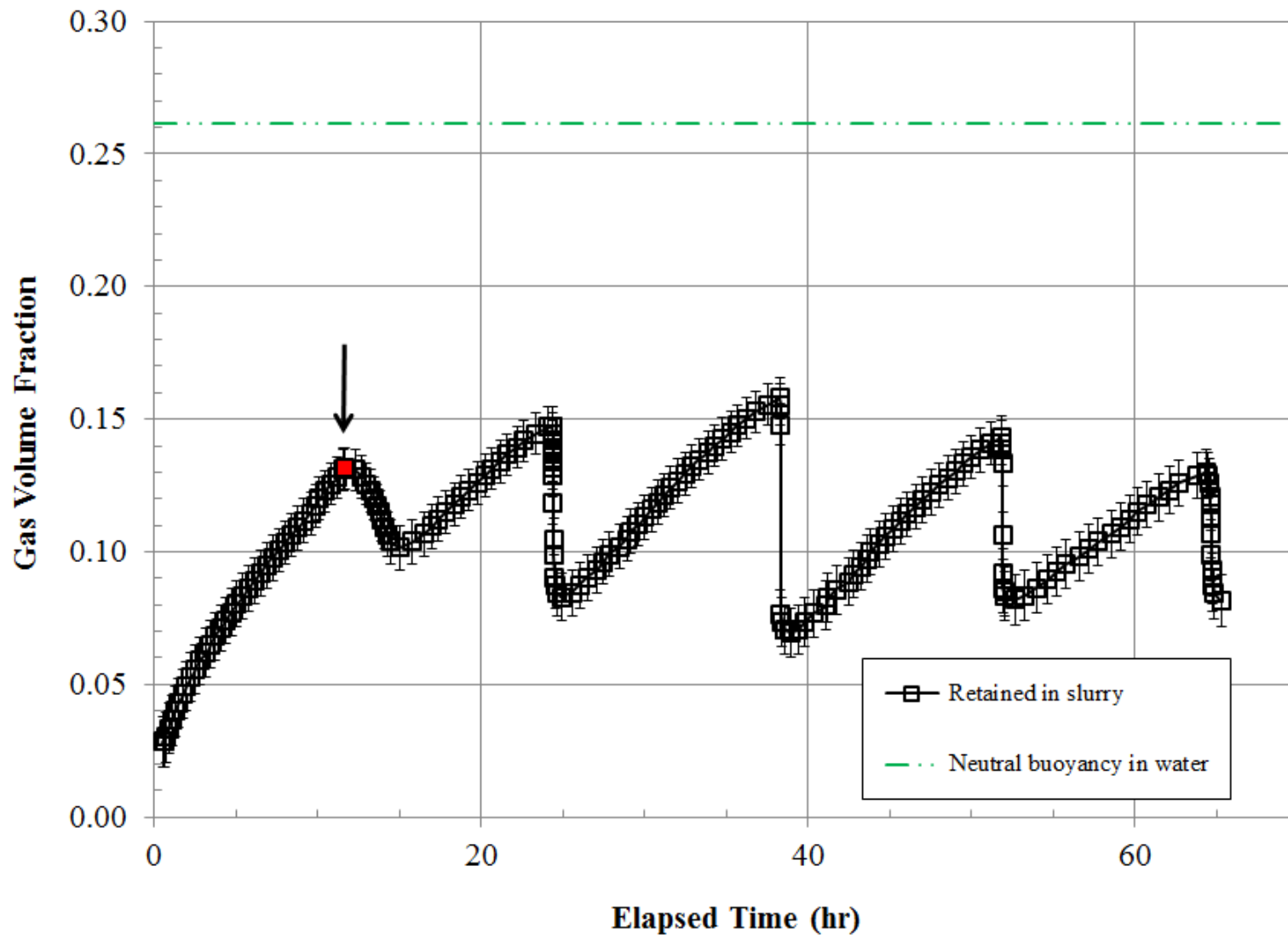
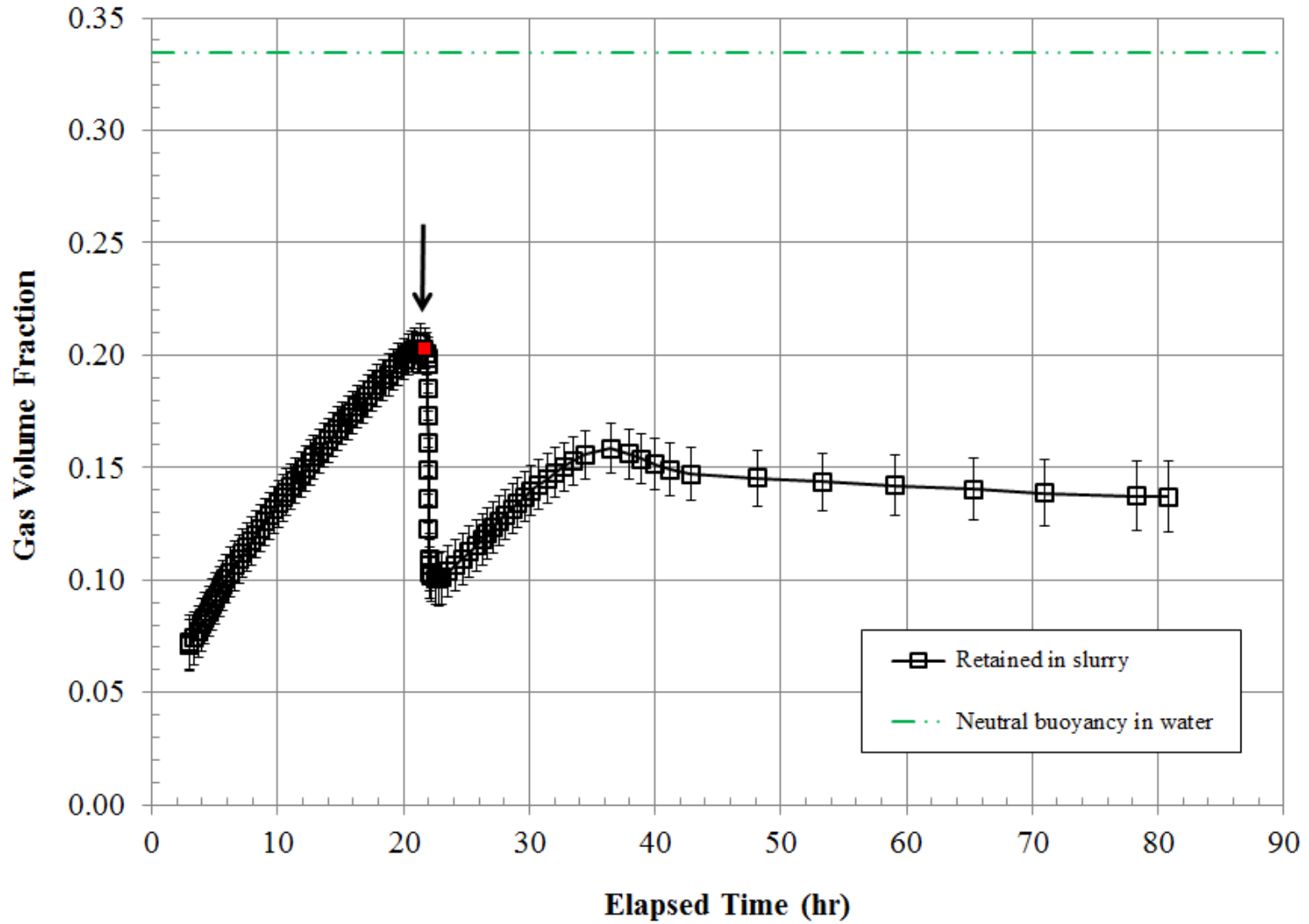


Figure C.18. Time Dependence of Retained Gas Fraction α from Level Measurements for RT Test 23-19 (assumes all gas retained in lower layer)

Test 70-20



C.23

Figure C.19. Time Dependence of Retained Gas Fraction α from Level Measurements for RT Test 70-20 (assumes all gas retained in lower layer)

Test 23-21

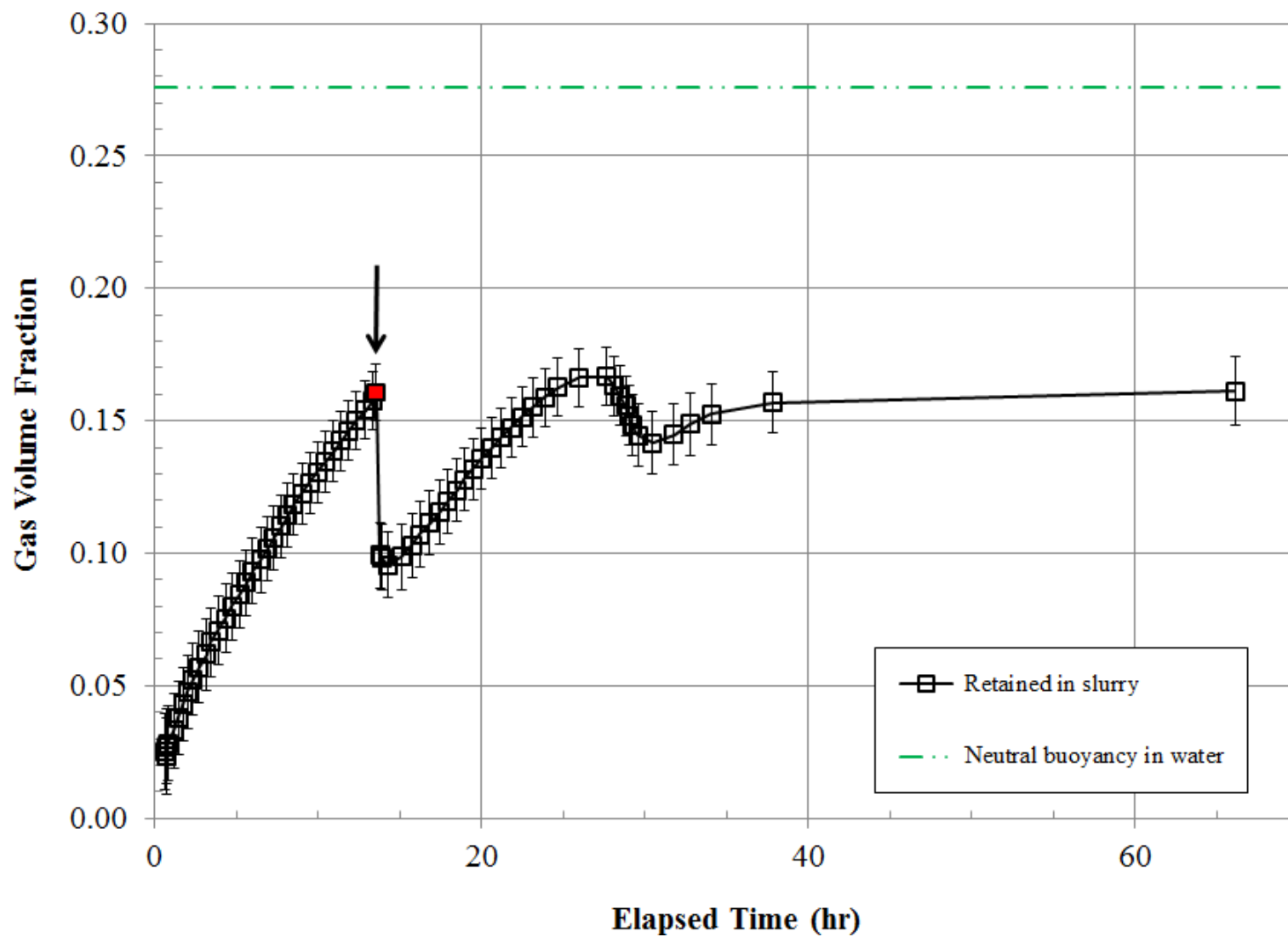
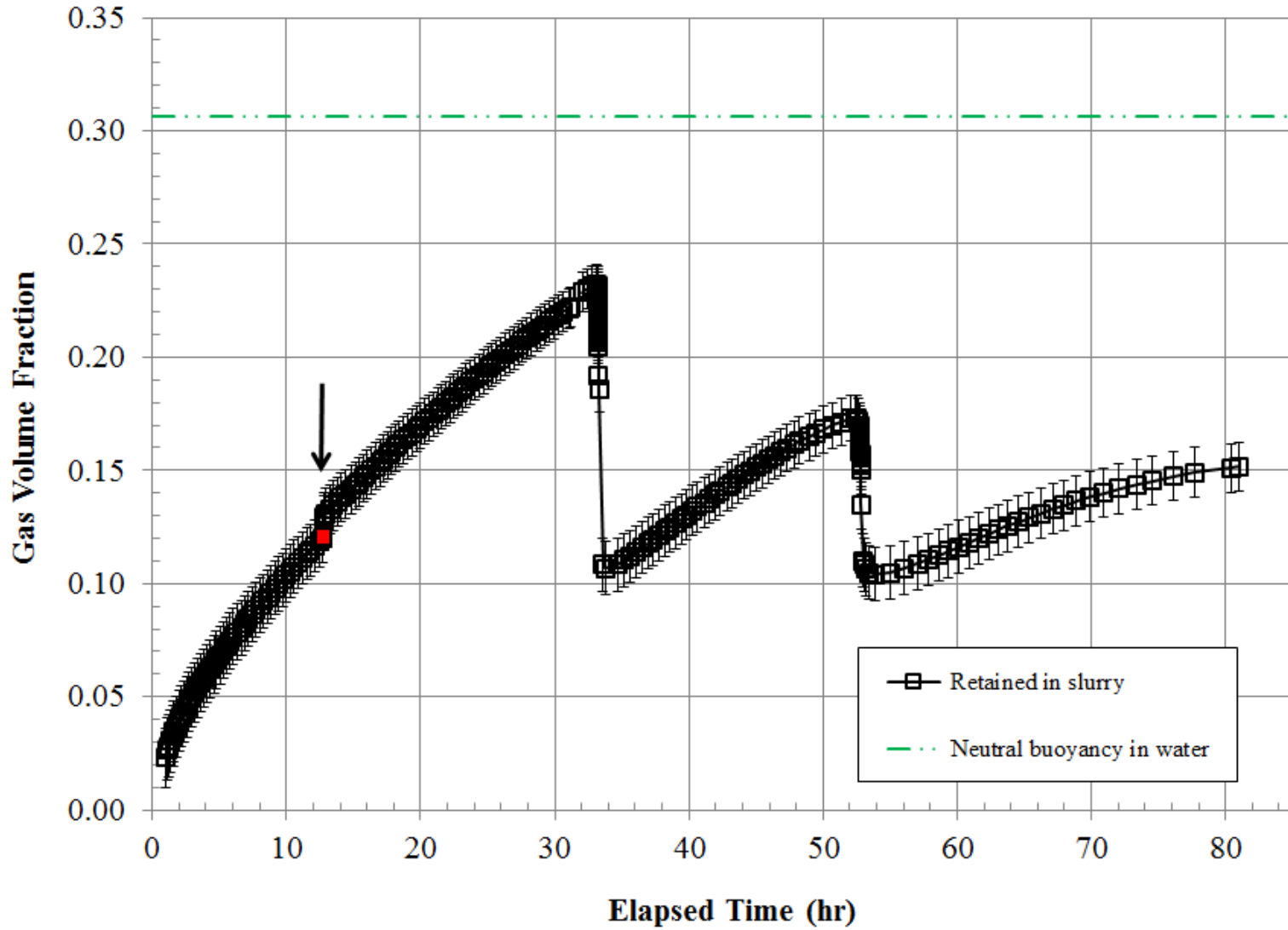


Figure C.20. Time Dependence of Retained Gas Fraction α from Level Measurements for RT Test 23-21 (assumes all gas retained in lower layer)

Test 70-22



C.25

Figure C.21. Time Dependence of Retained Gas Fraction α from Level Measurements for RT Test 70-22 (assumes all gas retained in lower layer)

Test 23-23

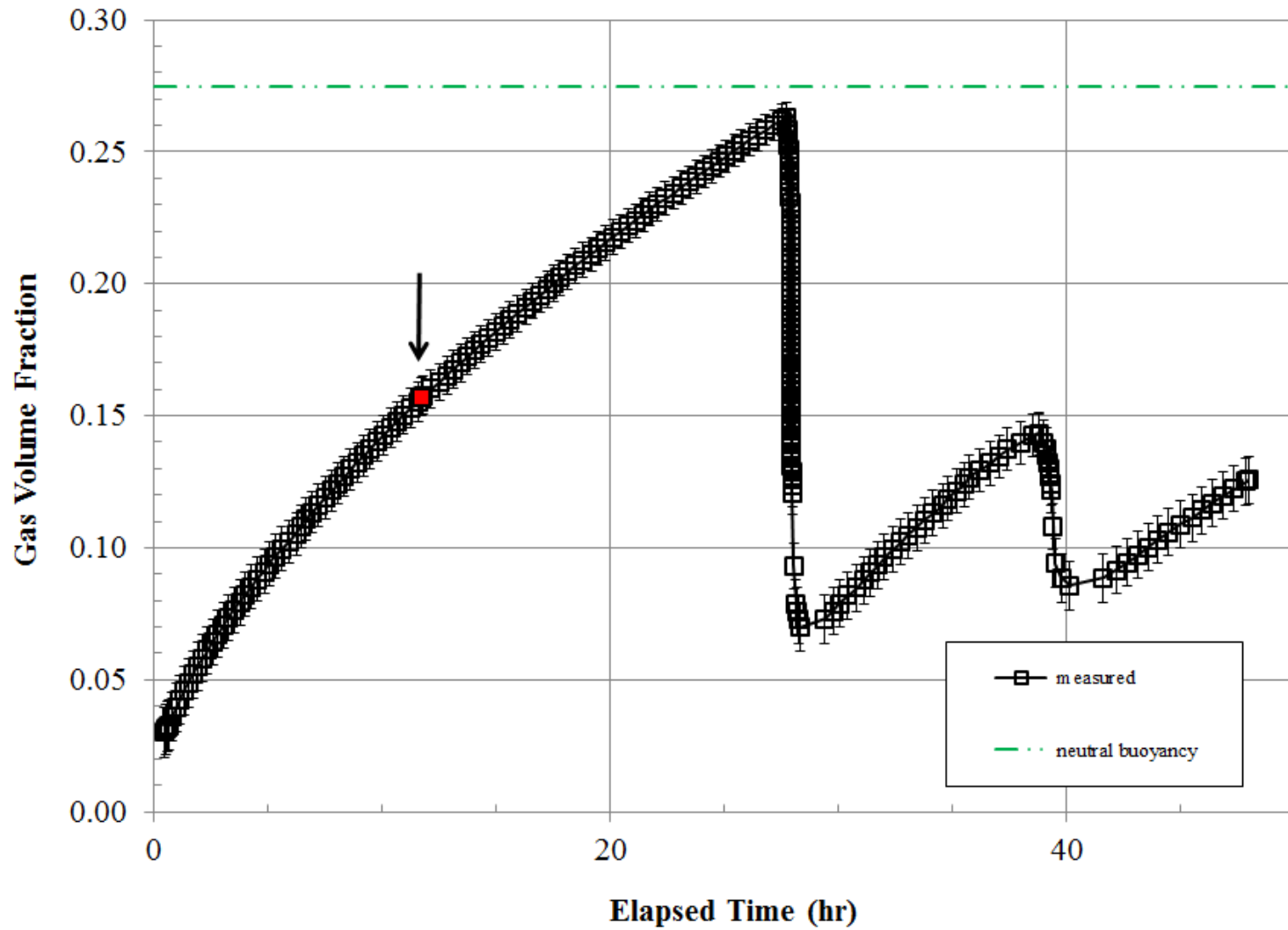


Figure C.22. Time Dependence of Retained Gas Fraction α from Level Measurements for RT Test 23-23 (assumes all gas retained in lower layer)

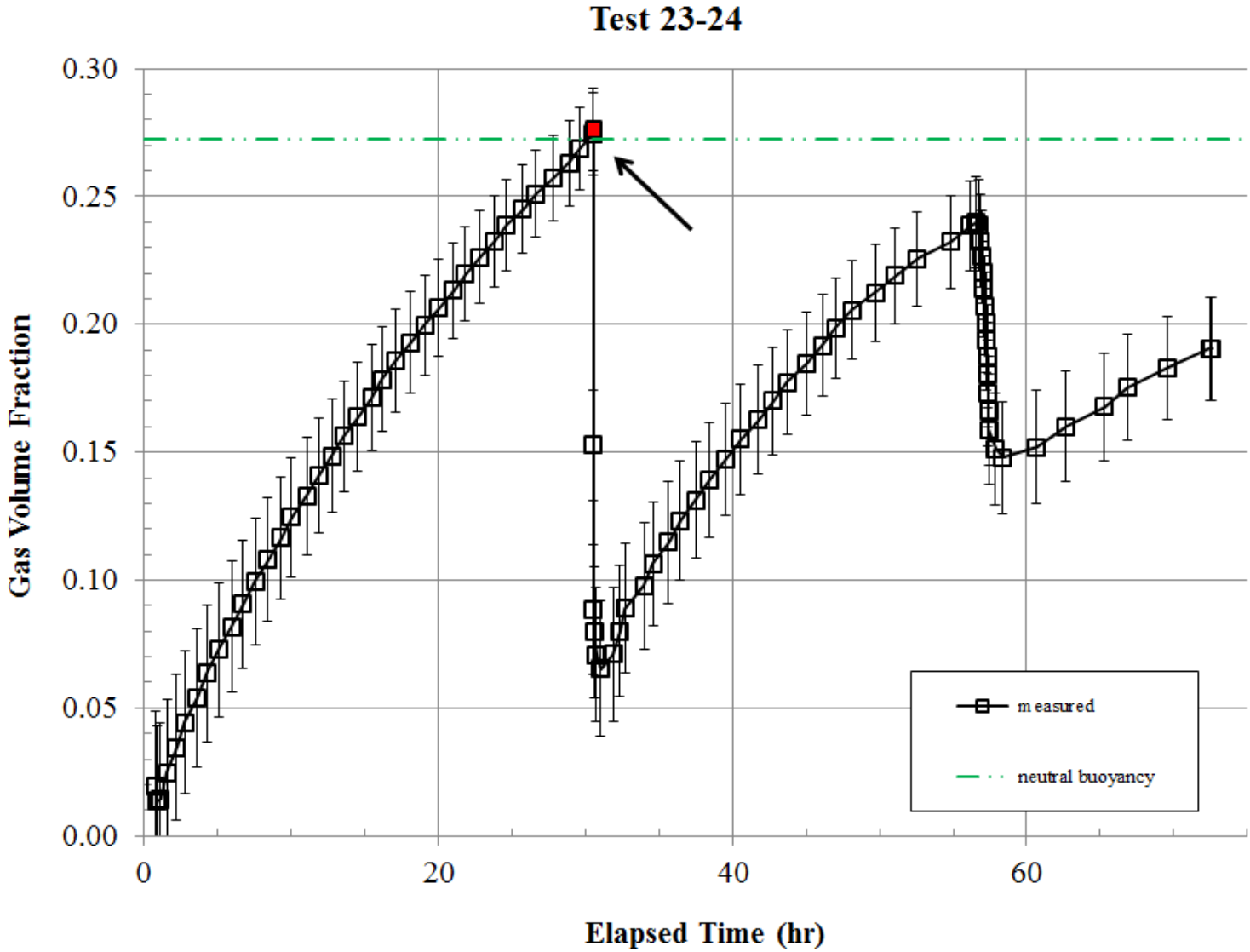


Figure C.23. Time Dependence of Retained Gas Fraction α from Level Measurements for RT Test 23-24 (assumes all gas retained in lower layer)

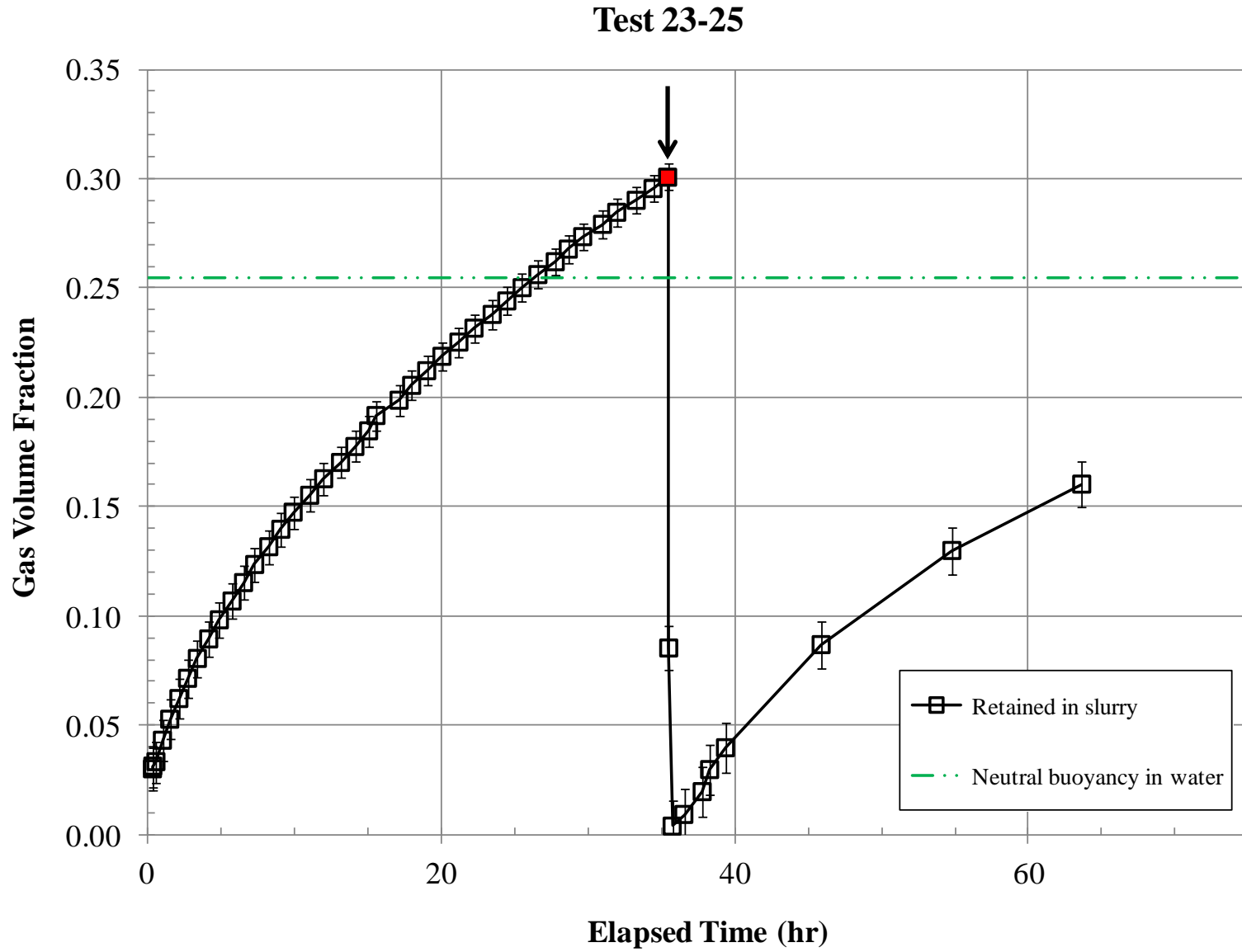


Figure C.24. Time Dependence of Retained Gas Fraction α from Level Measurements for SL Test 23-25

Test 70-26

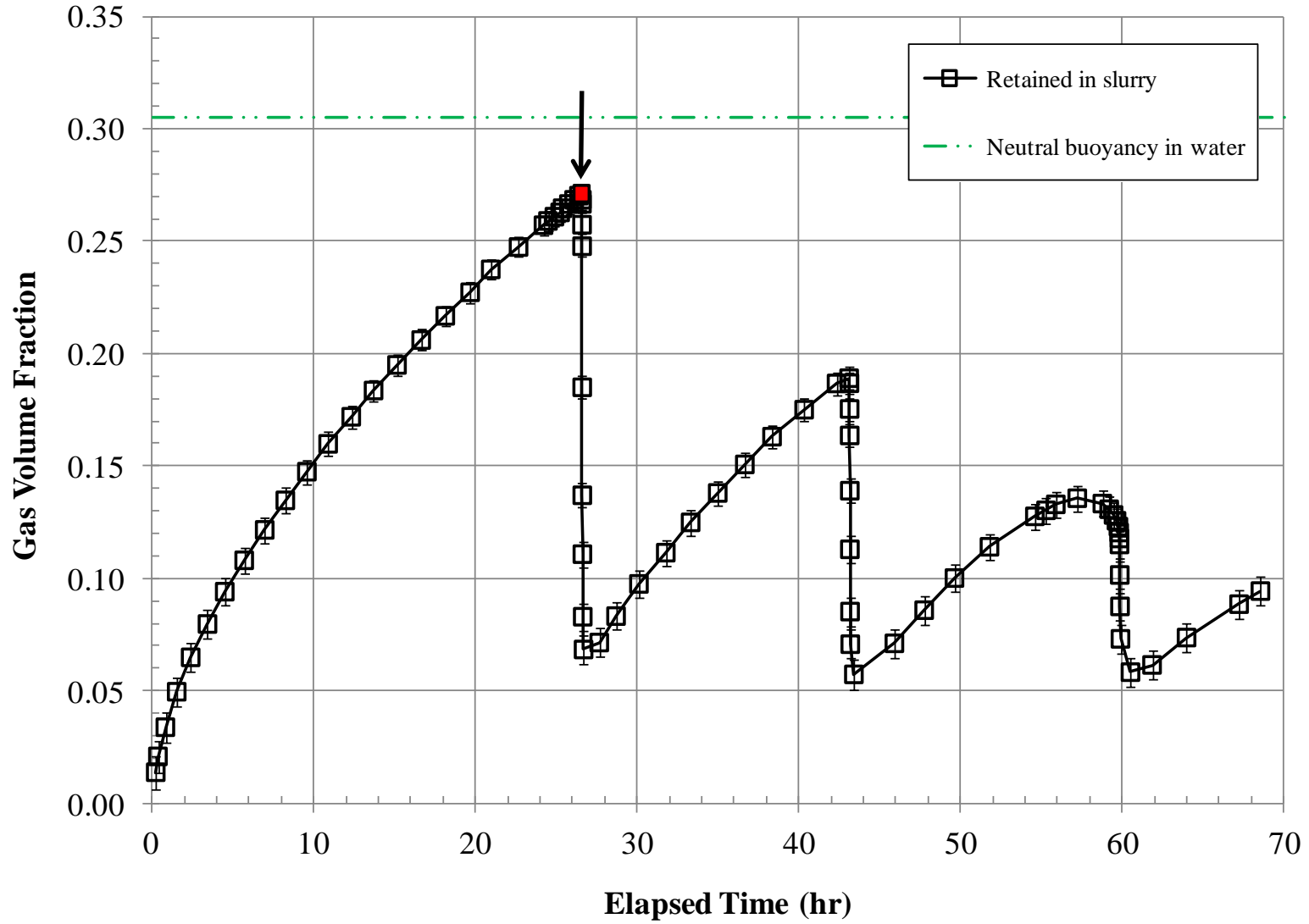


Figure C.25. Time Dependence of Retained Gas Fraction α from Level Measurements for SL Test 70-26

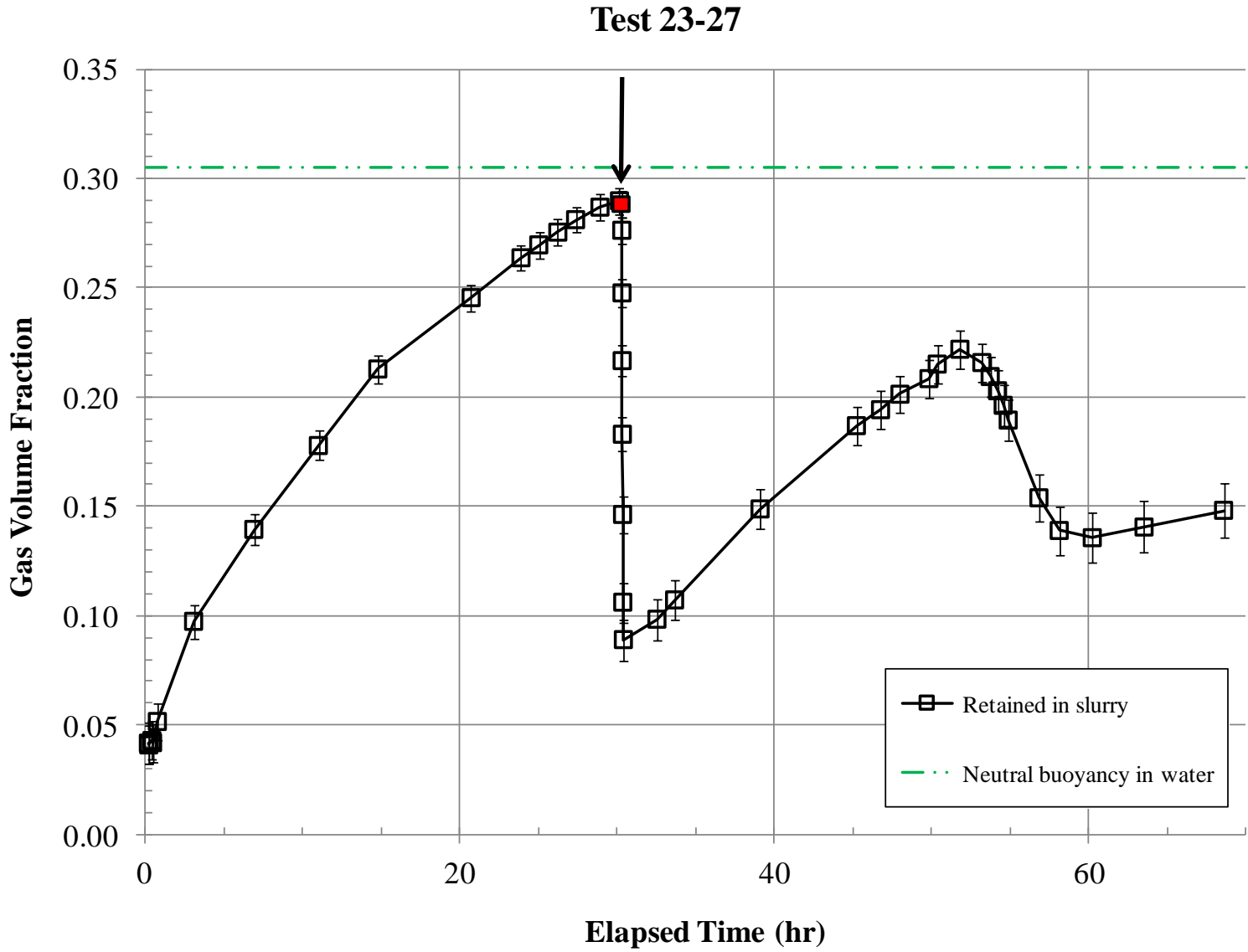


Figure C.26. Time Dependence of Retained Gas Fraction α from Level Measurements for SL Test 23-27

Test 70-28

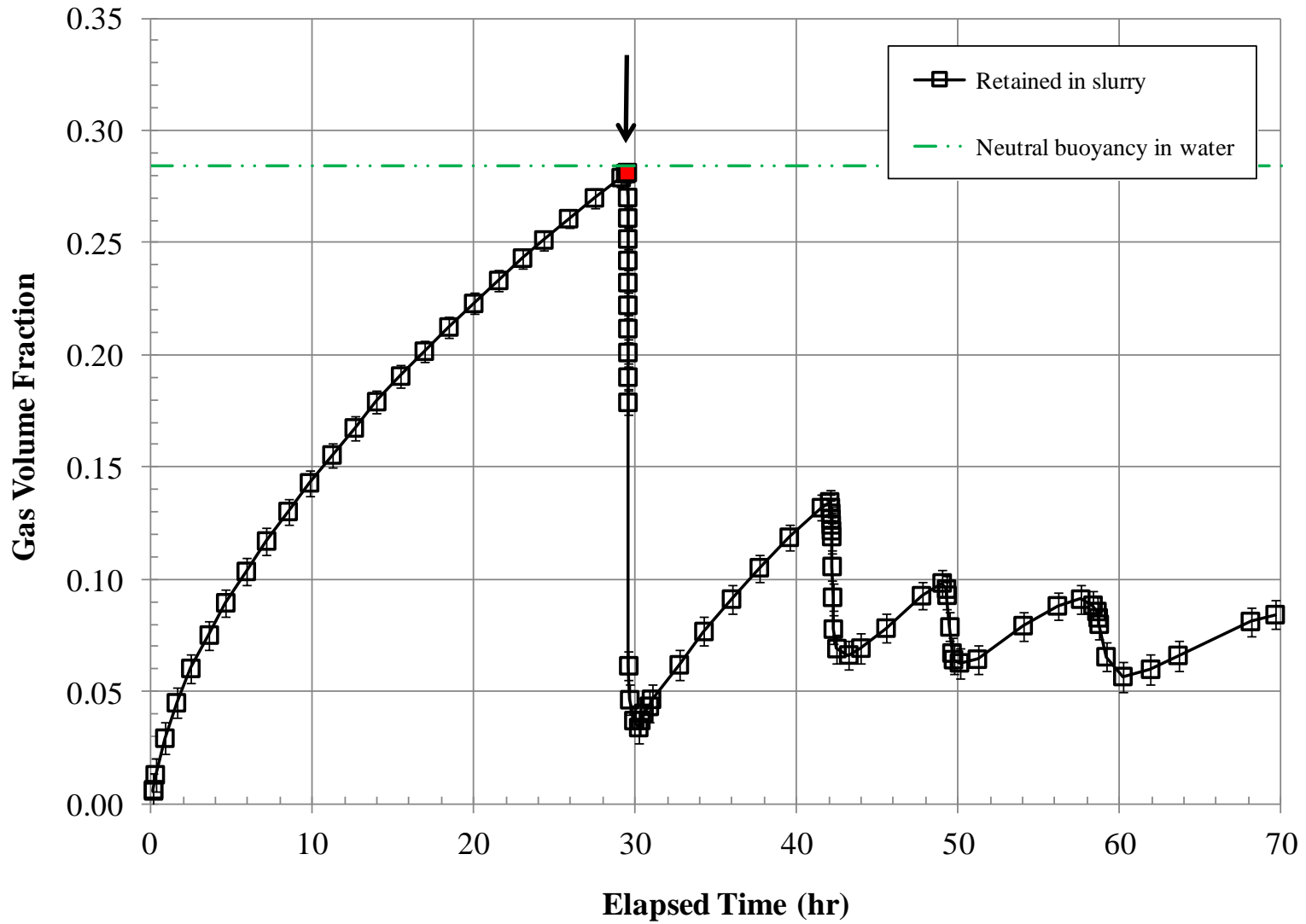


Figure C.27. Time Dependence of Retained Gas Fraction α from Level Measurements for SL Test 70-28

Test 23-29

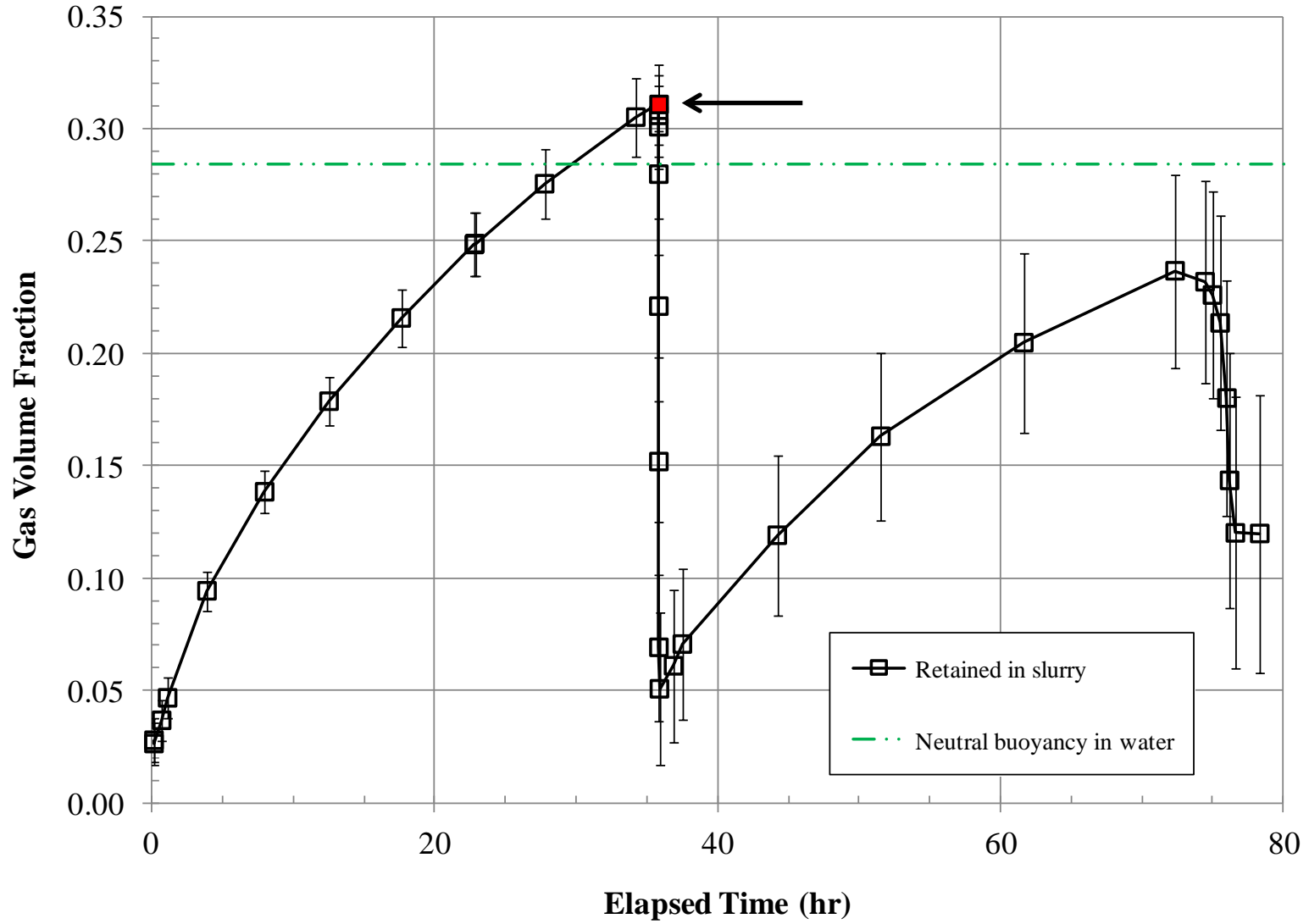


Figure C.28. Time Dependence of Retained Gas Fraction α from Level Measurements for SL Test 23-29

Test 70-30

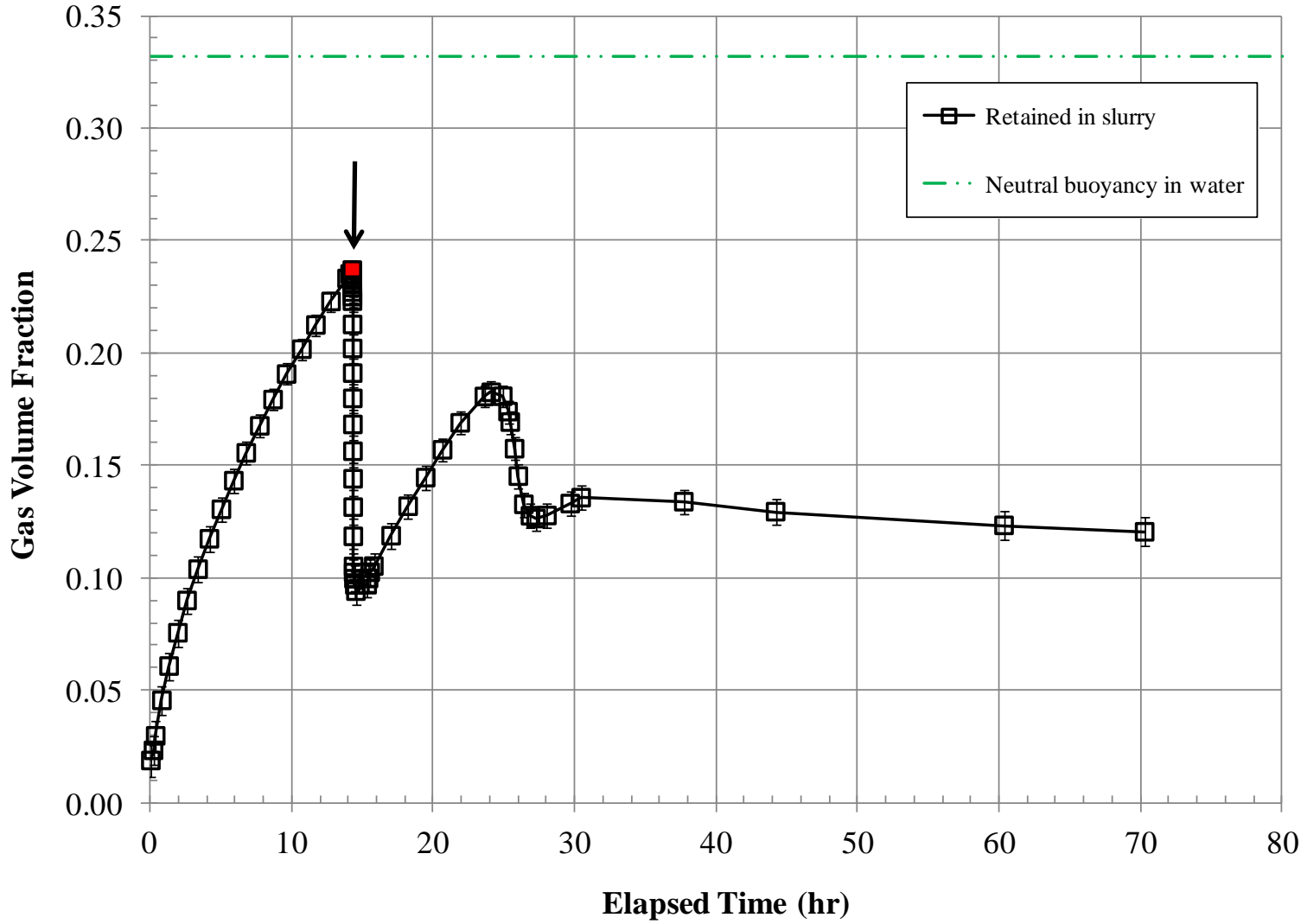


Figure C.29. Time Dependence of Retained Gas Fraction α from Level Measurements for SL Test 70-30

Test 23-31

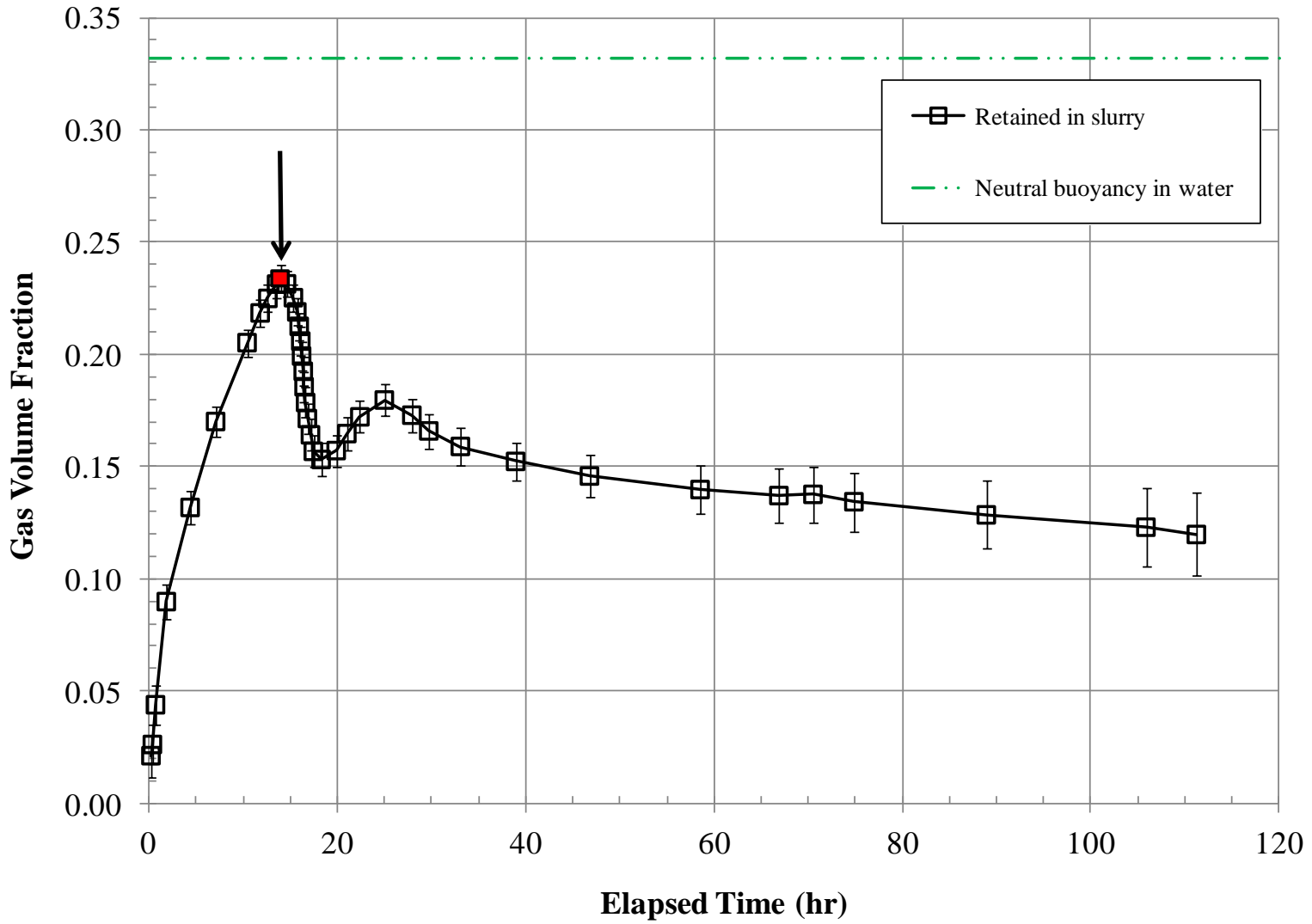
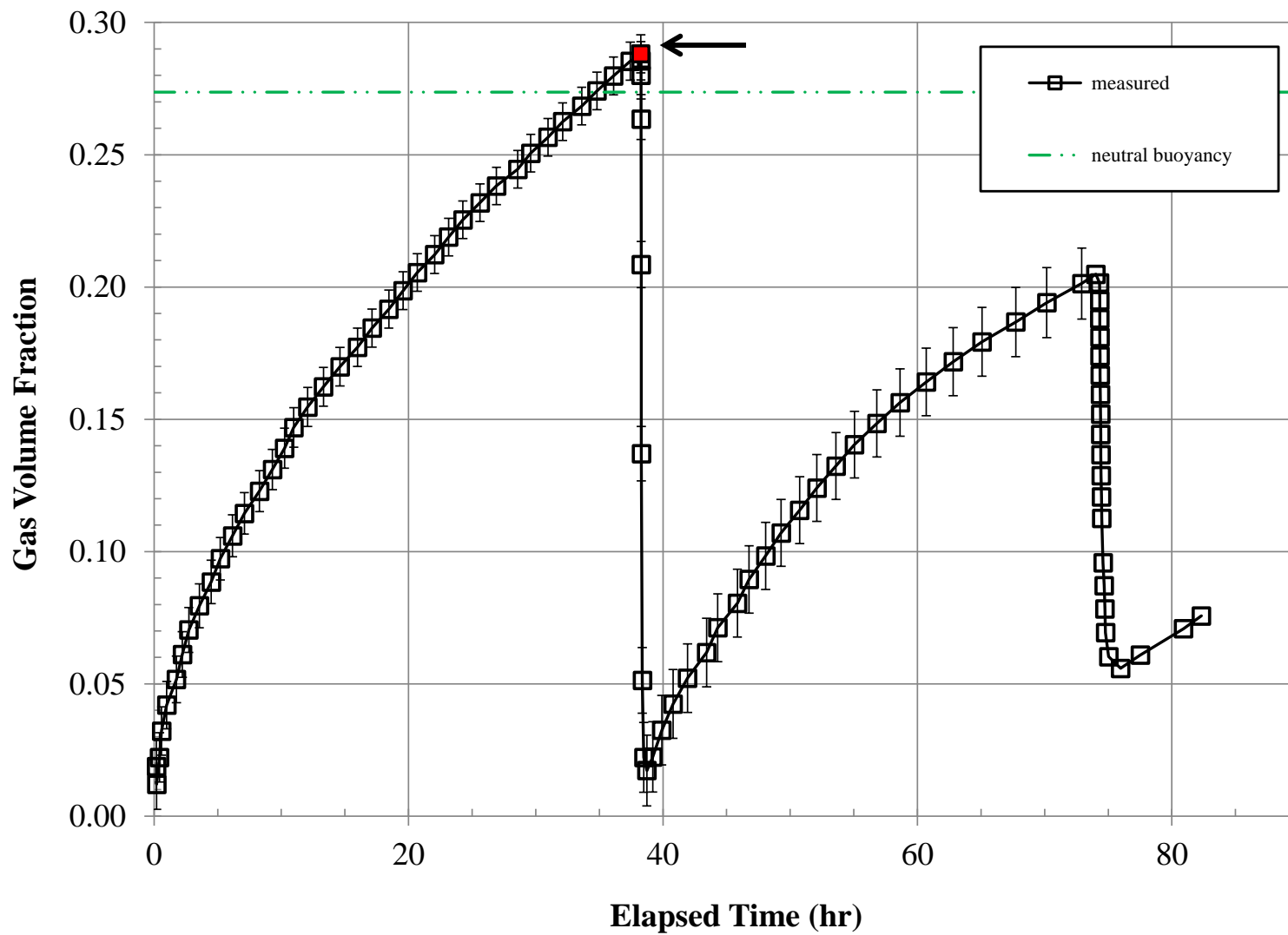


Figure C.30. Time Dependence of Retained Gas Fraction α from Level Measurements for SL Test 23-31

Test 23-32



C.2 References

Gauglitz PA, SD Rassat, PR Bredt, JH Konynenbelt, SM Tingey, and DP Mendoza. 1996. Mechanisms of Gas Bubble Retention and Release: Results for Hanford Waste Tanks 241-S-102 and 241-SY-103 and Single-Shell Tank Simulants. PNNL-11298, Pacific Northwest National Laboratory, Richland, Washington.

Distribution

**No. of
Copies**

**No. of
Copies**

OFFSITE

ONSITE

- 1 M Epstein
Fauske and Associates, LLC
1118 3rd Street, #308
Santa Monica, CA 90403
- 1 G Terrones
Applied Physics Division (X-4)
MS: T086
Los Alamos National Laboratory
Los Alamos, NM 87545
- 2 Savannah River National Laboratory
Savannah River Site
Aiken, SC 29808
C Nash
B Wilmarth
- 1 RD Holtz
Civil & Environmental Engineering
University of Washington
201 More Hall, Box 352700
Seattle, WA 98195-2700

- 7 **Washington River Protection Solutions**
- | | |
|------------|-------|
| WB Barton | S7-90 |
| R Calmus | H8-04 |
| JM Grigsby | S7-90 |
| NW Kirch | R2-58 |
| DB Little | R2-58 |
| JE Meacham | R2-58 |
| TL Sams | R2-52 |
- 28 **Pacific Northwest National Laboratory**
- | | |
|------------------|-------|
| GK Boeringa | K7-15 |
| WC Buchmiller | K6-26 |
| RC Daniel | P7-22 |
| MR Elmore | K6-24 |
| JA Fort | K7-15 |
| PA Gauglitz (10) | K7-15 |
| LA Mahoney | K7-15 |
| RP Pires | K6-28 |
| MR Powell | K6-24 |
| SD Rassat (5) | K6-28 |
| DR Rector | K7-15 |
| PP Schonewill | P7-25 |
| DN Tran | K6-24 |
| BE Wells | K7-15 |
| Project Records | |



Pacific Northwest
NATIONAL LABORATORY

*Proudly Operated by **Battelle** Since 1965*

902 Battelle Boulevard
P.O. Box 999
Richland, WA 99352
1-888-375-PNNL (7665)
www.pnnl.gov



U.S. DEPARTMENT OF
ENERGY